Open Research Online

The Open University's repository of research publications
and other research outputs

Role of sedlin, a TRAPP complex subunit, in membrane trafficking and in the pathogenesis of Spondyleopyphiseal Dysplasia Tarda

Thesis

oro.open.ac.uk

Role of sedlin, a TRAPP complex subunit, in membrane trafficking and in the pathogenesis of Spondyloepyphiseal Dysplasia Tarda

Rossella Venditti

Discipline: Life and Biomolecular Sciences

Affiliated Research Center: Telethon Institute of Genetics and Medicine and

Consorzio Mario Negri Sud

Thesis submitted in accordance with the requirements of the Open

University for the degree of Doctor of Philosophy

August 2011

Date of Submission: 22 August 2011
Date of Award: 7 February 2012

To my parents

*"It's the possibility of having a dream come true
that makes life interesting"*

*(Paulo Coelho,
The Alchemist)*

Abstract

Genetic defects occurring in the sedlin gene, a conserved component of TRAPP complex, cause Spondyloepiphyseal Dysplasia Tarda (SEDT), a rare progressive condition characterised by impaired chondrogenesis resulting in short stature, flattening of the vertebrae, and premature osteoarthritis. The role of sedlin in the pathogenesis of SEDT disease so far is still unknown. Prompted by the consideration that sedlin is ubiquitously expressed but that sedlin mutations cause cartilaginous-restricted dysfunctions, I hypothesized that sedlin might exert a role in membrane trafficking generally but in particular in the transport of chondrocyte-specific cargoes, such as type II procollagen (PCII). This hypothesis was reinforced by the fact that mutations in PCII give rise to autosomal dominant forms of spondyloepiphiseal dysplasia. I tested this hypothesis by analyzing the involvement of sedlin in the transport of different classes of secretory cargoes and found that sedlin is selectively required for PCII to exit the ER, while it is not essential for ER exit of small soluble and membrane-associated cargoes. I have also identified the molecular mechanism underlying this role of sedlin in its ability to bind the GTPase Sar1 and to control the membrane–cytosol cycle of Sar1 itself and of the COPII coat complex at the level of the ER exit sites. Sedlin depletion and/or mutation in SEDT patients slows down the Sar1 cycle and prolongs the membrane association of Sar1-GTP at the ER exit sites, thus inducing constriction and premature fission of nascent carriers which fail to incorporate the large PC protofibrils but are still competent for smaller

secretory cargoes. All together these findings provide new insights not only into understanding the role of sedlin but also shed new light on the molecular mechanisms underlying the onset of the SEDT disease.

Table of Contents

Abstract

Chapter 1

Chapter 2

V

Chapter 4

Chapter 5

Chapter 6

List of Figures

Chapter 1

Chapter 3

Chapter 4

Chapter 5

Chapter 6

List of Tables

Chapter 2

Chapter 1

Introduction

Newly synthesised proteins destined to enter the secretory pathway are translated at the level of the rough endoplasmic reticulum (ER) and translocated into the ER lumen or ER membrane. Here, secretory proteins undergo folding, assembly and post-translational modifications.

Proper folded and assembled proteins are then separated from ER resident proteins and transported to the Golgi complex (GC) for further processing, modifications and transport to their final destination.

The transport of newly synthesized proteins from one organelle to another (such as from the ER to the Golgi complex) or through a single organelle (such as transport through the Golgi stacks: intra-Golgi transport) is tightly regulated so that a large amount of cargo can flow through the secretory pathway without compromising the integrity and steady-state composition of the constituent organelles (**Figure 1.1**).

1
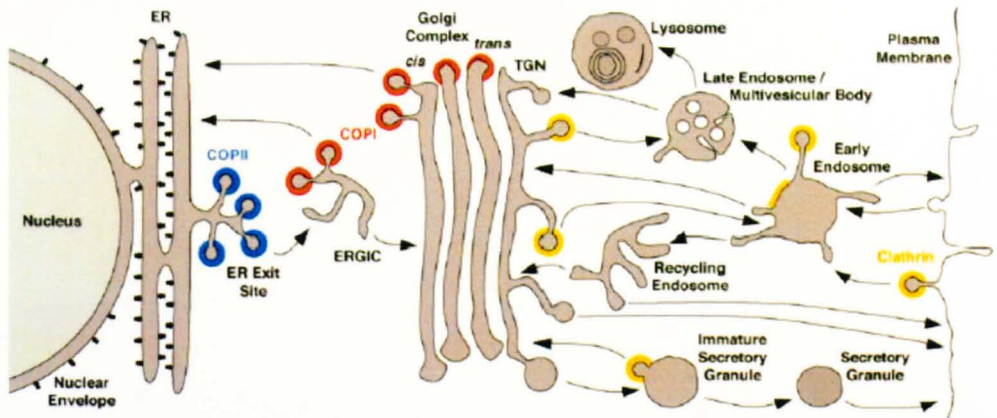
Figure 1.1 The secretory pathway. Schematic representation of the intracellular transport pathway. The scheme depicts the compartments of the secretory, lysosomal/vacuolar, and endocytic pathways. Transport steps are indicated by arrows. Colors indicate the known or presumed locations of COPII (blue), COPI (red), and clathrin (orange). Adapted from Bonifacino and Glick, 2004.

Although the protein subunits of the different machineries acting along the secretory pathway are largely known (as in the case of COPII subunits that mediate the formation of carriers at the ER-exit sites (ERES) and the SNARE proteins that are involved in membrane fusion), a number of important aspects and questions remain to be resolved.

One open question is whether different proteins that differ in size and composition are incorporated into the same or different carriers. Moreover, the debate about the shapes and sizes of these transpost carriers (i.e. 60-80 nm vesicles or large pleiomorphic tubular carriers: Mironov et al. 2003; Fromme and Schekman, 2005) also remains an important open question, with some proteins thought to be transported in distinct carriers (such as vesicles) while others are thought to move via large carriers that are formed by "en-bloc protrusions" from the ER (Mironov et al., 2003).

Indeed, beyond the recruitment of nascent cargo for delivery to downstream compartments, other transport components must be integrated with the recruitment of nascent cargo, such as targeting and fusion proteins, including the tethering and SNARE complexes that direct COPII vesicles to the Golgi complex.

In the following sections, I will briefly describe and discuss what is known about protein transport and the machineries that are involved, with particular reference to the questions that remain to be answered.

1.1 COPII

1.1.1 COPII coat recruitment and assembly

The ER-to-Golgi transport step is thought to occur via membrane-bound transport carrier intermediates, which are formed by the assembly of the coat protein complex II, the COPII coat, on the ER membranes.

COPII (coatomer protein II) has been shown to be involved in the direct capture of cargo molecules and in the physical deformation of the ER membranes that drives the formation of the so-called COPII carriers or transport intermediates in ER-to-Golgi anterograde trafficking.

The COPII proteins directly participate in the selection of the cargo that is incorporated, either by recognizing sorting signals that are present in the cytosolic domains of the transmembrane cargo proteins, or indirectly, via specific cargo receptors in the case of soluble cargoes and some transmembrane cargoes (Bonifacino and Glick, 2004).

Protein export by COPII vesicles from the ER represents the default ER-to-Golgi route in yeasts and mammals. Cargo proteins that are destined for the GC not only include newly synthesised biosynthetic cargo molecules, but also a variety of other machinery proteins that constantly cycle between the ER and the GC.

The molecular mechanistic details of COPII vesicle formation and cargo delivery to the GC have been defined through yeast genetics and *in vitro* reconstitution.

The components of the COPII machinery identified using the yeast model *Saccharomyces cerevisiae* as being necessary for ER exit include: Sar1 (Nakano and Maramtsu, 1989), Sec23/24 (Hicke et al., 1992), Sec13/31 (Salama et al., 1993) and the Sar1 regulator Sec12 (Nakano et al., 1988). Only few years after the original discovery of these proteins, their physical interaction and their capability to generate COPII vesicles *in vitro* were demonstrated (Barlowe et al., 1994).

A wealth of biochemical and genetic experiments led to a general consensus that COPII vesicles were formed through a precise sequence of events (**Figure 1.2**).

1.1.1.1 Sar1 and Sec12

COPII coat assembly is initiated by the exchange of GDP for GTP on the small GTPase Sar1, a process catalyzed by the ER-localized guanine nucleotide exchange factor (GEF) Sec12. As a small Ras-like GTPase, Sar1 needs to be activated by a guanine nucleotide exchange factor (GEF). Activation from the GDP- to the GTP-bound form occurs thanks to the GEF Sec12p first identified in the yeast *S. cerevisiae* (Barlowe et al., 1993). Sec12p is a type II transmembrane ER glycoprotein composed of a 40-kDa cytoplasmic domain and 10-kDa luminal domain. The cytosolic domain has been reported to function independently of membranes as a Sar1-specific
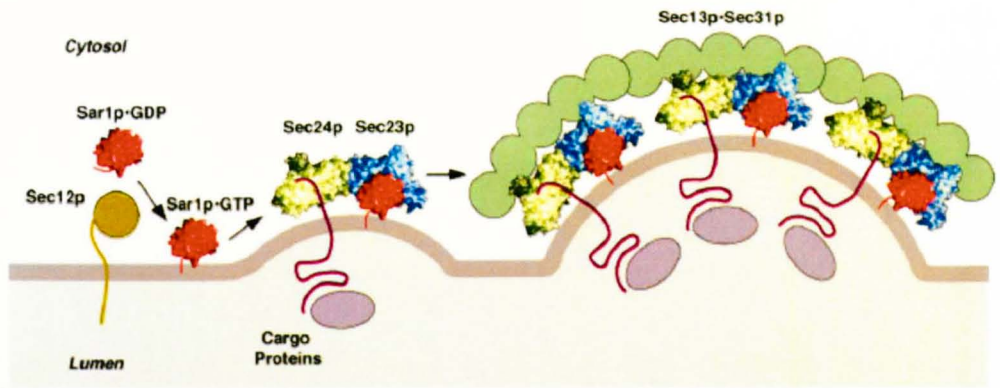
Figure 1.2 Assembly of the COPII machinery and cargo sorting/packaging. Sar1 is activated to Sar1-GTP by the ER-localized exchange protein Sec12. Sar1-GTP assembles into the Sar1-Sec23/Sec24-cargo pre-budding complex that is successively clustered by the outer layer Sec13-Sec31 protein complex. Adapted from Bonifacino and Glick, 2004.

GEF (Nakano et al., 1988; D'Enfert et al., 1991). Since Sec12 is strictly localised to the ER membranes by static retention (Sato et al., 1996), Sar1 activation is restricted to the ER membranes.

Activation of Sar1 by Sec12 at the ERES in mammalian cells (Aridor et al., 2001), leads to the recruitment of cargo to "prebudding" complexes (Aridor et al., 1998; Kuhen et al., 1998) and assembly of the COPII cytosolic coat complexes Sec23/24 and Sec13/31, directing vesicle budding from the ER.

In its GTP-bound state, Sar1 interacts with the ER membranes by the exposure of the N-terminal amphipathic α-helix (Huang et al., 2001; Bi et al., 2002) and recruits the Sec23/Sec24 heterodimeric complex, and this Sar1–Sec23/Sec24 complex then recruits the Sec13/Sec31 proteins.

Together with Sec23/Sec24, Sar1 forms the layer of the coat that is proximal to the membrane, the *inner* layer, while Sec13/Sec31 form a second, more distal, *outer* or membrane layer.

In addition to its established role in recruiting the Sec23/Sec24 complex, Sar1 also appears to facilitate membrane bending and to contribute also to membrane-bound carrier fission (Lee et al., 2005; Long et al., 2010). Sar1 with bound GTP (or non-hydrolyzable GTP analogs) has been shown to generate curvature and tubulation *in vitro* from liposomes with lipid composition mimicking that of the ER (Lee et al., 2005; Bielli et al., 2005, Bacia et al., 2011). The incubation of Sar1-GTP with ER membranes in the absence of the Sec23/Sec24 and Sec13/Sec31 proteins leads to the formation of tubules at the ERES, and these tubules can be resolved into functional transport carriers by the addition of the missing Sec23/Sec24 and

Sec13/Sec31 components, indicating that Sar1 can control membrane curvature and has an important role in the generation of the ERES (Aridor et al., 2001; Long et al., 2010).

This tubulation is dependent on the Sar1 N-terminal amphipathic α-helix (possessing a hydrophobic face and a hydrophilic face; Lee et al., 2005; Long et al., 2010), formed by 23 amino acids that are exposed when the protein is GTP-bound, allowing the hydrophobic hemicylinder to insert into the lipid bilayer (Matsuoka et al., 1998). By contrast, Sar1-GDP binds membranes with lower affinity.

The expression of a GTP-restricted mutant form of Sar1 has differential effects on the segregation of cargo during export from the ER, blocking the transport of these cargoes to the Golgi complex (Stephens and Pepperkok, 2004). In addition, the microinjection of a GDP-restricted form of Sar1p inhibits the ER exit of both large molecules, such as procollagen type-I (~300 nm in size), and small proteins, such as the viral protein VSV-G, suggesting that, despite their differences in size, ER exit is COPII-dependent for both large and small cargoes (Aridor et al., 2001; Mironov et al., 2003).

X-ray crystallography studies revealed details of the Sar1 structure. It consists of four distinct domains: a guanine nucleotide binding pocket, switch I domain, switch II domain, and N-terminal amphipathic α-helix, each of which plays a specific role in Sar1 function (Rao et al., 2006; Bi et al., 2002; Huang et al., 2001). Six β sheets compose the core of the protein that forms the guanine nucleotide binding pocket (the G domain) typical of

8

the Ras superfamily (Huang et al., 2001). This G domain is essential for Sar1 function: mutation of Thr39 to Asn creates a GDP-restricted dominant-negative mutant by interfering with the association to its guanine nucleotide exchange factor, Sec12 (Weissman et al., 2001). Another position important in regulating Sar1 GTPase activity is His79 in the switch II region which, if mutated, results in a loss of ability of Sar1 to hydrolyze GTP thus inhibiting the disassembly of the COPII complex (Huang et al., 2001).

Sar1 has a very slow intrinsic rate of GTP hydrolysis because, like other Ras-like small GTPases, it lacks key catalytic residues (Bi et al., 2002; Vetter and Wittinghofer, 2001). As mentioned above, Sar1-GTP recruits the Sec23/24 heterodimer by binding Sec23 to form the so-called "prebudding complex" (Kuehn et al., 1998). Sec23 acts as a GTPase-activating protein (GAP) for Sar1 (Yoshihisa et al., 1993), and it binds to Sar1-GTP on the side opposite to the Sar1 membrane anchor.

Therefore, Sec23 stimulates Sar1 GTP hydrolysis upon binding to Sar1, an event that leads to the loss of Sar1 from membranes (Antonny et al., 2001). However, the presence of Sec12, which continuously provides "fresh" Sar1-GTP guarantees a constant presence of Sar1-GTP, and hence the full assembly of the COPII coat at the ERES (Futai et al., 2004).

The Sec23/24 heterodimer is responsible for binding cargo molecules and accelerating the Sar1 GTPase activity (Yoshihisa et al., 1993). The crystal structure of the Sec23/24 heterodimer revealed a general bow tie shape (Lederkremer et al., 2001) with a concave inner face that closely matches the arc of the 60 nm cages, likely favouring deformation of the membrane (Bi et al., 2002). Interestingly, the two structures of Sec23 and Sec24 are very similar, albeit they share only 14% sequence identity (Bi et al., 2002). The two structures share common features: they both possess a β barrel, a zinc finger, an α-helical region and a trunk domain (**Figure 1.3**). The trunk domain plays an important role in the binding of Sar1 and is responsible for the binding between Sec23 and Sec24.

The carboxyl-terminal gelsolin-like domain of Sec23 is responsible for the activation of the GTPase activity of Sar1. The mechanism by which Sec23 acts as a GAP to accelerate the GTP hydrolysis of Sar1 involves the insertion of an arginine side chain, Arg722, into the active site to form bonds with the phosphates via its guanidinum group (Bi et al., 2002).

This type of mechanism, involving an "arginine-finger" residue that neutralizes negative charge in the GTPase transition state is a common feature of Ras-like GTPases (Vetter and Wittinghofer, 2001).

The lifetime of the Sar1–Sec23/Sec24 prebudding complex is believed to be sufficiently long to allow its lateral diffusion on the ER membrane and cargo capture. The subsequent recruitment of Sec13/Sec31 accelerates the Sec23-mediated GAP activity on Sar1 by an order of magnitude (Antonny
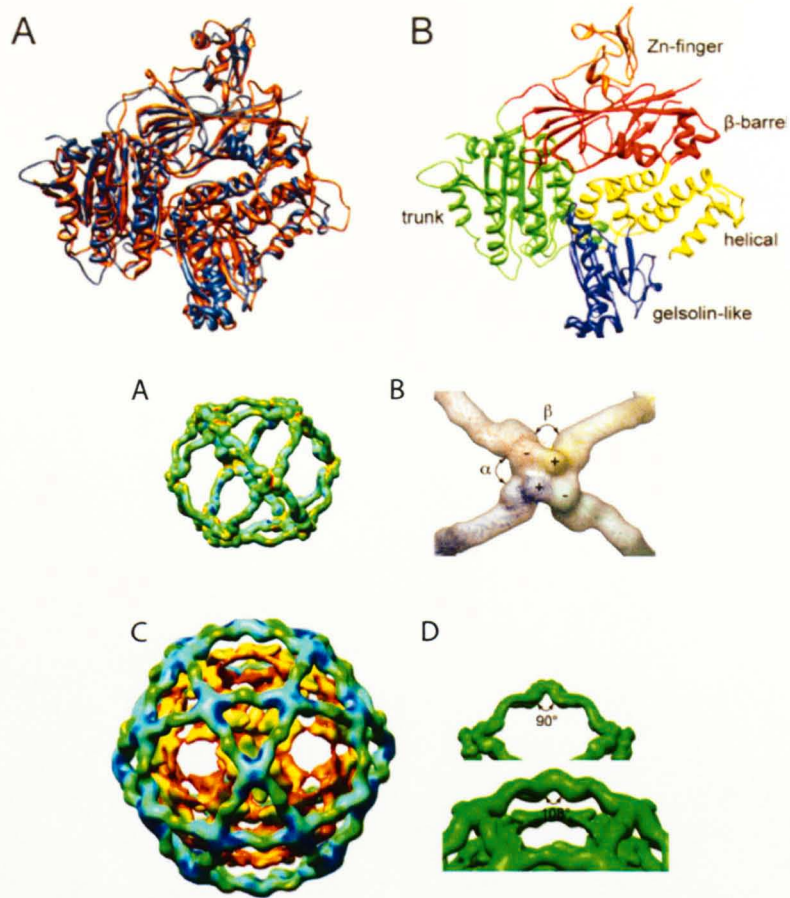
Figure 1.3 The structure of the COPII components. Upper panel: Sec23/24. (**A**) Superposition of Sec23 and Sec24 shows the high degree of homology between the two proteins. (**B**) Sec23/24 domains: the trunk (green), Zn-finger (orange), β-barrel (red), helical (yellow), and gelsolin-like (blue). Lower panel: Sec13/Sec31. (**A**) Sec13/Sec31 structure derived from cryo-EM. (**B**) WD domains mediate the formation of the vertices of the cage. (**C**) Sec13/sec31 structure with Sec23/24 (**D**) β angle of 90°C dictates the 600 Å diameter structure, while β angle of 108 dictates the formation of a larger structure of 1000 Å in diameter. Adapted from Russell and Stagg, 2010.

et al., 2001). Sec31 binds as an extended polypeptide (heterotetramer) across the Sec23 and Sar1 molecules, and inserts amino-acid side chains in the proximity of the Sar1 active site, thus accelerating GTP hydrolysis in combination with Sec23 (Bi et al., 2007).

Sec24 functions as the primary cargo adaptor element of the COPII coat, as it is generally responsible for the direct interaction with cargo molecules (Miller et al., 2003).

Basically, the selective capture is driven by export signals located within the cytoplasmically exposed regions of transmembrane proteins, but some of these transmembrane proteins and the majority of soluble cargo proteins need specific transmembrane receptors/adaptors to mediate the interaction with the COPII coat.

Although a universal ER-export signal has not yet been described, a number of different signals appear to regulate the interaction with the COPII coat, including di-acidic motifs and hydrophobic/aromatic motifs (Bonifacino and Glick, 2004). Sec24 was initially studied in yeast and at least three interaction domains have been identified on its membrane-facing surface: the A, B and C sites that control which cargo is selected (Mossessova et al., 2003; Miller et al., 2003). The Sec24 A site is the binding site for the NPF motif, the dominant signal for ER exit of the Syntaxin SNARE protein Sed5 (Mossessova et al. 2003; Miller et al. 2005). The B site on Sec24 binds to the LxxLE-class signals that are present on the SNAREs Bet1 and Sed5, as well as to the DxE transport signal that directs the ER exit of VSV-G and yeast Sys1p (Nishimura et al. 1999; Votsmeier and Gallwitz 2001). The C

site was defined through the mutagenesis of Sec24, and it is specific for packaging the SNARE Sec22.

The presence of multiple binding sites allows for diversity in the number of exit codes that Sec24 can bind, and multiple Sec24 isoforms (four isoforms, A, B, C and D, have been identified in mammals) expand the range and specificity of Sec24-cargo interactions.

Intriguingly, distinct Sec24 family members, by interacting with Sec23, are able to recognize export signals different from those bound by Sec24 alone (Pagano et al., 1999; Miller et al., 2003), thus expanding the cargo multiplicity captured by COPII coat.

1.1.1.3 Sec13/Sec31

After the "prebudding complex" is formed, the subsequent recruitment of Sec13/Sec31 accelerates the Sec23-mediated GAP activity. The GAP activity associated with these components of the COPII complex makes the complex unstable in principle, and raises the question of how sufficient stability for cargo capture and carrier formation is achieved.

Notably, Sec31 cannot act alone on Sar1 because it only binds to the Sec23-Sar1 complex (Bi et al., 2007). In this scenario, the sequential binding reaction confers a two-gear mechanism for GTP hydrolysis on Sar1 (Antonny et al., 2001), whereby hydrolysis is initiated upon Sec23/24 binding and is accelerated further upon recruitment of Sec13/31. Thus, GTP hydrolysis is programmed into the COPII system upon assembly, since the

slow rate of reaction on Sar1-Sec23/24 may provide the prebudding complex the opportunity to gather cargo and SNARE molecules prior to Sec13/31 binding (Antonny et al., 2001).

However, some cell types have to secrete extremely large macromolecular cargoes, such as the lipoprotein chylomicrons (~400 nm in diameter) and the procollagen molecules that assemble into a triple helical molecule of >300 nm in length (see below). These types of cargo exceed the regular COPII size and they are clearly too large to fit into these conventional 60-80 nm vesicles that bud from the ER. New insights came from the full determination of the crystal structure of COPII machinery that has revealed new rules in COPII formation (Stagg et al., 2008).

A conventional model of coat assembly suggested the possibility that each Sar1-Sec23/24-cargo ternary prebudding complex (Aridor et al., 1999; Supek et al., 2002) will recruit a Sec13/31 heterotetramer that will subsequently assemble a vertex. But new detailed structural information led to a different model: Sec23/24 first form an oligomer to define a site for Sec13/31 recruitment (Stagg et al., 2008). While other permutations are possible, such a pathway based on assembly of Sec23/24 tetramer clusters could establish the polarity and geometry of the observed vertices as well as facilitate regulation by cargo. The formation of a vertex depends on two angles: α and β. α is invariant for all the COPII structures observed. β, varies between 90° and 108°, and this is what allows COPII cages to form with different diameters.

The COPII structures observed should be capable of recruiting a huge variety of molecules of several classes that differ in term of size and dimensions including single and multi-membrane spanning proteins. If COPII cages are to incorporate cargo molecules larger than those that can be accommodated by the 1000 Å coat, β must be capable of assuming angles greater than 108°. If 1000 Å is the largest coat that can be formed, then large cargo such as procollagen and chylomicrons (up to 3,000 Å or 10,000 Å respectively) would have to be transported by some other means, perhaps a non-canonical COPII vesicle that lacks Sec13/31.

In another scenario, β angles larger than 108° (up to 120°) would make it possible to assemble any kind of structures from planar polygonal sheets to helical tubes. Thus, if β could take on different angles it would support the hypothesis that the COP II machinery possesses the capacity to accommodate large cargo molecules; however such structures have not been observed *in vitro* as yet (Russell and Stagg, 2010).

How such cargoes are packaged into transport carriers and how they are subsequently transported to and through the Golgi complex still remain an open question (Fromme and Schekman, 2005).

1.1.2 Maintenance and regulation of ERES

The molecular mechanisms controlling the positioning, biogenesis and maintenance of ERES have remained elusive. Recent evidence suggests a function for Sec16 in the homoeostasis of ERES (Watson et al., 2006; Bhattacharyya and Glick, 2007; Iinuma et al., 2007; Fahran et al., 2008;

Hughes and Stephens, 2009). Sec16 is a large peripheral membrane protein of 250 kDa. It is a highly evolutionarily conserved protein that associates with ERES and is thought to form a scaffold for the assembly of COPII (Gimeno et al., 1996). Sec16 is also an essential gene in *S. cerevisiae* and *Pichia pastoris* (Espenshade et al., 1995; Connerly et al., 2005). *In vitro* COPII binding reactions performed with isolated ER membranes stripped of Sec16 showed less efficient vesicle formation (Gimeno et al., 1996; Supek et al., 2002). Sec16 has then been shown to act as a protein scaffold to direct the assembly of the COPII coat through its binding to Sar1 (Ivan et al., 2008), to Sec23 (Bhattacharyya and Glick, 2007), and to Sec13 (Hughes and Stephens, 2009).

COPII turnover at a single ERES has been analyzed in living cells, and the half-lives for Sar1, Sec23 and Sec24 were determined as 1.1, 3.7 and 3.9 sec, respectively (Forster et al., 2006). Moreover, decreasing the amount of transport-competent cargo in the ER has been shown to accelerate the turnover of the Sec23/24p and to slow down that of Sar1. The combination of several experimental *in vivo* FRAP kinetic studies, the mathematical model of membrane turnover by COPII, and existing *in vitro* data predicts that Sec23/24p remains membrane associated even after GTP is hydrolysed by Sar1, for a duration that is strongly increased by the presence of cargo. Thus the cargo retains the COPII complex on membranes even after the release of Sar1, and prevents the premature disassembly of COPII during cargo sorting and transport-carrier formation (Forster et al., 2006).

Indeed, Guo and Linstedt showed the importance of cargo in the recruitment of COPII (Guo and Linstedt, 2006). Quantification of COPII assembly during *de novo* biogenesis of the Golgi complex during wash-out of brefeldin A (BFA, a fungal toxin that induces a reversible redistribution of the Golgi complex into the ER), showed that a dramatic up-regulation of COPII at the ERES was driven by increased levels of cargo (i.e. Golgi proteins) in the ER (Guo and Linstedt, 2006).

This up-regulation of COPII assembly occurred in the absence of GTP hydrolysis and any cytosolic factors, other than the COPII prebudding complex of Sar1–Sec23/Sec24. These findings suggest that the interaction between the cargo (i.e. Golgi proteins exiting the ER) and COPII components regulates ER exit (Guo and Linstedt, 2006). Moreover, an acute increase in cargo load causes fusion of ERES leading to an increase in ERES size (Farhan et al., 2008). This response was dependent on a limiting amount of either PI4-kinase III α (PI4K-IIIα) or Sec16. By contrast, a chronic increase in cargo load resulted in the neo-formation of additional ERES. This response was in turn independent of PI4K-IIIα but required Sec16. The chronic increase in cargo load induced the expression of COPII and Sec16 through the unfolded protein response (UPR). These results suggest that acute and chronic cargo loads are handled in a different mechanistic way at the level of ERES (Farhan et al., 2008).

ERES align along microtubules in several cell lines (Ralston et al., 2001) ERES undergo predominantly short- but also long-range movements in mammalian cells that are completely inhibited following depolymerization of microtubules. In metazoans, ER-to-Golgi transport carriers are

transported along microtubules in a dynein motor-dependent manner (Presley et al., 1997). Moreover a subunit of the dynactin complex, which is essential for dynein function, has been shown to directly interact with the human Sec23A paralog (Watson et al., 2005). This interaction paired with observation of both dynactin and Sec23A at the plus-end of growing microtubules in living cells, corresponding to ER exit sites. Interfering with the Sec23A–dynactin interaction resulted in an increased turnover rate of COPII components at ER exit sites, coupled with a decrease in the kinetics of ER export, but it did not affect the velocity of ER-to-Golgi transport carriers (Watson et al., 2005).

Dynactin is important for an early stage of ER exit, but not for microtubule transport. A subsequent study found that microtubule plus-end localization of dynactin was dependent upon EB1 (End-Binding protein 1) and CLIP-170 (Cytoplasmic Linker Protein 170; Watson et al., 2006). EB1 and CLIP-170 mediate the microtubule plus-end loading of p150 (Glued) (Watson et al., 2006). Disruption of the plus-end localization of dynactin did not affect ER-to-Golgi transport, implying that dynein-based transport is not dependent upon localization to plus-ends. This work suggests the hypothesis that the COPII coat functions as the link between the vesicle membrane and the microtubule motor.

1.2 Procollagens

A central question is whether the huge variety of cargoes leaving the ER use different types of carriers. Studies in yeast have shown that different carriers forming in a COPII-dependent manner at the ER membrane have differential molecular requirements (Castillon et al., 2009; Morsomme and Riezman, 2002; Morsomme et al., 2003). A number of approaches have been undertaken to address this question in mammals but a definitive answer is still missing (Stephens and Pepperkok, 2002; Mironov et al., 2003). This issue is particularly relevant for cargoes that are considered special because of their size, as is the case for types I and II procollagen (PCI and PCII), which form large 300 nm rigid triple helices whose size greatly exceeds the size of a "regular" COPII carrier vesicle (60-80nm).

Collagen is a very abundant structural protein in all animals. In humans, collagen comprises one third of the total protein and is the most prevalent component of the extracellular matrix (ECM). So far, twenty-eight different types of collagen composed of at least 46 distinct polypeptide chains have been identified in vertebrates (Veit et al., 2006; Brinkman et al., 2005; **Figure 1.4**).

Xaa-Yaa-Gly is the amino-acid motif responsible for the assembly of the triple helix of all collagen types, where Xaa and Yaa can be any amino acid. The amino acids in the Xaa and Yaa positions of collagen are often (2S)-proline (Pro, 28%) and (2S, 4R)- 4-hydroxyproline (Hyp, 38%),

A

B

Type	Class	Composition	Distribution[b]	Pathology[c]
I	Fibrillar	α1[I]₂α2[I]	Abundant and widespread: dermis, bone, tendon, ligament	OI, Ehlers–Danlos syndrome, osteoporosis
II	Fibrillar	α1[II]₃	Cartilage, vitreous	Osteoarthrosis, chondrodysplasias
III	Fibrillar	α1[III]₃	Skin, blood vessels, intestine	Ehlers-Danlos syndrome, arterial aneurysms
IV	Network	α1[IV]₂α2[IV] α3[IV]α4[IV]α5[IV] α5[IV]₂α6[IV]	Basement membranes	Alport syndrome
V	Fibrillar	α1[V]₃ α1[V]₂α2[V] α1[V]α2[V]α3[V]	Widespread: bone, dermis, cornea, placenta	Ehlers-Danlos syndrome
VI	Network	α1[VI]α2[VI] α3[VI][d] α1[VI]α2[VI] α4[VI]	Widespread: bone, cartilage, cornea, dermis	Bethlem myopathy
VII	Anchoring fibrils	α1[VII]₂α2[VII]	Dermis, bladder	Epidermolysis bullosa acquisita
VIII	Network	α1[VIII]₃ α2[VIII]₃ α1[VIII]₂α2[VIII]	Widespread: dermis, brain, heart, kidney	Fuchs endothelia corneal dystrophy
IX	FACIT[e]	α1[IX]α2[IX]α3[IX]	Cartilage, cornea, vitreous	Osteoarthrosis, multiple epiphyseal dysplasia
X	Network	α1[X]₃	Cartilage	Chondrodysplasia
XI	Fibrillar	α1[XI]α2[XI]α3[XI]	Cartilage, intervertebral disc	Chondrodysplasia, osteoarthrosis
XII	FACIT	α1[XII]₃	Dermis, tendon	—
XIII	MACIT	—	Endothelial cells, dermis, eye, heart	—
XIV	FACIT	α1[XIV]₃	Widespread: bone, dermis, cartilage	—
XV	MULTIPLEXIN	—	Capillaries, testis, kidney, heart	—
XVI	FACIT	—	Dermis, kidney	—
XVII	MACIT	α1[XVII]₃	Hemidesmosomes in epithelia	Generalized atrophic epidermolysis bullosa
XVIII	MULTIPLEXIN	—	Basement membrane, liver	Knobloch syndrome
XIX	FACIT	—	Basement membrane	—
XX	FACIT	—	Cornea (chick)	—
XXI	FACIT	—	Stomach, kidney	—
XXII	FACIT	—	Tissue junctions	—
XXIII	MACIT	—	Heart, retina	—
XXIV	Fibrillar	—	Bone, cornea	—
XXV	MACIT	—	Brain, heart, testis	Amyloid formation?
XXVI	FACIT	—	Testis, ovary	—
XXVII	Fibrillar	—	Cartilage	—
XXVIII[f]	—	—	Dermis, sciatic nerve	Neurodegenerative disease?

Figure 1.4 Collagens structure and classification. (**A**) Overview of the collagen triple helix. (**B**) List of all identified collagens. Adapted from Shoulders and Raines, 2009.

respectively. The most common triplet found in collagen is ProHypGly (10.5%, Ramshaw et al., 2009).

Collagens consist of three polypeptide (α) chains, displaying an extended polyproline-II conformation, a right-handed supercoiled triple helix and a one-residue stagger between adjacent chains (Brodsky and Persikov, 2005). Collagens can be heterotrimeric, i.e. type I collagen, which contains two identical α chains and a different third chain [$\alpha 1(I)]_2 \alpha 2(I)$. However, the majority of collagens are homotrimers, like collagen II that contains three identical α chains [$\alpha 1(II)]_3$.

Vertebrate collagens are classified by function and domain homology into different classes (**Figure 1.4**): classical fibril forming collagens, network-forming collagens, fibril-associated collagens with interrupted triple helices (FACITs), transmembrane collagens, membrane associated (MACITs), multiple triple-helix domains and interruptions (MULTIPLEXINs). Collagen types, their distribution, composition, and associated pathologies are listed in **Figure 1.4**.

Fibril-forming collagens occur as 67-nm D-periodic fibrils that constitute the principal source of tensile strength in animal tissues (Kadler et al., 1996). The periodic structure of the fibril is due to regular staggering of triple helical collagen molecules. Mammals have 11 fibrillar collagen genes, which cluster phylogenetically into three distinct subclasses (Huxley-Jones et al., 2007). Collagen type I and collagen type II belong to this family. Interestingly, the X-Y-Gly domain of fibril-forming collagens contains

~1000 residues and is usually uninterrupted, with the notable exception of collagen XXIV and collagen XXVII. Newly synthesised fibril-forming collagens are initially produced as pro-collagens containing N- and C-propeptides at each end of the triple helical domain. Cleavage of the C-propeptides is required for fibrillogenesis.

Collagen type II is found predominantly, but not exclusively, in hyaline cartilage where it accounts for 90% of the total cartilage collagen (Mayne 1989). Together with smaller amounts of other collagens (types IX and XI), type II collagen forms a three-dimensional fibrillar network which is fundamental for the tensile stiffness and strength of cartilage, providing the architecture of the tissue (Eyre et al., 1991).

Mutations occurring in the *Col2* gene are responsible for the onset of Spondyloepiphyseal dysplasia *congenita* (see 1.7.4 section).

Collagen fibrils formed from type I collagen (all fibrous tissues except cartilage) and fibrils formed largely from type II collagen (cartilage) have slightly different structures, but they share a rod-like structures of 300-400 nm.

1.3 COPII and genetic diseases

While there has been important progress recently in identifying receptors such as TANGO/MIA3 that can guide the soluble PCs into COPII transport vesicles (Saito et al., 2009; Wilson et al., 2011), the issue of steric

22

incompatibility between cargo (300 nm triple helices) and containers (80 nm vesicles) remains a puzzle. In this regard, studies of genetic diseases involving genes that encode components of the early secretory pathway have been illuminating. Though ubiquitous, these components turn out to be rate limiting only for selected tissues/cells, presumably because these tissues/cells have specific requirements in terms of efficiency, loads and/or types of cargo.

1.3.1 Sar1B: Anderson's disease (AD) and Chylomicron Retention Disease (CMRD)

Anderson' disease (AD; OMIM 246700) or Chylomicron Retention Disease (CMRD) is a disorder characterized by hypobetalipoproteinemia with selective absence of apo B-48 in the post-prandial state (Bonavent et al., 1997; Jones et al., 2003; Peretti et al., 2010).

Chylomicrons, the principal carriers of dietary lipids, are triglyceride (TG)-rich lipoproteins secreted exclusively from enterocytes. These large lipoproteins (700 to 6000 Å) contain a single molecule of apolipoprotein (apo) B-48, which is essential for chylomicron structure cohesion (Mansbach et al., 2010; Kindel et al., 2010). Apo B-100 is found within very-low-density lipoproteins (VLDL) secreted by the liver and in low-density lipoprotein (LDL), a catabolic product of VLDL.

It is a very rare recessive disease with less than 50 cases reported in the literature. Subjects with this disorder exhibit the clinical manifestations initially described by Anderson and her colleagues in 1961, which consist of a malabsorption syndrome with steatorrhea and failure to thrive (Anderson et al., 1961).

When the Sar1B gene is mutated, the pre-chylomicron transport vesicle delivered by the ER cannot fuse with the Golgi apparatus, which then induces an accumulation of pre-chylomicron transport vesicles in the cytoplasm of the enterocytes (Siddiqi et al., 2003). To date, 15 mutations in the *Sar1B* gene (including frameshifts, missense, or deletions) have been identified in patients with AD/CMRD. Interestingly, the *Sar1A* gene located on chromosome 10 encodes a second human isoform of Sar1, Sar1A. Sar1A is very similar to Sar1B (90,5 % of sequence identity), but so far no mutation in the *Sar1A* gene has been described in patients with AD/CMRD.

In AD/CMRD, the existence of another Sar1 paralogue- and cargo-specific transport could explain the rather modest and tissue specific manifestations of the disease. If, in enterocytes, the Sar1B paralogue is used specifically in pre-chylomicron transport vesicles (PCTV) for the transport of chylomicrons, and if the Sar1A paralogue is used for the transport of small soluble and membrane bound proteins, then mutations in Sar1B would be expected to affect primarily or only chylomicron transport. Indeed, it has been shown that Sar1B has a weaker affinity compared to Sar1A for Sec13/31A, which could lead to a less constrained structure (Fromme et al.,

2007). This less constrained structure would be permissive for the formation of larger COPII vesicles (which could transport large cargoes such as chylomicrons) as compared to those assembled with Sar1A (Fromme et al., 2008; Fromme et al., 2005).

It has been proposed, in fact, that mutated Sar1B protein leads to an absence of chylomicronemia in AD because the PCTVs that are produced in the absence of Sar1 do not fuse with the Golgi complex and are retained in the cytosol (Siddiqi et al., 2010).

Furthermore, the question arises as to whether AD/CMRD occurs only in tissues in which there is insufficient amounts of the second Sar1 paralogue to compensate for the loss of activity of the first paralogue or whether a specific cargo (chylomicrons) is strictly dependent on a specific paralogue(s) of the secretion machinery.

Both the Sar1A and Sar1B genes are expressed in the intestine (Jones et al., 2003; Su et al., 2004; Gurkan et al., 2005). In one AD patient, an increase in the expression level of Sar1A was detected, but Sar1A failed to rescue the phenotype (Georges et al., 2011). This increased expression of the Sar1A gene and, presumably, of its encoded protein does not appear to be sufficient to compensate the defect in Sar1B (Georges et al., 2011). This is consistent with a Sar1 paralogue-specific and cargo-specific transport of chylomicrons.

1.3.2 Sec23A: Cranio-Lenticulo-Sutural Dysplasia (CLSD)

CLSD is an autosomal recessive syndrome characterized by late-closing fontanels, sutural cataracts, facial dysmorphisms and skeletal defects (Boyadjiev et al., 2003). CLSD was originally described in five males and one female from a large consanguineous Saudi Arabian family of Bedouin descent (Boyadjiev et al., 2003), while the identification of Sec23A as the gene responsible for this syndrome came a few years later (Boyadjiev et al., 2006).

The process of endochondral ossification forms most of the skeletal elements in mammals where mesenchymally derived chondrocytes compose the matrix of future bones. The two exceptions to this rule are the bones of the calvaria and the clavicles, formed by the process of intramembranous ossification in which the mesenchymal cells bypass the intermediate cartilaginous step and differentiate directly into osteoblasts (Karsenty et al., 2002). One major type of calvarial malformation is failure of the fontanels and/or sutures to close, which is the process affected by the loss of Sec23A. A frequent missense substitution was identified in the primary sequence of Sec23A protein: F382L (Fromme et al., 2007). The molecular properties of this Sec23A mutant were analysed and compared to the wild-type Sec23A in several *in vitro* assays. F382L-Sec23A is able to bind to synthetic membranes at a level equivalent to the wild-type and retains intrinsic GAP activity similar to the wild-type protein (Fromme et al., 2007). However, F382L-Sec23A shows reduced recruitment of the Sec13/Sec31 outer coat complex both *in vitro* and *in vivo*.

Fibroblasts isolated from patients affected by CLDS have a dilated ER and a cytoplasmic mislocalization of Sec31, as shown by EM and immunofluorescence (Boyadjiev et al., 2006). Not surprisingly, nonsense mutations in Sec23 were also found to have serious developmental consequences in worms and fish (Lang et al., 2006; Roberts et al., 2003). Recently, mutation in position 702 (M702V) was found to be responsible for the CLSD (Boyadjiev et al., 2011).

Moreover, in zebrafish *crusher* mutants, chondrocytes accumulate proteins in a distended ER, resulting in a severe reduction in the extracellular matrix deposits of cartilage, including type II collagen (Lang et al., 2006).

1.3.3 Sec23B: Congenital dyserythropoietic anemia type II (CDAII)

Mutations occurring in the *SEC23B* gene cause the onset of a rare genetic disorder affecting erythropoiesis, Congenital dyserythropoietic anemia type II (Schwarz et al., 2009). Congenital dyserythropoietic anemias (CDA) were first described in the literature by Heimpel and colleagues in 1968 as a condition characterized by a paradoxical association of anemia and reticulocytopenia with erythroid hyperplasia of the bone marrow (Heimpel et al., 1968). These pathological conditions are phenotypically and genotypically heterogeneous (Heimpel et al., 1968), but the most frequent form of CDAs is the CDA type II (CDAII).

CDAII is an autosomal recessive condition characterised by moderate to severe normocytic or microcytic anemia, by a normal or insufficiently

increased reticulocyte count, chronic or intermittent jaundice and progressive splenomegaly (Iolascon et al., 2000).

In CDAII patients, bi- and multinucleated erythroblasts were found in bone marrow, with nuclei of equal size and DNA content, suggesting a cytokinesis defect (Queisser et al., 1971). Other features of the peripheral red blood cells are protein and lipid dysglycosylation (and additional hypoglycosylation of the band 3) and endoplasmic reticulum double-membrane remnants (Iolascon et al., 1996). By contrast, development of other hematopoietic lineages is normal. Only recently, the gene responsible for the development of CDAII was identified as Sec23B (Schwarz et al., 2009). Again, Sec23B selective impairment leads to a very specific erythropoietic phenotype. This CDAII phenotype might be caused by tissue-specific expression of Sec23B versus Sec23A. The hypothesis arose from the interesting finding that, while in normal dermal cells no gross difference was detectable between mRNA expression of the two genes, Sec23B mRNA expression increased 5–7 fold over Sec23A mRNA expression during *in vitro* erythroid differentiation of CD34+ blood cells (Schwarz et al., 2009). More interestingly, zebrafish Sec23B morphants mimicked the erythroid differentiation problems. In parallel, the Sec23A mutant zebrafish line, *crusher,* showed normal erythrocyte development (Schwarz et al., 2009).

1.4 Rab protein

One of the most important molecular machines operating within the secretory pathway is represented by the small GTPases of the Rab family. Rab (Ras-related proteins in brain) are highly evolutionarily conserved regulators of membrane trafficking. They regulate key steps of the exocytic secretory pathway and endocytosis. Rabs take part in all events of intracellular transport, as they participate in cargo selection, budding of vesicular structures in donor compartments, regulate the transport of these membrane-bound structures along cytoskeletal tracks and also control their docking and fusion to the target membrane. Moreover, they ensure organelle identity, in terms of protein and lipid composition as well as their correct position within the cell (Seabra et al., 2002; Grosshans et al., 2006). In yeast, 11 Rabs have been described, while more than 70 different Rab-like proteins are present in mammals, reflecting the higher complexity of transport events in higher eukaryotes (Pereira-Leal and Seabra, 2001; Gurkan et al., 2005).

Rabs function as small monomeric GTPases that cycle between a GDP-bound inactive state and a GTP-bound active state (Dumas et al., 1999; Pasqualato et al., 2004). The GTP-bound form is the active state that can recruit "effectors", which participate in different steps of membrane transport. The inactive form, the GDP-bound form, can be either cytoplasmic or membrane-associated (Wittman and Rudolph, 2004). Notably, Rabs possess low intrinsic rates of nucleotide exchange and

hydrolysis. For this reason, the activity switch function of Rabs is mediated by GDP-GTP exchange factors, called GEFs, and GTPase activating proteins, the GAPs (Bos et al., 2007). Hydrolysis of GTP leads to inactivation of the Rab and the GDP-bound form can be extracted from the membrane by GDI (GDP dissociation inhibitor, Ullrich et al., 1993). GDI delivers cytosolic Rab to the appropriate organelle (Pfeffer and Aivazian, 2004). When a Rab in its GDP-bound state becomes membrane-associated, a Rab GEF promotes the GDP exchange with GTP, thus converting the Rab to its active form (Bos et al., 2007; **Figure 1.5**).

Each individual GEF has a certain specificity profile for individual members of a G-protein family. The Sec2-, Vps9-, and Mss4-like proteins act as GEFs for members of the Rab family. In particular, Sec2 is a reversibly membrane-associated, multi-domain protein with guanine nucleotide exchange activity towards the yeast Rab-protein Sec4 (Itzen et al., 2007). The GEFs with VPS9 domains, like Rabex-5, activate Rab5, Rab21 and Rab22 in mammals (Delprato and Lambright, 2007).

On the other hand, the Mss4 protein was first identified as a mammalian GEF that interacted with several Rabs belonging to the same family, which included Rab1, Rab3, Rab8 and Rab10, but not Rab2, Rab4, Rab5, Rab6, Rab9 and Rab11 (Burton al., 1994).
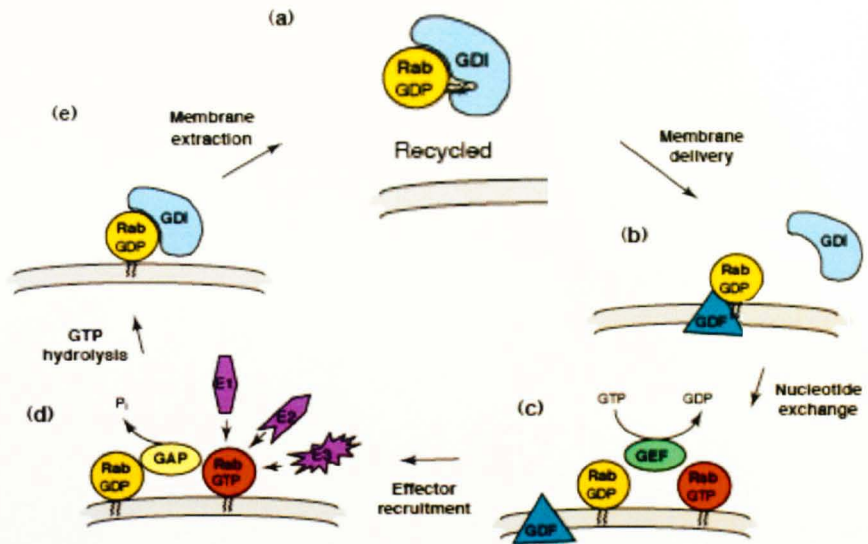
Figure 1.5 Schematic representation of the Rab cycle showing membrane recruitment and activation. (**A**) GDP-bound proteins form a cytosolic complex with Rab-GDI (GDP Dissociation Inhibitor). (**B**) Membrane delivery and Rab-GDI displacement are mediated by a GDF (GDI Displacement Factor), followed by (**C**) Rab activation through GEF-catalyzed nucleotide exchange. (**D**) GTP-bound Rab recruits effector molecules to the membrane. (**E**) GAP-mediated GTP hydrolysis returns the Rab to its inactive state, resulting in re-extraction from the membrane by GDI (modified from Seabra and Wasmeier, 2004).

Few years later, the same protein was shown not to be a GEF that mediated the activation of Rab, but rather a protein that interacts with the transient guanine-nucleotide-free state of the Rabs, acting as a chaperone that assists the Rabs that fail to undergo productive interactions with components of the transport machinery during guanine nucleotide exchange (Nuoffer et al., 1997).

Recently, the multisubunit tethering complex TRAPP has been shown to act as a GEF for the Ypt1p and Ypt31/32 proteins in yeast (Jones et al., 2000; Sacher et al., 2001; Wang and Ferro-Novick, 2002) and to target ER-derived vesicles to the Golgi complex by accelerating the nucleotide exchange on Ypt1p. A similar function has been first postulated and then demonstrated for the mammalian counterpart of the TRAPP complex (Morozova et al., 2006; Yamasaki et al., 2009).

In mammals, two Rabs have been shown so far to be involved in the early secretory pathway between the ER and the Golgi complex: Rab1 and Rab2.

Rab1 exists in two isoforms, Rab1A and Rab1B. Both of these are localized in the ER–Golgi compartments (Tisdale et al. 1992; Saraste et al. 1995) and they also have roles in intra-Golgi transport and in the maintenance of the structure of the Golgi complex (Pind et al., 1994; Wilson et al. 1994; Alvarez et al. 2003).

In particular, Rab1 mutants with a low affinity for both GDP and GTP ("inactive form") result in the disruption of the Golgi complex, with the redistribution of the Golgi enzyme mannosidase II (MannII) and the Golgi

protein Giantin to the ER. Moreover, the transport of the viral protein VSV-G is blocked, being retained in the ER (Tisdale et al., 1992).

In contrast, transient expression of mutants with a low affinity for GTP and a normal affinity for GDP leads to the partial disruption of the Golgi complex and the relocation of MannII and Giantin into perinuclear elements, while their microinjection into cells promotes the disassembly of the Golgi stacks (Wilson et al., 1994). The transport of the VSV-G protein to the plasma membrane is also blocked in cells expressing these mutants (Alvarez et al., 2003; Tisdale et al., 1992). Cells expressing wild-type Rab1 or the mutant "active form" with low GTPase activity have a normal Golgi complex, as visualized by the localization of the two Golgi-resident proteins, MannII and Giantin (Alvarez et al. 2003). Moreover, the transport of VSV-G is normal, as VSV-G is transported to the Golgi complex and to the plasma membrane (Alvarez et al., 2003; Tisdale et al. 1992).

On the other hand, the Rab2 protein (which shares 40% of identity with Rab1) localizes to pre-Golgi intermediates (VTCs; ERGIC) and its mutant form Rab2 Q65L that is predominantly in the GTP-bound-activated form inhibits the ER-to-Golgi transport of VSV-G (Tisdale et al., 1992; Tisdale 1999). However, differently from Rab1 mutants, the block of anterograde transport of VSV-G in this Rab2 mutant is a consequence of VTC fragmentation and a decrease in the membrane association of β-COP (Tisdale, 1999). Indeed, a peptide corresponding to the amino terminus of Rab2 (residues 2-14) causes a dramatic change in the distribution of pre-Golgi intermediates containing β-COP, and causes the persistent recruitment of COPI to the pre-Golgi compartment, which arrests protein transport due

to the inability of the membranes to uncoat (Tisdale and Balch, 1996; Tisdale and Jackson, 1998).

In addition, *in vitro* binding assays have demonstrated that the Rab2 Q65L mutant does not interfere with β-COP binding, but instead stimulates the release of slowly sedimenting vesicles that contain Rab2, β-COP and ERGIC markers and lack anterograde-directed cargo, suggesting their nature as retrograde vesicles (Tisdale, 1999).

Thus, in presence of Rab2 Q65L, the vesicles that bud from VTCs contain the mutant Rab2 protein and increase COPI recruitment. The retrograde carriers are therefore unable to uncoat and retrieve the components of the trafficking machinery, which would explain the ER-staining pattern of VSV-G in the presence of Rab2 Q65L (i.e. a block in retrograde traffic). Indeed, since the initial target for newly budded ER transport carriers is commonly believed to be the VTCs, in their absence or when they fail to reach a critical size, the carriers are stalled in their forward movement (Tisdale, 1999).

The important roles of the Rab proteins in membrane transport are supported by different studies that demonstrate that membrane tethering is a conserved mechanism that depends on the Rab effectors. A clear example comes from studies in yeast. Here the tethering of ER-derived carriers to the Golgi depends on the membrane recruitment of Uso1p (yeast homologue of mammalian p115) by Ypt1p (yeast homologue of mammalian Rab1). Uso1p is a soluble cytoplasmic protein that shows peripheral association with

34

membranes. Uso1p and p115 share homology in their head domains, but the coiled-coil region of Uso1p is at least twice the size of that of p115.

Uso1p was initially identified as yeast ER-to-Golgi transport factor by showing that the temperature-sensitive mutant, *uso1*, blocks the transport of the secretory protein invertase prior to its delivery to the Golgi complex. Moreover, Uso1 defects can be suppressed by over-expressing the ER-to-Golgi SNAREs (see below) Bet1p, Bos1p, Sec22 and Ykt6, and of the GTP-binding Ypt1p, confirming the role of Uso1p in ER-to-Golgi transport. *In vitro* studies have provided direct evidence for a role for Uso1p in tethering COPII vesicles to Golgi membranes. COPII vesicles do not bind to Golgi membranes in the absence of functional Uso1p, and the addition of functional Uso1p to the assays reconstituted COPII binding (Lupashin and Sztul, 2005).

However, no direct interactions between Uso1p and Ypt1p have been shown, while in mammals, p115 has been shown to bind directly to Rab1 (Allan et al., 2000). Moreover, while Rab1 recruits p115 onto COPII coats already at the budding step, in yeast the requirement for Ypt1p appears to be only at the level of the target membrane (Cao and Barlowe, 2000).

The final step in membrane transport is the fusion between the transport intermediate and the acceptor compartment. This process is mediated by the transmembrane SNARE proteins, which interact in specific combinations to bring the membranes of the transport intermediate and acceptor

compartment into close proximity and to drive their fusion. Upon membrane contact, the SNAREs form the trans-SNARE complexes, also known as the "SNAREpins", which catalyzes the apposition and fusion of the two membranes (Hong, 2005; Ungermann and Langosch, 2005).

1.5 SNAREs

In general, the SNAREs consist of a central "SNARE domain" flanked by a variable N-terminal domain and a C-terminal single α-helical transmembrane anchor. These transmembrane anchor domains not only anchor the SNAREs to the membrane, but also participate in SNARE-SNARE interactions. Functionally, SNAREs were initially classified as v-SNAREs, associated with the vesicle/transport intermediate, and t-SNAREs, associated with the target compartment. However, the demonstration that t-SNAREs are also present on vesicles and v-SNAREs are also present on target membranes has led to a new classification of these proteins. Based on the amino acid sequence of their SNARE domains, the SNAREs are divided in the R-SNAREs, with an arginine residue in the centre of their SNARE domain, and the Q-SNAREs, with a glutamine (or aspartate) residue.

In general, most of the previous v-SNAREs are R-SNAREs, while the Q-SNAREs are further classified into three groups: Qa, Qb and Qc (Hong,2005). It is now generally believed that one member of each subfamily contributes to the formation of the SNAREpin, which thus consists of three Q-SNAREs and one R-SNARE, resulting in a Qa:Qb:Qc:R SNARE complex. The formation of this SNARE complex is essential for

fusion between two separate membranes (also known as the trans-SNARE complex).

The functions of the SNAREs are under regulation by various factors. N-ethylmaleimide-sensitive factor (NSF) and soluble NSF-association protein-a (α-SNAP) represent the most essential regulators of the SNAREs (the SNAP receptors), as they promote the disassembly of the SNARE complexes. Thus, it is the concerted action of NSF and α-SNAP that causes the dissociation of the SNARE complexes that are formed after SNARE-mediated fusion, which releases the free SNAREs for repeated use (**Figure 1.6**).

α-SNAP is believed to serve as a folding sensor that binds to the assembled SNARE complex, mediates the recruitment of NSF, and supports the NSF-directed disassembly of the SNARE complex.

Soon after the disassembly, transport-intermediate-associated SNAREs can then be recycled to the donor compartment via retrograde transport, while the target-compartment-associated SNARE subunits can be re-organized into functional SNAREs for the next round of docking and fusion events.
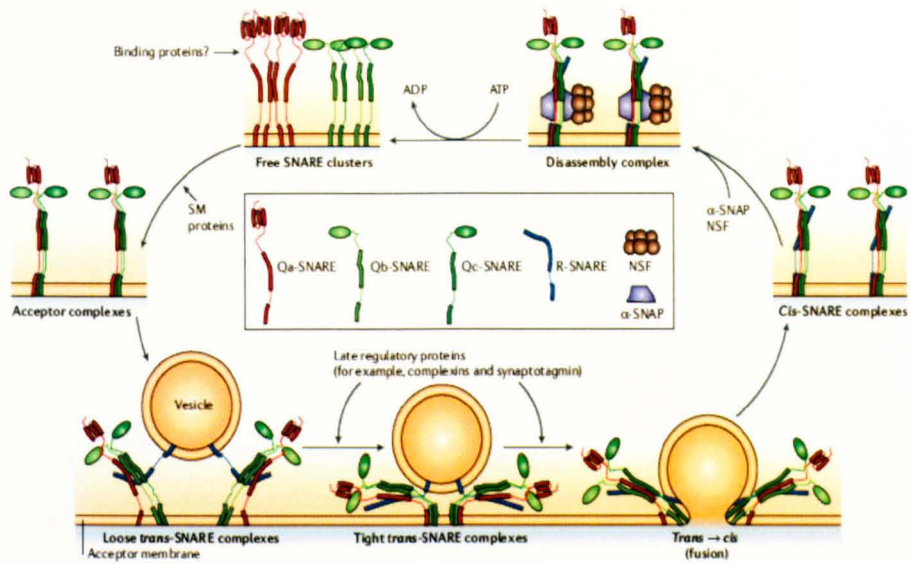
Figure 1.6 The SNARE conformational cycle during vesicle fusion. As an example, three Q-SNAREs are on the acceptor membrane and one R-SNARE is on the vesicle. Q-SNARES that are organized in clusters, assemble into acceptor complexes. Acceptor complexes interact with the vesicular R-SNAREs through the N-terminal end of the SNARE motif to form the four-helical trans SNARE complex. Trans-complexes proceed from a loose state to a tight state, and this is followed by the fusion between two membranes. Modified from Jahan and Scheller, 2006.

1.6 The Golgi complex

The Italian anatomist Camillo Golgi described the "apparato reticulare interno" as an extensive perinuclear network that is present in the cytoplasm of nerve cells more than one hundred years ago (Camillo Golgi, 1898). With the development of EM in the 1950s, the ultrastructure of the Golgi complex was first defined, confirming its unique organisation of stacks of flattened cisternae that are closely apposed to one another (Dalton and Felix, 1954).

Further investigations led to a more detailed description of the Golgi complex that together with the ordered stacks of *cisternae* (from 3 to 11 in mammalian cells) also included membranous vesicular/tubular structures (Farquhar and Palade, 1981; Rambourg and Clermont, 1990).

Progress in the morphological characterisation of the Golgi complex was accompanied by the discovery of its function. The Golgi complex is involved in the intracellular transport and glycosylation of proteins that are destined for secretion or for other intracellular organelles.

Biochemical studies revealed that carbohydrates are progressively added during the passage of proteins from the *cis* to the *trans* face of the Golgi complex. In particular, the enzymes involved in the terminal glycosylation steps, i.e. galactosyltransferases and sialyltransferases, reside in the trans-Golgi elements, confirming the observation that the Golgi subcompartments

(or *cisternae*) can be recognized by the presence of the enzymes involved in the specific steps of glycosylation of proteins and lipids. Indeed, the enzymes that process newly synthesised proteins are arranged through the Golgi stack in such a manner that the early acting enzymes reside on one side of the Golgi stack, while the late-acting enzymes are located at the other site. Together with morphological considerations, these observations have led to the classification of the Golgi complex into *cis-*, *medial* and *trans*-compartments within each single stack (**Figure 1.7**).

The architectural features of the Golgi complex were initially investigated in various animal, plant and yeast cells using EM analysis of ultrathin sections. This has been followed by more sophisticated analyses of EM tilt series combined with computer axial tomography, to study the three-dimensional structure of this organelle (Kepes et al., 2005). All of these studies revealed some common features and some particular differences in the morphology of the Golgi complex among plants, animals and yeast. Here the Golgi morphology and dynamics in yeast and mammals will be described briefly.

In mammalian cells, the Golgi complex localised typically around the centrosomes, where it remains due to a microtubule-dependent mechanism (Lippincott-Schwartz, 1998).

The Golgi complex undergoes fragmentation into hundreds of "islands" (known as mini-stacks) when the microtubules are depolymerised by specific agents (such as nocodazole).
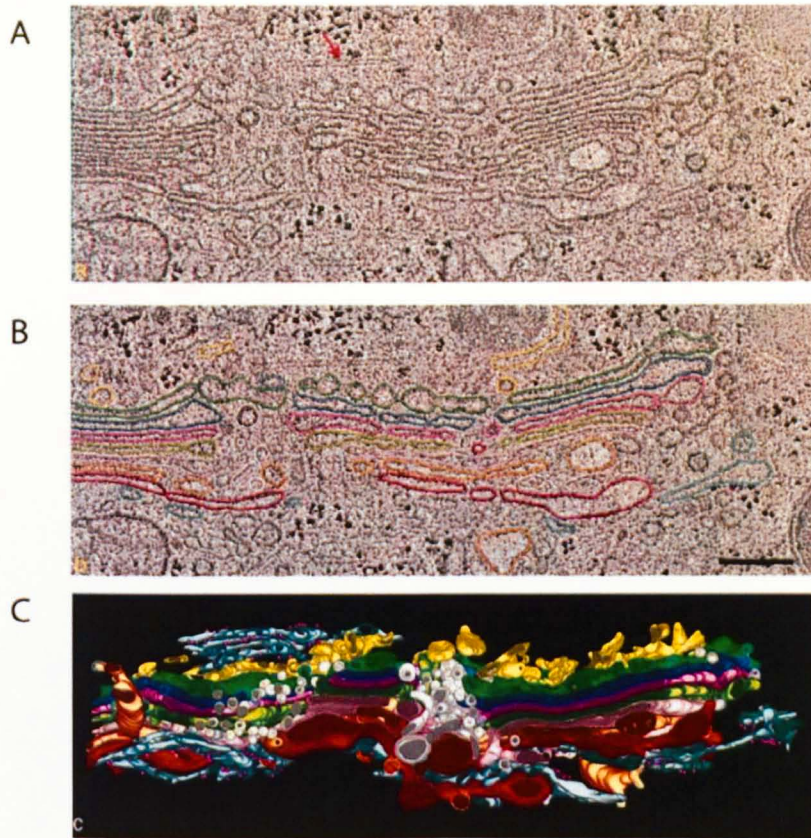
Figure 1.7 The Golgi structure in mammalian cells. Tomographic reconstruction of a portion of the Golgi ribbon from a fast frozen, freeze-substitution fixed NRK cells. Two serial 4-nm slices extracted from the tomogram are shown in (**A**) and (**B**). (**A**) Membranes of individual Golgi cisternae (G) are clearly seen. (**B**) Different cisternae were modelled by placing points along the membranes that delimit them. The model viewed in (**C**) is in the same orientation as the tomographic slices (modified from Ladinsky et al., 1999).

Through conventional or high-voltage EM, the Golgi complex appears as a single ribbon-like structure that is composed of a set of flattened parallel sacculi (*cisternae*) arranged into several stacks that are associated with an array of small vesicles, as well as with tubules emanating from both sides of the stacks (Rambourg and Clermont, 1990). Along its longitudinal axis, the Golgi ribbon has structural heterogeneity when examined at higher magnifications. Some of its regions are composed of closely apposed and poorly fenestrated cisternae; these are described as the "compact" regions (or zones). In contrast, other regions consist of highly fenestrated cisternae and/or membranous tubules that bridge the adjacent compact zones; these are described as the "non-compact" zones (Kepes et al., 2005). The compact region of the Golgi ribbon is usually subdivided into three morphologically distinct compartments: the *cis*, *medial* and *trans* compartments.

The *cis* compartment of the mammalian Golgi complex comprises a tubular network that is known as the cis-Golgi network (CGN). It is composed of branching tubules that are connected with the highly perforated *cis-cisternae*. The CGN receives proteins from the ERGIC, it is involved in the retrieval of a subset of proteins back to the ER, and it has a role in the initial Golgi-specific addition of carbohydrates to proteins that arrive from the ER.

In the *medial* compartment of the mammalian Golgi complex, most of the additions of carbohydrate moieties take place. This compartment comprises a number of closely apposed, more or less flattened *cisternae*, which are

strictly parallel to each other, and which form the "stacks of *cisternae*" that are characteristic of the mammalian Golgi complex. The number of *cisternae* that form the Golgi stacks varies from one cell type to another (three to eight *cisternae*, in the majority of cases), while the lengths of the *cisternae* frequently depend on the axis of the section.

The *trans* compartment and the TGN of the mammalian Golgi complex are involved in the terminal glycosylation events of proteins, as well as in cargo packaging into the membrane carriers destined for the plasma membrane and the endosomal/lysosomal system. The TGN was at first considered to be the trans-most cisternae of the Golgi stack, which is also seen to continue into a large anastomosed tubular network. However, different studies have indicated the TGN as an entirely independent organelle. Indeed, in some cell types, the TGN is positioned at some distance from the trans aspect of the Golgi ribbon (Clermont et al., 1995).

On the other hand, in many cell types, connections between the TGN and the stack of *cisternae* can be easily visualized. Various cargo proteins need to be moved within the TGN to the different exit domains where the transport carriers are formed. Plasma-membrane-directed proteins leave the Golgi complex within Golgi-to-plasma membrane carriers (GPCs), which at the EM level have a complex, tubular-saccular morphology (Ladinsky et al., 1999).

The Golgi complex is the crossroads of many intracellular trafficking pathways that is being constantly traversed by huge amounts of proteins and membranes, each undergoing its correct processing and following its own route, in an amazingly efficient way. In spite of this massive flow of material, the typical architecture of the Golgi complex remains almost unaltered. How this "highly dynamic" stability is accomplished is largely unknown, and thus represents the subject of many studies.

Indeed, there are conditions in which the Golgi complex loses its organisation but not its function. One example is represented by the depolymerisation of microtubules with nocodazole, which results in the ribbon-breakdown of the Golgi complex in mammalian cells. This does not significantly alter Golgi function, since the transport of newly synthesised proteins to the plasma membrane continues unperturbed (Cole et al., 1996).

Microtubules are the major component of the cytoskeleton of mammalian cells and they have a vital role in the control of cell morphology and function. The microtubules delineate the tracks along which membranes are transported during exocytosis and endocytosis, they form the spindle that separates the chromosomes during mitosis, and they provide the physical strength for maintenance of the shape and internal arrangements of cells. Moreover, microtubules have a central role in the perinuclear localization of the Golgi complex: agents that alter the distribution of microtubules have profound effects on the distribution and integrity of the Golgi complex (Thyberg and Moskalewski, 1999).

A dramatic example of this is the reversible scattering of the Golgi complex during nocodazole-induced microtubule depolymerization, due to the binding of nocodazole to the tubulin heterodimers and the successive inhibition of their polymerization (**Figure 1.8**). EM has shown us that these fully scattered Golgi fragments are composed of short, stacked *cisternae* that resemble intact Golgi stacks. Notably, the fragmentation of the interconnected Golgi stacks and the dispersal of these fragments require metabolic energy and continuing membrane trafficking (Turner and Tartakoff, 1989).

As microtubule depolymerisation does not prevent the formation of stacks of *cisternae*, but induces the dispersal of the Golgi complex into "mini-stacks" in the cytoplasm (Cole et al., 1996), it might be concluded that these Golgi mini-stacks are the minimal requirement for the correct processing and transport of cargo proteins.

Interestingly, the transitional ER sites (tER) redistribute rapidly to form clusters next to the Golgi mini-stacks (Hammond and Glick, 2000).

Another useful tool for the study of the Golgi complex dynamics is the use of brefeldin A (BFA). BFA was initially isolated from the fungus *Penicillium brefeldianum* and characterized as an antiviral antibiotic.
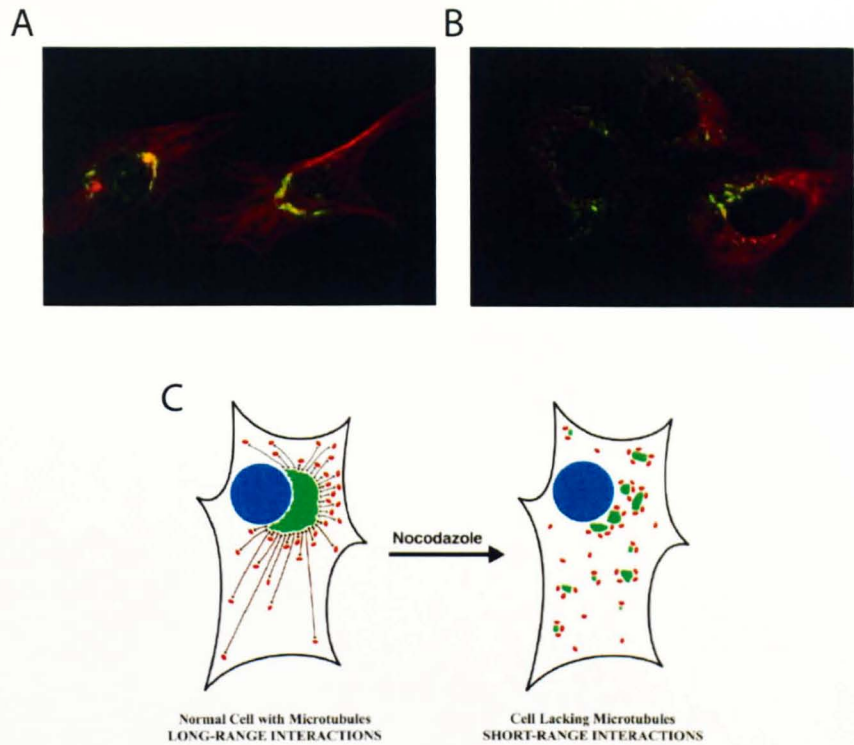
Figure 1.8 Effect of depolymerizing microtubules on the Golgi apparatus. (**A**) In this endothelial cell, the microtubules are labelled in red, and the Golgi apparatus is labelled in green (using an antibody against a Golgi protein). As long as the system of microtubules remains intact, the Golgi is localized near the centrosome, close to the nucleus at the center of the cell. (**B**) After exposure to nocodazole, which causes microtubules to depolymerize the Golgi apparatus fragments and is dispersed throughout the cell cytoplasm (modified from Alberts et al., Molecular Biology of the Cell, fourth edition). (**C**) (Left) In normal cells, tER sites (red) and Golgi structures (green) exchange material by microtubule-directed transport (bidirectional arrows). Retrograde transport events terminate . This recycling of proteins to the ER causes tER sites to proliferate. (Right) When microtubules are disrupted with nocodazole, each Golgi structure receives input only from adjacent tER sites, and the number of these sites determines the size and stability of the Golgi structure. Conversely, membrane recycling from a given Golgi structure induces a localized proliferation of the tER. (adapted from Hammond and Glick, 2000).

BFA gained importance with cell biologists due to the fact that protein secretion was inhibited at a very early step in the secretory pathway in BFA-treated cells. Moreover, the Golgi structure was completely lost by the extensive retrograde transport of the Golgi components to the ER, which was mediated by the growth of Golgi tubules (Klausner et al., 1992).

The mechanism of action of BFA is caused by the inhibition of nucleotide exchange on Arf, which prevents the assembly of cytosolic COPI coat protein on target membranes. The removal of the coatomer from membranes is then followed by the delivery of Golgi enzymes and Golgi proteins to the ER (Scheel et al. 1997; Sciaky et al. 1997).

1.7 The TRAPP complex (Transport Protein Particle)

1.7.1 Yeast TRAPP complex

The TRAPP complex was initially characterized in the yeast _S. cerevisiae_ by Sacher et al. thirteen years ago (Sacher et al., 1998, **Figure 1.9**). Bet3 was the first member of the TRAPP complex to be identified through its genetic interaction with BET1, a gene encoding a SNARE protein that acts in ER-to-Golgi transport (Rossi et al., 1995).
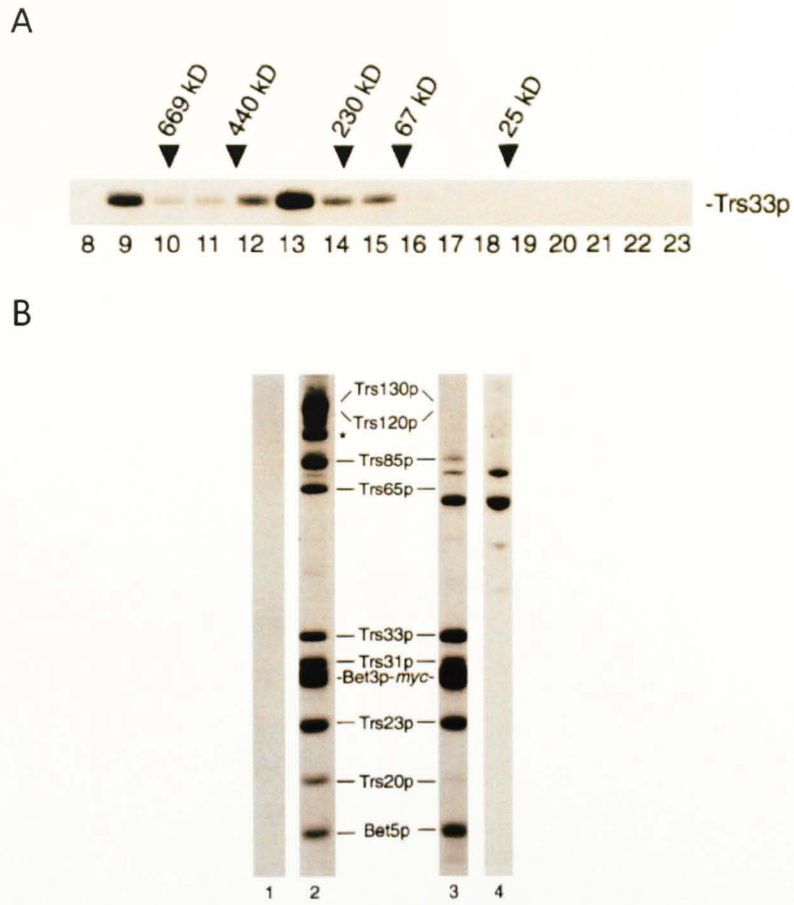
Figure 1.9 Identification of yeast TRAPPI and TRAPPII. (**A**) Gel filtration experiment showed Trs33p in two high-molecular weight fractions, corresponding to the TRAPP complexes (**B**) Trs65p, Trs120p and Trs130p are only found in TRAPP II. Radiolabeled lysates were prepared from an untagged strain (lanes 1 and 4) and a Bet3p-myc tagged strain (lanes 2 and 3), fractionated by gel filtration, and immunoprecipitated using Trs33p. Fractions 9 (lanes 1 and 2) and 13 (lanes 3 and 4) are shown. TRAPP subunits are indicated between lanes 2 and 3 (modified from Sacher et al., 2001).

Studies using a temperature-sensitive mutant of Bet3 (*bet3-1*) revealed an involvement in the regulation of ER-to-Golgi transport of several cargo molecules: invertase, α-factor and carboxypeptidase Y (CPY). These cargoes are all soluble proteins that are modified on their passage through the different compartments of the secretory pathway.

Invertase is initially synthesized as a 62-kDa protein that is transformed into an 80-kDa form in the lumen of the ER by the addition of oligosaccharide units (Moreno et al., 1975). This ER form of invertase accumulates in mutants that block trafficking from the ER to the Golgi complex.

The α-factor is synthesized as a 19-kDa precursor that is subsequently converted into a 26-kDa form in the lumen of the ER. The 26-kDa ER form is the core-glycosylated molecule that is successively modified inside the Golgi complex by the addition of mannose-rich outer chains (Julius et al., 1984; Brigance et al., 2000). Then, a proteolytic process begins in the Golgi complex and is completed within the secretory vesicles, after which the mature form of the α-factor can be secreted (Julius et al., 1984).

Finally, CPY is synthesized and translocated into the lumen of the ER (as its p1 form) before it is transported to and modified in the early (p1' form) and late (p2 form) Golgi compartments (Franzusoff and Schekman, 1989; Banfield et al., 1995). Proteolytic activation in the vacuole yields the mature form (Stevens et al., 1982).

At 37 °C, the *bet3-1* mutant accumulated the ER form of invertase (80 kDa), the 26-kDa ER form together with a partially glycosylated form of α-factor, and finally the p1 form of CPY, suggesting a block in ER-to-Golgi transport

of these soluble cargo proteins (Rossi et al., 1995). However, the block of ER-to-Golgi transport in this mutant was not complete, since small amounts of the p1' CPY form (early Golgi) and small amounts of the Golgi form of invertase accumulated inside the cells (Rossi et al., 1995; Sacher et al., 2001), indicating that these proteins proceeded through an initial block between the ER and the Golgi complex and were then transported to the Golgi. EM analysis of thin sections of the *bet3-1* mutant at 37 °C revealed an accumulation of small and large vesicles and a dilated ER.

After the identification of the Bet3 protein (Rossi et al., 1995), it emerged that it was a member of a large complex (~800) that was named TRAPP (Sacher et al., 1998). Later, gel filtration chromatography revealed the presence of two complexes; these were then isolated and identified as TRAPP I and TRAPP II (Sacher et al., 2001). Today it is well known that TRAPP I is ~300 kDa in size and contains six subunits (Trs33p Trs31p, Trs23p, Bet3, Trs20p, Bet5p), while TRAPP II is ~1,000 kDa and contains all of the TRAPP I subunits plus three additional subunits (Trs65p, Trs120p, Trs130p). Additional factors, such as a homolog of Trs20 called Tca17, may also contribute to the formation and functions of TRAPP (Scrivens et al., 2009; Montpetit et al., 2009).

Moreover, recently a third TRAPP complex was identified, the TRAPP III complex, involved in the regulation of autophagosome formation (Lynch-Day et al., 2010).

Studies on the possible network of interactions between the TRAPP I subunits revealed the presence of two subcomplexes (Kim et al., 2006;

Menon et al., 2006) that according to Kim and co-workers were linked together by the TRAPP subunit Trs23 to form a stable six subunit complex where the Bet3 subunit is present twice (Kim et al., 2006). Moreover, additional studies have shown the importance of the role of the Bet3 subunit in the organization of the TRAPP complex (Kim et al., 2006; Menon et al. 2006).

TRAPP complex localization was determined by analysis of yeast lysate fractions on sucrose density gradients, capable of resolving subcompartments of the Golgi complex. TRAPP I and TRAPP II appeared to co-fractionate to early Golgi compartments of similar size and density (Sacher et al., 2001). Successively, using modified sucrose density gradients to better resolve the different compartments of the Golgi complex, it was clear that the TRAPP II complex co-fractioned with late Golgi/early endosomal markers, indicating the localization of this complex in that specific compartment (Cai et al., 2005).

The first experiments that demonstrated the role of the TRAPP complex in vesicle tethering were performed by the Ferro-Novick group (Sacher et al., 1998; Barrowman et al., 2000) using an *in vitro* transport assay (Ruohola et al., 1988; Groesch et al., 1990) from permeabilized yeast cells (PYCs) and following the glycosylation of α-factor, which in its 26-kDa form marks vesicles that bud from the ER. These vesicles, which are formed and released from PYCs, are incubated with exogenously added Golgi membranes. In the exogenous Golgi, the 26-kDa form of α-factor is

converted to a heterogeneous high molecular weight product. This conversion of the α-factor can be measured with an antibody (anti-outer chain) that specifically recognizes outer chain carbohydrates that are only added to the yeast glycoprotein in the Golgi complex. ATP and exogenously added cytosol are also required for this assay (Groesch et al., 1990). Using this *in vitro* assay, they demonstrated that when Bet3-depleted Golgi membranes were incubated with vesicles in the presence of Bet3-depleted cytosol, the vesicles that formed failed to fuse with the Golgi (Barrowman et al., 2000). Thus, in the absence of Bet3, the budding of the vesicles was not blocked, but their tethering to the acceptor membranes did not occur, causing a block of vesicle fusion.

It is of note that reconstitution of the transport activity was possible by adding cytosol containing Bet3 (Sacher et al., 1998; Barrowman et al., 2000). This means that a certain amount of Bet3 is present also in the cytosol of the cells and this amount is sufficient to have a partial recovery of vesicle docking. In spite of this important finding, today the yeast TRAPP complex is considered to be localized "exclusively" to Golgi membranes (Barrowman et al., 2000).

The concept that the TRAPP complex acted as a tethering factor before membrane fusion and thus before SNARE pairing came from the finding that over-expression of SNAREs such as Bos1p, Sec22 (Rossi et al., 1995) or Sed5 (Sacher et al., 1998), suppresses the *bet3-1* mutant.

Moreover, the SNARE complex containing the SNAREs Sed5 and Bos1 did not form in *bet3-1* mutant cells (Rossi et al., 1995). These data confirmed

that Bet3, and then the TRAPP complex, acts upstream of the SNAREs, i.e. during the tethering of the vesicles to the acceptor membranes. More precisely, Sacher and co-workers (2001) demonstrated that TRAPP I functions in ER-to-Golgi transport, while TRAPP II functions in intra-Golgi trafficking and/or exit from the Golgi (Sacher et al., 2001).

Indeed, TRAPPI binds ER-derived COPII vesicles *in vitro*. As reported by Barlowe and co-workers (Barlowe et al., 1994), when a chemically pure TRAPPI was immobilized on IgG-Sepharose beads and COPII vesicles were formed with purified COPII coat components, COPII vesicles bound to TRAPPI in a concentration-dependent manner (Sacher et al., 2001). The finding that this binding was drastically reduced by the addition of GTPγS, a non-hydrolyzable analogue of GTP that is known to stabilize the COPII coat, led to the suggestion that COPII vesicles must uncoat before TRAPPI can bind (Sacher et al., 2001).

However, the same group showed subsequently that yeast TRAPPI tethers COPII vesicles via an interaction with Sec23, suggesting that vesicle tethering precedes vesicle uncoating (Cai et al., 2007). Indeed, they demonstrated that TRAPPI binds efficiently to vesicles formed in the presence of GTPγS. Furthermore, when they stripped vesicles of their COPII coat by sedimentation through a sorbitol cushion, TRAPPI loses the ability to bind them. Thus, they suggested that ER-derived vesicles recognize and bind to their target membrane before uncoating (Cai et al., 2007).

Recently it has been demonstrated that Bet3 is involved in ensuring the sequential directionality of COPII carriers from the ER to the Golgi complex (Lord et al., 2011). Sec23, a component of the inner layer of the COPII coat, sequentially interacts with three different binding partners, Sar1, TRAPPI and Hrr25, to control the direction of ER–Golgi traffic. These interactions should define the three different stages in vesicle traffic: budding, tethering and a pre-fusion step (Lord et al., 2011).

Studies of the components of the TRAPP II complex have shown that a trs130 temperature-sensitive mutant accumulated aberrant Golgi structures that had been described in other mutants where the products acted at the level of the Golgi complex, like sec-7 and sft1 (Sacher et al., 2001). Moreover, trs130 mutants accumulated Golgi forms of CPY and invertase, confirming the role of TRAPP II in late Golgi/ Golgi exit transport.

Notably, the trs130 mutant showed synthetic interactions with ret2-1 (a mutant with a defect in a COPI subunit), and arf1Δ (a mutant that lacks Arf1p that is required for COPI vesicle formation), but not with mutants defective in COPII subunits, like sec13-1, sec23-1, sec24-1 and sec31-1 (Sacher et al., 2001).

Based on these finding, it was speculated that TRAPP II has a role in the binding of retrograde vesicles to the Golgi complex: these vesicles would arise from a late Golgi compartment and bind to an earlier Golgi compartment (Sacher et al., 2001). Later, mutants in Trs120 were reported to mis-localize COPI subunits and a specific, even if weak, interaction between TRAPP (purified using the Bet3-tagged subunits that are common

to TRAPP I and TRAPP II) and COPI was demonstrated *in vitro* (Cai et al., 2005). However, a mutation in the TRAPP II subunit Trs120 blocked neither invertase secretion nor trafficking of CPY, but showed a defect in the recycling of the R-SNARE Snc1p (which resides on the plasma membrane and moves through the early endosomes before reaching the late Golgi), and of the Chs3 enzyme (which has a recycling pathway similar to Snc1p). Thus, Trs120 appeared to be involved in trafficking from the early endosomes to the late Golgi (Cai et al., 2005). The trafficking of GFP-Snc1p and Chs3-GFP was also defective in trs130 mutants, where, in contrast to trs120 mutants, invertase and CPY transport were also affected.

Therefore, Trs130 may be required at multiple steps on the secretory and endocytic pathways, whereas Trs120 appears to be required only in the endocytic pathway. Given these differences between trs120 and trs130 mutants, one possibility is that Trs120 acts independently of the TRAPP II complex. However, the quantitative depletion of Bet3 from lysates was also shown to result in the complete depletion of Trs120 and Trs130 (Cai et al., 2005), suggesting that Trs120 is a part of the TRAPP II complex.

Trs85 is another TRAPP subunit that appears to act independently of the TRAPP I and TRAPP II complexes. This subunit is a non-essential component of TRAPP, as it is dispensable for yeast growth, and its absence does not block the early secretory pathway. Trs85 appears to be required for the biogenesis of Cvt vesicles (cytoplasm to vacuole targeting; Meiling-Wesse et al., 2005). The Cvt pathway was discovered as a variant of starvation-induced non-selective autophagy, and in contrast to the degradative autophagic pathway, it acts under nutrient-rich conditions as a

biosynthetic route that delivers specific cargo proteins to the vacuole. Δtrs85 cells are defective in the biogenesis of Cvt vesicles and in the recruitment of the GFP-Atg8 protein (that has an essential role during the formation of Cvt vesicles) to the pre-autophagosomal structure (PAS). Moreover, these cells show a defect in the organization of the PAS.

According to the "maturation model" for the formation of the PAS, the components of the PAS travel through the ER and Golgi complex and are segregated in a specific compartment. This compartment matures into the PAS by retrograde transport of specific proteins and lipids back to the donor compartment. A block in a retrograde transport step would then result in the generation of a premature PAS, which would probably not be able to recruit GFP-Atg8 and would thus be unable to fulfil its function (Reggiori et al., 2004). This is exactly what occurs in Δtrs85 cells, suggesting a role for this TRAPP subunit in the retrograde transport step during the generation of the PAS (Meiling-Wesse et al., 2005).

1.7.2 The Guanine exchange activity of the TRAPP complex

The yeast TRAPP complex has been shown to act as a nucleotide exchange factor for the Ypt/Rab family of small GTP-binding proteins that cycle between their GDP-bound and GTP-bound forms through nucleotide exchange and GTP hydrolysis, respectively. It was known previously that Ypt1, which encodes a small GTP-binding protein that regulates ER-to-Golgi membrane trafficking, interacted genetically with the Bet3 and Bet5 genes, and its over-expression suppressed the *bet3-1* mutation (Rossi et al., 1995; Jiang et al., 1998). Further studies have demonstrated that TRAPP can

stimulate guanine nucleotide exchange on Ypt1p (the yeast homologue of mammalian Rab1), suggesting a role for TRAPP as a GEF for Ypt1p (Wang et al., 2000).

Biochemical analysis confirmed that purified TRAPP can bind to the nucleotide-free form of Ypt1p and stimulate GDP release (Wang et al., 2000). After the characterization of the TRAPP I and TRAPP II complexes, it was then shown that both of the TRAPP complexes can stimulate the uptake of GTPγS onto Ypt1p, and thus both can exchange nucleotides on this small GTP-binding protein (Sacher et al., 2001).

The architecture of the TRAPP I complex was solved and the minimal complex core needed for the exchange factor activity was identified (Kim et al., 2006, **Figure 1.10**). This minimal unit consists of Bet5-Trs23-Bet3-Trs31 and is capable of releasing the nucleotide specifically from Ypt1p, suggesting that TRAPP I is a GEF for Ypt1p and not for Ypt31/32 (Kim et al., 2006).
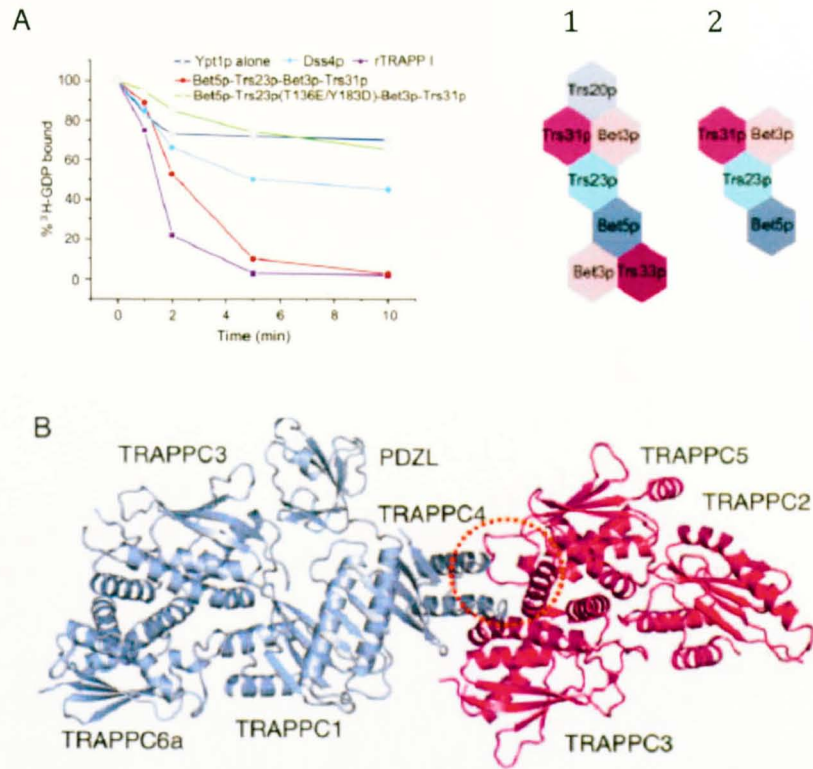
Figure 1.10 TRAPP complex acts as a guanine exchange factor. (**A**) Nucleotide exchange activity was assayed for recombinant TRAPPI (Bet5p-Trs23p-Bet3p-Trs31p-Trs20-Trs33, purple line), Bet5p-Trs23p-Bet3p-Trs31p (red line), Bet5p-Trs23p (double mutant T136E/Y183D)-Bet3p-Trs31p (green line), Dss4p (protein with a broad spectrum of GEF activity; cyan line), or Ypt1p alone (blue line). Beyond the recombinant TRAPPI (1), the minimal unit required for GEF activity is Bet5-Trs23-Bet3-Trs31 (2). Notably, Trs20-sedlin is not required for the minimal GEF activity of the TRAPP complex (modified from Kim et al., 2006). (**B**) Crystal structure of the mammalian TRAPP complex (modified from Cai et al., 2008).

On the other hand, the TRAPP complex was also identified to act as a nucleotide exchanger not only for Ypt1p but also for Ypt31/32, a functional pair of GTPases that are essential for exit from the trans-Golgi (Jones et al., 2000). Indeed, TRAPP stimulated both GDP release and GTP uptake by Ypt32p, and to a lesser extent, by Ypt31. The ability of the TRAPP complex to act as a GEF for Ypt31/32 was previously excluded by Wang and co-workers (Wang et al., 2000), who successively confirmed that chemically pure TRAPP stimulated guanine nucleotide exchange selectively on Ypt1p but not on Ypt32p (Wang and Ferro-Novick, 2002). The different results obtained by these two groups could be due to their different methods of TRAPP purification. This issue is still hotly debated.

Intriguingly, TRAPP III complex has been shown also to act as an exchange factor for Ypt1 during autophagy processes (Lynch-Day et al., 2010). The Trs85 subunit of the TRAPPIII complex directs this Ypt1 GEF to the phagophore assembly site (PAS) that is involved in autophagosome formation. Consistent with the observation that a Ypt1 GEF is directed to the PAS, Ypt1 was found to be essential for autophagy. This finding represents the first example of a Rab GEF that is specifically required for canonical autophagosome formation (Lynch-Day et al., 2010).

1.7.3 The mammalian TRAPP complex

The TRAPP complex in mammalian cells was first isolated in HeLa cells by gel filtration analysis as a 670 kDa complex (Sacher et al., 2001).

As mentioned above, *S. cerevisiae* TRAPP I consists of Bet5p, Trs20p, Bet3p, Trs23p, Trs31p, and Trs33p (Sacher et al., 1998; Sacher et al., 2000; Sacher et al., 2001), with the mammalian orthologues named TRAPPC1, TRAPPC2 (sedlin), TRAPPC3 (Bet3), TRAPPC4 (synbindin), TRAPPC5, and TRAPPC6a/b, respectively (Sacher et al., 2008).

Together with the so-called "human Bet3 complex", i.e. the human TRAPP complex, gel filtration revealed an additional peak with Bet3 and sedlin suggesting the presence of a free pool of TRAPP subunits, since the peak-size was coherent with the monomeric size of Bet3 and sedlin (Sacher et al., 2000). This finding was in apparent contrast to what was observed in yeast, where no free pool of any of the subunits was detected. One possibility is that in higher eukaryotes, TRAPP subunits exert several functions independently of the complex.

However, as in yeast, the mammalian TRAPP complex was resistant to extraction by Triton X-100, suggesting that it is anchored to a Triton X-100-resistant matrix in the cell (Sacher et al., 2000). Adopting the TAP methodology, the other TRAPP subunits were identified (Gavin et al., 2002).

All TRAPP subunits except Trs65 are conserved from yeast to mammals (Sacher et al., 2008).

The primary and secondary structures of the two essential TRAPP II subunits Trs120 and Trs130 are conserved from yeast to man (Cox et al. 2007), whereas the non-essential Trs65 is conserved only among some unicellular eukaryotes. Indeed, it has been suggested that TRAPP II, like

TRAPP I, is a conserved complex, and that the function of both of their TRAPP complexes in their regulation of trafficking through the Golgi complex is also conserved (Cox et al., 2007). The mammalian homologue of Trs120 has been identified as the NIBP/TRAPPC9 protein, which is a protein that when mutated cause postnatal mental retardation with microcephaly (Philippe et al., 2009; Mochida et al., 2009), while TMEM1/EHOC1 (TRAPPC10) has been identified as the Trs130 orthologue. This protein was previously identified by TAP methodology (Gavin et al., 2002), and it is a candidate for several human disorders, including certain types of epilepsy (Cox et al., 2007).

Recently, a distantly related human sequence C5orf44 (FLJ13611) was identified as the human orthologue of Trs65. This sequence was shown to interact with a number of known mammalian TRAPP subunits (Choi et al., 2011).

Moreover, two novel TRAPP proteins, C4orf41/Gryzun (now designated TRAPPC11) and TTC-15 (now designated TRAPPC12) were identified throughout eukarya including diverse fungi, but they are absent in *S. cerevisiae* (Scrivens et al., 2011).

However, since the conclusions of Cox and co-workers (2007) were based on sequence and predicted secondary structure analyses and are not supported by any *in vivo* evidence, the existence of a mammalian TRAPP II remains still remains to be proved.

Instead, mammalian TRAPP proteins elute as a single high-molecular-weight complex, suggesting the absence of a small complex equivalent to TRAPP I (Loh et al., 2005; Scrivens et al., 2008; Yamasaki et al., 2009).

Among the human TRAPP subunits, some have been previously identified in other contexts, such as sedlin (human homologue of Trs20) and synbindin (human homologue of Trs23).

Sedlin was previously known as the protein associated with the pathogenesis of Spondyloepiphyseal Dysplasia Tarda (or late; SEDT), (see below). Synbindin was identified as a protein that is expressed in neuronal cells and that co-localizes with the cell-surface heparan sulfate proteoglycan Syndecan-2 in the spines of cultured hippocampal neurons (Ethell and Yamaguchi, 1999; Ethell et al., 2000). Its homology with the TRAPP subunit Trs23 suggested a role in membrane trafficking for synbindin.

The most conserved of the TRAPP subunits is Bet3, and its crystal structure and possible role in mammalian membrane trafficking have been determined. Moreover, the finding that this subunit, and probably the entire mammalian TRAPP complex, is mostly localized in the cytosol of mammalian cells (Loh et al., 2005), suggests that there are some differences in the roles and functions of the mammalian TRAPP complex as compared with the yeast TRAPP complex.

Although the understanding of mammalian TRAPP (mTRAPP) lags behind that of yeast TRAPP (yTRAPP), yTRAPP and mTRAPP have both common and distinctive features. Both yTRAPP and mTRAPP are required to maintain the organization of the Golgi complex (Barrowman et al., 2000; Yu et al., 2006) and possess guanine nucleotide-exchange (GEF) activity for the small GTPases Ypt1 and Rab1, respectively (Wang et al., 2000; Yamasaki et al., 2009). In contrast, mTRAPP is implicated in the homotypic tethering of ER-derived vesicles (Yu et al., 2006), while yTRAPPI is required for the heterotypic tethering of the ER-derived COPII vesicles to Golgi membranes (Sacher et al., 2001, **Figure 1.11**).

Despite these attempts to describe a possible function of the mammalian TRAPP complex, very little data are available to date. Mammalian TRAPP is involved in homotypic fusion of COPII carriers (Yu et al., 2006; Cai et al., 2007; Lord et al., 2011), mediates the guanine exchange factor for Rab1 (Yamaski et al., 2009) and recently TRAPP has been implicated in ciliogenesis (Westlake et al., 2010).

Indeed, most of the available information regards the mBet3 subunit, the most conserved subunit of the TRAPP complex (Loh et al., 2005), while little is known about the other mammalian TRAPP subunits.
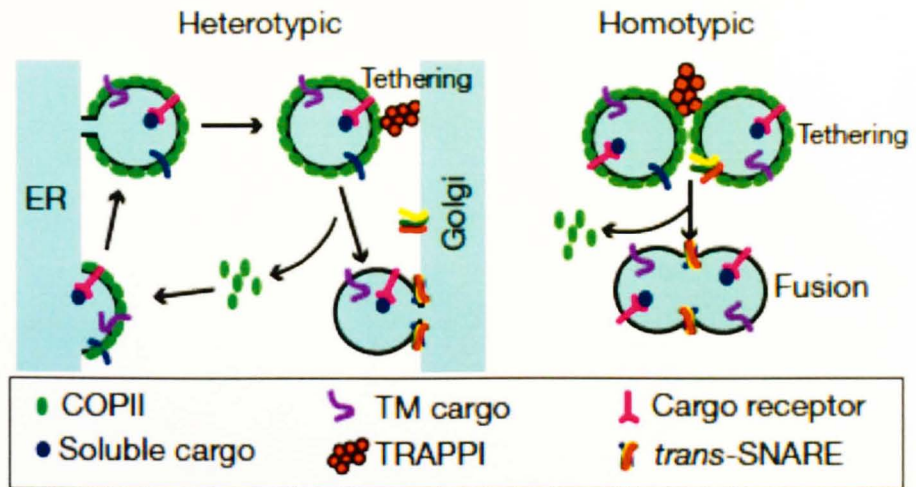
Figure1.11 A model for heterotypic and homotypic COPII vesicle .(Left) In heterotypic tethering, yeast TRAPPI acts as a tethering factor on ER-derived vesicles, allowing their fusion to the Golgi through *via* a direct interaction with Sec23p. Coat complexes dissociate from vesicles, followed by the formation of trans-SNARE pairs and membrane fusion. (Right) In homotypic vesicle tethering, TRAPPI links two COPII-coated vesicles via an interaction between mBet3 and mSec23 (modified from Cai et al., 2007).

1.7.4 Sedlin and Spondyloepiphyseal Dysplasia Tarda (SEDT)

The mammalian TRAPP complex subunit sedlin (TRAPPC2, human homologue of yeast Trs20) was first identified as the protein coded by the gene SEDL. This gene appeared to be truncated/mutated in males affected by Spondyloepiphyseal Dysplasia Tarda (SEDT) or late (Gedeon et al., 1999).

The term spondyloepiphyseal dysplasia (SED) defines a heterogeneous group of disorders, which share typical radiographic defects of the vertebral bodies and epiphyseal regions. Frequent additional features are short stature and early development of degenerative joint disease. SED has been divided into a severe *congenita* and a more benign *tarda* form reflecting the broad range of clinical severity. The genetic background responsible for its onset is variable and it is associated with autosomal dominant, autosomal recessive, or X-linked recessive modes of inheritance. Several genes have been found to be mutated in patients affected by spondyloepiphyseal dysplasia. Collagen type II, the most abundant collagen of cartilage, is mutated in autosomal dominant forms of SED (Spranger et al., 1994) or spondylo-epimetaphyseal dysplasia (SEMD) Strudwick type (Tiller et al., 1995). Since collagen type II is also a component of the vitreous humor, these patients may have additional ophthalmological problems, like severe myopia and/or retinal detachment. A rare autosomal recessive form of SED associated with insulin-dependent diabetes mellitus (Wolcott-Rallison syndrome) has been attributed to mutations in the translation factor EIF2AK3 (Delepine et al., 2000). In another autosomal recessive form of SEMD, mutations have been described in the ATPSK2 gene that is involved

in sulfate activation (Faiyaz ul Haque et al., 1998). X-linked spondyloepiphyseal dysplasia tarda (SEDT) is a mild variant with moderately short stature, barrel chest deformity and minor epiphyseal alterations, but characteristic, vertebral body dysplasia comprising platyspondyly and a central hump (Iceton and Horne, 1986; Whyte et al., 1999). Degenerative joint disease is common in male patients and often makes hip replacement necessary in the fourth or fifth decade. Mutations in WISP3 cause progressive pseudorheumatoid dysplasia (PPD; Ehl et al., 2004, Hurvitz et al., 1999), an autosomal recessive form of a spondyloepiphyseal dysplasia tarda. Individuals with PPD appear normal at birth, have subtle clinical symptoms by 3 years of age, manifest radiologic changes of the axial and appendicular skeleton by 5 years of age, and develop severe degenerative joint disease necessitating joint replacement surgery by their second decade of life.

Spondyloepiphyseal dysplasia tarda (SEDT, MIM 313400) is a rare recessive X-linked osteochondrodysplasia that results in short stature, flattening of the vertebrae and premature osteoarthritis, with the absence of systemic complications (Gedeon et al., 1999).

As outlined by the name, SEDT is a late onset skeletal disorder, which manifests in childhood, with the usual age of presentation being after the first decade of life. It is caused by mutations in the Sedlin gene (SEDL) located on Xp22.12-p22.31 (Gedeon et al., 1999). Carrier females appear to be asymptomatic, while the development of SEDT in affected males appears normal until just before puberty, when longitudinal growth slows, with the appearance of a "barrel chest" deformity. Following malformation of the

growing vertebrae, intervertebral disks deteriorate and may appear absent later in life. Patients develop joint pain and limited mobility.

Most of the disease-associated mutations that have been identified throughout the SEDL gene are splice alterations, insertions and deletions that can lead to premature termination signals and truncated proteins (Gedeon et al., 2001), while only four missense mutations have been described (**Figure 1.12**). No apparent correlation between genotype and phenotype was detected.

Five Y-chromosome-linked and another two pseudogenes of SEDL have been reported (Gecz et al., 2000). One of these pseudogenes is SEDLP1, located on chromosome 19, which has been described as a transcribed pseudogene. More precisely, two different transcripts were identified by Northern-blot hybridization (Gedeon et al., 1999): one at approximately 2.8 kb, encoding the X-linked SEDL, and the other at approximately 0.75 kb, encoding the truncated transcript of the chromosome 19 pseudogene (SEDLP1). The two sequences have only six nucleotide differences in the ORF, none of which alter the amino-acid sequence.

SEDL and SEDLP1 are expressed in a wide range of tissue/cell types, showing their highest expression levels in kidney, heart, skeletal muscle, liver and placenta (Mumm et al., 2001; **Figure 1.13**). The most striking difference between SEDL and SEDLP1 is the absence of SEDLP1 expression in skeletal muscle (Ghosh et al., 2003).
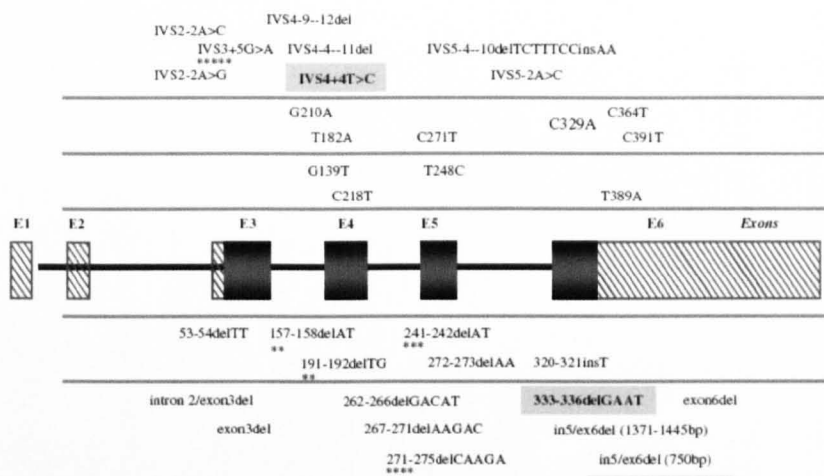
Figure 1.12 Sedlin mutations responsible for the onset of SEDT disease. Schematic representation of the sedlin gene (6 exons) and of the SEDT isolated mutations into the sedlin gene. Mutations are spread all over the sedl gene: there is no evident correlation between phenotype and genotype (adapted from Shaw et al., 2003).

Despite the ubiquitous expression of these two genes, the SEDT phenotypes are very specific. However, since SEDL and SEDLP1 are under the control of different promoters, the lack of phenotypic effects in different tissues could be due to a function attributable to SEDLP1.

SEDLP1 was also isolated via a yeast two-hybrid analysis as a cDNA where the protein product was seen to interact with the *c-myc promoter-binding protein 1* (MBP-1), and to relieve the activity of MBP-1 as a transcriptional repressor (Ghosh et al., 2001). This protein was thus defined as MIP-2A, standing for "MBP-1 interacting protein-2A". MBP-1 negatively regulates both human and mouse c-myc promoter activity and its ectopic expression induces cell death, reduction of c-myc expression and regression of tumour growth.

MIP-2A was identified also as a transcriptional repressor of MBP-1 that antagonized MBP-1-mediated cell death, suggesting a functional interaction between MIP-2A and MBP-1 in cell growth regulation.

This interaction of sedlin with the transcriptional repressor MBP-1 is interesting in light of the finding suggesting that truncated sedlin accumulates in or around the nucleus (Gecz et al., 2000). This could suggest that full-length sedlin may cycle in and out of the nucleus during its itinerary which would make interaction with nuclear proteins a likely possibility (Sacher, 2003). Thus, the interaction with MBP-1 raises the intriguing possibility of a dual function for sedlin, both in membrane trafficking and in the regulation of gene expression.

Indeed, it has been reported that MIP-2A acts as a transcription factor by inhibiting the transactivation of the luteinizing hormone-β (LHb) promoter that is mediated by the SF-1 nuclear receptor and by the pituitary homebox 1 (Ptx1) protein (Ghosh et al., 2003). In addition, sedlin mutations disrupt the interactions with Ptx1 and SF1 suggesting a potential cause of delayed puberty in boys with SEDT (Jeyabalan et al., 2007). Thus, a role for sedlin/MIP-2A in the regulation of gene expression appears plausible. It would be of interest to determine whether sedlin interacts with chondrocyte-specific factors involved in transcription.

Another sedlin interactor has been identified by yeast two-hybrid screening. This screening reported an interaction between sedlin and a chloride intracellular channel proteins-1 (CLIC1; Fan et al., 2003). The CLICs have been reported to be present in membranes of the ER, mitochondria and nucleus. They are involved in the homeostasis of cell membrane potential, substance transfer, and maintenance of intracellular pH and cell volume. Considering their extensive homologies but distinct localizations, different CLICs may function similarly at distinct locations.

CLIC1 is a transmembrane protein that is sufficient to form a functional ion channel as a tetrameric assembly of subunits. Fan and co-workers (2003) demonstrated that GFP-CLIC1 co-immunoprecipitated with FLAG-sedlin. Moreover, both proteins co-localized extensively in cytoplasmic vesicular/ reticular structures in COS-7 cells, suggesting their interaction at intracellular membranous organelles (Fan et al., 2003). According to this study, since both sedlin and CLIC are membrane-associated proteins, their interactions might be important either for functions of the TRAPP complex

or for the proper targeting and functions of the intracellular chloride channels. However, the implications of this interaction in the development in the SEDT remain to be established.

Very recently, a new sedlin interactor was identified, SPATA4, a spermatocyte-specific protein of unknown function (Duarte et al., 2011). The implications of this novel interactor with sedlin functioning and the onset of the disease have still to be elucidated.

From the few studies that have appeared to date, the specific role of sedlin is still unknown. The link to collagen transport has also been proposed as sedlin is part of the TRAPP complex that is involved in secretory trafficking.

Indeed, Sedlin has 34% identity with the yeast TRAPP subunit Trs20. Moreover, the human Sedlin gene can complement the lethality caused by deletion of the Trs20 gene, illustrating conservation of function (Gecz et al., 2003). Interestingly, although the different SEDL mutations display the same clinical phenotype, expression of three of the four missense mutations that are associated with the development of SEDT have shown that one of the mutations could not complement the yeast deletion, while the other two led to very subtle effects on yeast growth (Gecz et al., 2003).

The involvement of sedlin in membrane trafficking is also confirmed by the finding that its structure suggests a role in regulatory or adaptor functions via multiple protein-protein interactions (Jang et al., 2002). Indeed, despite having no sequence homology, the crystal structure of sedlin reveals a

similarity to the structures of the N-terminal regulatory domain of two SNAREs, Ykt6 and Sec22, suggesting a possible interaction between sedlin and SNAREs (Jang et al., 2002; **Figure 1.13**).

Recently, the relative position of sedlin inside the TRAPP I complex has been described: sedlin occupies a peripheral position in the complex and its yeast homologue Trs20 is not required for the GEF activity of the TRAPP complex (Kim et al., 2006). However, despite these structural insights into the sedlin protein, its function remains completely unknown. In particular, the role of sedlin and how it operates in membrane trafficking, whether it has other functions, and how these result in the development of SEDT remain open questions.
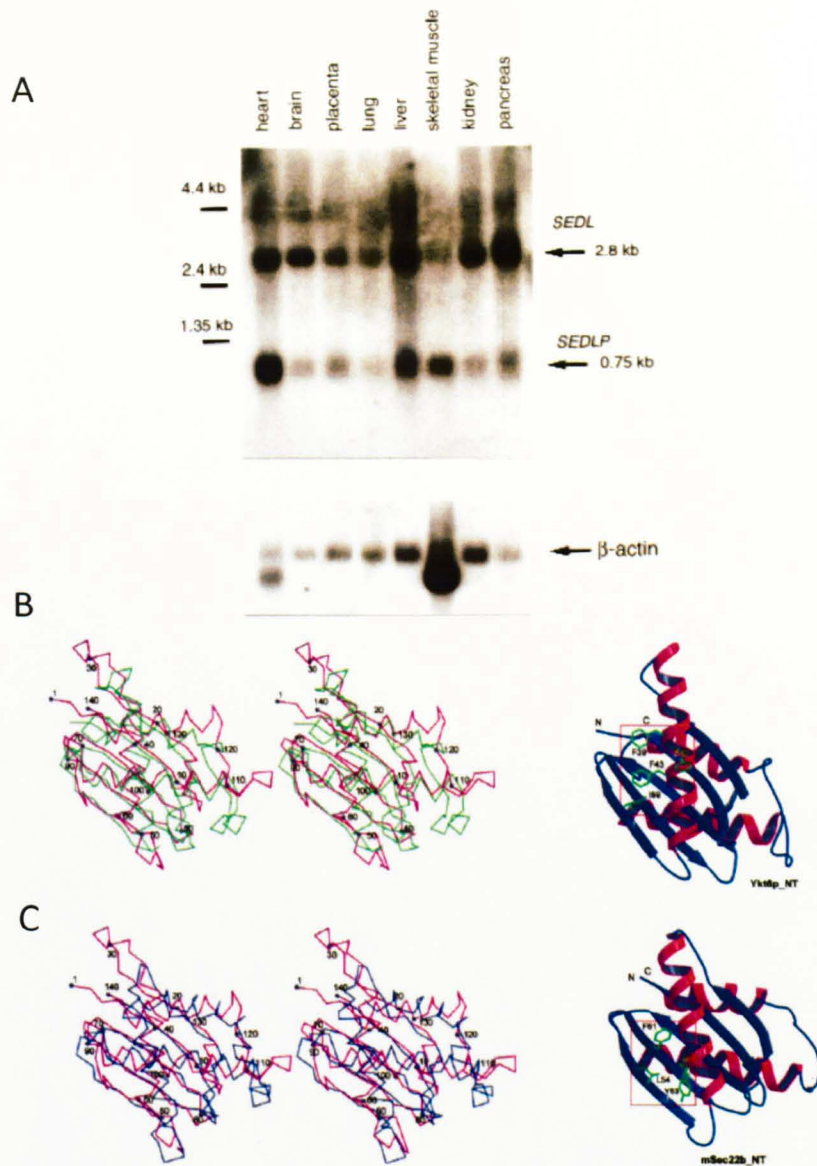
Figure 1.13 Sedlin: gene expression and protein structure. (**A**) Pattern of mRNA expression from several tissues. Sedlin is ubiquitously expressed, as its pseudogene located on chromosome 19 (modified from Gecz et al., 2003). (**B**) Superimposition of the sedlin structure and Ykt6p-NT (140 residues). (**C**) Superimposition of the sedlin and mSec22b-NT (127 residues, modified from Jang et al., 2002).

Chapter 2

Materials and Methods

2.1 Cell culture

2.1.1 Materials

Hepatocellular carcinoma (HepG2), NRK fibroblasts (NRK49F) and HeLa cells were bought from American tissue type collection (ATTC, number HB-8065, CRL-1570 and CCL-2, respectively).

Human fibroblasts (HFs) were kindly provided by Dr. M. De Luca, Istituto Dermatologico dell' Immacolata, Rome, Italy.

Rat chondrosarcoma chondrocytes (Rx chondrocytes) were provided by J. Kimura and B. Vertel .

Primary fibrobalsts isolated from SEDT patient were provided by the Genetics Unit, IRCCS Casa Sollievo della Sofferenza, San Giovanni Rotondo, Foggia, Italy.

Dulbecco's Modified Eagles Medium (DMEM), Minimum Essential Medium (MEM), RPMI-1640 Medium, Foetal Calf Serum (FCS) and Calf

Serum (CS), penicillin, streptomycin, trypsin-EDTA, non-essential amino acids (NEAA) and L-glutamine were from GIBCO™ (Invitrogen, USA). All these reagents were 10 x stock solutions. All the plastic materials were from Corning (USA). Filters (0.45 and 0.2 μm) were from Amicon (USA).

2.1.2 Propagation of cell lines

2.1.2.1 Growth media

Rx chondrocytes and HeLa cells were grown in DMEM supplemented with 4.5 g/l glucose, 2 mM L-glutamine, 1 U/ml penicillin and streptomycin, and 10% FCS. HepG2 cells were grown using MEM supplemented with non-essential amino acids (NEAA) and 4.5 g/l glucose, 2 mM glutamine, 1 U/ml penicillin and streptomycin, and 10 % FCS. HFs were grown in DMEM supplemented with 4.5 g/l glucose, 2 mM L-glutamine, 1 U/ml penicillin and streptomycin, and 10% CS. Primary fibroblasts (control and SEDT isolated cell lines) were grown in RPMI-1640 supplemented with 4.5 g/l glucose, 2 mM L-glutamine, 1 U/ml penicillin and streptomycin, and 10% FCS.

2.1.2.2 Growth conditions

All cell lines were grown in a controlled atmosphere in the presence of 5% CO_2 at 37°C. Cells were grown in a flask to 80-90% confluence. The medium was removed and trypsin-EDTA solution (0.05% trypsin, 0.02% EDTA) was added for 3-5 min at 37°C. The medium was added back to block the protease action, cells were collected into a plastic tube and

75

centrifuged for 5 min at 2000 x g. The pellet was resuspended in fresh medium and placed in a new plastic flask.

2.1.2.3 Establishment of primary fibroblast cultures from a SEDT patient

This procedure was carried out by Dr. Zelante (IRCCS Casa Sollievo della Sofferenza, San Giovanni Rotondo, Italy).

Briefly, cutaneous specimens were placed in RPMI 1640 medium without serum immediately after biopsy removal, repeatedly washed with PBS and placed in a 30 mm Petri dish. The specimens were then fragmented in 1-2 mm pieces and transferred to flasks containing D-MEM (Invitrogen) supplemented with 10% Foetal Bovine Serum (FBS, Invitrogen), 100 units/ml penicillin and 100 µg/ml streptomycin. Primary cultures were incubated at 37°C in 5% CO_2 humidified atmosphere, and 5 ml of complete medium were added 24 hours later. After one week primary cultures were washed with PBS to remove non-adherent fragments and fresh medium prewarmed at 37°C was added. These procedures were repeated every 3 days until primary cultures reached local confluence. The mutational analysis of the sedlin gene was carried out as follows by Dr. Zelante. Coding exons 3-6 (including exon/intron boundaries) of the SEDL gene were amplified by PCR under standard conditions using the primers for genomic PCR amplification and sequencing described in Gedeon et al. (1999). PCR products were purified using an ExoSAP IT Kit (USB Corporation, GE Healthcare) and sequenced using a Big Dye Terminator ready reaction Kit (PE Applied Biosystems, CA, USA) according to the

manufacturer's specifications, on an ABI PRISM 3100 Genetic Analyzer (Applied Biosystems).

2.2 Preparation of recombinant proteins and affinity-purified polyclonal antibodies

The following procedures were carried out in collaboration with G. Di Tullio and M. Santoro (Consorzio Mario Negri Sud, Italy and TIGEM, Italy).

2.2.1 Materials

Restriction endonucleases were purchased from Amersham Pharmacia Bio-Tec (UK). The pEGFP-N, pEGFP-C vectors were purchased from Clontech (USA).

Gluthathione, lysozyme, IPTG, sodium azide, Triton X-100, Freund's adjuvant, potassium acetate, RbCl, $CaCl_2$, $MnCl_2$ were from Sigma Chemical Co. (MO, USA). The gluthathione sepharose resin and the pGEX-4T vectors were from Pharmacia Bio-Tec, UK. Leupeptine, benzamidine, and PMSF (Protease Inhibitors Cocktail, PIC) were from Sigma Chemical Co. (MO, USA).

The human Bet3 cDNA was purchased from the I.M.A.G.E Consortium (I.M.A.G.E clone 3051295).

pGEX-4T-Synbindin was kindly provided by Dr. Yu Yamaguchi (The Burnham Institute, La Jolla, California; Ethell et al., 2000).

GFP-Sedlin, with the GFP at the amino-terminus of the protein, was kindly provided by J.Gecz (Centre for Medical Genetics, Department of Cytogenetics and Molecular Genetics, Women's and Children's Hospital, Australia, (Gecz et al., 2000).

The DNA-oligonucleotides were purchased from SIGMA-Genosys Ltd.

Tris (hydroxymethyl) aminomethane (TRIS), lysozyme, RbCl, $MgCl_2$, $MnCl_2$, 4-morpholinepropanesulfonic acid (MOPS), agarose, kanamycin, chloramphenicol and the SIGMA GenElute plasmid miniprep kit for mini-scale plasmid DNA preparation were purchased from SIGMA (USA). The Qiagen plasmid kit for large-scale plasmid DNA preparation and the QIAEX® II kit were purchased from Qiagen (USA). BL21 DE3 E.coli bacteria were purchased from Novagen (Merck, Germany). XL1-blue E.coli bacteria were purchased from Stratagene (USA), T4 DNA ligase from Promega (USA), agar from GIBCO™ (Invitrogen, USA), ampicillin and kanamycin from Fluka (SIGMA, USA), glycerol from Merck (Germany), and isopropyl-β-D-thiogalactopyranoside (IPTG) from Calbiochem (Merck, Germany). Yeast extract and tryptone peptone were purchased from DIFCO (USA), DNase from Boeringher Mannheim (USA) and the Bio-Rad Protein Assay Kit from Bio-Rad (USA).

2.2.2 Sub-cloning

The PstI/BamHI restriction sites were inserted in the Bet3 I.M.A.G.E clone by PCR reaction using the primers GCGCTGCAGATGTCGAGGCAGGCGAACCGT (PstI forward primer) and GCGGGATCCTTATTCCTCTCCAGCTGG (BamHI reverse primer).

After its purification with the JET-QUICK® PCR Purification Spin Kit (GENOMED,USA) the product of PCR-reaction was ligated in frame with the pGEX vector, previously digested with the same restriction enzymes, by using the T4 DNA ligase (30 fmol of the product of PCR-reaction were ligated with 10 fmol of the purified PstI/BamHI pre-digested vector).

The pGEX4T2-Sedlin was obtained by excision of Sedlin-insert from the pEGFP-C1-Sedlin vector digested with BglII and SalI restriction enzymes, and the insert was subsequently ligated in frame with the pGEX4T2 vector previously digested with the BamHI and SalI restriction enzymes.

The products of ligation were used to transform competent bacteria. On the following day, some isolated bacterial colonies for each construct were picked up and used to inoculate 2 ml of LB-broth containing 50μg/ml of the appropriated antibiotic. The culture was incubated at 37 °C overnight. Seven hundred and fifty μl of sterile glycerol were added to 750 μl of bacterial culture and stored at -80 °C. Bacteria cultures were used to prepare cDNAs (section 2.7.1) and these were digested for 3 h at 37 °C with the respective restriction enzymes in order to verify the presence of the inserts. Moreover, the obtained plasmids were sent to be sequenced by MWG Biotech (Italy).

The full-length Sec23 coding sequence was inserted into the BglII/XhoI sites of the vector pEGFP-C2 (Clontech Laboratories). TRS31 was purchased from imaGenes GmbH (IMAGE number 4869377). The CD8 cDNA was kindly provided by Professor Stefano Bonatti. Rab1b-GFP was a kind gift of the Alvarez lab.

2.2.3 Preparation of competent cells

Competent bacterial cells were prepared with the help of G. di Tullio (Consorzio Mario Negri Sud, Santa Maria Imbaro, Italy).

A single colony of XL-1 Blue *E. coli* bacteria was picked from a LB-agar plate (10 g/l NaCl, 5 g/l yeast extract, 10 g/l tryptone peptone and 15 g/l agar) and used to inoculate 10 ml of LB-broth (10 g/l NaCl, 5 g/l yeast extract and 10 g/l tryptone peptone). Bacteria were grown overnight, then diluted in 190 ml of fresh LB broth and incubated at 37 °C until the optical density (OD) reached 0.5 (at λ=600 nm). Bacteria were harvested by centrifugation at 6,000 rpm in a JA10 rotor for 10 min at 4 °C. The bacterial pellet was resuspended in 40 ml of 30 mM potassium acetate, 100 mM RbCl, 10 mM $CaCl_2$, 50 mM $MnCl_2$, 15% (v/v) glycerol, pH 5.8, and left on ice for 2 h. After centrifugation and resuspension of the pellet in 4 ml of 10 mM MOPS, 75 mM $CaCl_2$, 10 mM RbCl, 15% (v/v) glycerol, pH 7, cells were stored at -80 °C in 400 μl aliquots.

2.2.4 Transformation of bacteria by heat shock

The plasmid cDNA of interest (10 ng) was added to 200 μl of competent bacteria previously thawed on ice. After gentle mixing, cells were left on ice for 30 min, heat shocked for 90 sec at 42°C and, after addition of 800 μl LB broth, incubated with shaking at 37 °C for 45 min. Bacteria were plated on LB-agar containing the appropriate selective antibiotic and incubated overnight at 37°C. The following day, an isolated bacterial colony was picked and used to inoculate 2 ml of LB-broth containing the appropriate antibiotic. The culture was incubated at 37°C overnight. For storage, 750 μl of sterile glycerol were added to 750 μl of bacterial culture and stored at -80 °C.

2.2.5 Expression and purification of GST-fusion proteins

A single colony of *E. coli* transformed with a pGEX vector containing the GST-fusion protein of interest was used to inoculate 100 ml of LB broth. The bacterial culture was grown to an OD_{600} of 0.6. Expression was induced with 1mM IPTG for 3 h at 37°C. Bacteria were harvested by centrifugation (6000 rpm, JA10 rotor, Beckman, CA, USA) for 10 min at 4°C. The bacterial pellet was resuspended in 25 ml of 20 mM Tris-HCl pH 8,0, 100 mM NaCl, 1 mM EDTA, 1 mg/ml lysozyme in the presence of a cocktail of protease inhibitors (leupeptin, benzamidine, and PMSF). TritonX-100 was added to a final concentration of 1% and the suspension agitated continuously for 30 min, and then sonicated for 2 min on ice. The lysed bacteria were centrifuged for 20 min (1800 rpm, JA20) and the pellet

discarded. Meanwhile, 2.5 ml of a glutathione-Sepharose resin were diluted to 40 ml and centrifuged (2000 x g) for 5 min. The supernatant was discarded and the resin was resuspended in PBS. This procedure was repeated twice. The cleared bacterial lysate was then added to the glutathione-Sepharose resin, and incubated for 30 min at 4°C with occasional agitation. The beads were washed 3 times with 50 ml of PBS and packed onto a column. The resin was allowed to pack for 10 min, and the protein was eluted with 1 ml of elution buffer (100 mM Tris-HCl, 20 mM gluthathione, 5 mM DTT). The eluate was collected and this operation was repeated an additional five times. The protein content of each of the six fractions collected was analysed by SDS-PAGE and fractions containing the higher protein concentration were pooled together and stored in aliquots.

2.2.6 cDNA mutagenesis

2.2.6.1 Materials

The QuickChange® Site-Directed Mutagenesis Kit and Dpn I restriction enzyme were purchased from Stratagene (USA).

2.2.6.2 Site-directed mutagenesis

Mutagenesis was performed using pGEX-4T1-Sedlin as a template in order to generate two sedlin mutants, H13A and del387A.

The mutagenic oligonucleotides containing the desired mutation were designed following the instructions of the QuickChange® Site-Directed Mutagenesis Kit (Stratagene, USA) manual:

SedlinH13A (+)

5'-CTACTTTGTAATTGTTGGCCACGCTGATAATCCAGTTTTTGAAA

TGGAG -3'

SedlinH13A (+)

5'-CTCCATTTCAAAAACTGGATTATCAGCGTGGCCAACAATTACA

AAGTAG -3'

Sedlin del387 (+)

5'- CAAGTGCATTTGACAGAAAGTTCAGTTTCTTGGGAAG -3'

Sedlin del387 (-)

5'- CTTCCCAAGAAACTGAACTTTCTGTCAAATGCACTTG -3'

The polymerase chain reaction (PCR) was performed uing the following conditions:

5 μl of 10X reaction buffer;

5 μl (5 ng) of DNA template;

1.25 μl (125 ng) of oligonucleotide primer forward;

1.25 μl (125 ng) of oligonucleotide primer reverse;

1 μl of dNTP (10mM) mix;

36.5 μl of sterile double distilled water;

1 μl of Pfu Turbo DNA polymerase.

The cycling parameters for the QuickChange Site-Directed Mutagenesis Method are: 95°C for 30 sec. (1 cycle); 95°C for 30 sec., 53°C for 1 min., 68°C for 12 min (12 cycles); 72°C for 10 min (1 cycle). Amplification was checked by electrophoresis of 10 μl of the PCR product on a 1% (w/v) agarose gel. One μl of the Dpn I restriction enzyme (10 U/μl) was added directly to each amplification reaction and then the PCR product was incubated for 1 h at 37 °C, in order to digest the parental non-mutated DNA. XL1-Blue supercompetent cells were transformed with 2 μl of the Dpn I-treated DNA. On the following day, one colony was used to inoculate 2 ml of LB-broth containing the selective antibiotic and plasmid DNA was prepared. A DNA aliquot was precipitated as follows: to 20 μl of DNA, 3 μl of sodium acetate (3 M, pH 8), 66 μl of ethanol and 14 μl of sterile double distilled water were added. The sample was mixed and incubated for 10 min on ice and then centrifuged at maximum speed for 30 min at 4 °C. The supernatant was removed and the pellet air dried for 5-10 min. and then sent for sequencing by MWG Biotech (Italy).

2.2.7 Procollagen type II cloning

To generate fluorescently tagged procollagen type II, the cDNA sequence corresponding to amino acids 26-1487 of COL2A1 was PCR-amplified

84

from the Image clone IRCFp5008C071D (imaGenes GmbH) using the forward primer 5'-TTCAAGCTTGTCAGGATGTCCAGGAGGCTG-3' and reverse primer 5'-GAGGGATCCTTACAAGAAGCAGACCGGCC-3' and cloned HindIII/BamHI into the pmCHERRY-C2 vector, a derivative of pEGFP-C2. This construct was digested NheI/AgeI and a stuffer fragment corresponding to the procollagen signal peptide (amino acids 1-25) that included the Kozak consensus sequence was ligated, upstream of the mCHERRY, by annealing the oligos 5'-CTAGCACCATGGCAATTCGCCTCGGGGCTCCCCAGACGCTGGTG CTGCTGACGCTGCTCGTCGCCGCTGTCCTTCGGTGTCAGGGCA-3' and 5'-CCGGTGCCCTGACACCGAAGGACAGCGGCGACGAGCAGCGTCA GCAGCACCAGCGTCTGGGGAGCCCCGAGGCGAATTGCCATGGTG -3'.

2.2.8 Preparation of antibodies

The preparation of the anti-Bet3, anti-Sedlin and anti-Synbindin antibodies has been performed by G. Di Tullio and M. Santoro (Consorzio Mario Negri Sud, Italy). Briefly, 1 mg of the specific antigen was resuspended in 2 ml of PBS (1.5 mM KH_2PO_4, 8 mM Na_2HPO_4, 137 mM NaCl and 2.7 mM KCl, pH 7.4). Two ml of complete Freund's adjuvant were added and this mixture used to immunize New Zealand rabbits. The rabbits were boosted after 21 and 42 days with 1 mg of antigen containing the same volume of incomplete Freund's adjuvant. The rabbits were bled and the serum

prepared as described below. After collection, blood was allowed to clot at 37 °C for 60 min, then kept overnight at 4 °C in order to make the clot contract. The serum was removed from the clot and the insoluble material, by centrifugation at 10000 x g for 10 min at 4 °C, and stored at -80 °C in aliquots. Protein-A-sepharose beads (500 mg), suspended in 5 ml of distilled water, were packed into a column and washed with 100 ml of distilled water under constant flow. The packed beads were washed with 20 ml of PBS and 2 ml of anti-TRAPP subunit (Bet3 or Sedlin or Synbindin) serum were loaded onto the column at 0.5 ml/min in a FPLC (Fast Protein Liquid Chromatography) system (Pharmacia Bio-Tec, UK). The beads were washed with 30 ml of PBS and the retained IgGs were detached using 15 ml of 100 mM glycine pH 2.5. Fractions of 1 ml were collected and their protein content quantitated by spectrometry (by the FPLC system). The six fractions containing the highest concentration of protein were pooled and the pH neutralised with 1 M Tris, pH 11. The protein concentration of the pooled fractions was determined using a commercially available protein assay kit (Biorad, UK) according to the manufacturer instructions. Typically this was 2.5 mg/ml. Different dilutions of the IgGs were tested both in Immuno-fluorescence (IF) and in Western blot (WB) and optimal working dilutions were reported in the **Table 2.1.**

After the affinity-purification (see above) the anti-Bet3 antibody was dialysed against 70mM KCl, 10mM Na_2HPO_4 pH7.2 for 4h using dialysis membranes with a molecular weight cut off of 6000/8000 Da (1ml of

Antibody	Company or other source	Animal source	Dilution WB	Dilution IF	Catalog n°
β-Actin	Sigma	Rabbit	1:10000	–	#A2066
collagen type I	Daichii chemical	Mouse	–	1:200	#F-56
collagen type I(SP1D8)	Hybridoma Bank	Mouse	1:1000	1:200	–
collagen type II	Hybridoma Bank	Mouse	–	1:300	–
albumin	Dako	Rabbit	1:1000	–	#A 0001
α 1 anti-trypsin	Dako	Rabbit	1:1000	–	#A 0012
CD8	G. Di Tullio (CMNS)	Mouse	–	1:800	–
GM130	BD	Mouse	1:5000	1:1000	#61082
GST	G. Di Tullio (CMNS)	Rabbit	1:10000	1:500	–
GST	G. Di Tullio (CMNS)	Mouse	–	1:500	–
giantin	G. Di Tullio (CMNS)	Rabbit	–	1:1000	–
GRASP55	G. Di Tullio (CMNS)	Rabbit	–	1:500	–
TGN38	Serotech	Sheep	–	1:750	–
TGN46	Serotech	Sheep	–	1:1500	#AHP500G
PDI	StressGen	Mouse	–	1:200	#SPA-891
Rab1A	Santa Cruz	Rabbit	1:1000	–	#sc-311
Rab1B	Santa Cruz	Rabbit	1:1000	1:200	#sc-599
Sar1	Upstate	Rabbit	1:2000	1:200	#07-692
Sec23	ABR	Rabbit	1:3000	–	#A300-592A
Sec31	G. Di Tullio (CMNS)	Rabbit	1:2000	1:1000	–
Sec31	G. Di Tullio (CMNS)	Mouse	–	1:30	–
VSV-G (P5D8)	Bethyl	Rabbit	–	1:1000	#A190-231A
VSV-G (lum domain)		Mouse		1:2000	–
Bet3	G. Di Tullio (CMNS)	Rabbit	1:5000	1:200	–
sedlin	G. Di Tullio (CMNS)	Rabbit	1:5000	1:200	–
synbindin	G. Di Tullio (CMNS)	Rabbit	1:5000	1:200	–
TRS33A	Heinemann lab	Rabbit	1:1000	–	–
TRS33B	Heinemann lab	Rabbit	1:1000	–	–
aggrecan	Vertel lab	Rabbit	–	1:1000	–
poly-His	Sigma	Mouse	1:1000	–	#34660
GRP78/BiP		Rabbit	–	1:50	–

Table 2.1. List of antibodies used in this study both for immunofluorescence (IF) and immunoblotting (WB).

antibody in 500 ml of buffer for two times). The antibody was then ready to be microinjected inside the cells.

2.3 Cell transfection and RNA interference

2.3.1 Materials

TransIT-LT1 transfection reagent was from Mirus (USA). OligoFectamine and LipoFectamine 2000 were from Invitrogen (USA), Dharmafect4 from Dharmacon (USA) and OptiMEM serum-free reduced culture medium was from GIBCO (UK).

2.3.2 Preparation of plasmid DNA and transfection of DNA

2.3.2.1 Mini scale

A single colony of XL-1 Blue E. Coli bacteria, transformed with the plasmid of interest was used to inoculate 2 ml of LB-broth containing the selective antibiotic. After 15-20 h incubation with shaking at 37 °C, bacteria were collected by centrifugation at 14,000 rpm in a Microfuge®18 centrifuge [Beckman Coulter (USA)] for 1 min at RT and processed accordingly to the mini-plasmid preparation protocol of the "SIGMA-plasmid-miniprep kit". The cDNA obtained was resuspended in 10 mM TRIS-HCl pH 8 and stored at 4 °C or, for long-term, at -20 °C.

2.3.2.2 Large scale

A single colony of XL-1 Blue *E. Coli* bacteria, transformed with the plasmid of interest was used to inoculate 500 ml of LB-broth containing the selective antibiotic. After 15-20 h incubation with shaking at 37 °C, bacteria were collected by centrifugation at 6000 rpm in a JA10 rotor for 10 min at 4 °C and processed according to the maxi-plasmid purification protocol of the "Qiagen-plasmid-kit". The cDNA obtained was resuspended in TE buffer (10 mM TRIS-HCl, 1 mM EDTA pH 7.5) to a final concentration of 1 mg/ml and stored at 4 °C or, for long-term, at -20 °C.

2.3.3 TransIT-LT1-reagent-based cell transfection

HeLa cells were seeded into 24-well plates at a concentration suitable to have 50%-70% confluence for transfection. The transfection mixture was prepared in a polypropylene tube: for each well, 0.3 µl TransIT-LT1 transfection reagent was diluted in 50 µl OptiMEM culture medium. The mixture was shaken and incubated at RT for 5 min. Then 100 ng of total DNA was added to the transfection mixture, which was shaken and kept at RT for 15 min, to allow the DNA-TransIT-LT1 complex to form. The cells were then incubated with the transfection mixture at 37 °C in the presence of 5% CO_2 for 16-20 h.

2.3.4 siRNA duplexes

SiRNA oligonucleotides for sedlin, Bet3, Rab1A were purchased from Dharmacon (USA), while for Sec23 and Rab1B they were purchased from Sigma (USA). Non-targeting siRNA sequences were used as controls; the siRNAs sequences are listed in **Table 2.2**.

2.3.5 siRNA-duplex transfection

HeLa cells were transfected using OligoFectamine (Invitrogen, USA), Rx chondrocytes and NRK using LipoFectamine 2000 (Invitrogen, USA), and HepG2 cells using DharmaFect 4 (Dharmacon). The Cell Microporator System (CellBio) was used or electroporation of human fibroblasts according to the manufacturer's instructions (using the programme number 5 of the Microporator System Software).

HeLa cells were plated in 24-well plates to sub-confluent density on glass coverslips, in antibiotic-free medium. The day after, a transfection mixture was prepared: for each well, 50 pmol of specific siRNA duplexes were diluted in 40 μl of OptiMEM culture medium in a polypropylene tube. In a separate polypropylene tube, for each well, 1μl of Oligofectamine Reagent was diluted in 7.5 μl of the same medium. The mixtures were first shaken and incubated at RT for 7 min, then combined, shaken and kept at RT for 20 min, to allow the siRNA-Oligofectamine complex to form.

90

name	Sense sequence 3'-5'		Species	Purchased from
Sedl n1	GGGCAUAUGAGGUUUAUUA	UU	human	Dharmacon
Sedl n2	GAGCUUCUACUUUGUAAUU	UU	human	Dharmacon
Sedl n3	ACAUGUGGCUAUCGAACAA	UU	human	Dharmacon
Sedl n4	CAUAAGACAAGAAGAUGGA	UU	human	Dharmacon
Sedl n5	GGGCAUAUGAGAUUUAUUA	UU	rat	Sigma
Sedl n6	AAGCUUCUACUUUGUAAUU	UU	rat	Sigma
Sedl n7	AUAUGUGGCUUUCUAACAA	UU	rat	Sigma
Sedl n8	UGUGAGGCAAGAAGAUGGA	UU	rat	Sigma
Sedl S1	UCCAUUUUAUGAACCCAAU	UU	human/rat	Sigma
Sedl S2	CAAUUCUCCUAUUCGAUCA	UU	human/rat	Sigma
Bet3 n1	GAUAACCACUCAUCCCUUA	UU	human	Dharmacon
Bet3 n2	GGGCAUCACUCCAAGCAUU	UU	human/rat	Dharmacon
Bet3 n3	GAAAGGAGACGGUGUGACA	UU	human	Dharmacon
Bet3 n4	GGAAACUGCGGAUGUCAUU	UU	human	Dharmacon
Rab1An1	CAGCAUGAAUCCCGAAUAU	UU	human/rat	Dharmacon
Rab1An2	GUAGAACAGUCUUUCAUGA	UU	human/rat	Dharmacon
Rab1An3	GGAAACCAGUGCUAAGAAU	UU	human	Dharmacon
Rab1An4	UGAGAAGUCCAAUGUUAAA	UU	human	Dharmacon
Rab1B	CGUACACAGAGAGCUACAU	UU	human/rat	Ambion

Table 2.2. List of siRNA sequences used in this study.

The cells were incubated with the transfection mixture at 37 °C in the presence of 5% CO_2 for 72 h.

A similar protocol was adopted for Rx chondrocytes and NRK49F. SDS-PAGE, Western blotting and densitometry analyses were carried out to evaluate the efficiency of siRNA treatment for each experiment.

2.4 Immunofluorescence Confocal Microscopy

2.4.1 Materials

Potassium acetate and magnesium acetate were from Merck (Germany). Paraformaldehyde was from Electron Microscopy Sciences (USA). Bovine serum albumin (BSA), saponin, NaCl were purchased from Carlo Erba (Italy). Alexa-Fluor-546, -568, -488 and -633 conjugated goat anti-mouse or anti-rabbit secondary antibodies were from Molecular Probes (USA). DAPI was from Molecular Probes (USA). Mowiol was from Calbiochem (USA). Primary antibodies used in this study and their origin are listed above,in **Table 2.1.**

2.4.2 Solutions

Phosphate buffered saline (PBS): 1.5 mM KH_2PO_4, 8 mM Na_2HPO_4, 2.7 mM KCl, 137 mM NaCl, pH 7.4.

Paraformaldehyde: as 8% in H_2O, the paraformaldehyde was diluted in PBS (pH 7.4) to the appropriate concentration, and stored at 4 °C.

Blocking solution: 0.05% saponin, 0.5% BSA, 50 mM NH_4Cl in PBS. Mowiol: 20 mg Mowiol were dissolved in 80 ml of PBS, stirred overnight and centrifuged for 30 min at 12000× g.

2.4.3 Immunofluorescence procedures

HeLa, HFs, NRK49F and Rx chondrocytes were grown to sub-confluent density on glass coverslips and treated as follows. They were fixed with 4% paraformaldehyde for 10 min at RT and washed twice in PBS. Blocking reagent was then added to the cells for 20 min, followed by a 1-h incubation with the primary antibody in blocking reagent (see **Table 2.1** for the dilutions used). When required, cells were permeabilised with 0.01% Triton-X 100 in PBS. The cells were then extensively washed with PBS and incubated with secondary antibodies (1:400) and with DAPI (where indicated, at a final dilution of 1:1000 from a 1 mg/ml stock) for 45 min, diluted in blocking solution. After immuno-staining, the cells were washed three times in PBS and once in sterile water, to remove salts. The coverslips were then mounted on glass microscope slides (Carlo Erba, Italy) using Mowiol.

2.4.4 Immunofluorescence analysis by laser scanning confocal microscopy

IF samples were examined under a confocal laser microscope (Zeiss LSM510 META and LSM710 confocal microscope systems; Carl Zeiss, Gottingen, Germany) equipped with 63x1.4 NA oil objective. Optical confocal sections were taken at 1 Airy unit with a resolution of 1024×1024 pixels or 2048×2048 pixels, and exported as TIFF files. Images were cropped with Adobe Photoshop and composed using Adobe Illustrator.

2.4.5 Image processing and quantification of colocalisation on fixed cells

For quantification experiments, 10-15 randomly chosen fields each containing 8-10 cells were scanned with the same microscope settings (i.e. laser power and detector amplification) below pixel-saturation. The mean intensity per cell was determined using the histogram function in the Zeiss LSM 510 Software (version 3.2), where all pixel values above the background level were quantified. All experiments were repeated at least three times.

To quantify the level of co-localisation, confocal serial sections were acquired at the same magnification from 20 cells per experimental condition, exported in TIFF format, and processed. Briefly, an intensity threshold of 50 (in a range of 0-255) was applied. The percentage of co-localisation represents the percentage of total pixels in the reference channel that were positive for the other channel.

2.4.6 Fluorescence Recovery After Photobleaching (FRAP)

Human fibroblasts microinjected with the plasmid encoding GFP-Sec23 were incubated at 37°C using a humidified temperature-controlled incubation chamber equipped on Zeiss LSM710 in carbonate-free culture medium. Cells were imaged using an LSM710 confocal microscope (Zeiss) fitted with a 488 and nm argon ion laser lines, using a 63x PlanApochromat NA 1.4 DIC oil immersion objective. FRAP experiments and time-lapse laser-scanning confocal microscopy were performed as described (Watson et al., 2005). Briefly, a single ER exit sites was acquired 5 frames before bleaching (0.8 sec/frame). Bleaching was performed with 100% power of the 488 laser for 3 iterations. Recovery was monitored for 90 seconds after the bleaching event. At least 60 independent ERES were analysed for each condition in three different experiments. Data were exported using Zen software (Zeiss) and corrected for bleaching, by dividing the fluorescence intensity of the bleached area by that of an unbleached area. Bleaching was minimal during the time course of recovery, between 0-10% and where bleaching exceeded 10%, the recovery sequences were discarded. The half time for recovery, $t_{1/2}$, was calculated as previously described (Watson et al., 2005).

2.4.7 Fluorescence loss in photobleaching (FLIP) and Fluorescence recovery after photobleaching (FRAP) assays.

Human fibroblasts (HF) plated on 35-mm glass bottom wells (Mattek, USA) were treated with siRNA against sedlin and Bet3, as described above.

95

After 96 hours, plasmids encoding GFP-Sec23 or GFP-Rab1 (stock solution 20 ng/µl and 10 ng/µl, respectively) were micro-injected into the nuclei and analyzed 6 h after transfection.

Fluorescence Loss In Photobleaching (FLIP) was performed (using Zeiss 510 confocal microscope) by bleaching iteratively (100 times) the GFP-associated fluorescence in the whole cell area except for the Golgi and monitoring the Golgi-associated fluorescence over time and the relative fluorescence intensity (% of pre-bleaching) was plotted. For the Golgi dissociation constant (K_{off}) and Golgi dissociation half time ($t_{1/2}$) calculations, FLIP curves were linearised according to the formula:

$$F(t)=e^{-K_{off}*t}$$

where K_{off} represents the dissociation constant of the fluorescent protein from the Golgi membranes and t represents the time in sec.

The $t_{1/2}$ value was obtained according to the formula:

$$t_{1/2} = \ln(1/2)/K_{off}$$

Fluorescence Recovery After Photobleaching (FRAP) was performed by bleaching the GFP-associated fluorescence in an area encompassing a single ER exit site (5 bleaching iterations at the maximum laser fluorescence power) and then monitoring the fluorescence intensity recovery in the bleached area. Relative fluorescence intensity (% of pre-bleaching) was plotted (the time required to bleach the samples is not

reported in the graphs). For the Golgi association constant (K_{on}) calculation, FRAP curves were linearised according to the formula:

$$F(t) = e(K_{on} + K_{off}) * t$$

where K_{on} represents the association constant of the fluorescent protein to the Golgi and K_{off} represents the dissociation constant of the fluorescent protein from the Golgi membranes and t represents the time in sec.

2.5 Transport assays

2.5.1 VSV-G transport assay

For VSV-G assays, cells were infected with the VSVts045 variant for 1 hr a 32°C in serum-free medium. After infection, the cells were washed several times and shifted for 3 hrs at 40°C in complete medium. Cycloheximide was added to a final concentration of 100 μg/ml and the cells were shifted to 32°C for the indicated times. To follow endogenous PC-I in fibroblasts and NRK cells or PC-II in Rx chondrocytes (both endogenous and expressed in primary fibroblasts), cells were incubated for 3 hrs at 40°C in DMEM supplemented with 1% serum and 20mM HEPES pH 7.2, then shifted to 32°C in the presence of cycloheximide (100 μg/ml) and ascorbate (50 μg/ml). Then, the cells were fixed and processed as described above.

Quantitative evaluation of VSV-G and PC (both I and II) transport was performed by analysing the immunofluorescence staining patterns of at least 200 cells in three separate experiments.

2.5.2 CD8 transport assay

For CD8 transport, a CD8 cDNA was injected into the cell nuclei, incubated 6 hrs at 37°C and then chased in the presence of cycloheximide (100 µg/ml) for the indicated times. Cells were fixed and processed for immunofluorescence.

2.5.3 Albumin secretion assay

2.5.3.1 Materials

[^{35}S]-Met-Cys Protein Labelling Mix was from Perkin Elmer (USA). Rabbit polyclonal anti-human-Albumin antibody was from DakoCytomation (Denmark).

2.5.3.2 Procedure

Human hepatoma HepG2 cells were plated in a 12-well culture tissue multiwell plate to reach 80% confluence the day of the experiment. Cells were treated with non-targeting, sedlin and Bet3 siRNAs for 72 hours. The day of the experiment, cells were washed 3 times with 600 µl PBS at 37°C, to remove any source of albumin from the serum. Then cells were incubated with 500 µL of DMEM without methionine (Met) and cysteine

(Cys) for 30 min at 37 °C. Subsequently, cells were pulse labelled with 500 μL DMEM [^{35}S]-Met-Cys 100μCi/ml for 5 min at 37 °C. Cells were washed and chased in 500 μL DMEM without FCS and for the indicated times.

Medium was withdrawn and centrifuged (16,000 g for 5 min), the supernatant transferred to a new tube and immunoprecipitated overnight at 4°C using the anti-albumin antibody. In the meanwhile, the cells were washed 3 times with ice cold PBS and lysed by adding 400 μL of lysis buffer (70 mM TRIS-HCl pH 7.5; 150 mM NaCl; 0.05% SDS; 1% TX-100; 1 mM EDTA) on ice for 15 min. Lysates were collected, centrifuged (16,000 g for 5 min) and the supernatant was immunoprecipitated overnight at 4°C using the anti-albumin antibody.

Antibody/antigen complexes were recovered by adding 20 μL of Protein A-Sepharose equilibrated in lysis buffer to each sample (45 min at 4°C). After extensive washing (at least 6 washes were performed), samples were processed for SDS-PAGE and Western blotting. Immunoprecipitated albumin was revealed by autoradiography and the percentage of albumin released into the medium after the indicated time points was calculated.

2.5.4 α1 anti-trypsin glycosylation and secretion assays

2.5.4.1 Materials

[^{35}S]-Met-Cys Protein Labelling Mix was from Perkin Elmer (USA), Endoglycosidase-H was from New England Biolabs (USA).

Rabbit polyclonal anti α1 anti-trypsin was from DakoCytomation (Denmark).

2.5.4.2 Procedure

HepG2 cells were siRNA treated in 12 well culture tissue multiwell plates to reach 80% confluence the day of the experiment. Cells were pulsed and chased as described in the previous sections (albumin secretion, 2.5.3.2).

After washing 3 times with PBS, the cells were lysed using 400 μl (25 mM Tris-HCl pH 7.5; 150 mM NaCl; 1mM EDTA; 1% TX-100; protease inhibitors) 15 min on ice. Lysates were immunoprecipitated with 2.5 μl of anti-α 1-AT rabbit polyclonal antibody per sample. 150 μl of denaturing buffer (0.5% SDS; 1% β-Mercaptoethanol) was added to the samples that were then boiled for 10 min. Each sample was divided into two aliquots of 75 μl, and then 9 μl of 10X glycosidase buffer (0.5 M Na-Acetate pH 5.5, 50 mM CaCl$_2$) was added to each aliquot. 40U/sample of endoglycosidase-H (Endo-H, Calbiochem) were added to one of the two samples. Samples were incubated 5 h at 37 °C and then processed for SDS-PAGE and Western blotting. After autoradiography, the Endo-H resistant form was evaluated as a % of the total α 1-AT (as a measure of ER to medial-Golgi transport).

2.6 Metabolic labelling

2.6.1 Materials

100

[^{35}S]-Met-Cys Protein Labelling Mix was from Perkin Elmer (USA), BFA was from Sigma-Aldrich, Germany.

2.6.2 Procedure

Total secretion experiments were performed essentially as described previously (Saito et al., 2009). Briefly, sedlin or Bet3 siRNA-treated or untreated Rx chondrocytes and HeLa cells were cultured in DMEM without L-methionine and L-cysteine for 1 h and then pulsed with 40 μCi of ^{35}S-methionine and ^{35}S-cysteine (Protein Labelling Mix, Perkin Elmer) for 1 h at 37°C. Cells were then washed and chased for 3 h in DMEM. Medium was collected and each sample was resolved by SDS–PAGE, followed by autoradiography. For BFA-treated cells, 10 μg/ml of BFA was added 10 mins before the end of the pulse and left throughout the chase. Samples were resuspended in Sample Buffer and subjected to SDS-PAGE and followed by autoradiography and quantified using Instant-Imager (Perkin Elmer).

2.7 Microinjection experiments

Rx chondrocytes were plated on glass coverslips in complete culture medium the day before injection. Pre-immune IgG and anti-Bet3 antibody were injected (2 mg/ml) into cells using a 5246 transjector controlled by a 5171 micromanipulator (Eppendorf, Germany). For the effects of the anti-Bet3 antibody on PC and VSV-G transport, the antibody was injected into infected cells during the second hour of the 40 °C block.

His-Sar1H79G was injected at different dilution (2.5 mg/ml, 0.5 mg/ml and 0.1 mg/ml) dissolved in 70 mM KCl, 10 mM NaH_2PO_4, pH 7.2. Injections were performed into infected cells as described above.

For the DNA microinjection, plasmids encoding the protein of interest (GFP-Sec23 and CD8) were diluted to a final concentration of 20 μg/ml with the same microinjection buffer. Briefly, cells were treated with sedlin and Bet3 specific siRNAs for 72 hours. After this procedure, the different plasmids were microinjected in the nuclei and left to express the protein at 37°C for at least 3 hours. For PC-II mCherry expression in primary fibroblasts, microinjections were performed as described above (20ng/μl). After the injections, cells were incubated for 3 hrs at 37°C and then shifted to 40°C for an additional 3 hrs. Co-injection of PC-II mCherry plasmid with wild-type sedlin (100ng/μl) was carried out under identical conditions. For rescue experiments, a plasmid encoding human sedlin was injected both in control and sedlin siRNA-treated Rx chondrocytes (100ng/μl). Cells were incubated for 4 hrs before the experiments. For each microinjection experiment at least 150 cells were injected.

2.8 SDS-PAGE

2.8.1 Solutions

Running buffer: 0,2 M glycine, 20 mM Trizma base, 4 mM SDS, pH 8.3; 1X sample buffer: 0.125 M Trizma base, 4% (w/v) SDS, 20% (v/v) glycerol, 10% (v/v) β-mercaptoethanol, pH 6.8.

2.8.2 Assembly of polyacrylamide gels

Two 16 x 15 cm glass plates were assembled to form a chamber using two 1.5 mm plastic spacers lined on the lateral edges of the plates. This chamber was fixed using two clamps and mounted on a plastic base that sealed the bottom (Hoefer Scientific instruments, Germany). The polyacrylamide gel was then prepared using one solution of the desired polyacrylamide concentration (usually 13% to better separate the TRAPP subunits) or two solutions of 4 and 15% (v/v) polyacrylamide in a gradient maker device, to prepare a 4-15% (v/v) gradient gel.

2.8.3 Samples preparation and run

Samples were prepared by adding sample buffer and boiling for 5 min at 95 °C before loading onto the gel. The end wells were loaded with 3 μl of pre-stained molecular weight standards (Sigma, USA). The chamber was then assembled into the electrophoresis apparatus (Hoefer Scientific Instruments, Germany) and electrophoresis was carried out under a constant current of 8 mA (for overnight runs) or 30-40 mA (for 4 h runs).

2.8.4 Western blotting

2.8.4.1 Solutions

Transfer buffer: 0.2 M glycine, 20 mM Trizma base, pH 8.3; blocking buffer: 1% (w/v) BSA [or alternatively 5% (w/v) dry skim milk], 0.05% (v/v) Tween 20, 150 mM NaCl, 50 mM TRIS-HCl pH 7.5.

ECL^{TM} Western Blotting Detection Reagents was purchased from GE Healthcare (Sweden).

2.8.4.2 Nitrocellulose blotting

The polyacrylamide gel was soaked for 15 min in transfer buffer, placed on a sheet of 3 MM Whatman paper and covered by a nitrocellulose filter (Schleicher & Schuell, USA). The filter was covered by a second sheet of 3 MM paper to form a "sandwich" that was subsequently assembled into the blotting apparatus (Hoefer Scientific Instruments, Germany). Protein transfer occurred at 400 mA for 4-5 h. At the end of the run, the "sandwich" was disassembled and the nitrocellulose filter was soaked in 0.2% (w/v) red Ponceau in 5% (v/v) acetic acid for 5 min to visualise the protein bands and then rinsed with 5% (v/v) acetic acid to remove the excess of the unbound dye.

2.8.4.3 Immunodetection of antigens

Nitrocellulose filters were cut with a razor blade into strips. Strips containing the proteins of interest were incubated in blocking buffer for 30 min at RT and then with fresh blocking buffer containing the primary antibody at its working concentration (see Table 2.1 for the antibody dilution used).

After 2-3 h of incubation at RT, or overnight at 4 °C, the antibodies were removed and the strips washed with TTBS 3 times, 3min each wash. Strips were incubated for 1 h with the appropriate HRP-conjugated secondary antibody (diluted 1:10,000 (goat anti-mouse) or 1:20,000 (goat anti-rabbit) for ECL development) and washed 2 times, 3min each wash, with TTBS

and 2 times, 3min each wash, with TBS. After washing, strips were incubated with the developing solution:

ECLTM from GE Healthcare (UK).

Strips were incubated with the ECL developing solution for 1 min at RT and visualised by chemoluminescence.

2.9 Pull-down assays

Increasing concentrations (0.1, 0.3 and 1 μM) of His-Sar1 were incubated with GST-fusion proteins or GST alone (0.5 μM) as previously described (Cai et al., 2007). After overnight incubation at 4°C in 300 μl binding buffer (50 mM TRIS pH 7,4, 100 mM NaCl, 1mg/ml BSA, 0.1% Triton X-100, 0.1% NP-40, 0.1 mM GTP or GDP), glutathione-beads were added, incubated for 2 hrs at 4°C, washed extensively at least 5 times (50 mM TRIS pH 7.4, 100 mM NaCl), eluted and analysed by SDS-PAGE.

2.10 Sar1 GTPase activating assay

These experiments are carried out in collaboration with Giuseppe Di Tullio and Michele Santoro (CMNS, Santa Maria Imbaro , Chieti, Italy and TIGEM, Naples, Italy respectively).

2.10.1 Sar1 Protein purification

Overnight cultures of Escherichia coli BL21(DE3) carrying pet28a-Sar1 WT or pet28a-Sar1H79G were diluted into Luria Broth. The cells were

grown at 37 °C to an A600 of 0.3, transferred to 25 °C, and further grown to an OD_{600} of 0.5. Expression of hamster Sar1a was induced with 0.1 mM isopropyl 1-thio-β-d-galactopyranoside for 3 h. The induced cells were harvested by centrifugation at 4,500 rpm for 10 min in a JA10 (Beckman) rotor at 4 °C. The pellet was resuspended according to manufacturer's instructions (Qiagen, NiNTA agarose beads). Proteins were quantified by the Bradford assay using bovine serum albumin as a standard.

2.10.2 Preparation of Rat Liver Cytosol

Rat liver cytosol was prepared as described previously (Nohturfft et al., 2000). Briefly, male Sprague-Dawley rats were anesthetized by halothane inhalation and livers were excised and disrupted in 2 mL/g ice-cold buffer E (50 mM HEPES- KOH pH 7.2, 250 mM sorbitol, 70 mM KOAc, 5 mM potassium-EGTA, 2.5 mM $Mg(OAc)_2$) supplemented with protease inhibitor cocktail (Roche). Livers were each cut in 20 smaller pieces and homogenized using a T18 UltraTurrax dispenser (IKA). All subsequent steps were carried out at 4°C. Homogenates were centrifuged at 960 × g for 10 min. Supernatants were sequentially centrifuged 186,000 × g for 1 hour. This resulting supernatant (the rat liver cytosol, 15–22 mg protein/ml), was divided into multiple aliquots, snap-frozen in liquid nitrogen, and stored at −80°C. To prepare TRAPP-depleted rat liver cytosol, equal amount of preimmune IgG and Bet3 specific antibody (250 µg) were cross-linked to Protein A Sepharose beads (Sigma) and packed into a 0.3 cm diameter column. 3 mg of rat liver cytosol were loaded onto the column on an FPLC system (ÄKTAmicro™, GE Healthcare Lifesciences) at a flow rate of 0.5

ml/cm. Fractions were collected and blotting analyses were performed to assess the efficiency of TRAPP depletion.

2.10.3 Sar1 GAP assay

The protocol used in this study was adapted from Jacques et al. (2001). 0,5 µM recombinant Sar1-His was incubated in buffer C (25mM HEPES-KOH pH 7.2, 1mM DTT, 0.25 mM BSA, 0.25 mM $Mg(OAc)_2$, 1 mM ATP and 50nM α-32P-GTP) at 32°C alone or in presence of 60 µg of wild type or TRAPP-depleted rat liver cytosol. At variuos times (15, 30, 60, and 120 minutes) 2.5 µl of the samples were removed and diluted in 50 µL of 2M formic acid. 2.5 µl of these mixtures were spotted onto a TLC plate (PEI Cellulose F, Merck), rapidly air dried and subjected to a separation run. Radiolabeled GTP and GDP were separated by placing the bottom of the TLC plate in a shallow reservoir containing TRIS-HCl 1.2 M, pH 7.4. The buffer was allowed to migrate up the TLC plate until it reached 2-3 cm from the top. Radiolabeled nucleotides were measured using Istant-Imager (Perkin-Elmer), and expressed as a percentage of the sum of the two detected species.

2.11 Assay in permeablilised cells

2.11.1 Materials

Streptolysine O (Sclavo, Italy).

2.11.2 Procedure

HeLa cells were treated with specific siRNAs for 72 hours, then treated as previously reported (De Matteis et al., 1993) with some modifications.

Mock, sedlin-KD and Bet3-KD Cells were incubated with streptolysine-O (Sclavo, Italy, 1 UI/mL) for 10 minutes on ice, in a buffer containing 20 mM HEPES-KOH pH 7.2, 110 mM KOAc, 2 mM $Mg(OAc)_2$, 1 mM DTT. Cells were washed twice with the same buffer, then they were shifted to 37°C for 20 minutes, to allow membrane pore formation. Reactions contained 1 mM ATP, and/or 0.1 mM GTPγS, an ATP regeneration system (5mM creatine phosphate and 20 UI/mL creatine phosphate kinase) and transport buffer (25 mM HEPES KOH, 2.5 mM $Mg(OAc)_2$, 120 mM KOAc, 5 mM EGTA and 1.8 mM $CaCl_2$). The media was collected as the cytosolic fraction while the cells were considered as the membrane-bound part. The media was precipitated with TCA while cells were lysed at 4°C using a Lysis buffer (25mM TRIS pH 7.4, 150 mM NaCl, 1 mM EDTA, 1 % Triton X-100 and a protease inhibitors cocktail).

Both media and cellular fractions were analysed by Western blot. As negative and positive controls, antibodies against GM130 (a bona fide membrane marker) and GAPDH (a cytosolic marker) were used, respectively. In parallel, the same experiment was performed for immunofluorescence analyses. GM130 antibody was added during the 37°C incubation, as a read-out of the extent of the permeabilisation step. After this incubation, cells were fixed in 4% paraformaldehyde and processed for indirect immunofluorescence. Sec31 antibody was used to visualise ERES,

while for GM130 only the Alexa-conjugated secondary antibody was used. For fluorescence analyses, only cells positive for double-staining were considered.

2.12 Electron microscopy techniques

The following experiments were performed in collaboration with A. A. Mironov, G. Beznoussenko and D. Di Giandomenico (Consorzio Mario Negri Sud, Italy) and Elena Polishchuck (IBP, Naples, Italy).

2.12.1 Post-embedding techniques

The name of these techniques derives from the fact that the labelling is performed after the sample embedding. The cryosectioning technique is the most important technique for post-embedding sub-cellular immunocytochemistry.

2.12.2 Materials

MultiwellTM (6 well) tissue culture plates were purchased from Becton Dickinson (France). Acetylated bovine serum albumin (BSA-cTM) was purchased from Aurion (Wageningen, The Netherlands). Protein A conjugated with 5, 10 and 15 gold particles were provided by J. Slot (Utrecht University, Utrecht, The Netherlands). Grids, paraformaldehyde and glutaraldehyde were purchased from Electron Microscopy Sciences

(USA). Uranyl acetate and glycine were purchased from Fluka (CH). Cold fish skin gelatin, gelatin, BSA and methyl cellulose were purchased from Sigma (USA). Sucrose was purchased from Carlo Erba (Italy). Whatman 50 filter papers were purchased from Whatman (UK).

2.12.3 Ultrathin cryosectioning

The cells were fixed by adding to the culture medium the same volume of a mixture of PHEM (10 mM EGTA, 2 mM MgCl2, 60 mM PIPES, 25 mM HEPES, pH 6.9) buffer, 4% paraformaldehyde, 2% glutaraldehyde for 2 h, and finally stored in storage solution (PHEM buffer, 0.5 % paraformaldehyde) overnight. After washing with 0.15 M glycine buffer in PBS, the cells were scraped and pelleted by centrifugation, embedded in 10% gelatin, cooled on ice, and cut into 0.5-mm blocks in the cold room. The blocks were infused with 2.3 M sucrose, which acts as a cryo-protectant, and then placed onto small specimen pins. The pins were frozen by immersion in liquid nitrogen, quickly transferred to a pre-cooled (–60 °C) cryo-chamber fitted onto an ultramicrotome (Leica Ultracut R) and trimmed to a suitable shape. The sections were cut at –120 °C using a dry diamond knife and collected on the knife surface. Sections were retrieved from the knife by picking them up on a small drop of a 1:1 mixture of 2.3 M sucrose and 2% methyl cellulose and transferred onto formvar- and carbon-coated specimen grids. Samples were processed for immuno-labelling as described in the following section.

During immuno-labelling, the grids were kept floating on drops of buffered saline solution, with the section side in the liquid. The back of the grid was kept dry and the section side was kept hydrated at all times. The grids were washed in 500 μl droplets of PBS for 3× 10 min and then additionally washed 3× 3 min with 0.02 M glycine in PBS, pH 7.4. For double immuno-labelling, the grids were incubating with anti-Sar1 and anti-Sec31 antibodies diluted 1:20, then with goat anti-mouse or rabbit immunoglobulin antibodies (bridge antibody). Finally, sections were incubated with Protein A-gold of different sizes (10 nm and 15 nm). Then, the grids were washed 5× 1 min in distilled water and stained for 5 min in 1.8% methyl cellulose plus 0.4% uranyl acetate, on ice. The grids were retrieved with a stainless steel loop, onto a piece of Whatman 50 filter paper at an angle of 45°. After air-drying, the grids were examined under a Philips Tecnai-12 electron microscope (Philips, Einhoven, The Netherlands) using an ULTRA VIEW CCD digital camera.

2.13 Sedlin expression in Medaka

Total RNA, total lysates and sections derived from *Orytias Latipes* (Medaka) were kindly provided by Dr. Ivan Conte.

RT-PCR to detect sedlin transcript was performed using the following primers:

Sedlin-Medaka-fw   5'- GGAAGCAAATTTCAACAAAGG -3'

Sedlin-Medaka-rev   5'- GTGTGATTGGTAGACTACAC -3'

Western blotting analyses and immunofluorescence studies were carried out as described in the previous sections.

AIM

The main aim of my Ph.D. project was to investigate the role of sedlin, a component of the TRAPP complex and the product of the gene (SEDL) mutated in Spondylo-epiphyseal dysplasia tarda (SEDT). To date, the TRAPP complex has been implicated in the homotypic fusion of COPII carriers (Yu et al., 2006; Cai et al., 2007) and as a guanine exchange factor (GEF) for Rab1 in mammals (Yamasaki et al., 2009 and see Introduction section). However, the specific role of sedlin has not been determined so far. Defining the role of sedlin will not only shed light on the role of the mammalian TRAPP complex but will be also extremely important for understanding the molecular mechanisms underlying the onset of SEDT.

It has been proposed that mutations in the SEDL gene cause defects in collagen homeostasis/transport (Tiller et al., 2001; Sacher, 2003). However, there is little direct evidence at present to substantiate this hypothesis, which is based mainly on the histology of a single SEDT patient whose chondrocytes showed a dilated rough ER and some short or frayed collagen fibrils (Tiller et al., 2001). Whether these characteristics are truly representative of the SEDT disorder is uncertain, due to the lack of more extensive histopathological analyses (Tiller et al., 2001). How sedlin might regulate this homeostasis/transport remains elusive and there are no data available about the role of sedlin in membrane trafficking.

As mentioned above, the link to collagen homeostasis and transport has been also proposed as sedlin is a component of the TRAPP complex that is involved in early steps of the secretory pathway (Sacher et al., 2001; Yu et al., 2006; Cai et al., 2007; Barrowman et al., 2010). Many hypotheses about the role of sedlin in cartilage development or in membrane trafficking have been generated, but so far no evidence about its functions has been provided.

The main goals of my Ph.D. project were thus to:

1. investigate the role of sedlin in membrane trafficking;

2. define molecular mechanisms in which sedlin is involved (through the identification of novel interactors);

3. study the impact of the sedlin KD/mutations reported in SEDT patients on membrane trafficking in SEDT-related cell lines (i.e. chondrocytes);

4. set up the basis for the development of an animal model of SEDT.

In Chapter 3, I will focus on the results related to tasks 1 and 2, while the task described in point 3 will be discussed in Chapter 4, and finally task 4 will be discussed in Chapter 5, the last of the Results section.

Chapter 3

Results

The role of sedlin in membrane trafficking

Previous studies performed in Dr. De Matteis' laboratory in mammalian systems regarding the most evolutionarily conserved TRAPP subunit, Bet3, led to the finding that this TRAPP subunit is specifically required for ER exit of large secretory cargoes (i.e. procollagen I, PCI). Injection of a blocking anti-Bet3 antibody caused a block in PCI transport at the level of the ER, while different cargoes, such as the reporter protein vesicular stomatitis virus glycoprotein (VSV-G), reached the GC (Scanu T., PhD Thesis, 2008 unpublished data). This suggested that TRAPP is selectively required for procollagen incorporation into transport carriers leaving the ER.

Based on these results, and on the consideration that SEDT had been hypothesized to result from defective secretion of ECM components, I focused my studies on the role of sedlin in membrane transport.

3.1 Sedlin depletion in different cell lines

At the beginning of this study nothing was known about the effects of silencing sedlin in human cells, so I developed a cell model system in which to study the impact of sedlin knock-down (KD) using siRNA inhibition. Sedlin KD was compared not only to control conditions (using non-targeting siRNAs), but also with the KD of another component of the TRAPP complex, namely Bet3, which is a key component of the TRAPP complex (Sacher et al., 2001). Moreover, from the comparative analyses of the two conditions, I sought to discriminate whether the consequences of sedlin KD could be ascribed to the impairment of the function of the TRAPP complex or to sedlin-specific dysfunction, unrelated to the TRAPP complex.

Conditions for the transient silencing of sedlin in different cell lines (HeLa, human fibroblasts and HepG2) were established using siRNAs against sedlin (**Figure 3.1**). These siRNAs target both sedlin and the "transcribed" sedlin pseudogene *SEDLP1* (see Introduction). The efficiency of the siRNA silencing was measured by Western blot analysis with sedlin-specific antibodies that were developed in the lab (see Materials and Methods).

Sedlin levels were significantly reduced (to 10-15% of the level in untreated cells or in cells treated with non-targeting siRNAs) after 72 hrs of treatment (96 hrs for HF, **Figure 3.1**). Sedlin KD did not affect the levels of other TRAPP subunits (**Figure 3.1** and Scrivens et al., 2009), in contrast to Bet3

A

```
CH X   ATGTCTGGGAGCTTCTACTTTGTAATTGTTGGCCACCATGATAATCCAGTTTTTGAAATG  60
CH19   ATGTCTGGAAGCTTCTACTTTGTAATTGTTGGTCACCATGATAATCCAGTTTTTGAAATG
       ***   ** ***************** ***** **** ***********************

CH X   GAGTTTTTGCCAGCTGGGAAGGCAGAATCCAAAGACGACCATCGTCATCTGAACCAGTTC
CH19   GAGTTTTTGCCAGCTGGGAAGGCAGAATCCAAAGACGACCATCGTCATCTGAACCAGTTC
       ************************************************************

CH X   ATAGCTCATGCTGCTCTCGACCTCGTAGATGAGAACATGTGGCTATCGAACAACATGTAC  180
CH19   ATAGCTCATGCTGCTCTCGACCTCGTAGATGAGAACATGTGGCTGTCGAACAACATGTAC
       ********************************************* ************** **

CH X   TTGAAAACTGTGGACAAGTTCAACGAGTGGTTTGTGTCGGCATTTGTCACTGCGGGGCAT
CH19   TTGAAAACTGTGGACAAGTTCAACGAGTGGTTTGTGTCAGCATTTGTCACCGCGGGGCAT
       ************************************** ************ ********

CH X   ATGAGGTTTATTATGCTTCATGACATAAGACAAGAAGATGGAAATAAAGAACTTCTTTACT  300
CH19   ATGAGGTTTATTATGCTTCATGACATAAGACAAGAAGATGGAAATAAAGAACTTCTTTACT
       *****************************************************************

CH X   GATGTTTATGATTTATATATAAAGTTTTCAATGAATCCATTTTATGAACCCAATTCTCCT
CH19   GATGTTTATGATTTATATATAAAATTTTCAATGAATCCATTTTATGAACCCAATTCTCCT
       ***********************  **************************************

CH X   ATTCGATCAAGTGCATTTGACAGAAAAGTTCAGTTTCTTGGGAAGAAACACCTTTTAAGC  420
CH19   ATTCGATCAAGTGCATTTGACAGAAAAGTTCAGTTTCTTGGGAAGAAACACCTTTTAAGC
       ****** *****************************************************

CH X   TGA                                                           423
CH19   TGA
       ***
```

Name	Sequence 3'-5'
SedlN1	GGGCAUAUGAGGUUUAUUA UU
SedlN2	GAGCUUCUACUUUGUAAUU UU
SedlN3	ACAUGUGGCUAUCGAACAA UU
SedlN4	CAUAAGACAAGAAGAUGGA UU
SedlS1	UCCAUUUUAUGAACCCAAU UU
SedlS2	CAAUUCUCCUAUUCGAUCA UU

B
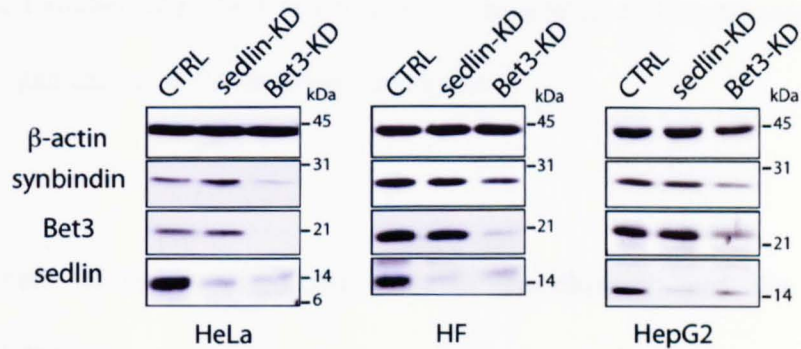
Figure 3.1 Sedlin depletion in different cell lines. (A) Sequence alignment between the SEDL ORF on chromosome X and the SEDLP1 ORF on chromosome 19, generated using ClustalW software. The two sequences differ from each other only by six nucleotides. Asterisks mark nucleotide identity. The start (ATG) and stop (TGA) codons are boxed. siRNAs used in this Thesis are highlighted with two different colours: green refers to the Dharmacon pools used in this study (n1-n4), pink to the published sequences (S1 and S2, Scrivens et al., 2009). The sequences are listed in the bottom part of the panel. **(B)** Western blot analyses of HeLa, HF and HepG2 cells after treatment with control, sedlin and Bet3 siRNAs. 60 µg of total lysate from each sample were separated by SDS-PAGE (13% gel). In sedlin-KD cells only the sedlin protein is reduced, while in Bet3-KD cells the three analysed TRAPP subunits (sedlin, Bet3 and synbindin) were strongly reduced compared to control cells. β-actin was used as a loading control.

117

KD where the levels of the other TRAPP subunits are decreased (**Figure 3.1**), as also reported by Yu et al., 2006.

Since Bet3 KD caused the depletion of the entire TRAPP complex, such cells will hereafter be referred to as TRAPP-depleted cells. The mechanism by which Bet3 controls the levels of the other TRAPP components is unclear, be it through the regulation of gene expression or protein stability. The latter possibility appears more likely considering the central position that Bet3 occupies in the TRAPP complex. Sedlin, instead, occupies a peripheral position in the complex (Kim et al., 2006), which may explain the lack of consequences of sedlin KD on the stability of the other TRAPP complex subunits.

After setting up efficient conditions for transient knock-down of sedlin by siRNAs, I studied the effect of its absence on general cell morphology and on the organization of the secretory apparatus.

3.2 Effects of sedlin depletion on cell morphology and the actin cytoskeleton

HeLa cells lacking sedlin appear flatter and larger than control cells. To test whether this reorganisation depends on alterations of actin cytoskeleton, I performed fluorescence-based analyses of sedlin-KD and mock-treated HeLa cells. Sedlin depletion affects dramatically not only the organization but also the dynamics of the actin cytoskeleton and focal adhesions in HeLa

cells, resulting in increased formation of stress fibres, decreased sensitivity to actin depolymerizing drugs (i.e. latrunculin B, LA-B) and an increase in number of focal adhesions (**Figure 3.2**). Immunofluorescence studies revealed that actin tips of the newly-formed stress fibres colocalised with markers of focal adhesions such as vinculin and phospho-tyrosine (**Figure 3.2**). Furthermore, compared to control cells, the actin stress fibres observed in sedlin-KD cells were refractory to treatment with the actin-depolymerising agent LA-B, but were totally disassembled in the presence of the selective non-muscle myosin II inhibitor, blebbistatin (**Figure 3.2**). After LA-B wash-out, the reformation of these stress fibers in sedlin-KD cells was faster than in control cells where it was possible to detect only subcortical fibres. These findings indicate that sedlin regulates actin dynamics. As a role for actin in membrane trafficking is emerging from the literature, this stabilisation of the actin cytoskeleton observed upon sedlin impairment deserves further and more detailed analyses to assess whether it is connected with the secretory phenotype we have identified in sedlin-depleted cells, which is described below.

3.3. Effects of sedlin depletion on the structure of the Golgi complex

The effect of sedlin depletion on the structural organization of the Golgi complex was examined by immunofluorescence analysis, using different Golgi markers (GM130 and TGN46), and by EM analysis (in collaboration with Sasha Mironov).
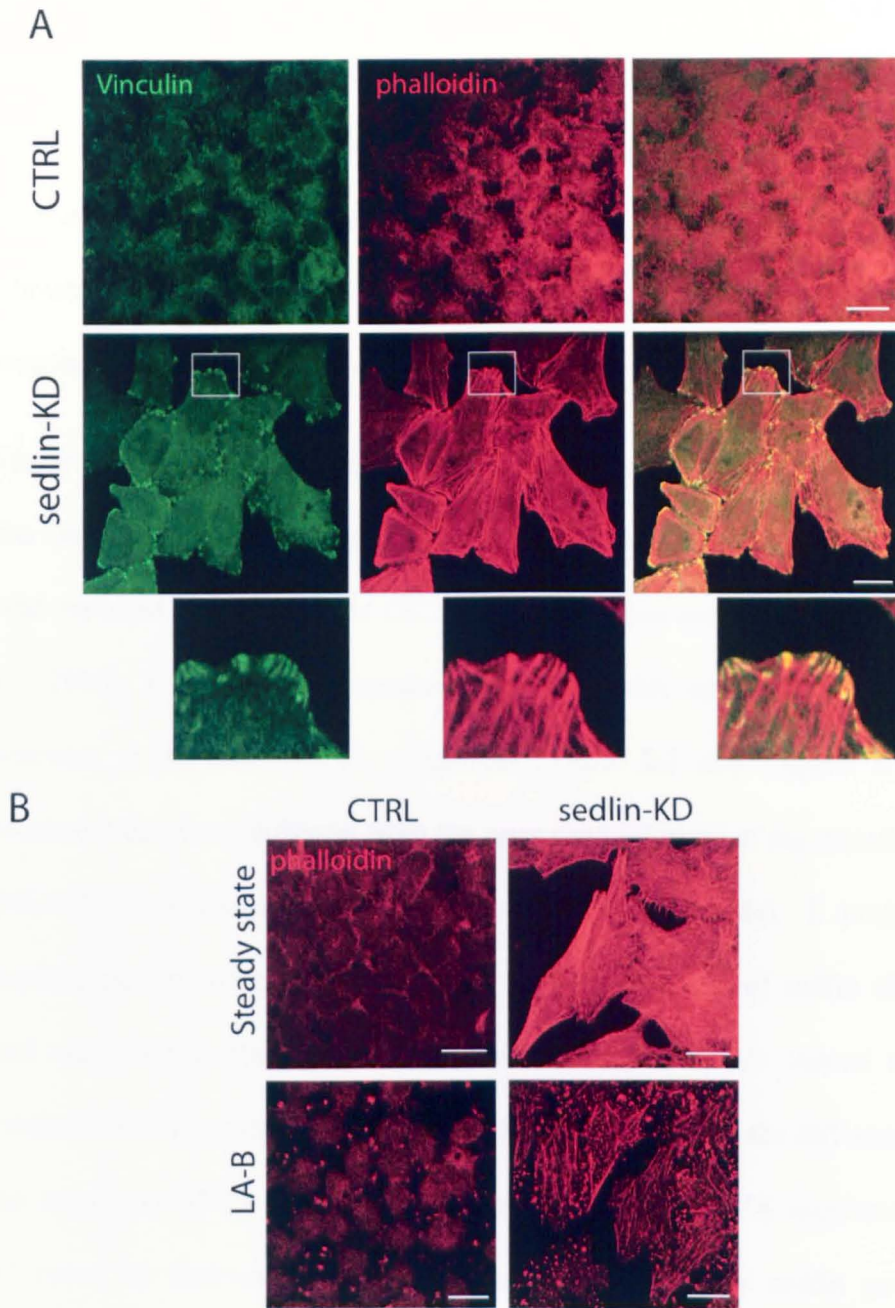
Figure 3.2 Sedlin depletion affects actin organisation. (A) siRNA-treated HeLa cells were fixed, permeabilised and incubated with a primary antibody against vinculin (focal adhesion marker) and with phalloidin (to visualise actin). Sedlin KD causes reorganization of the actin cytoskeleton (which is not found in control cells) with the appearance of stress fibres and focal adhesions localised at the tips of these structures. Scale bar 20μM. **(B)** Sedlin KD causes the formation of stress fibres resistant to latrunculin-B treatment. siRNA-treated HeLa cells were fixed and processed with phalloidin or treated for 30 minutes at 37°C with 1 μM latrunculin-B. In control cells the actin redistributes completely into round phalloidin-positive aggregates, while in silenced cells the stress fibres are still present. Scale bar 20 μm.

In contrast to Bet3 KD, which has been shown to induce Golgi fragmentation (Yu et al, 2006, **Figure 3.3**), the Golgi complex in sedlin-KD cells appears well developed and organized, both at the immunofluorescence and ultrastructural levels (**Figure 3.3**). Indeed, the ultrastructural analysis showed a well-preserved ribbon and the average lengths of the Golgi cisternae were twice that of control cells (**Figure 3.3**).

These findings, i.e. that sedlin depletion does not induce fragmentation of the Golgi complex, are in apparent contrast with data from Scrivens et al. who reported a compromised GC morphology upon sedlin KD (Scrivens et al., 2009). I explored the reasons underlying this apparent discrepancy. Scrivens et al. used siRNA sequences (**Table 2.2** and **Figure 3.1**, see Methods) that were different from the ones used for most of my experiments (N1-N4 from Dharmacon, see Materials and Methods). I performed experiments to compare the effects of the different sets of sedlin siRNAs and verified that the siRNAs used by Scrivens et al. do indeed induce extensive GC fragmentation (**Figure 3.4**). Then I analysed the differences in the sequences of the siRNA used (**Figure 3.1**). The siRNA sequences S1, S2 (used by Scrivens et al.) target transcripts from the sedlin gene on chromosome X and SEDLP1 on chromosome 19, but also one from another pseudogene located on chromosome 8 (Gecz et al., 2000). This gene, called SEDLP2, is not translated, but it could be transcribed and thus it might play a role in the stability of sedlin mRNA, as recently reported for other products of processed pseudogenes (Berger et al., 2011). This difference may underlie the higher efficiency of depletion achieved with the siRNA sequences S1, S2 (to 5% residual sedlin) compared to the sequences I used

A

CTRL — TGN46 | GM130 | merge

sedlin-KD — TGN46 | GM130 | merge

Bet3-KD — TGN46 | GM130 | merge

B

CTRL | sedlin-KD

GC | GC

Length of golgi cisternae (µm)

■ CTRL
□ sedlin-KD

2.0
1.5 — 1.59
1.0 — 0.89
0.5
0

n = 50
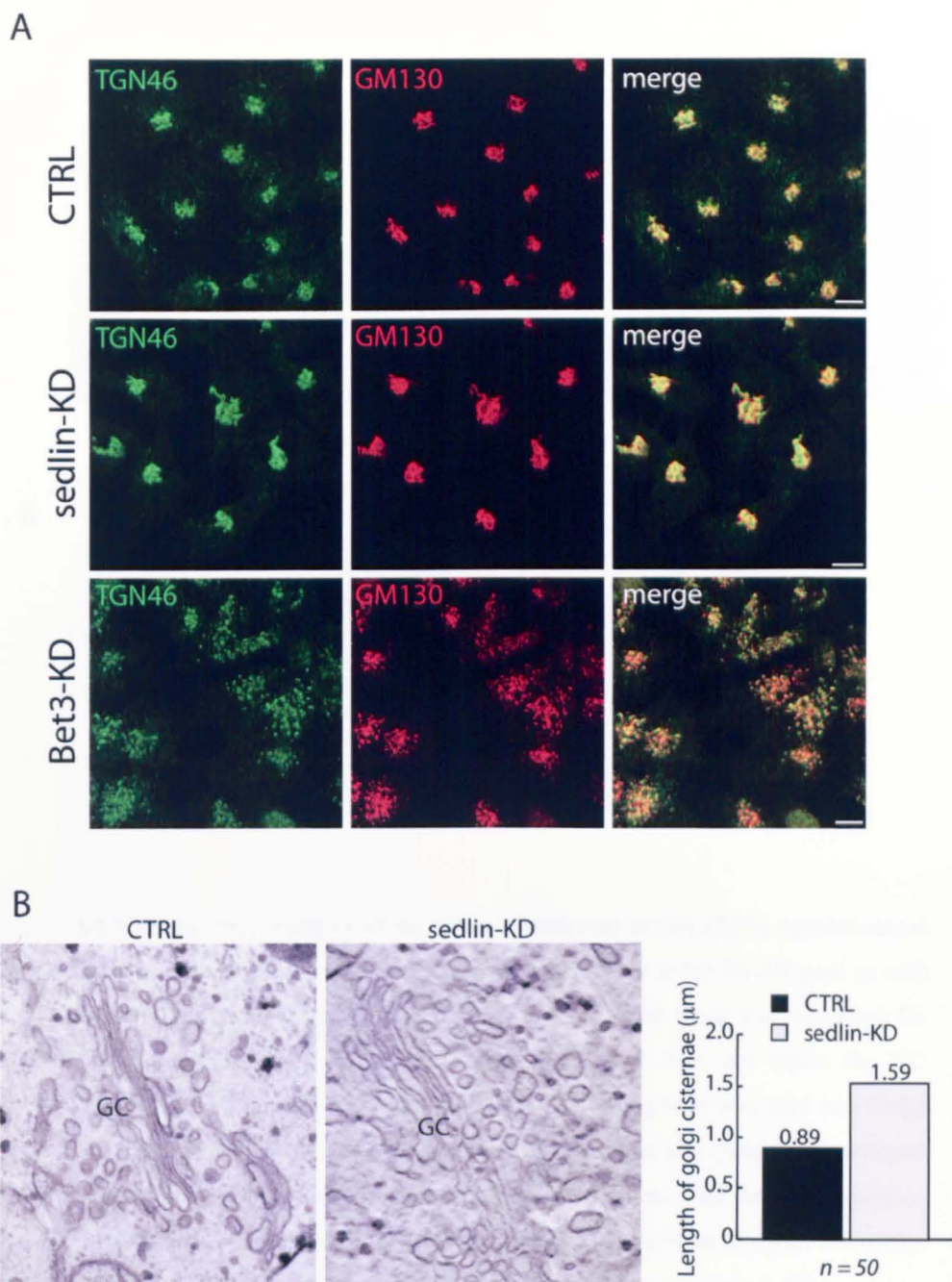
Figure 3.3 Sedlin depletion does not affect the structure of the Golgi complex. (**A**) HeLa cells were mock (CTRL), sedlin- or Bet3-siRNA treated for three days. Cells were then fixed and stained using two different Golgi markers: TGN46 (green) and GM130 (red). In control cells, the GC appears as a continuous structure concentrated in the perinuclear region. A similar GC morphology is evident also in sedlin-KD HeLa cells, while upon Bet3 depletion, the GC shows a fragmented staining pattern, in accordance with previous reports (Yu et al., 2006). Scale bars, 10 µm. (**B**) Ultrastructural analysis of sedlin-KD HeLa cells show an intact GC morphology. (Left) HeLa cells were treated as described in (A) and then processed for EM (see Materials and Methods). Notably, in sedlin-KD cells the GC appeared unaltered compared to control conditions. Scale bars, 200 nm. (Right) Morphometric analyses show that the average length of the Golgi *cisternae* is doubled in sedlin KD cells compared to control cells (n=50).
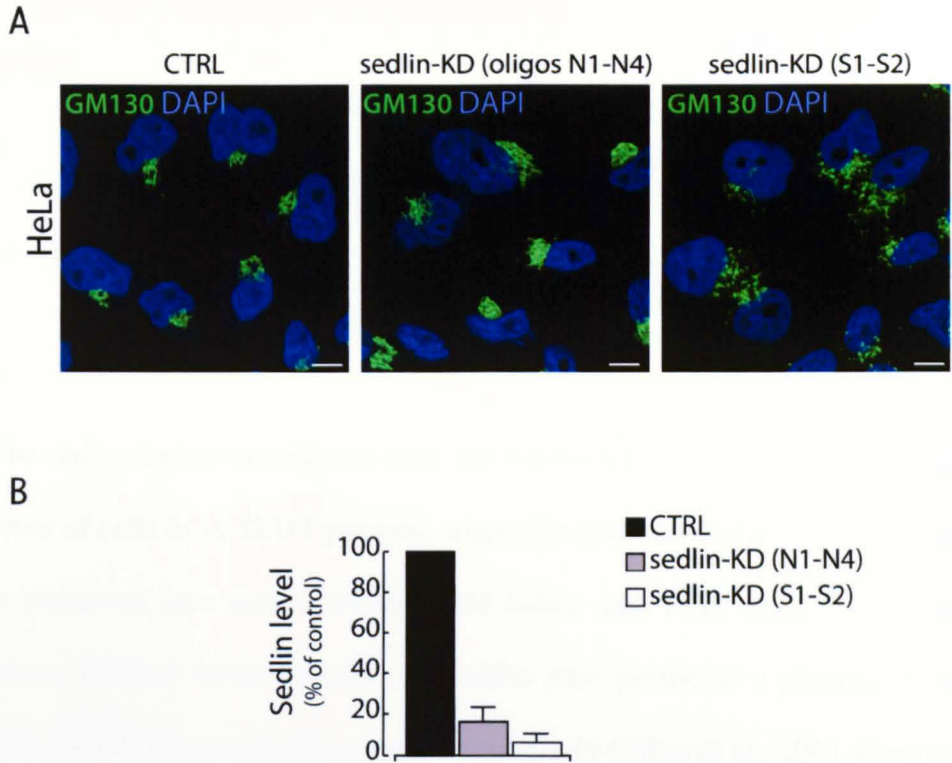
Figure 3.4. Comparative analysis of the effect of different sedlin siRNA combinations on Golgi complex morphology. (A) HeLa cells were treated with the N1-N4 pool or with S1-S2 pool at a final concentration of 60 nM. Cells were then fixed and processed for immunofluorescence analysis. Sedlin-KD with N1-N4 pool does not effect the GC structure, while the S1-S2 pool fragments the Golgi. GM130 (green) was used as a Golgi marker and DAPI (blue) for nuclear staining. Scale bars, 10 μm. (B) Quantitative analysis of the amount of the sedlin protein in cells after siRNA treatment with the N1-N4 pool or the S1-S2 pool, as determined by Western blot analysis of cell lystaes using an anti-sedlin antibody. Data represent mean values from three independent experiments ± SD.

throughout this work, N1-N4 (to 10-15% of control value). A possibility that remains to be explored for the S1, S2 siRNAs (and that we have excluded for the N1-N4 siRNAs with rescue experiments, see below) is that of off-targeting effects.

The sedlin depletion achieved with the N1-N4 siRNAs more closely mimic those of cells from SEDT patients, where the structure of the Golgi complex is preserved (see section **Figure 4.14** below and Tiller et al., 2001) and where residual levels of wild type sedlin may persist as a product of the transcribed retropseudogene on chromosome 19 (Tiller et al., 2001, Scrivens et al., 2009).

3.4 Sedlin in membrane transport: analyses of different classes of cargo upon sedlin depletion

The trafficking of different classes of cargo molecules was analysed to study the impact of sedlin KD on ER-to-Golgi transport. I chose several model proteins as representative of distinct classes: VSV-G and CD8 as membrane cargoes, albumin and α1-antitrypsin as small soluble cargoes, procollagen I (PCI) as a large soluble cargo.

3.4.1 Transmembrane cargoes

Secretory transport has been typically studied using ts045-G, a temperature sensitive transmembrane glycoprotein derived from the vesicular stomatitis virus, VSV-G (Balch and Keller, 1986; Kreis, 1986; Presley et al., 1997; Scales et al., 1997; Stephens et al., 2000), which enables one to follow a synchronized wave of transport along the secretory pathway. The transport of VSV-G along the secretory pathway can be synchronized by incubating cells at 40°C, which results in reversible misfolding and retention in the ER, and then shifting the cells to 32°C to release the ER block. Adopting this synchronisation protocol I followed the intracellular transport of VSV-G in sedlin-KD and Bet3-KD cells by immunofluorescence. HeLa cells were treated with non-targeting (control), sedlin and Bet3 siRNAs for three days. The cells were then VSV-infected at 32°C for 45 minutes and incubated for 3 hrs at 40°C, to allow VSV-G accumulation inside the ER. They were then shifted to the permissive temperature (32°C) in the presence of cycloheximide (CHX, 50 µg/ml, to inhibit further protein synthesis) and fixed at different times (0, 15, 30, 60, 90 and 120 minutes) for immunofluorescence analyses.

In control cells, VSV-G reached both the GC and the PM after 60 minutes at the permissive temperature. At 90 minutes, VSV-G was no longer visible at the GC, but only at the PM.

Sedlin-KD cells did not show any significant delay in the transport of VSV-G compared to control cells (there was a delay of about 10% between control and treated cells after 60 minutes at 32°C), while Bet3-KD showed a

125

marked delay in VSV-G arrival to the PM, in agreement with previous reports (Loh et al., 2005; Yu et al., 2006 and **Figure 3.5**).

Moreover, in Bet3-KD cells VSV-G reached the fragmented GC but failed to leave the GC, revealing a defect in intra-Golgi or in Golgi-to-PM transport. The arrival to the GC was also deduced by the results of experiments in which the glycosylation state of VSV-G was assessed by pulse-labelling, immunoprecipitation and treatment with endo-H glycosidase. Here it was shown that VSV-G acquires endo-H resistance (Scanu T., PhD Thesis, 2008), which is a hallmark of arrival at the medial Golgi (see Methods).

To study the transport of the transmembrane cargo CD8, which is not synchronizable, a CD8 cDNA was micro-injected into the nuclei of control, sedlin-KD and Bet3-KD cells. Three hours post-injection the cells were treated with CHX (to inhibit further protein synthesis) and the transport of CD8 through the secretory pathway was followed by IF. CD8 was detected at the GC and at the PM 30 minutes after CHX addition and at the PM after 60 minutes in both control and sedlin-KD cells. In contrast CD8 was retained in the GC and failed to reach the PM in Bet3-KD cells (**Figure 3.6**). These findings clearly demonstrate that these transmembrane cargoes exit the ER both in sedlin and in TRAPP-depleted cells, but that TRAPP-depleted cells suffer a Golgi secretory defect compared to sedlin-depleted cells.
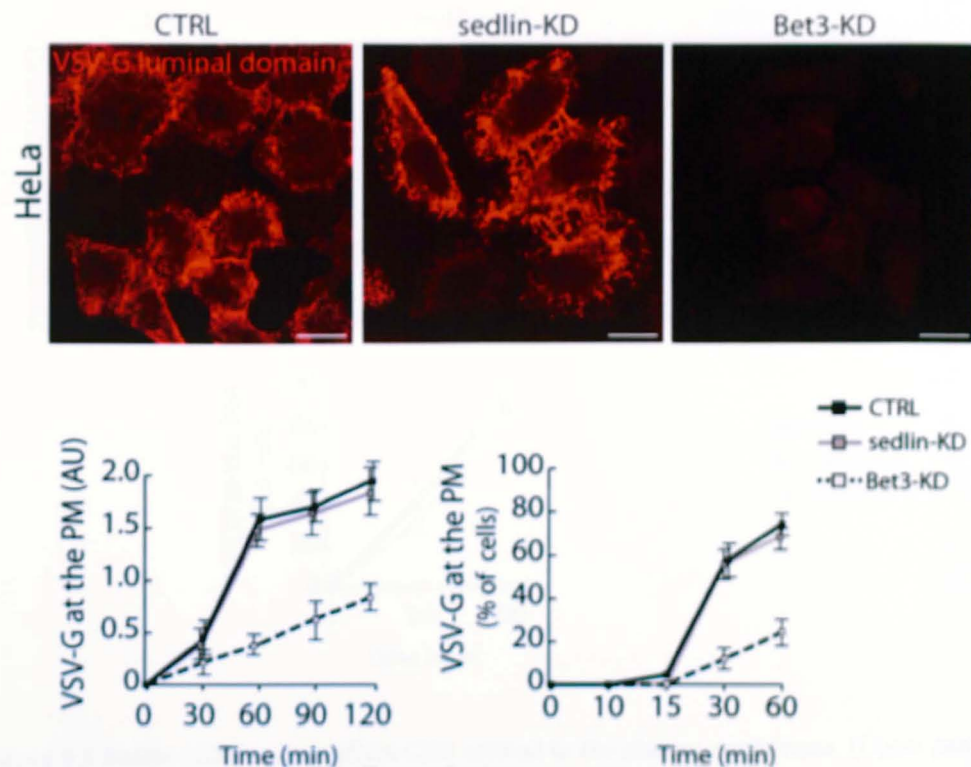
Figure 3.5 Sedlin depletion does not inhibit VSV-G arrival to the plasma membrane. (Upper panel) HeLa cells were mock (CTRL), sedlin- or Bet3-siRNA treated for three days. Cells were then infected with VSV-ts045 virus at 32°C for 1 hour, and subsequently incubated at 40°C for 3 hours, to allow VSV-G to accumulate into the ER. Cells were then shifted to the permissive temperature of 32°C in presence of CHX for 60 minutes. To measure the arrival of VSV-G to the PM, a specific antibody recognising the VSV-G luminal domain was used before permeabilising cells. Arrival of VSV-G to the PM is similar in control and sedlin-KD cells, while its delivery to the PM is strongly inhibited in Bet3-KD cells. Scale bars, 20 μm. Images were taken using the same laser parameters. (Bottom panel) Quantification of VSV-G transport in control, sedlin- and Bet3-KD HeLa cells. HeLa cells were treated as described above. After the 40°C block, the cells were incubated at 32°C for the indicated time points. (Left) VSV-G arrival at the PM was measured by evaluating the ratio between VSV-G at the PM (assessed in intact cells with an Ab directed against the luminal portion of VSV-G) and the total amount of the viral protein (assessed in permeabilized cells with an Ab directed against the cytosolic portion of VSV-G). Mean values (±SD) from 4 independent experiments (n=100). (Right) Quantification of the arrival of VSV-G to the PM in sedlin and Bet3 siRNA-treated or mock-treated (CTRL) cells. HeLa cells were treated as described above and fixed at the indicated time points. The data are expressed as % of cells with VSV-G at the PM. Each experiment was repeated at least 4 times in duplicate and the data are represented as mean values (± SD), n=200 for each time point.

127
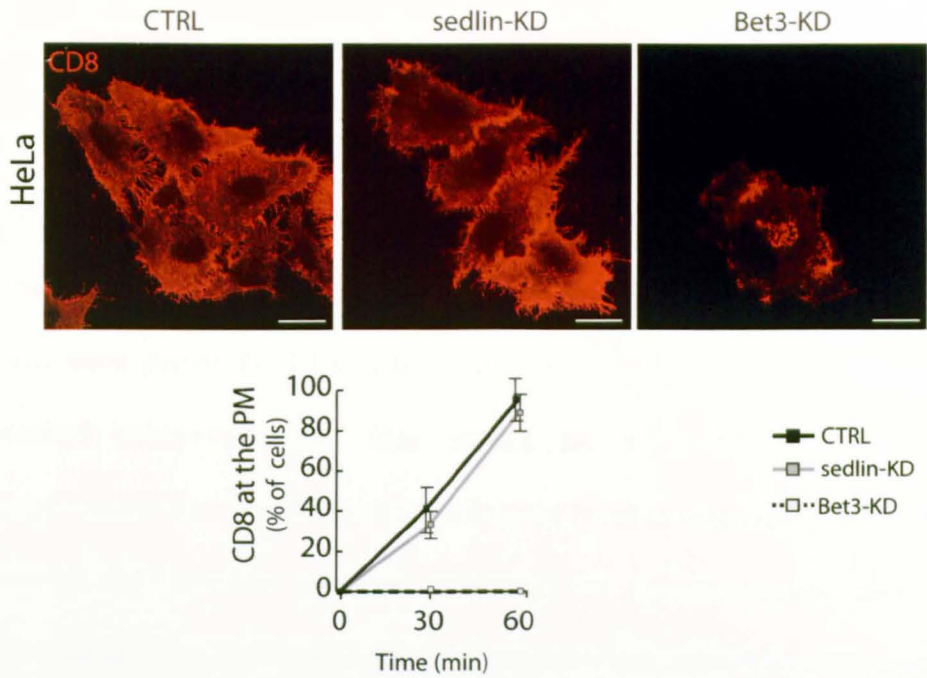
Figure 3.6 Sedlin-KD does not affect CD8 arrival to the plasma membrane. (Upper panel) HeLa cells were mock (CTRL), sedlin- or Bet3- siRNA treated for three days. Cells were then micro-injected with a plasmid encoding a CD8 cDNA. Five hours post-injection, CHX was added for 30 minutes and then the cells were fixed and processed for immunofluorescence analyses. A monoclonal antibody recognising CD8 was used. CD8 reaches the PM in control and sedlin-KD cells, while its delivery to the PM is strongly inhibited in Bet3-KD cells. Scale bars, 20 μm. Images were taken using the same laser parameters. (Bottom panel) Quantification of CD8 transport in control, sedlin- and Bet3-KD HeLa cells. HeLa cells were treated as described above. After injection the cells were incubated at 37°C for the indicated time points. Mean values (±SD) from 5 independent experiments (n=100). The data are expressed as % cells with CD8 at the PM.

3.4.2 Small soluble cargoes

To analyse small soluble molecules, the trafficking of the endogenous cargoes albumin and α1-antitrypsin was measured in HepG2 cells by pulse-chase experiments. Non-targeting (control), sedlin and Bet3 siRNA-treated cells were pulsed for 10 minutes with [^{35}S]-methionine and [^{35}S]-cysteine, washed extensively, and then chased for the indicated times. The supernatant was collected and the cells were lysed at each time point and the amount of labelled proteins analyzed by immunoprecipitation and autoradiography. Sedlin-KD cells did not show any significant difference in the amount of secreted albumin or α1-antitrypsin compared to control cells (**Figure 3.7**). By contrast, TRAPP depletion significantly inhibited the release of the two soluble cargoes (**Figure 3.7**).

I then defined the trafficking step where the transport of the different cargoes was impaired as a consequence of TRAPP depletion by evaluating the glycosylation state of the neosynthesized α1-antitrypsin as an index of its progression along the secretory pathway.

As shown in **Figure 3.7**, TRAPP depletion only marginally inhibited the ER-to-Golgi transport of α1-antitrypsin (as judged by the acquisition of the endo-H resistance after 20 minutes). These data suggested the existence of a intra- or post-Golgi transport block that would explain the marked inhibition of α1-antitrypsin release in TRAPP-depleted cells. Similarly to VSV-G, the rate of arrival of the protein to the Golgi complex was almost indistinguishable from that measured in control cells, while its progression to the PM was markedly inhibited.
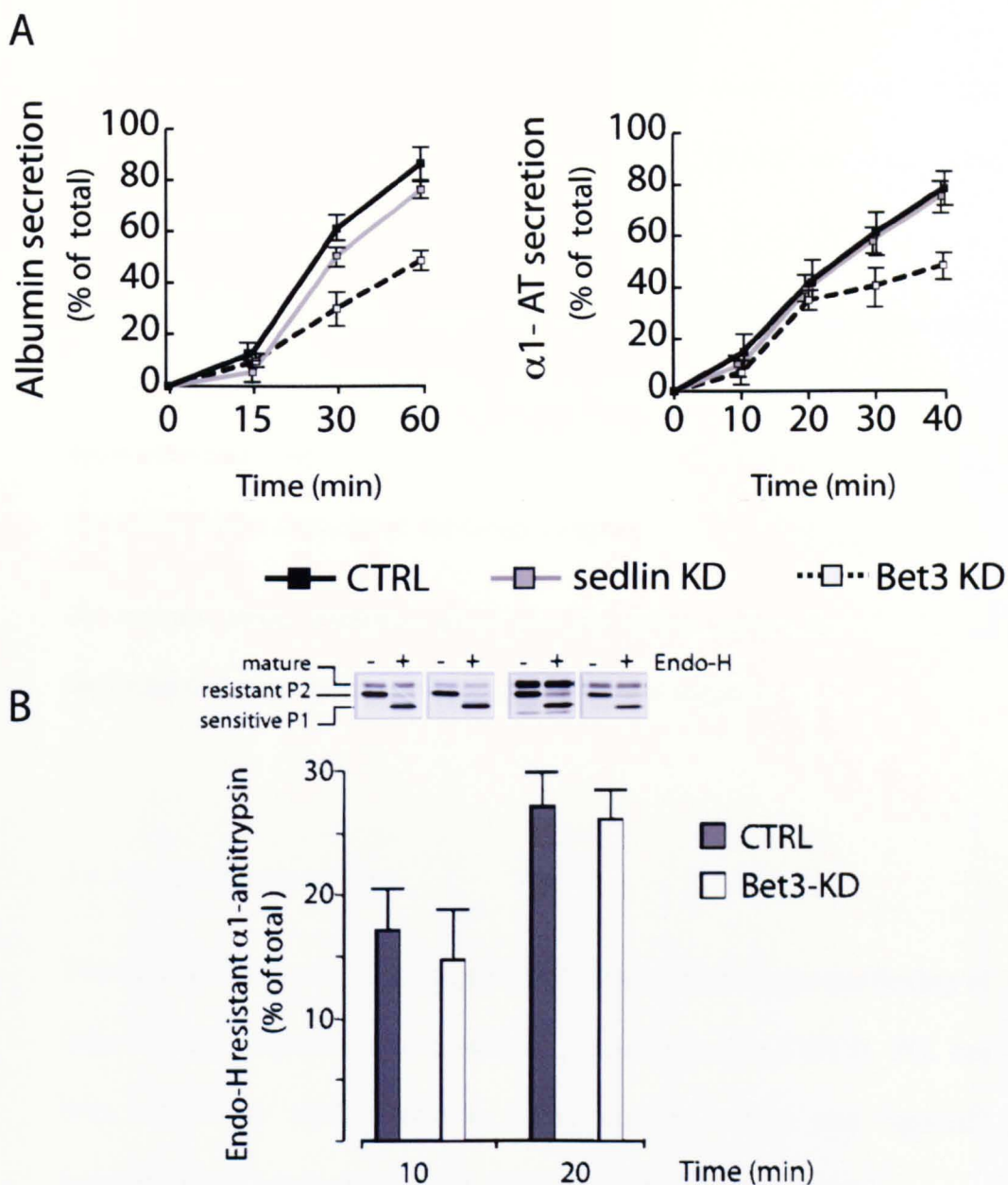
Figure 3.7 Sedlin depletion does not inhibit small soluble cargo secretion in HepG2 cells. (A) HepG2 cells were mock (CTRL), sedlin- or Bet3-siRNA treated for three days. Cells were then pulse/chased as described in Materials and Methods. Media and cell lysates were immunoprecipitated with anti-albumin (left) or anti-α1-anti-trypsin (α1-AT, right) antibodies, separated by SDS-PAGE and quantified using InstantImager. Mean values (±SD) from three independent experiments performed in duplicate. Control and sedlin-KD cells secrete both albumin and α1-AT at a similar rate, while Bet3-KD cells show a significant delay in the secretion of both cargoes. (B) Endoglycosidase H resistance analysis of α1-AT in control and Bet3-KD HepG2 cells. Control and Bet3-KD HepG2 cells were pulse/chased as described in (A). After immunoprecipitation of cell lysates the samples were treated (+) or not (-) with endoglycosidase H and then analysed by SDS-PAGE and autoradiography (top panel). α1-AT shows three discrete bands (mature, P1 and P2). P1 is the α1-AT band sensitive to the EndoH. (Panel labels in top). The graph shows quantification of the P1 band, mean data (±SD) from 3 independent experiments run in duplicate. No differences are detected between mock and TRAPP depleted cells, meaning that the α1-AT arrival to the GC is not impaired.

Moreover, similar results from the CD8 analysis (whose arrival to the PM but not to the GC was severely impaired in TRAPP depleted cells) reinforced this hypothesis.

Together with the above results on the Golgi complex disorganization induced by TRAPP depletion, these results on the trafficking of neosynthesized proteins show that the TRAPP complex is required for the structure and the function of the Golgi complex.

By contrast, sedlin depletion alone does not affect neither the structure of the Golgi complex nor the trafficking of analysed cargoes.

3.4.3 Large soluble cargoes

To evaluate the impact of sedlin and TRAPP depletion on the trafficking of large soluble cargo, I chose to analyse procollagen type I (PCI). PCI has been extensively studied because of its unique features and "special" requirements in terms of synthesis, folding, transport and secretion.

PCI is a thermo-sensitive synchronizable cargo as it is partially unfolded and blocked in the ER at 40°C: in order to leave the ER it needs the permissive temperature of 32°C and ascorbic acid (ascorbate), a cofactor for prolyl 4-hydroxylase which regulates synthesis and folding of collagens to generate a trimeric collagen in the ER (Pinnel et al., 1987). Following exit from the ER, PCI is transported to the Golgi complex and then to the PM where it is secreted into the extracellular medium (Mironov et al., 2001).

First, I set up a protocol to obtain very efficient reduction of sedlin and Bet3 protein levels in human fibroblasts (professional PCI secretory cells) by electroporation of the siRNAs and by prolonging the treatment to 96 hours. The synchronizable PCI transport assay was then applied to these cells.

The exit of PCI from the ER was strongly inhibited both in sedlin-KD and Bet3-KD fibroblasts (**Figure 3.8**), in contrast to the other cargo molecules described above. The small fraction of PCI that reached the GC in these fibroblasts remained blocked in this compartment.

I measured also the ability of control, sedlin and Bet3 siRNA-treated HFs to secrete PCI into the extracellular medium. Both sedlin-KD and Bet3-KD cells showed a decreased amount of secreted PCI compared to control cells (**Figure 3.8**).

To test whether the impaired exit of PCI from the ER upon sedlin/TRAPP depletion was induced or exacerbated by cargo overload in the ER during the 40°C block, sedlin-KD and Bet3-KD fibroblasts were treated with ascorbate for 24 hours at 37°C, to facilitate PCI intracellular trafficking. The cells were then fixed and PCI distribution analysed by immunofluorescence. PCI was found at the GC in control cells but was localised in the ER and in the GC in both sedlin-KD and Bet3-KD cells (**Figure 3.8**). Thus, the defect in PCI exit from the ER in sedlin and TRAPP depleted cells is not due to protein overload or temperature stress, but instead is a very specific effect of sedlin/TRAPP impairment.
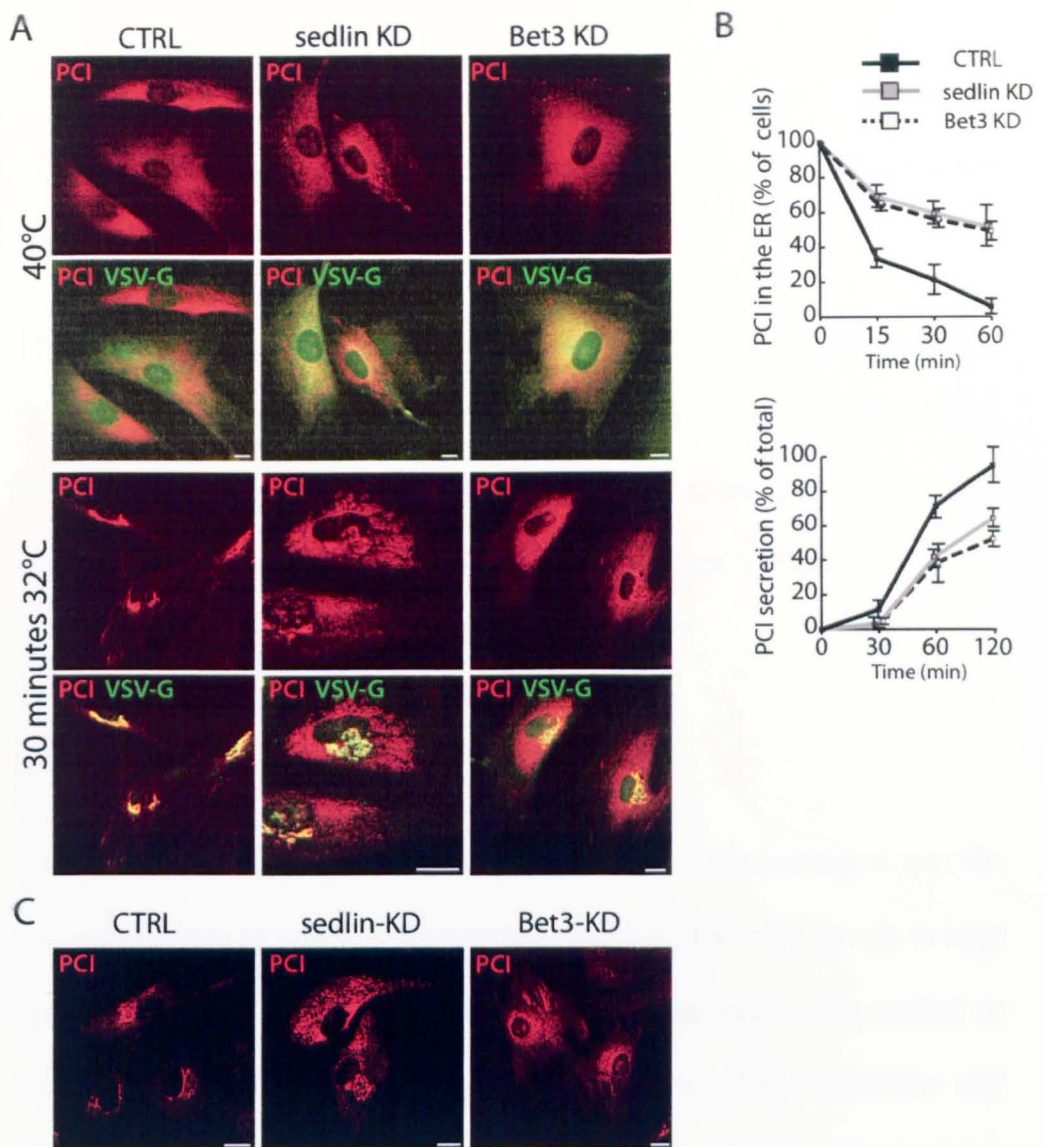
Figure 3.8 Sedlin and TRAPP complex are selectively required for ER exit of procollagen type I in human fibroblasts. (A) HF cells were mock (CTRL), sedlin- or Bet3-siRNA treated for 96 hours. Cells were infected with VSV-ts045 for 1 hour at 32°C and then shifted to 40°C for 3 hours, to accumulate both PCI (red) and VSV-G (green) into the ER. Fibroblasts were either fixed or incubated for 30 minutes at 32°C in the presence of ascorbate and CHX and fixed. (Upper panels) During the temperature block, mock, sedlin-KD and Bet3-KD cells accumulate PCI and VSV-G inside the ER. (Bottom panels) After the addition of CHX and ascorbate, cells were shifted to 32°C for 30 minute, fixed and stained. In control cells both VSV-G and PCI localise in the perinuclear area. PCI fails to exit the ER in sedlin-KD and Bet3-KD cells while VSV-G reaches the GC similarly to control cells. Scale bars, 10 μm. (B) Quantitative analysis of the ER exit of PCI (top) and of PCI secretion (bottom) in human fibroblasts. ER exit is expressed as % of cells with PCI in the ER while PCI secretion is expressed as % of total PCI (PCI in the medium/PCI in the medium+PCI in the cell). The data refer to 5 independent experiments run in duplicate. The graphs report mean values (±SD) (n=200). (C) PCI transport in HFs without the synchronisation protocol. Mock, sedlin-KD and Bet3-KD cells were incubated at 37°C for 24 hours in the presence of ascorbate. Cells were then fixed and stained for PCI (red). In control cells, PCI is mainly localised in the perinuclear area, while in sedlin-KD and Bet3-KD cells it is still present into the ER. Scale bars, 10 μm.

Identical results were obtained analysing ER-to-Golgi transport of endogenous PCI in rat fibroblasts (NRK) after sedlin and Bet3 depletion (**Figure 3.9**).

To directly compare the differential effect of sedlin and TRAPP depletion on ER exit of different cargoes, I then studied the trafficking of VSV-G and PC-I within the same cells. As above, while VSV-G reached the GC, PCI was retained into the ER in sedlin-KD and Bet3-KD cells (**Figure 3.9**).

3.4.4 Total protein secretion

Finally, in order to assess in an "unbiased" way (i.e. not looking at specific cargoes) the role of sedlin in the secretory pathway, I studied its role in total protein secretion. To this end, HeLa cells were transfected with control or sedlin siRNAs and the cells were then pulsed with [^{35}S]-methionine and [^{35}S]-cystheine for 1 hour followed by a chase for 3 hours. As a positive control for conditions that block total protein secretion, HeLa cells were treated with brefeldin A (BFA), an inhibitor of protein export, and subjected to the same pulse-chase experiment. Media from the three conditions were collected at 0, 1, 2, and 3 hours of the chase and analyzed by SDS-PAGE on 4%-15% gradient gels (to separate the high- and low-molecular weight polypeptides on the same gel) followed by autoradiography.

BFA treatment, as expected, efficiently inhibited total protein secretion from HeLa cells, since no bands were visible even after 3 hours (**Figure 3.10**).
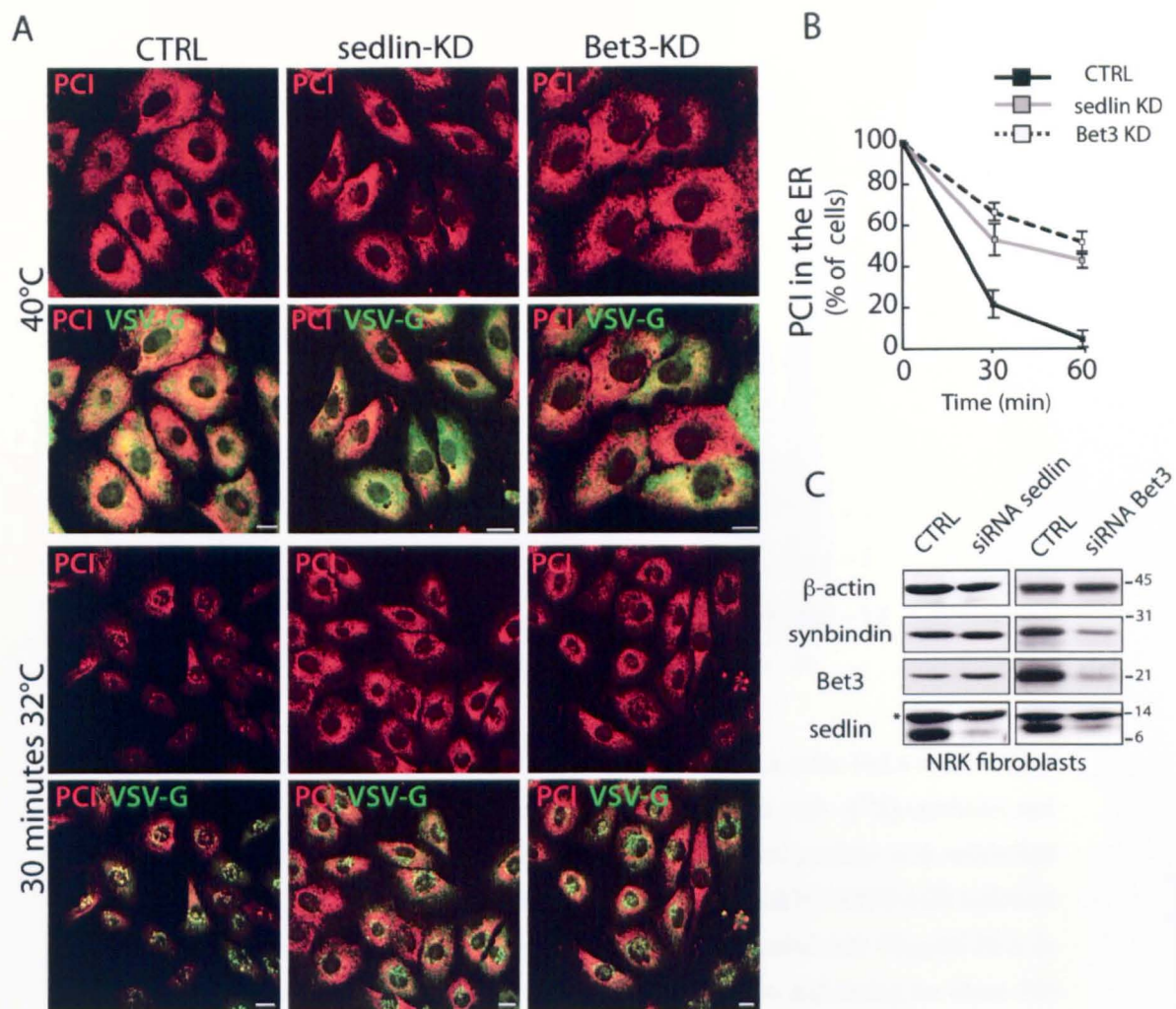
Figure 3.9 Sedlin and TRAPP complex are selectively required for ER exit of procollagen type I in NRK49F fibroblasts. (**A**) Mock (CTRL), sedlin-KD, and Bet3-KD NRK49F were analyzed for PCI and VSV-G trafficking as described in Figure 3.8 (A). Scale bars, 10 μm. (**B**) Quantitative analysis of the ER exit of PCI in NRK fibroblasts. ER exit is expressed as % cells with PCI in the ER. The data (means ±SD) refer to 3 independent experiments run in duplicates (n=100). (**C**) NRK fibroblasts (NRK49F) were treated with the indicated siRNA. Cell lysates (60 μg/sample) were analyzed by SDS-PAGE and immunoblotting with the indicated antibodies. β-actin was used as a loading control. Asterisk indicates non-specific band. Note that sedlin KD does not the affect protein levels of other TRAPP subunits, Bet3 or synbindin.
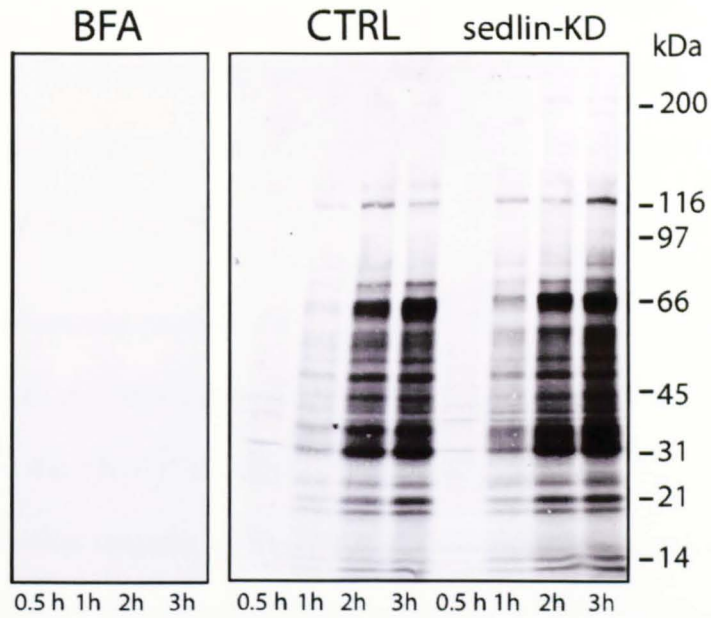
Figure 3.10 Sedlin-KD does not affect total secretion in HeLa cells. HeLa mock treated (CTRL) or sedlin siRNA (sedlin-KD) treated cells were pulsed with $-[^{35}S]$-cystheine and methionine for 60 minutes, then washed and cultured in standard medium with unlabelled methionine. After 0.5, 1, 2 and 3 hours the medium was analyzed by SDS-PAGE followed by autoradiography. As a negative control, mock cells were treated with 10μg/ml BFA (a blocker of protein secretion) for the last ten minutes of the pulse and during the chase. No significant difference is detectable between sedlin-KD and control cells, while BFA-treated cells fail to secrete any protein.

Importantly, sedlin knockdown did not affect the overall amount of protein secreted by HeLa cells (**Figure 3.10**). These findings indicate that sedlin does not have a role in global protein secretion but in contrast exerts a specific role in PCI secretion.

Sedlin is selectively required for PCI to exit the ER, but it is dispensable for ER exit of all the other analysed cargoes (transmembrane and small soluble ones). Also the TRAPP complex is selectively needed for ER export of PCI but not of other cargoes, even though the absence of a functional TRAPP has an inhibitory effect on intra-Golgi and Golgi-to-PM trafficking steps.

3.5 Rab1 is not involved in the selective inhibition of the ER exit of PCI

Next, I dissected the molecular mechanism underlying the requirement for sedlin/TRAPP in PCI export by analyzing the involvement of a known TRAPP effector, the small GTPase Rab1.

Rab1 has been implicated in the tethering and fusion reactions occurring during ER-to-Golgi trafficking. COPII vesicles, which develop from specialized exit sites on the endoplasmic reticulum (ER exit sites: ERES), are tethered together by the action of Rab1 together with its effector p115 to give rise to vesicular-tubular clusters (VTCs) adjacent to the Golgi (Allan et al., 2000; Alvarez et al., 1999; Bannykh et al., 1996; Cao et al., 1998). As mentioned above, recent findings show that TRAPP binds COPII vesicles

by direct interaction with the coat, thus providing a mechanism to ensure that all vesicles can recruit active Rab1 (Cai et al., 2007). Indeed, the TRAPP complex acts as a GEF for Rab1. In addition to its role in COPII vesicle tethering, Rab1 may also have a function in regulating the exit of secretory cargo from the ER. This idea derives from the observation that Ypt1 and Uso1, the yeast homologues of Rab1 and p115, respectively, were found to play a role in coupling the sorting of secretory cargo to vesicle formation (Morsomme and Riezman, 2002).

Thus, I assessed whether the defect in PCI transport out of the ER observed in TRAPP depleted cells could be ascribed to Rab1. To this end I used two approaches: I assessed the effect of sedlin/TRAPP depletion on the Rab1 cycle in living cells and examined whether or not the depletion of Rab1 (both Rab1a and Rab1b) reproduced the secretory phenotype of sedlin/TRAPP depletion. Rab GTPases switch between a GTP-bound state in which they are membrane-associated and a GDP-bound state in which they become cytosolic upon membrane extraction by the Rab GDI (Seabra and Wasmeier, 2004). Thus, the membrane-cytosol cycle of Rab GTPases reflects their GTP/GDP bound state and the rate of membrane release of Rab GDP (as assessed by FLIP) gives an indication of the RabGDP/RabGTP ratio (McCray et al., 2010).

The rate of release of Rab1 from membranes, as measured by FLIP (see Materials and Methods) was unaffected in sedlin-KD cells (**Figure 3.11**), thus indicating that sedlin depletion does not affect the Rab1 cycle. This observation is consistent with the report that sedlin is not required for the Rab1 GEF activity of TRAPP *in vitro* (Kim et al., 2006).

138
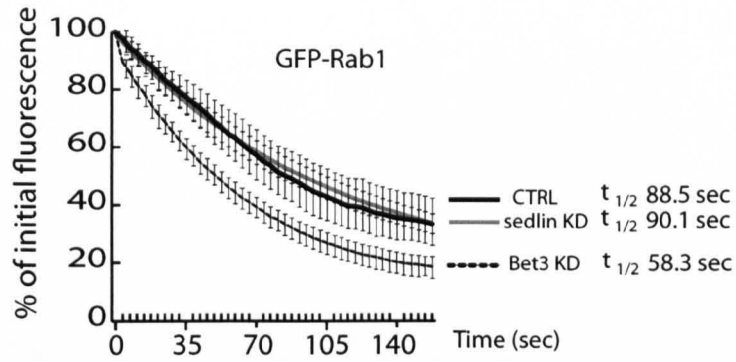
Figure 3.11 Bet3-KD, but not sedlin-KD, affects the Rab1 cycle. Human fibroblasts were treated with non-targeting (CTRL), sedlin, or Bet3 siRNAs and then transfected with a Rab1-GFP construct by micro-injection. The control and silenced cells were analyzed in Fluorescence Loss In Photobleaching (FLIP) experiments to assess the cycle of Rab1 at the Golgi complex (see Materials and Methods). While GFP-Rab1 has comparable dynamics in control and sedlin-KD cells, it dissociates faster from membranes in Bet3-KD cells. The values are the mean (±SD) from 4 independent experiments, n=15. The FLIP half-life ($t_{1/2}$) is indicated.

By contrast, depletion of the entire TRAPP complex by Bet3 KD severely altered the cycle of Rab1, which was more readily released from the Golgi membranes (**Figure 3.11**). Since Bet3 KD causes Golgi fragmentation, I considered the possibility that the faster dissociation of Rab1 from Golgi membranes might be a non-specific consequence of this fragmentation. To this end, the GFP-Rab1 cycle was measured using an alternative approach that leads to GC fragmentation. Cells were treated with GM130 siRNAs (Marra et al., 2007) to induce Golgi vesiculation. Upon GM130 depletion GFP-Rab1 showed the same rate of association and dissociation to and from membranes as control and sedlin-KD cells (not shown). This finding rules out the hypothesis that the Rab1 cycle depends on the integrity of the GC.

Importantly, the depletion of Rab1 by the combined KD of Rab1a and Rab1b mimicked the effects of TRAPP depletion on the Golgi complex, which was extensively vesiculated (**Figure 3.12**), but did not reproduce the selective inhibition of PCI exit from the ER observed upon sedlin (and TRAPP) depletion in HFs (**Figure 3.13**).

The above data solicited a search for molecular mechanisms underlying the requirement for sedlin in the ER export of PCs. Our first consideration was the possibility that sedlin affects the machinery responsible for cargo export from the ER, which is driven by the small GTPase Sar1.
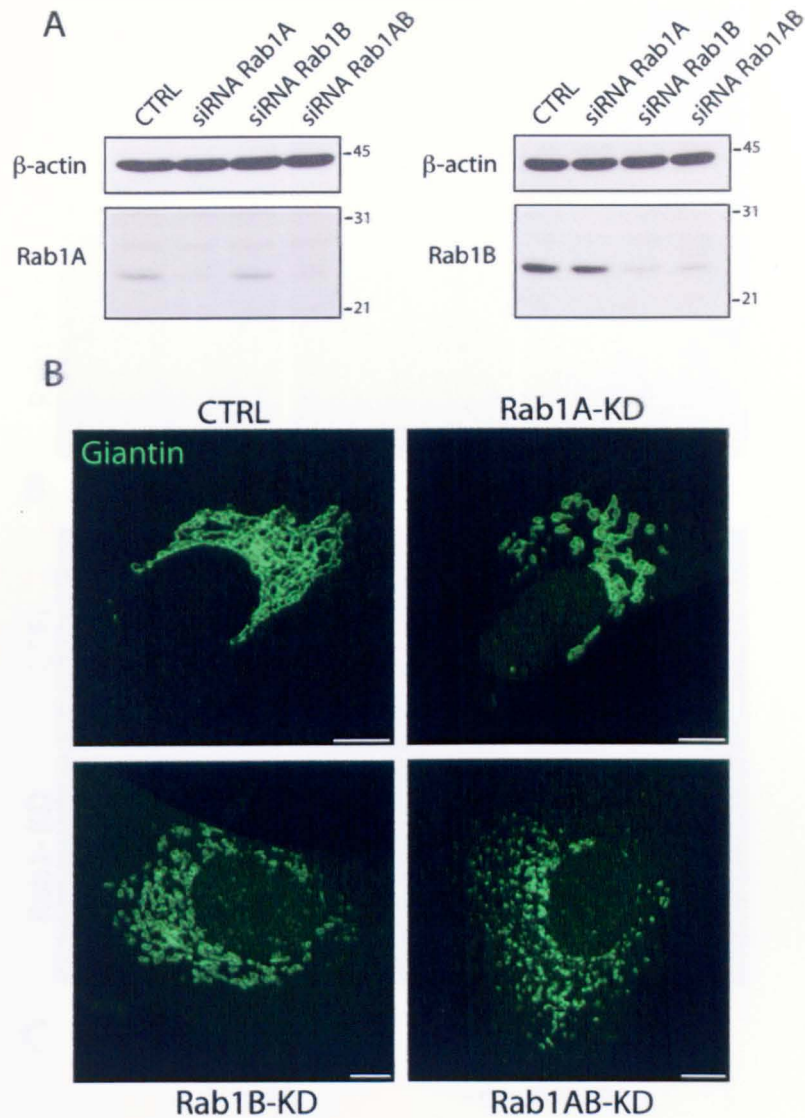
Figure 3.12 Rab1 depletion affects Golgi complex morphology. (**A**) HFs were mock (CTRL) treated or treated with specific siRNA directed against the A and/or B isoforms of Rab1. 96 hours after electroporation (see Materials and Methods), cells were lysed and 30 µg of total lysates were separated by SDS-PAGE and processed for immunoblot analysis. Notably, Rab1A-KD does not cause any alteration in Rab1B levels and vice versa. β-actin was used as a loading control. (**B**) HFs were treated with siRNAs as described in (A), then fixed and stained to evaluate the GC structure by indirect immunofluorescence. While in control cells giantin (green) highlights a continuous Golgi structure, under Rab1 depletion giantin marks a very fragmented GC. Scale bars, 10 µm.
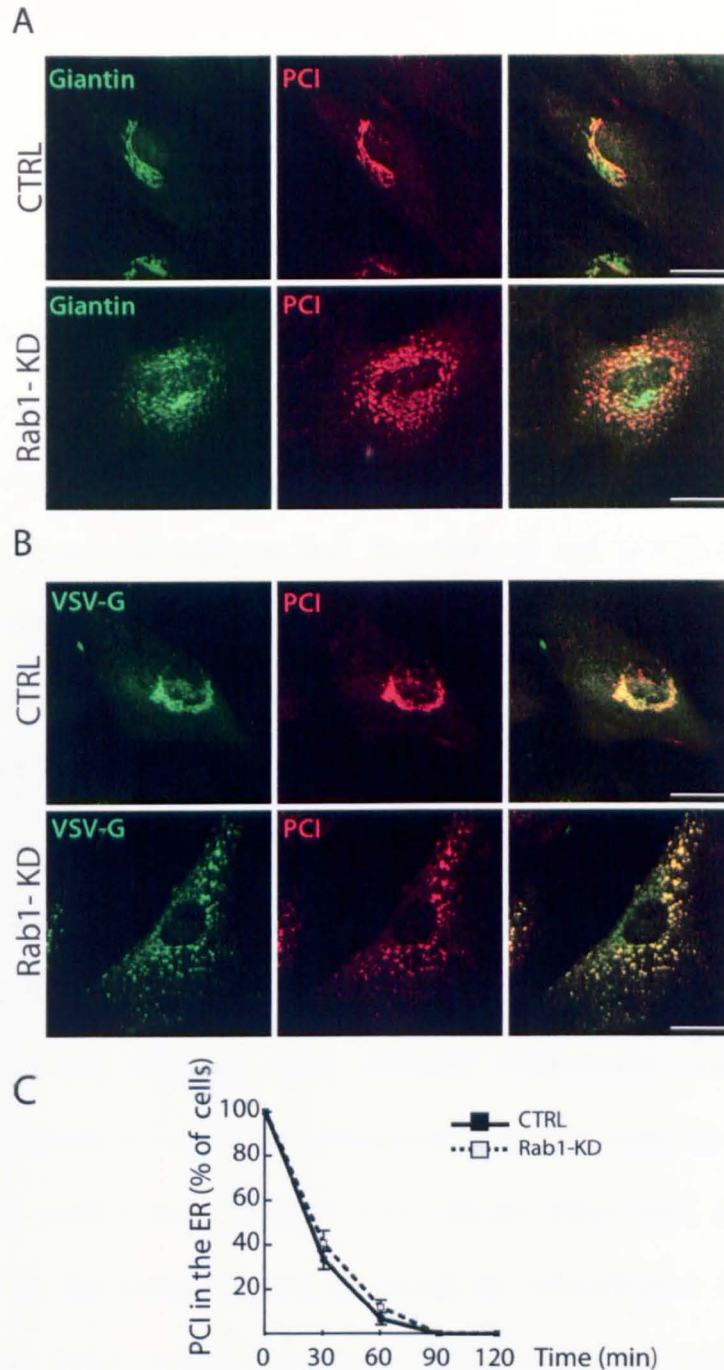
Figure 3.13 Rab1 depletion induces vesiculation of the Golgi complex but does not induce the selective inhibition of PCI exit from the ER. (A) Human fibroblasts were treated with non-targeting siRNA (CTRL) or siRNAs against both Rab1A and Rab1B isoforms (Rab1 KD) for 96 hrs, incubated at 40°C to synchronize cargo transport, shifted to 32°C for 30 minutes and then stained for PCI (red) and giantin (a Golgi marker). PCI reaches the giantin positive compartment under both control and Rab1-KD conditions. Scale bars: 20 µm. (B) VSVts045-infected human fibroblasts were treated as in (A) and stained for PCI and VSV-G. Both analysed cargoes leave the ER similarly in control and Rab1-KD cells. Scale bars: 20 µm. (C) Quantitative analysis of the transport of PCI out of the ER. The data, expressed as % of cells with PCI in the ER, are mean values (± SD) of four independent experiments in duplicate (n=200).

3.6 Sedlin effectors: sedlin binds Sar1

To characterize the role of the sedlin protein, I first assessed its subcellular localisation using a specific anti-sedlin antibody. Western analysis of total cell lystaes from HeLa cells identified a band of 14 kDa, corresponding to the molecular weight of sedlin. Moreover, this band is sensitive to sedlin siRNA treatment, implying that this antibody can specifically recognize sedlin (**Figure 3.14**). Immunofluorescence experiments on HeLa cells with the anti-sedlin antibody showed a spotty perinuclear staining pattern together with a very bright nuclear staining (**Figure 3.14**). The presence of sedlin in the nucleus has been reported previously where it may regulate transcription by interacting with PAM14, MBP-1, SF-1 and PTX-1 (Liu et al., 2010; Jeyalaban et al., 2010). The identity of the spotty perinuclear stuctures was analysed using different compartment-specific markers. Sedlin shows a very clear colocalisation pattern with the ER exit site (ERES) marker Sec31 (**Figure 3.14**). On the other hand, sedlin was not found on the Golgi complex as shown by colocalisation analyses using different Golgi markers, either under control conditions or after nocodazole treatment (**Figure 3.15**). Nocodazole, a microtubule-depolymerising drug, is widely used to precisely define the localisation of a protein on the GC. The formation of so-called "mini-stacks" allows the clear determination of the protein at the GC and its cis- or trans-side localisation. After nocodazole treatment, sedlin does not localise at the GC, but remains in the proximity of the mini stacks. Similar behaviour was also observed for COPII components (**Figure 3.16**).
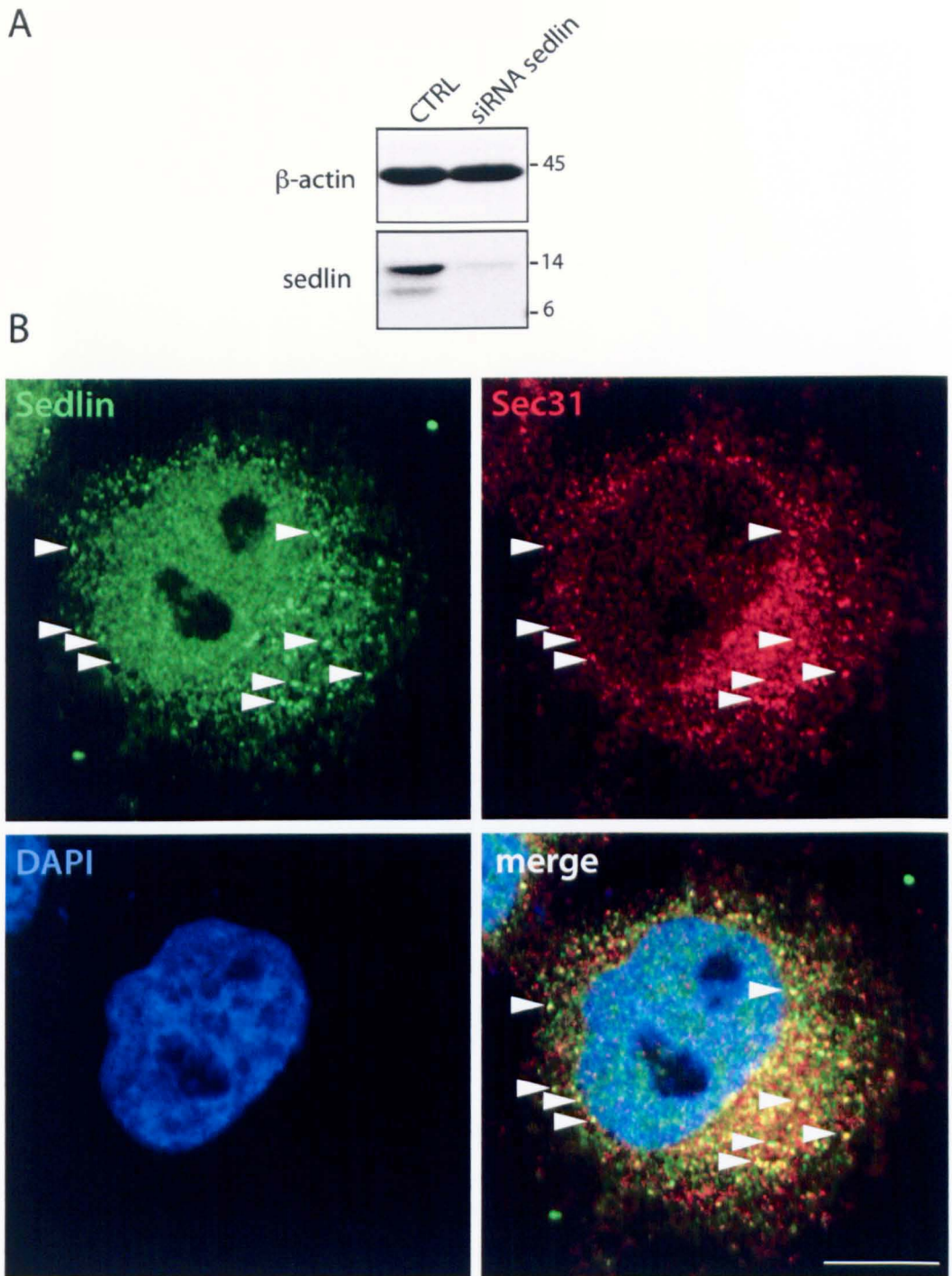
Figure 3.14 Sedlin localises at the ER exit sites in HeLa cells. (**A**) HeLa cells were treated with non-targeting siRNA (CTRL) or sedlin siRNAs for 72 hrs, then cells were lysed and 60 μg of total proteins were subjected to SDS-PAGE analysis. Immunoblot using a pAb against sedlin recognises a protein of 14 kDa (corresponding to sedlin) sensitive to the siRNA treatment. β-actin was used as a loading control. (**B**) Control HeLa cells were fixed and stained with the same anti-sedlin Ab used in (A) (green) and with an anti-Sec31 Ab (red). DAPI stain cell nuclei. White arrows indicate sedlin-Sec31 positive ERES. Scale bars: 10 μm.
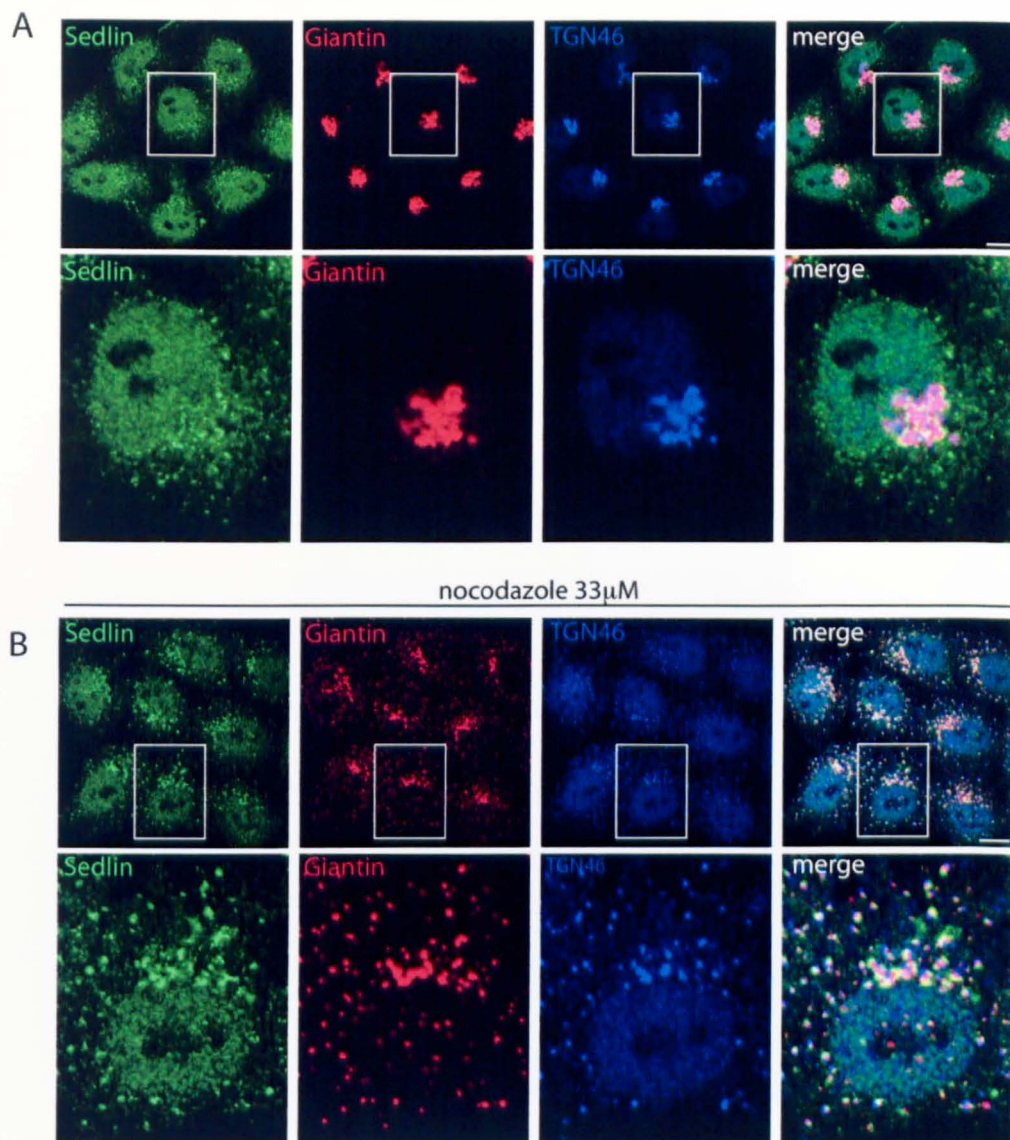
nocodazole 33µM

Figure 3.15 Sedlin does not localise at the Golgi complex. HeLa cells were seeded on glass coverslips. The next day, cells were fixed immediately or treated for 3 hours with nocodazole at 37°C and fixed. **(A)** Immunofluorescence analyses of control cells show that sedlin (green) appears localised in spotty structures (corresponding to ERES, see Figure 3.12) in proximity to the GC, stained using giantin (red) and TGN46 (blue). **(B)** After nocodazole treatment, sedlin localises close to but does not co-localise with the Golgi mini-stacks. White boxes delimitate higher magnifications, shown in the lower panels of (A) and (B). Scale bars: 10 µm.
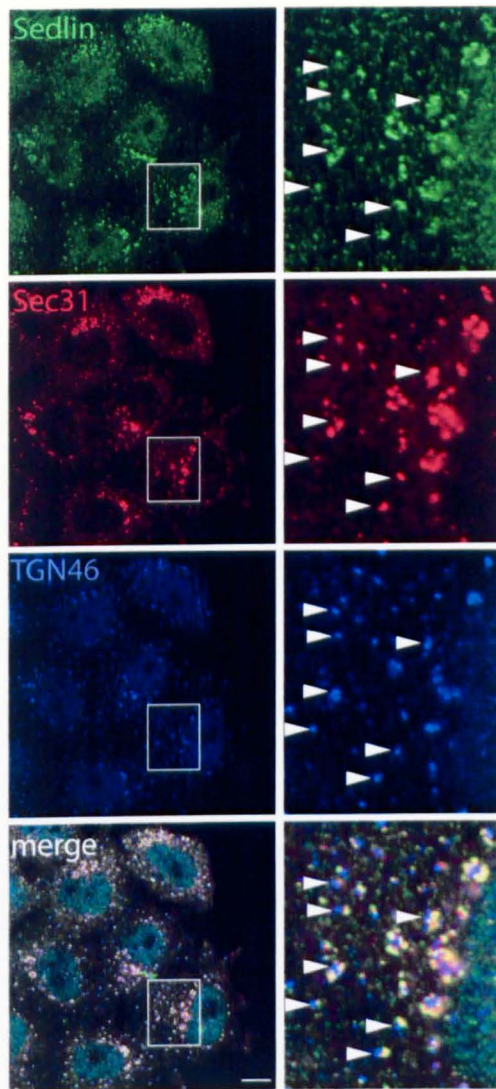
Figure 3.16 Sedlin colocalises with Sec31 upon nocodazole treatment. Control HeLa cells were treated as described in Figure 3.15. Immunofluorescence analyses show that sedlin (green) is still close to the Golgi mini-stacks after nocodazole treatment, but does not co-localise with TGN46. Instead, sedlin co-localises perfectly with Sec31 (red). White boxes delimitate higher magnifications, shown on the right side. White arrows indicate the TGN46 mini-stacks. Scale bar: 10 μm.

The COPII-sedlin localisation was performed under the same conditions and sedlin still colocalised with Sec31, indeed to an even greater extent (**Figure 3.16**).

I also followed the distribution of sedlin in (HeLa) cells treated cells with Befreldin A (BFA). BFA is a fungal toxin that provokes the redistribution of the GC into the ER, by inactivating Arf1, a GTPase that governs the structure and function of the GC. Upon BFA treatment the GC disassembles and Golgi enzymes are redistributed into the ER while Golgi matrix proteins of the cis-compartments relocalize in small punctate structures representing Golgi remnants. The ERES components are instead unchanged upon BFA treatment. Confirming its association with ERES, sedlin did not undergo redistribution upon BFA treatment, but still colocalized with Sec31-positive structures (**Figure 3.17**).

To further test the association of sedlin to ERES, I treated HeLa cells with CI-976, a compound that inhibits lysophospholipid acyl-transferase activity thus preventing COPII budding events (Brown et al., 2008) and leading to accumulation of COPII at the ERES. Under these conditions, I observed that sedlin was even more associated to Sec31, demonstrating that its binding to COPII components is dynamically dependent on their cycling (**Figure 3.18**).

The localisation of sedlin at ERES is not completely unexpected, considering the fact that Bet3, the protein mainly responsible for sedlin presence into the TRAPP complex, binds directly to another COPII protein Sec23 (Cai et al., 2007).
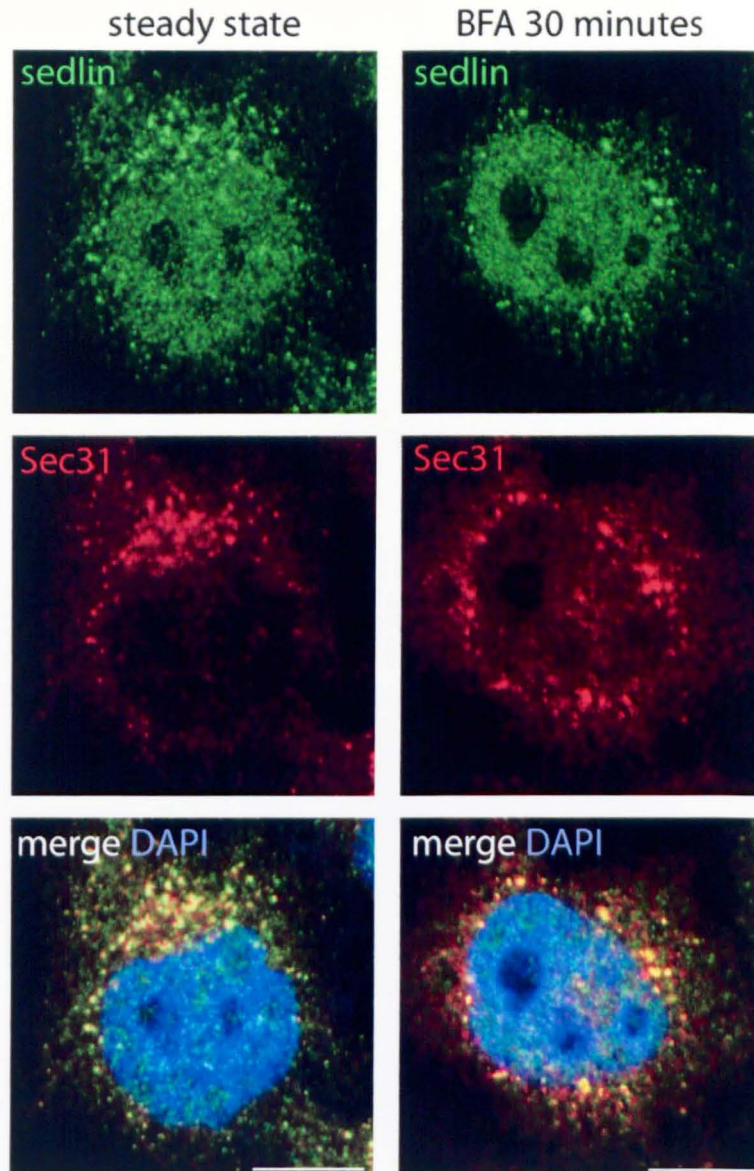
Figure 3.17 Sedlin still colocalises with Sec31 upon BFA treatment. Control HeLa cells were fixed or treated for 30 minutes with BFA (2.5 µg/ml) and then fixed and processed for immunofluorescence analysis. Sedlin (green) still colocalises with Sec31-positive structures (green) after BFA treatment. DAPI was used as a nuclei marker. Scale bar: 10 µm.
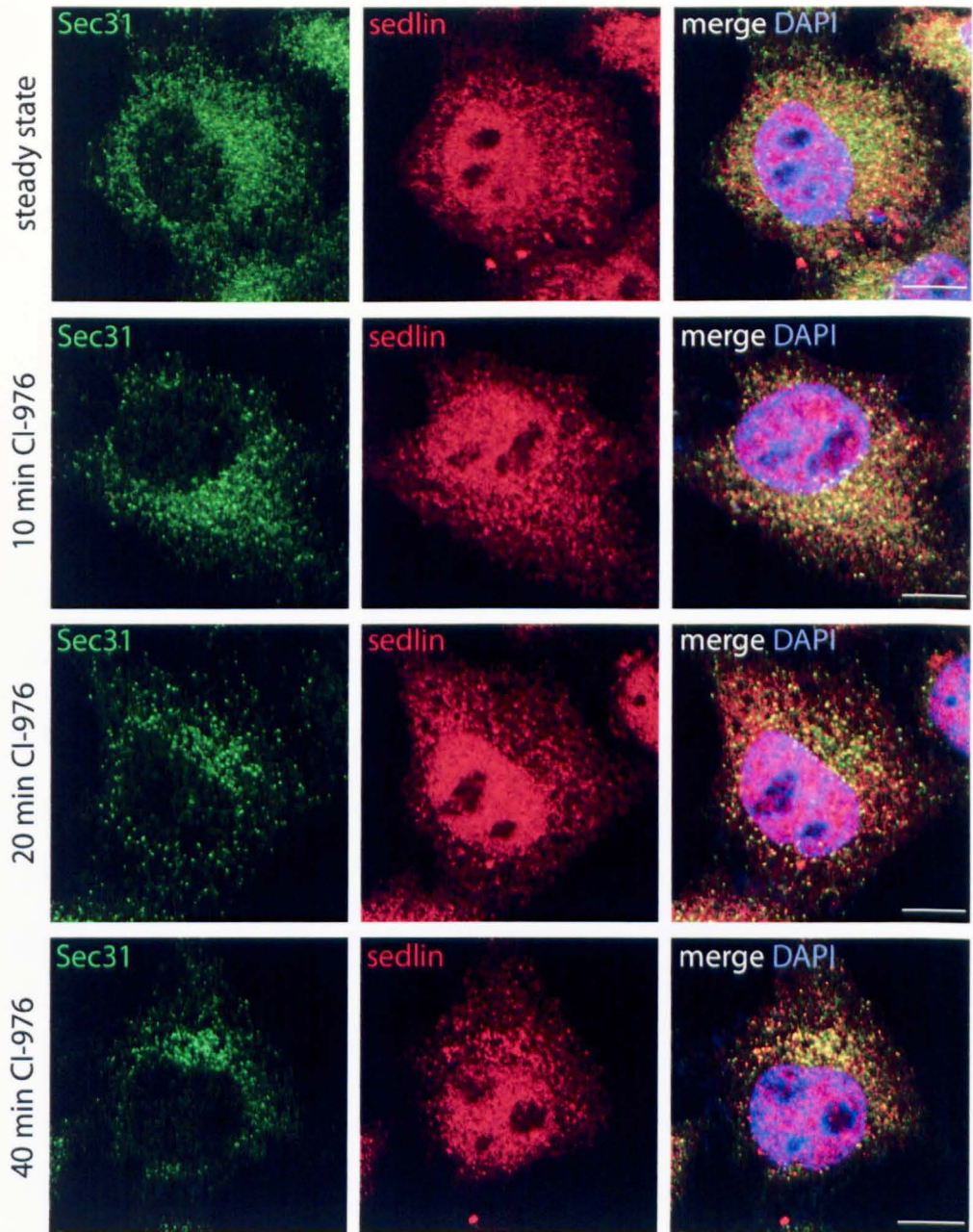
Figure 3.18 Sedlin is recruited to the ERES in the presence of the CI-976 fission inhibitor. Control HeLa cells were fixed or treated with CI-976 for the indicated time (10 µM) and then fixed and processed for immunofluorescence analysis. Since CI-976 is an inhibitor of COPII fission, Sec31 (green) is progressively recruited to the central ERES after the addition of the inhibitor. Under the same conditions, sedlin (red) is recruited to Sec31-positive structures (green). DAPI was used as a nuclear marker. Scale bar: 10 µm.

In this scenario, one possibility is that the whole TRAPP complex localises at ERES via Bet3-Sec23 interaction and that sedlin localisation is driven by Bet3-binding to COPII. The second possibility is that sedlin can localise to the ERES independently of Bet3.

I explored this possibility, also in the light of peculiar structural features of sedlin that, as described in the Introduction), is essentially composed of a longin domain. Longin domains have been proposed to exert a large variety of membrane trafficking processes (Rossi et al., 2004). Members of this family act as regulatory modules in different classes of proteins, mainly SNAREs, such as Ykt6, Sec22b, Vamp7 and others (Schenkler et al., 2006). Recently, longin domains have been also shown to be involved in the regulation of small GTPases belonging to Arf/Sar family (Schenkler et al., 2006). This is the case of signal recognition particle (SRP) and its receptor (SR).

SRP and its receptor (SR) are involved in targeting of nascent secretory and membrane proteins to ER membranes (Keenan et al., 2001; Luirink and Sinning, 2004). SRP recognizes N-terminal hydrophobic signal sequences as they emerge from the ribosomal polypeptide exit tunnel. The complex is targeted to the SR at the membrane, and the ribosome-nascent chain complex is transferred to the translocon. Thus, SRP and SR are the "initiation factors" of protein translocation mediating both targeting and the formation of the ribosome/translocon junction. Upon GTP hydrolysis in SRP and SR the complex dissociates (Doudna et al., 2004; Wild et al., 2004). Both SR and SRP are complex structures: SRP is a ribonucleoprotein consisting of six distinct protein subunits and one RNA subunit (Walter and

Blobel, 1980; Walter and Blobel, 1982). The SR complex consists of a heterodimeric membrane protein of two GTPases, SRα and SRβ, of 69 kDa and 30 kDa, respectively (Tajima et al., 1986). SRα mediates the binding to SRβ anchored to the ER membranes through its N-terminal domain, called SRX. SRX is a globular domain of 130 amino acids belonging to the SNARE-like superfamily, known as longin domains (Schwartz et al., 2003; Filippini et al., 2001). The interaction of SRX (the longin domain) and SRβ is very similar to other GTPase-effector complexes, strongly suggesting a co-GAP function (Schenkler et al., 2006). Sequence homology within the members of the longin domain family is very low, but the structural homology is remarkably high. The structural homology between sedlin and SRX had been noted by Schenkler et al. (2006) who reported a very nice fit of sedlin with SRX (Figure..in Schlenker et al.). As noted above, SRX binds SRβ, which belongs to the Arf-Sar family and Sar1 is the GTPase responsible for the assembly, formation and regulation of COPII carriers. Thus, I tested whether sedlin and Sar1 might interact similarly to SRX/ SRβ. In collaboration with Dr. Alex Spaar, based on this structural similarity existing between the two proteins, we superimposed Sar1A-GTP and sedlin onto the SRβ:SRX complex and generated a model of a putative complex between Sar1 and sedlin (**Figure 3.19**).

Prompted by this homology modelling I investigated whether sedlin can directly interact with Sar1. I assessed sedlin-Sar1 binding (both the A and B isoforms) in pull-down assays and found that GST-sedlin, but not GST alone, was able to bind both Sar1A and Sar1B (**Figure 3.20**).
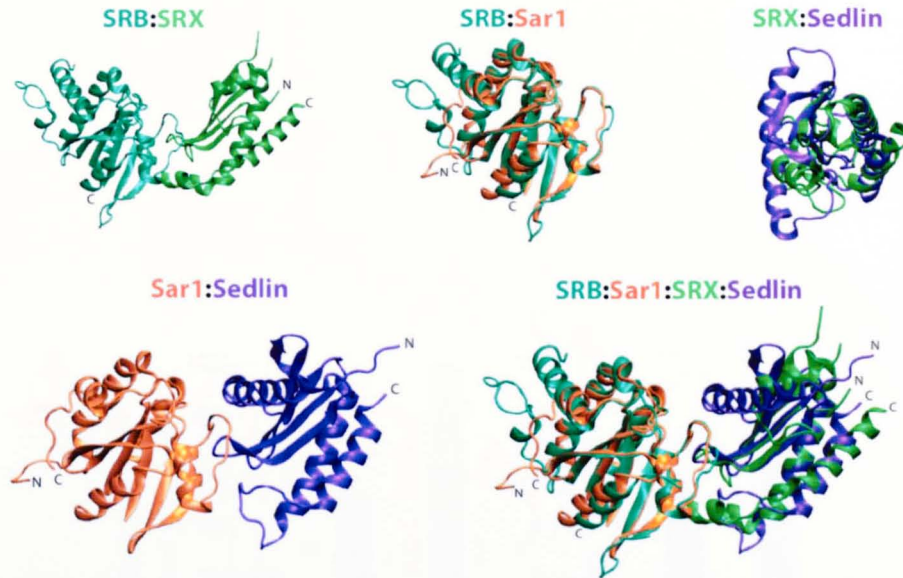
Figure 3.19 Modelling of the sedlin-Sar1 interaction. Superimposition modelling shows that the sedlin structure overlaps with that of the longin domain of SRX. Sar1 is the GTPase most similar to SR (SRB), as reported by Schenkler et al., in 2006. The modelling was created in collaboration with Dr. Alex Spaar.
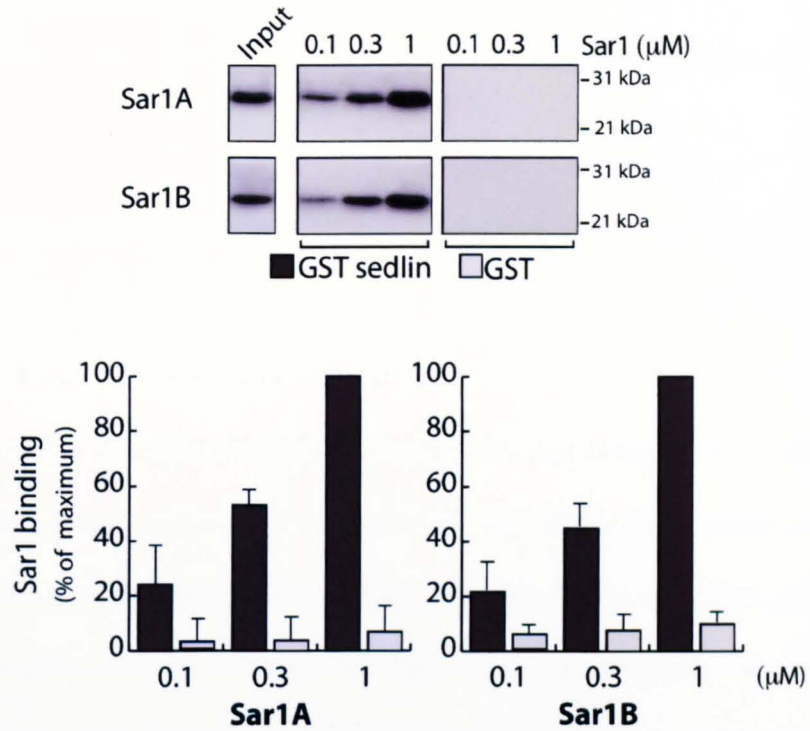
Figure 3.20 Sedlin binds directly to Sar1 *in vitro*. Pull-down assays were performed on glutathione-Sepharose beads using increasing concentrations of His-Sar1 (both A and B isoforms, 0.1, 0.3, 1 μM) with GST-sedlin or GST alone (each 0.5 μM). Input, 200ng Sar1 (equivalent to 2.5% of the amount used in the 1 μM incubation). Sedlin binds similarly to both Sar1 isofroms. The graphs report the results of the quantitative analysis of sedlin-Sar1 binding. Values are expressed as % of the sedlin-Sar1 binding relative to 1 μM His-Sar1 (Maximum), and are the means (± SD) of three experiments performed in duplicate.

Among the TRAPP subunits tested, only Sar1 bound specifically to sedlin, as neither Bet3 nor Trs31 could pull down Sar1 in the same assay (**Figure 3.21**).

I next checked the dependence of this interaction on the nucleotide bound state of Sar1 and found that sedlin preferentially interacts with Sar1-GTP (**Figure 3.22**). Taking advantage of the structural homology existing between sedlin and SRX (Schlenker et al., 2006) and between Sar1 and SRβ we modelled the sedlin-Sar1 complex on the SRX- SRβ complex and identified a putative interaction surface between sedlin and Sar1 (**Figure 3.23**). To define the site of interaction between sedlin and Sar1, we used the docking programs PatchDock (Schneidman-Duhovny et al., 2005) together with FireDock (Mashiach et al., 2008), and identified the energetically more favorable configurations of the sedlin-Sar1 complex. Several of the lowest energy docking models basically showed the same binding interface as the structure obtained by superimposing sedlin-Sar1 with SRX-SRβ (shown in **Figure 3.19**), but with a rotation of around 180°. From this docking analysis and from the collaboration with Dr. Spaar, I was able to predict that the His13 residue of sedlin should participate in the sedlin-Sar1 interaction (**Figure 3.24**). Indeed, we found that the single point mutant H13A sedlin has a greatly impaired ability to interact with Sar1 (**Figure 3.24**). This finding was very important as it adds a new level of interaction between the COPII-TRAPP machineries.
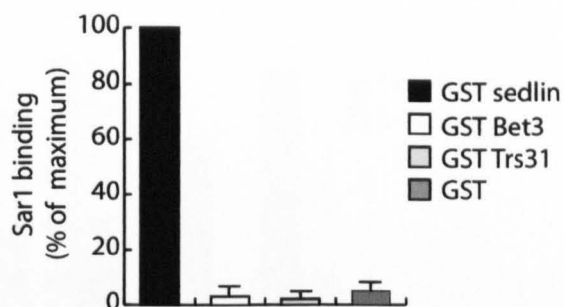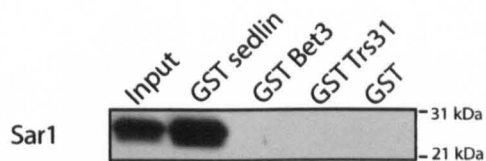
Figure 3.21 Sedlin, but not other TRAPP subunits, specifically interacts with Sar1.
Pull-down assays were performed on glutathione-Sepharose beads using 1 μM of His-Sar1
with GST-sedlin, GST-Bet3, GST-Trs31 or GST alone (each 0.5 μM). Input, 200ng Sar1
(equivalent to 2.5% of the amount used in the 1μM incubation). Sedlin is the only TRAPP
subunit to bind Sar1. The graph reports the results of the quantitative analysis of Sar1
binding. Values are expressed as % of the sedlin-Sar1 binding relative to 1 μM His-Sar1
(Maximum), and are the means (± SD) of three experiments performed in duplicate.
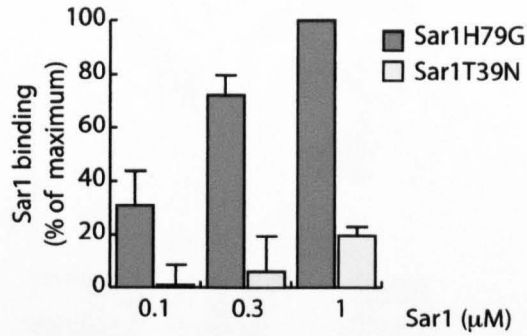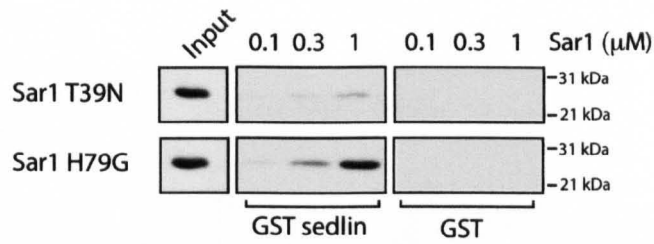
Figure 3.22 Sedlin interacts with Sar1 in a GTP-dependent manner. Pull-down assays were performed using increasing concentrations (0.1, 0.3 and 1 μM) of His-Sar1T39N (the GDP-restricted mutant) or His-Sar1H79G (the GTP-restricted mutant) with GST-sedlin, or GST alone (each 0.5 μM). Input, 200ng Sar1 (equivalent to 2.5% of the amount used in the 1μM incubation). Sedlin binds efficiently to the H79G mutant of Sar1, but has a lower affinity for the GDP-bound mutant. Thus, the nucleotide association state of Sar1 affects sedlin binding. The graph reports the results of the quantitative analysis of Sar1 binding. Values are expressed as % of the sedlin-Sar1 binding relative to 1 μM His-Sar1 (Maximum), and are the means (± SD) of three experiments performed in duplicate.
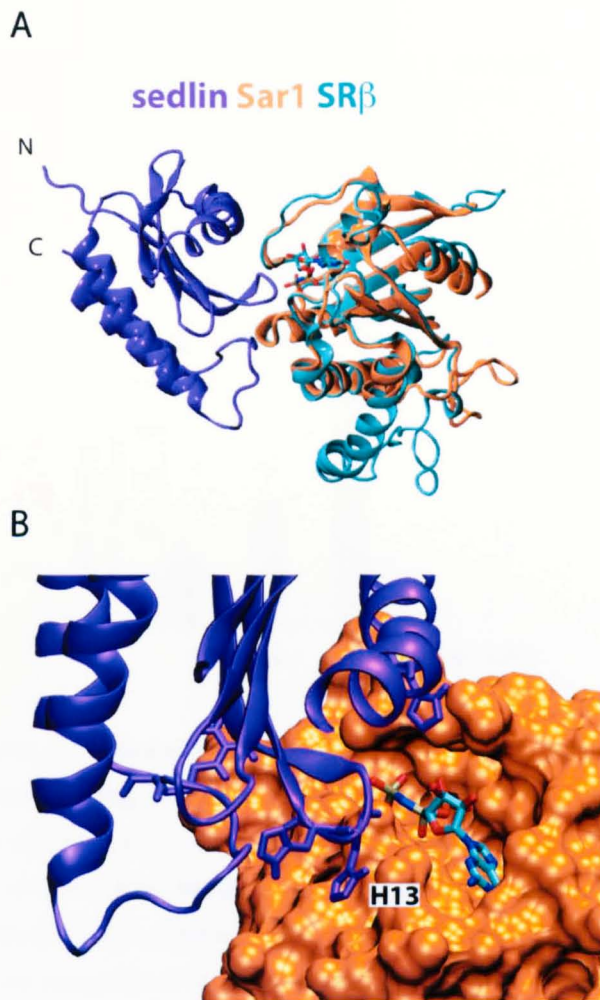
Figure 3.23 Homology modelling of sedlin-Sar1 interaction based on SRX-SRB interaction. (**A**) Homology modelling of the sedlin-Sar1 complex on the SRX-SRβ complex (see Schlenker et al., 2006). Sedlin has structural homology with SRX (Figure 9 in Schlenker et al., 2006, not shown here); Sar1 was modelled on SRß as also described in Figure 3.17. (**B**) Close up of the interaction surface between sedlin (cyan) and Sar1 (orange) showing the involvement of the H13 residue, predicted to be critical for the interaction between the two proteins.
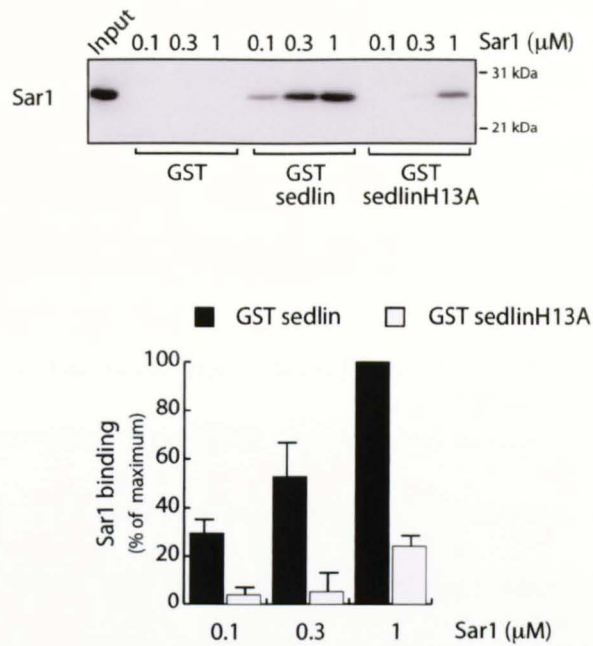
Figure 3.24 Sedlin H13 residue is critical for the interaction with Sar1. Pull-down assays were performed using increasing concentrations (0.1, 0.3 and 1 μM) of His-Sar1 with GST-sedlin wild type, GST-sedlin H13A or GST alone (each 0.5 μM). Input, 200ng Sar1 (equivalent to 2.5% of the amount used in the 1μM incubation). The H13A mutant has low affinity for Sar1. The graph reports the results of the quantitative analysis of Sar1 binding. Values are expressed as % of the sedlin-Sar1 binding relative to 1 μM His-Sar1 (Maximum), and are the means (± SD) of three experiments performed in duplicate.

Recent evidence has shown that, at least in yeast, Bet3 interacts with Sec23 only when Sec23 is not engaged in an interaction with Sar1 (Lord et al., 2011), in a fashion that guarantees the sequential and the proper direction to anterograde transport. Sar1 is associated with COPII carriers during the very early stages of COPII carrier formation but it is released faster than the other COPII components (i.e. Sec23/24 and Sec13/31). This is consistent with the observation that COPII vesicles have substoichiometric amount of Sar1 compared to Sec23/24 and Sec31/13 (Barrowman et al., 2000). The interaction I report here between sedlin and Sar1 would occur at an earlier step, i.e. during vesicle budding, suggesting a possible involvement of sedlin in a very initial stage of COPII assembly.

To ascertain whether sedlin binds Sar1 also in the presence of Sec23, I designed a GST-pull down assay to explore this possibility. Sar1 was loaded with GTPγS overnight at 4°C. The next day it was incubated with Sec23 and with GST-sedlin or GST alone. GST alone, as expected, failed to bind any protein, while GST-sedlin was able to bind Sar1 together with Sec23 (**Figure 3.25**). This experiment demonstrated clearly that the sedlin-Sar1 interaction is compatible with Sar1-Sec23 binding.
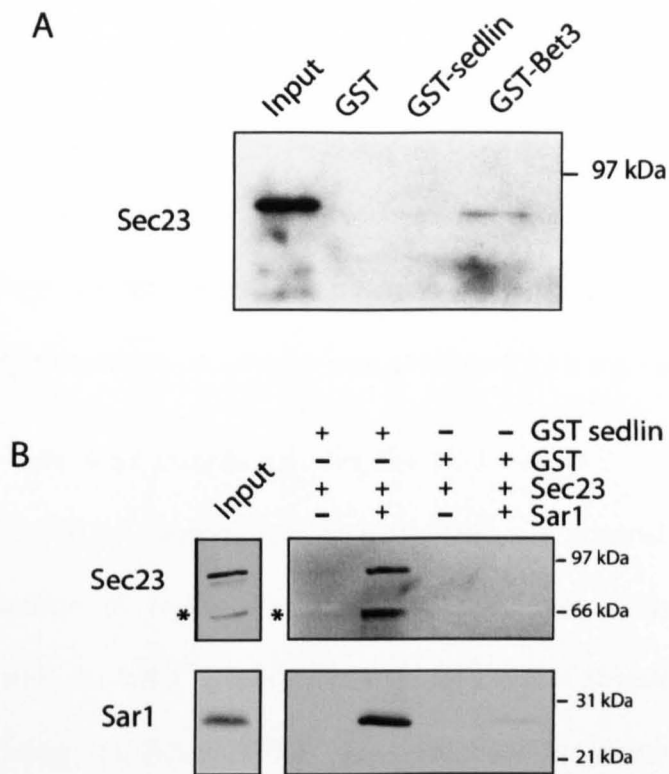
Figure 3.25 Sedlin binds Sar1 complexed with Sec23. (A) Pull-down assays were performed using 1 μM of His-Sec23 with GST-sedlin, GST-Bet3 or GST alone (each 0.5 μM). Input, Sec23 equivalent to 10% of the amount used in the 1μM incubation. GST sedlin fails to pull down Sec23, while GST-Bet3 interacts with Sec23, as expected and as reported by Cai et al. (2007). **(B)** Pull-down assays were performed using 1 μM of His-Sec23, 1 μM of His-Sar1 with GST-sedlin or GST alone (each 0.5 μM). His-Sar1 was pre-loaded overnight with GTPγS. Input, Sec23 equivalent to 2.5% of the amount used in the 1μM incubation. GST-sedlin on its own fails to pull down Sec23, but in presence of Sar1 it can bind to the complex. This finding shows that sedlin can contact Sar1 when it is active and bound to Sec23.

3.7 Sedlin associates to the ERES in a Sar1-dependent fashion

To corroborate the *in vitro* assays described above, I explored the functional correlates for the sedlin-Sar1 interaction *in vivo* by co-localization studies and by an assessment of reciprocal effects on their membrane-cytosol cycle.

Hela cells were transfected with the GFP-Sar1 wild type protein and the GFP-Sar1H79G mutant (see Introduction) and assayed for effects on the localisation of sedlin. No perturbation of the sedlin distribution was observed in cells over-expressing GFP-Sar1 (**Figure 3.26**). In cells expressing GFP-Sar1H79G, however, sedlin underwent a dramatic reorganisation and was recruited to Sar1H79G positive structures (**Figure 3.26**). To test whether sedlin recruitment to GFP-Sar1H79G structures was a primary effect mediated by sedlin-Sar1 interaction, I micro-injected the His-Sar1H79G protein into cells to observe the acute recruitment of sedlin to the ERES (**Figure 3.26**). As shown in **Figure 3.26**, sedlin was rapidly recruited to ERES (stained with Sec31 protein), soon after the injection and increased during the time course of the experiment (1, 1.5 and 3 hrs post injection).

Together these data support the hypothesis that sedlin and Sar1 can interact *in vivo*. Despite the fact that Sar1 locked in its active state recruits sedlin *in vivo*, this alone does not provide an answer about the role of Bet3 at this stage. To address this point, I analysed the role of Sec23 in the binding between sedlin and Sar1. HeLa cells were treated with specific siRNAs directed against Sec23 (A and B isoforms), which reduced the Sec23 protein in the cell (**Figure 3.27**).
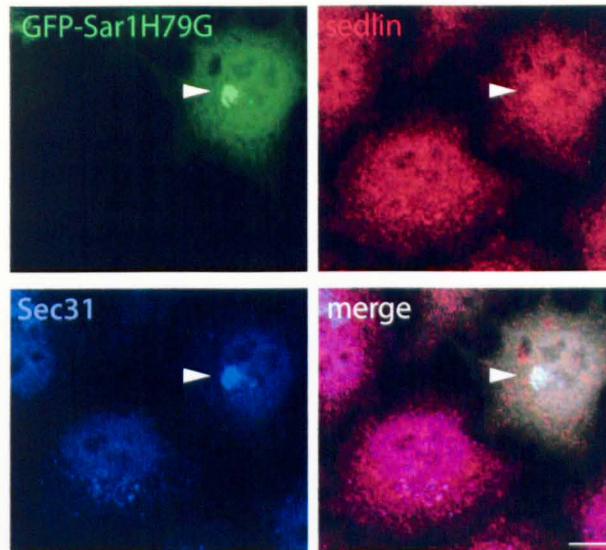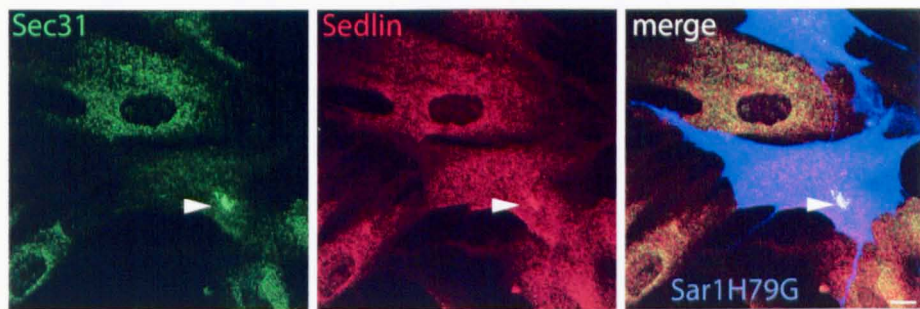
Figure 3.26 Sar1H79G recruits sedlin *in vivo*. (**A**) HeLa cells were transfected with a plasmid encoding a GFP-Sar1H79G protein. After 16 hours of expression, cells were fixed and processed for immunofluorescence analysis. Note that the GTP-restricted mutant of Sar1 (green) accumulates at the perinuclear region, as well as Sec31 (blue). Under these conditions, sedlin (red) is almost completely recruited to the positive Sar1-structures. White arrowheads highlight the recruitment to Sar1-positive structures. Scale bar, 10 μm. (**B**) HFs were micro-injected with 2.5 mg/ml of the His-Sar1H79G protein and left for 1 hour at 37°C. Cells were then fixed and stained for Sec31 (green) and sedlin (red). After injection, both sedlin and Sec31 change their usual localisation and appear to be concentrated at a perinuclear area. The white arrow-head indicates the injected cell. Bar, 10 μm.
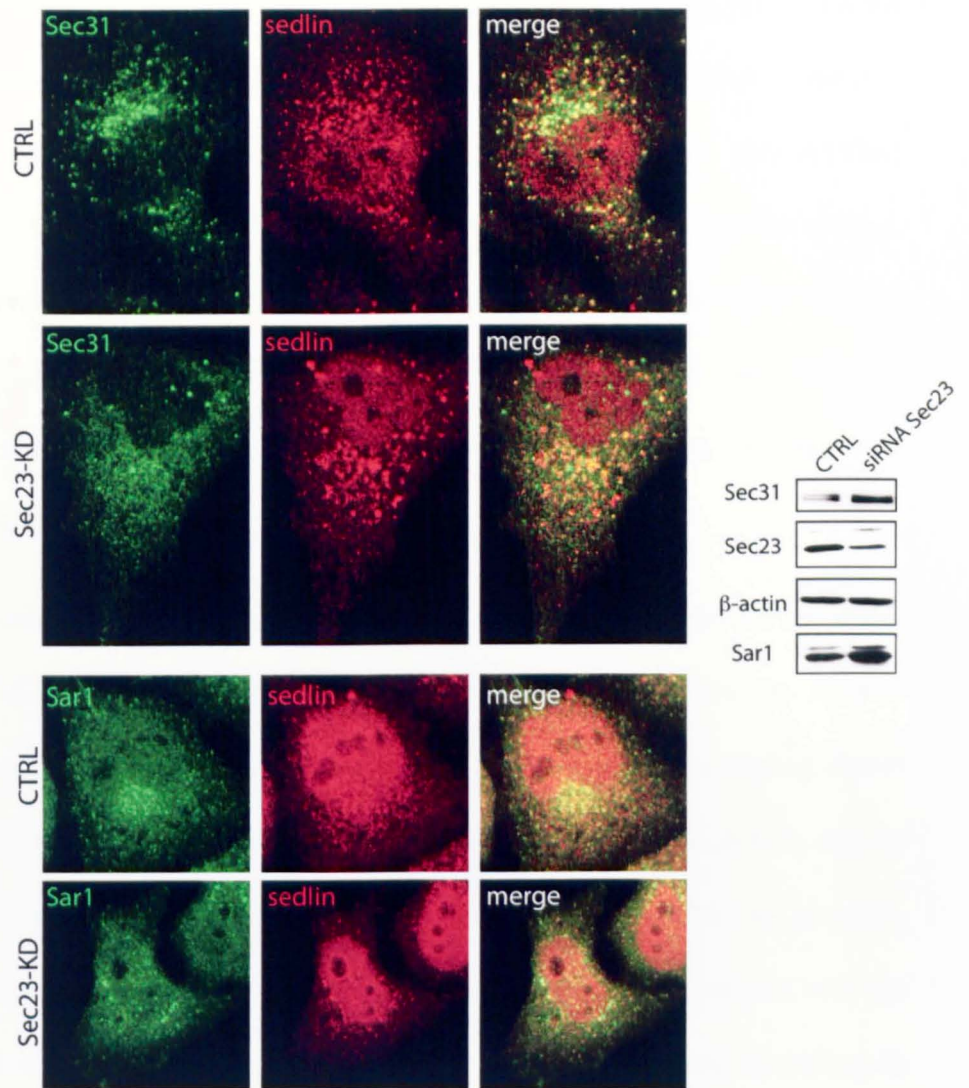
Figure 3.27 Sec23 depletion does not impair sedlin-Sar1 interaction in HeLa cells.
HeLa cells were mock or Sec23 siRNA treated as described in Materials and Methods.
Sec23 depletion does not cause destabilisation of the other COPII subunits analysed
(Sec31 or Sar1). Control and Sec23-KD cells were fixed and stained with a marker of the
ERES (Sec31, green) and with sedlin (red). In Sec23-KD cells, Sec31 appears to be
redistributed compared to control cells, while sedlin accumulates in structures mainly
localised in the perinuclear region. In parallel, control and Sec23-KD cells were fixed and
stained for the presence of Sar1 (green, bottom panels). In cells with reduced Sec23, sedlin
colocalises with Sar1. (Right) HeLa cells were treated as described above. Cell lysates (60
µg/sample) were analyzed by SDS-PAGE and immunoblot analysis with the indicated
antibodies. β-actin was used as a loading control.

After 72 hrs, control and siRNA treated cells were fixed and processed for indirect immunofluorescence experiments. After Sec23 siRNA treatment, Sec31 did not form the spotty structures with a perinuclear concentration typical of control cells but appeared to be dispersed throughout the cytosol. Moreover, Sec31 was present in few round structures distributed throughout the cell (**Figure 3.27**). By contrast, sedlin was distributed in very large and bright roundish structures located all around the nucleus, very different from the Sec31-positive structures (**Figure 3.27**).

The colocalisation of sedlin and Sec31 was no longer detectable under Sec23-KD conditions. The sedlin positive structures, however, showed positive staining for the presence of Sar1 (**Figure 3.27**). This finding shows clearly that sedlin binds Sar1 even in absence of functional Sec23, and by extension that Bet3 is dispensable for the interaction of the two proteins. Moreover, these data enforce the hypothesis that sedlin can interact with the COPII machinery before the Bet3-Sec23 interaction, which, according to the current literature, should occur after COPII formation and budding (Yu et al., 2006, Cai et al., 2007; Lord et al., 2011). These data shed a completely new light on the interactions between TRAPP-COPII, revealing a new and, until now, hidden player, sedlin.

3.8 Sedlin controls the membrane-cytosol cycle of Sar1 and COPII

I next investigated the role of sedlin in the Sar1/COPII cycle by following the dynamics of the membrane-cytosol cycle of a COPII component (GFP-

Sec23) in control and sedlin-KD cells using FRAP analysis. This method allows the precise calculation of the half-life of COPII subunits at the level of a single ERES (Watson et al., 2005; Forster et al., 2006).

It is essential to use low-level expression of fluorescently tagged proteins to ensure faithful replication of the behaviour of the endogenous protein. Moreover, to limit in time the expression of the fluorescent protein I also microinjected the GFP-Sec23 cDNA into the nuclei of cells. The GFP-Sec23 localised properly at ERES as shown by co-localisation with Sec31 (**Figure 3.28**).

Analyses of sedlin-KD and Bet3-KD HFs showed a partial redistribution of Sec31 structures from the perinuclear area to the cytoplasm, which still co-localised with the GFP-Sec23 protein (**Figure 3.28**).

Using FRAP analysis (see Materials and Methods), a consistently longer time of recovery of the GFP-Sec23 fluorescence was observed after photobleaching in sedlin KD cells compared to control cells (FRAP half-time of 9.2 sec and 4.9 sec, respectively, **Figure 3.29**), indicating that the membrane-cytosol cycle of the COPII coat is slowed down in the absence of sedlin. In order to understand whether the slower cycle of GFP-Sec23 was due to a delayed association to or delayed dissociation from membranes, I performed FLIP measurements (see Materials and Methods), to calculate the K_{off} of GFP-Sec23. Sedlin KD slowed down the dissociation of GFP-Sec23 from ERES membranes as the K_{off} was 0.032 sec^{-1} in control, 0.022 sec^{-1} in sedlin KD and 0.015 sec^{-1} in TRAPP-depleted cells.
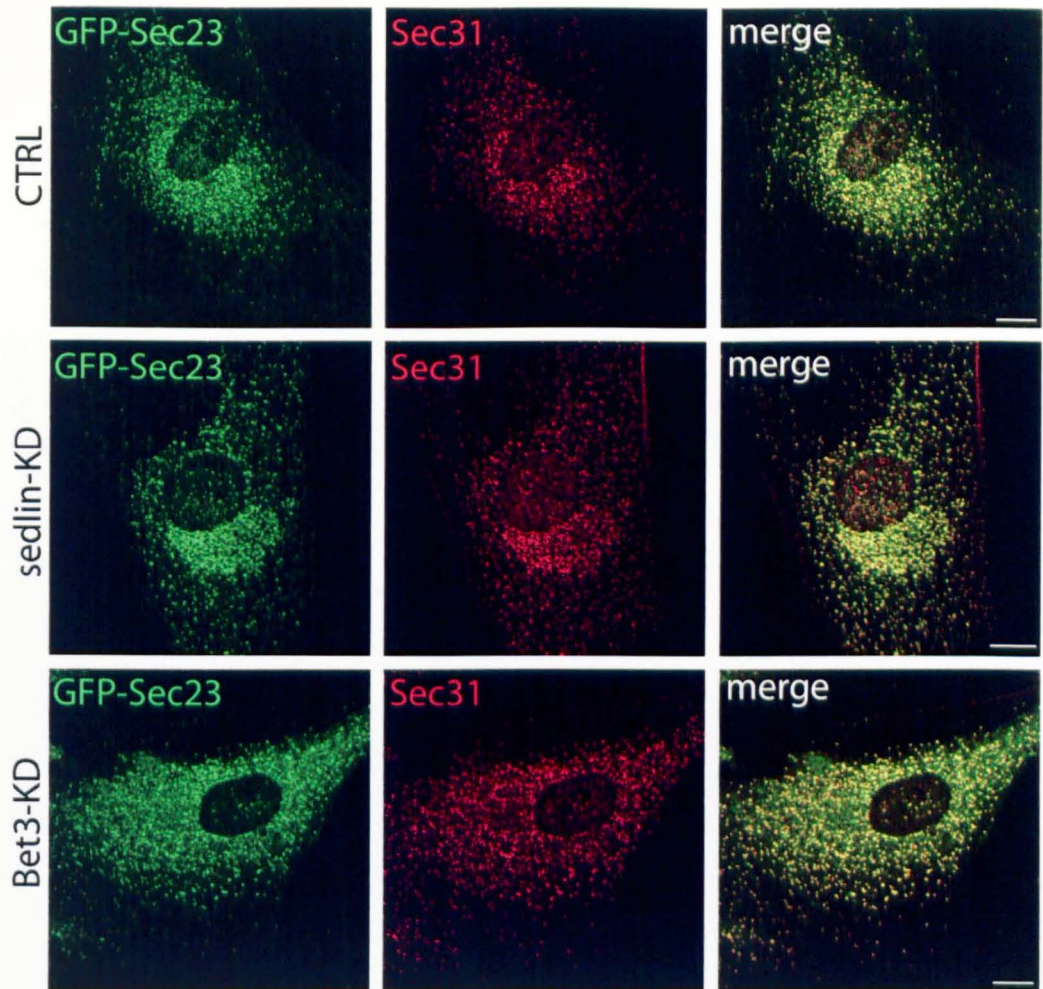
Figure 3.28 GFP-Sec23 properly localises at ERES in human fibroblasts. HFs were treated with non-targeting (CTRL), sedlin or Bet3 siRNA for 96 hours. Then, a cDNA encoding a GFP-tagged Sec23 protein (green) was micro-injected into the nuclei. Five hours post-injection, cells were fixed and processed for immunofluorescence analysis. GFP-Sec23 perfectly colocalises with Sec 31 (red), a marker of ERES. Scale bars: 10 μm.
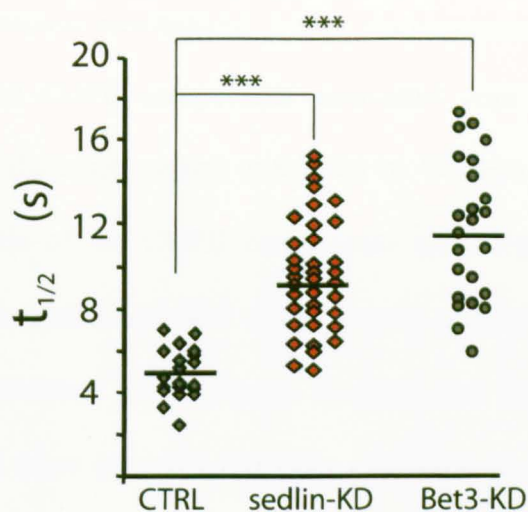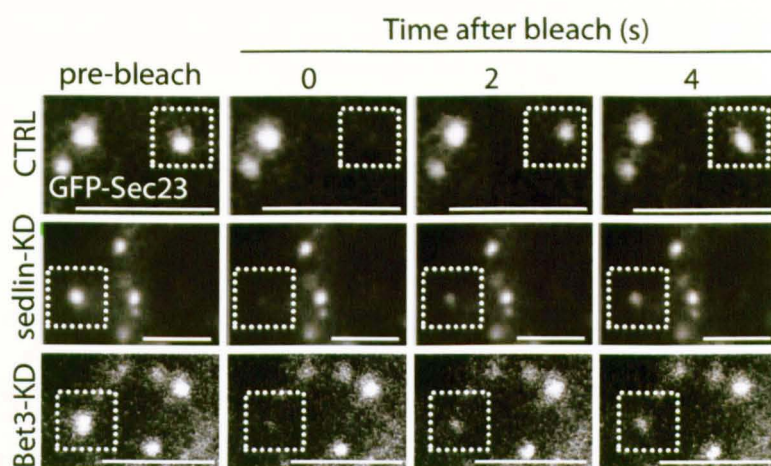
Figure 3.29 Sedlin depletion slows down the cycle of COPII. Human fibroblasts were treated with non-targeting (CTRL), sedlin or Bet3 specific siRNA for 96 hours. Cells were then micro-injected with GFP-Sec23 construct, and single ER exit site dynamics were analysed. An example of Fluorescence Recovery After Photobleaching (FRAP) of a single COPII (Sec23-GFP)-labelled ERES in non-targeting (CTRL), sedlin and Bet3 siRNA-treated human fibroblasts is shown. The four images show different time points (in seconds) of a time-lapse sequence. The white square indicates the bleached ERES. The bleaching area encompassing a single ER exit site was maintained constant during all measurements. "0" is the first image acquired after the bleaching. Scale bars, 2 μm. The graph shows the $t_{1/2}$ for the FRAP of the indicated number of ERES in human fibroblasts under the three conditions: non-targeting (CTRL), sedlin and Bet3 siRNA. CTRL, n=24; sedlin-KD, n=38; Bet3-KD, n=24, where n indicates the number of analyzed spots. P<0.0001. The experiment was run three independent times in duolicates with similar results. An average of 65 spots (corresponding to the single ERES) were analysed for each experiments.

I reached similar conclusions using an alternative and independent approach in which I evaluated the fraction of COPII components remaining associated with membranes in permeabilized cells. To this end, I took advantage of a temperature-sensitive bacterial toxin, streptolysine O (SLO), which can bind to cholesterol on the plasma membrane and produce holes in the membrane. With this procedure, it is possible to measure the release of cytosolic materials without permeabilising any other intracellular organelles (i.e. ER, GC or nuclear membranes). Using this procedure, I measured the amount of Sar1 and COPII components associated with membranes (visualised by immunofluorescence and quantified by Western blot analysis). I found that the levels of the COPII components were significantly and consistently higher in sedlin and Bet3 depleted cells compared to control cells (**Figure 3.30**). Western blot analyses revealed that Sec31, Sec23 and Sar1 are retained more in sedlin-KD cells compared to control conditions. GM130 and GAPDH, a membrane and a cytosolic marker, were monitored as negative and positive controls, respectively (**Figure 3.30**). The addition of GTPγS to the reaction leads to a disappearance of this difference, indicating that interfering with Sar1 cycle impaired the release of the COPII components from membranes (**Figure 3.30**).

Therefore, not only COPII coat components but also Sar1 are more stably associated with membranes in sedlin depleted and Bet3 depleted cells than in control cells (**Figure 3.30**). This increased association of Sar1 with the ERES in TRAPP-depleted cells was confirmed by IEM and morphometric analyses, which show a three fold increase in the labelling density of Sar1 on ERES membranes as compared to mock cells (Figure 4.12).
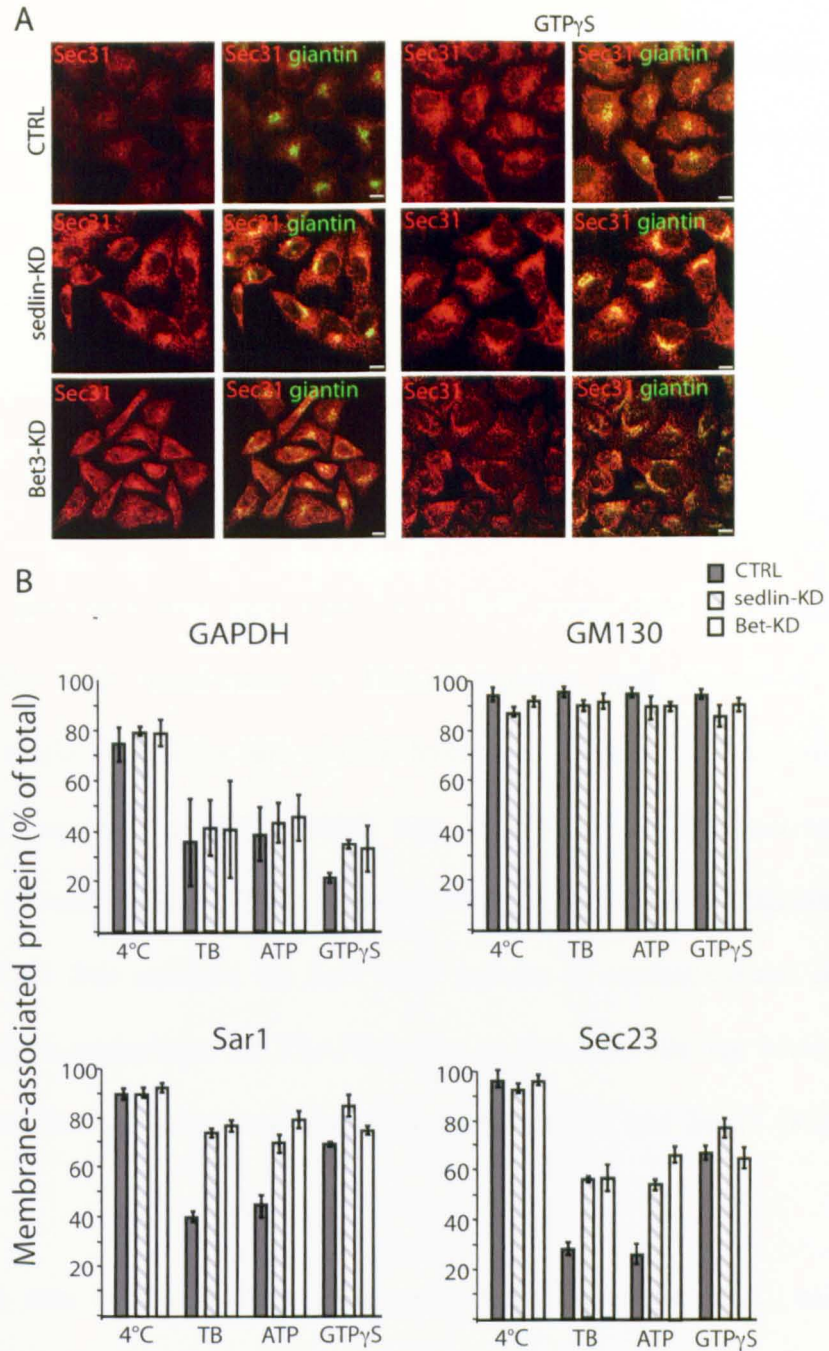
Figure 3.30 COPII subunits are more associated to membranes in sedlin and TRAPP depleted HeLa cells. (**A**) HeLa cells were mock, sedlin or Bet3 siRNA treated for 3 days. Cells were then incubated with streptolysine-O in order to remove the cytosolic pool of proteins. (see Materials and Methods) Images are single optical sections of paraformaldehyde fixed cells showing Sec31 localization. Giantin was used as a permeabilisation control. Scale bar, 10 μm.. (**B**) Western blot analyses shows that Sec23 and Sar1 are retained more both in sedlin-KD and in Bet3-KD cells compared to mock cells. GM130 and GAPDH were monitored as negative and positive controls, respectively. Note that the addition of GTPγS to the reaction leads to a disappearance of this difference. The graph reports mean values (± SD) from at least 4 independent experiments performed in duplicate.

Taken together, the above results strongly support the hypothesis that sedlin/TRAPP controls the membrane-cytosol cycle of Sar1, possibly acting as a co-GAP.

3.9 TRAPP acts as a co-GAP for Sar1

As Sar1 associates with membranes in its GTP-bound state, its prolonged association with membranes in TRAPP-depleted cells suggested that TRAPP might control the rate of GTP hydrolysis by Sar1. GTP hydrolysis on Sar1 requires Sec23/24, which acts as a GAP (GTPase-activating protein) (Yoshihisa et al., 1993), and is accelerated by Sec13/31 (Antonny et al., 2001). I thus assessed the Sar1 GAP activity of control cytosol or of cytosol immunodepleted for TRAPP (using an anti-Bet3 Ab, see Materials and Methods) but containing normal levels of Sec23 and Sec31 (**Figure 3.31**).

His-Sar1 was incubated alone or in presence of untreated RLC, mock-treated RLC or TRAPP-depleted RLC, in a buffer containing [^{32}P] α-GTP (Jacques et al., 2001) and the amount of GDP produced was measured by separating the two species ([^{32}P]-GDP versus [^{32}P]-GTP) by thin layer chromatography after 15, 30, 60, 90 and 120 minutes. Sar1 alone did not show any hydrolytic activity, as expected. Control RLC and mock-treated RLC induced a very high and similar activation of the GTPase activity of Sar1.
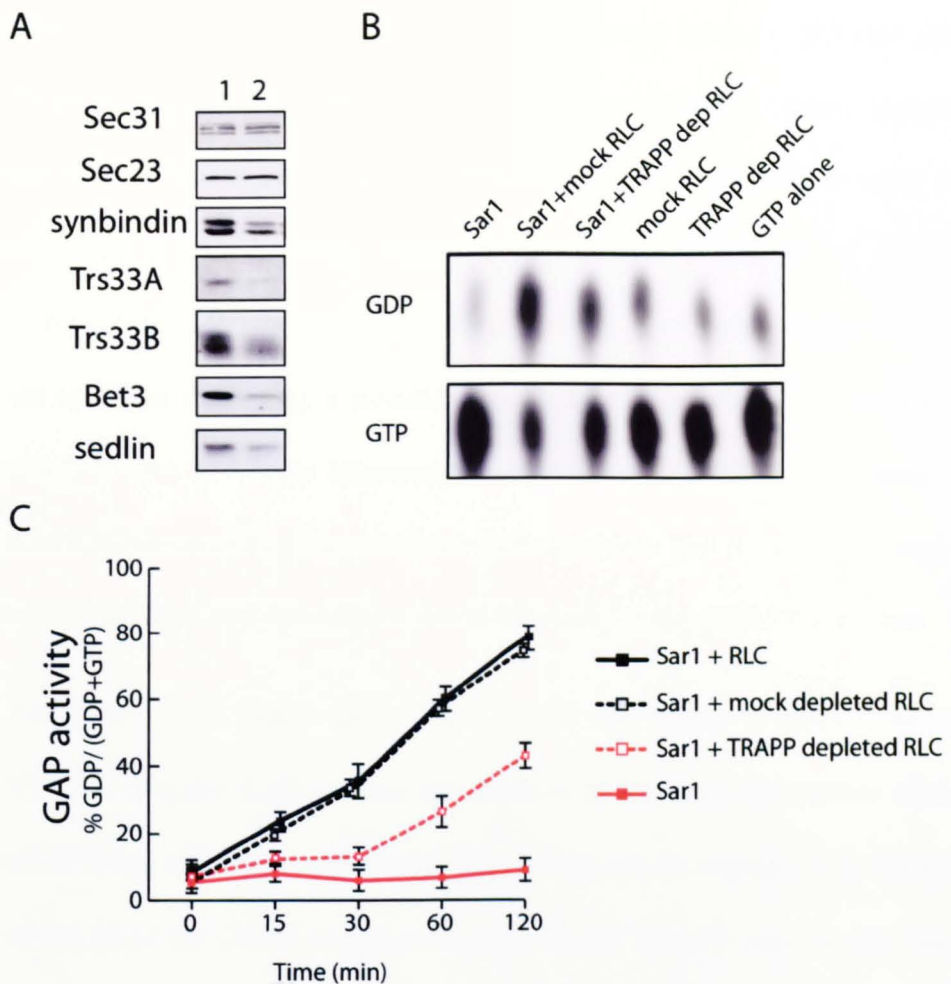
Figure 3.31 TRAPP depletion significantly reduces Sar1 GTPase activity *in vitro*.
(A) Rat liver cytosol (RLC, prepared as described in Materials and Methods) was incubated with pre-immune IgG (1) or with Bet3-Ab to deplete TRAPP (2). 60 µg of each RLC were subjected to SDS-PAGE and immunoblot analysis. TRAPP-depleted RLC has reduced levels of all the analysed TRAPP subunits (sedlin, Bet3, Trs33A, Trs33B and synbindin), while COPII components are similar to the mock-depleted RLC. (B) A representative TLC is shown of the GAP assay described in (C). (C) Recombinant His-Sar1 was incubated with α-^{32}P GTP alone or with 60 µg of mock-depleted RLC or TRAPP-depleted RLC for the indicated times. TLCs were analysed to quantify different α-^{32}P nucleotide species. As reported in the graph, TRAPP-depleted cytosol has a greatly impaired ability to promote Sar1 GTPase activity compared to mock-depleted cytosol. The GAP activity is expressed as % of α-^{32}P GDP over α-^{32}P GDP + α-^{32}P GTP. The graph shows mean values (± SD) from 7 different experiments performed in duplicate.

171

On the other hand, TRAPP depleted RLC showed strongly reduced Sar1 GTPase activity (the percentage of $[^{32}P]$-GDP produced in control samples after 60 minutes is 58.2% ± 1.68, while in TRAPP depleted cytosol the percentage is 26.6 ± 5.6%, **Figure 3.31**). Thus the absence of TRAPP severely impairs the cytosolic Sar1-GAP activity, prolonging its GTP-bound state and thus disclosing a possible mechanism underlying the increase in residence time and local concentrations of Sar1 on ERES membranes of TRAPP depleted cells. This confirms the hypothesis that it can function as a co-GAP for Sar1 and identifies a novel function for the TRAPP complex.

I performed GAP assays using Sar1, Sec23 and sedlin (**Figure 3.32**) or GST-Bet3 (**Figure 3.33**) without the addition of RLC but no increase of the Sar1 GTPase activity was observed. These data can be explained by the fact that not all of the COPII components or all of the TRAPP components were present that could favour the action of sedlin as a co-GAP. It cannot be excluded that the presence of the outer layer of the COPII machinery (Sec13/31) might be required to trigger the co-GAP activity of sedlin on Sar1 or that, in measuring the overall production of $[^{32}P]$-GDP, small changes were not considered statistically significant. I also prepared the cytosol from HeLa and HepG2 cells but they failed to stimulate Sar1 GTPase activity (not shown).
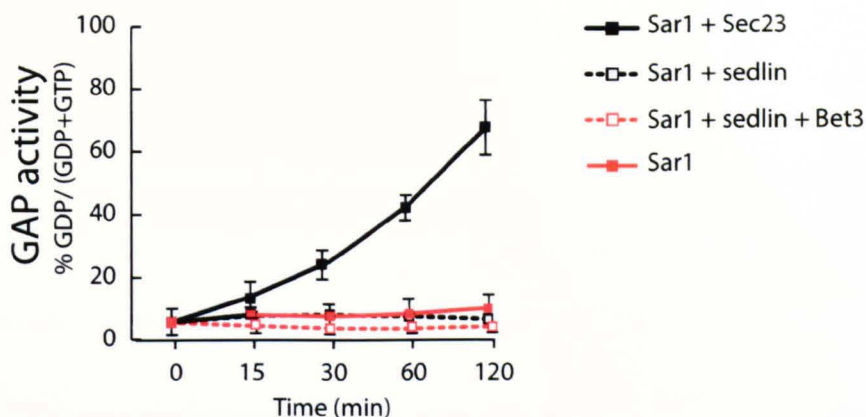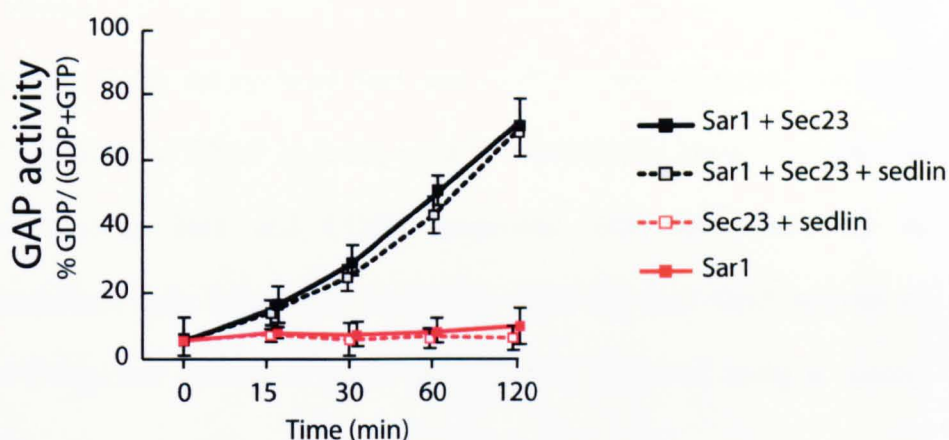
Figure 3.32 Recombinant sedlin does not stimulate the GTPase activity of Sar1 *in vitro*. **(A)** Recombinant His-Sar1 (1 μM) was incubated with α-^{32}P GTP alone or with His-Sec23 (0,5 μM) or GST-sedlin (0,5 μM) and GST-Bet3 (0,5 μM). TLCs were analysed to quantify different α-^{32}P nucleotide species. As reported in the graph, the presence of sedlin without Sec23 does not trigger the conversion of GTP in GDP. Similarly, the addition of Bet3 does not act on Sar1 activity. The GAP activity is expressed as % of α-^{32}P GDP over α-^{32}P GDP + α-^{32}P GTP. The graph shows mean values (± SD) from 3 different experiments performed in duplicate. **(B)** Recombinant His-Sar1 (1 μM) was incubated with α-^{32}P GTP alone or with His-Sec23 (0,5 μM) and GST-sedlin (0,5 μM). TLCs were analysed to quantify different α-^{32}P GTP species. As reported in the graph, the presence of sedlin together with Sec23 does not cause any change in the GTPase activity of Sar1. The GAP activity is expressed as % of α-^{32}P GDP over α-^{32}P GDP + α-^{32}P GTP. The graph shows mean values (± SD) from 3 different experiments performed in duplicate.

Discussion

Here I have reported that the transport particle complex TRAPP controls the formation of COPII-dependent transport carriers at the ERES where it is selectively required for the ER export of large soluble cargo, such as PCI.

TRAPP is required to keep the cycle of Sar1 and COPII efficient and fast. In the absence of the TRAPP complex (achieved by silencing its key component Bet3) the cycle of Sar1 and COPII is slowed down: the GFP-Sec23 halftime of FRAP in living cells is considerably higher, the fraction of endogenous Sar1 and COPII associated with the membranes in permeabilised cells is strongly increased, while the Sar1 GAP activity of TRAPP-depleted cytosol is lower than what is observed using a control cytosol.

In this scenario sedlin plays a key role in regulating this mechanism. Its depletion reproduces perfectly all the phenotypes induced by the whole TRAPP depletion: the slow down of Sar1 and COPII cycle and the inhibition of PCI export.

Interestingly, sedlin regulates proper COPII dynamics by binding directly and exclusively to Sar1p. Sedlin possesses a longin domain, a domain found in different classes of proteins including non-syntaxin SNAREs, adaptors, and a subunit of the signal recognition particle receptor SR (Schlenker et al., 2006). Based on the observation that the longin domain of SRX interacts with and acts as a co-GAP for the GTPase SRβ, a model has been proposed

174

according to which the longin domain is a general GTPase-interacting protein module. The observation that sedlin binds Sar1 and regulates its cycle supports this model.

Thus two subunits of the TRAPP complex, sedlin and Bet3, interact with Sar1 and Sec23, respectively, two components of the machinery controlling the packaging of nesosynthesized cargo into transport carriers at the ERES.

Intriguingly, the binding between sedlin and Sar1 can occur simultaneously with the Sar1 engagement with Sec23. As reported recently, the Bet3-Sec23 interaction, on the other hand, takes place only in the absence of Sar1, when COPII coated carriers are already formed (Lord et al., 2011).

Sedlin contacts Sar1 in its GTP-bound state thereby favouring the Sar1-GAP activity of Sec23 and accelerating the release of Sar1 from the membranes. Under these circumstances, it appears clear that sedlin binds to Sar1 during the first step of COPII formation.

Sar1 possesses a lower association/dissociation rate compared to the other members of the coat (i.e. Sec23 and Sec13, Watson et al., 2005; Forster et al., 2006), implying that it dissociates faster from the COPII-coated carrier. Bet3-Sec23 interaction occurs to guarantee the proper directionality of the formed carrier (homotypic fusion or heterotypic fusion, Cai et al., 2007; Lord et al., 2011).

This particular role of sedlin at the ERES appears dispensable for the ER exit of small cargo but is required for the ER exit of large cargo, such as PCI.

The efficient coupling between Sec23/24 and Sec13/31 is required for the ER exit of PCI but not for VSV-G (Townley et al., 2008), demonstrating that COPII dynamics are fundamental for the exit of special cargoes.

As mentioned above (see Introduction), protein sorting into different transport carriers occurs during their exit from the ER, as suggested by the different molecular requirements of different cargoes for their entry into the secretory pathway. This is the case for procollagen I as compared to VSV-G, which have common and also different molecular requirements during pre- and post-Golgi trafficking events (Starkuviene and Pepperkok, 2007), and for the angiotensin II type 1A receptor and the beta-2 adrenergic receptor (AR) compared to the alpha-2B AR (Wu et al., 2003).

Chapter 4

Results

The role of sedlin in membrane trafficking: insights into the pathophysiology of Spondylo-epiphyseal dysplasia tarda.

A defect in sedlin leads to SEDT, a condition characterized by a failure in the secretion and assembly of the ECM in chondrocytes (Tiller et al., 2001). In further consideration of the clinical overlap that results from some mutations of PCII (Bleasel et al., 1995; Zankl et al., 2004) and sedlin (Tiller et al., 2001), which both cause spondyloepiphyseal dysplasia, I initially examined the impact of sedlin depletion on the trafficking of PCII. PCII is the most abundant collagen in articular cartilage and it is found predominantly, but not exclusively, in hyaline cartilage where it accounts for 90% of the total collagen. Together with other tissue-specific collagens and proteoglycans, PCII provides the cartilage tissue with its shock-absorbing properties and its resilience to stress. Similarly to PCI, PCII forms homotrimeric helices and fibrils.

177

In this Chapter, I report the results obtained in assessing the impact of inhibiting sedlin on the transport of PCII in chondrocytes. As a control, I followed in parallel the effect of sedlin KD on the trafficking of a "generic" reporter cargo VSV-G. Lastly, I verified the relevance of the phenotypes observed in cultured cell lines by studying SEDT patient-derived fibroblasts.

4.1 Sedlin depletion in rat chondrosarcoma (Rx) chondrocytes

Firstly, I set up conditions to efficiently deplete sedlin and also Bet3 using rat chondrosarcoma (Rx) cells as a model (King and Kimura, 2003). siRNAs directed against sedlin efficiently reduced the levels of the protein by 75 to 90% while siRNA directed against Bet3 drastically reduced its levels as well (**Figure 4.1**).

I further analysed the impact of sedlin and Bet3 siRNAs on the GC in chondrocytes. I observed that, in line with the data obtained in the other previously analysed cell lines, the GC was well organized and properly polarized (cis-trans polarization, as verified by the cis and trans Golgi marker GM130 and TGN38) in mock-treated, sedlin-KD and Bet3-KD cells (**Figure 4.1**). The organization of the GC appeared severely compromised exclusively in Bet3-KD cells (**Figure 4.1**).
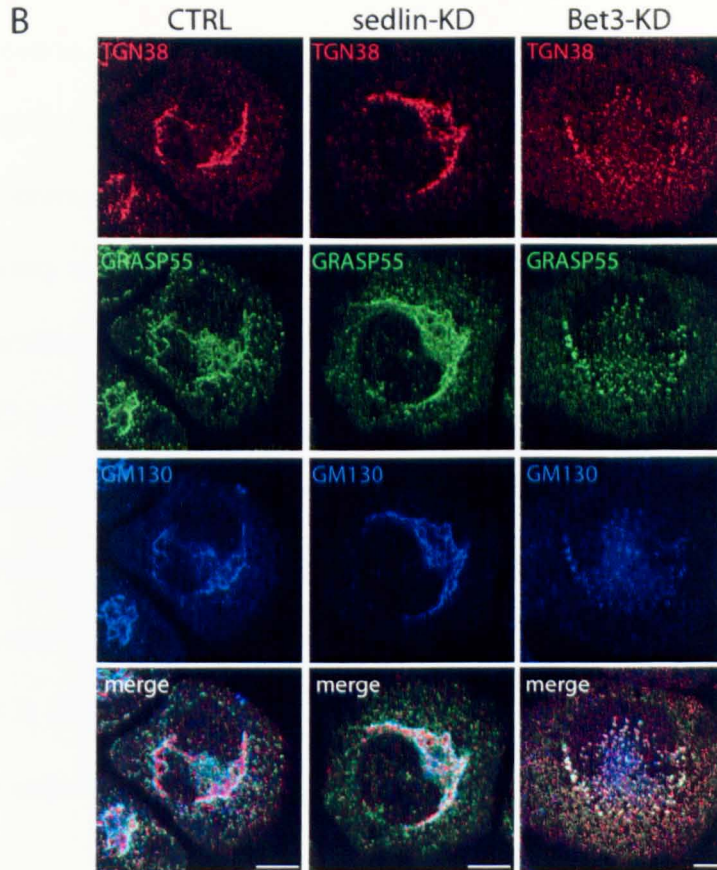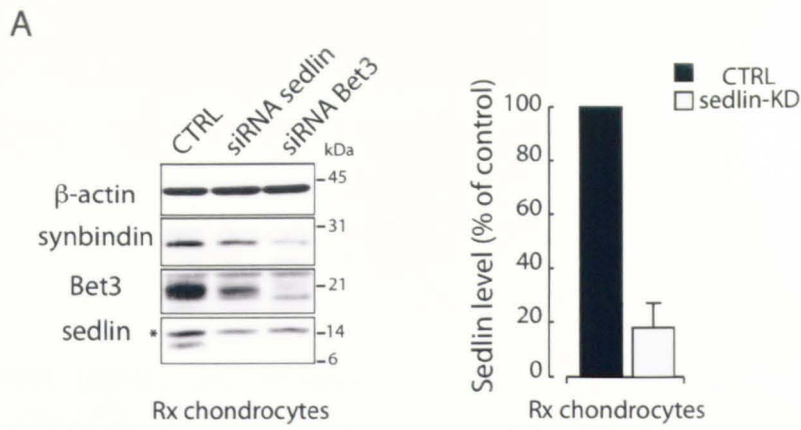
Figure 4.1 Sedlin KD in Rx chondrocytes does not affect TRAPP stability and Golgi structure. (**A**) Rx chondrocytes were treated with the indicated siRNAs as described in Materials and Methods. Cell lysates (60 μg/sample) were analyzed by SDS-PAGE and immunoblot analysis with the indicated antibodies. β-actin was used as a loading control. Sedlin does not cause destabilisation of the other analysed TRAPP subunits (i.e. Bet3 or synbindin) in contrast to Bet3 depletion. The graph shows the amount of the sedlin protein in Rx chondrocytes after siRNA treatment as determined by Western blot analysis of cell lysates using an anti-sedlin antibody. Mean values are reported (± SD) from 7 independent experiments. (**B**) Control, sedlin and Bet3 depleted chondrocytes were fixed and stained with several markers of the GC (TGN38, red; GRASP55, green and GM130, blue) to evaluate structure and proper polarity of the organelle. Sedlin-KD does not affect GC structure or the *cis-trans* distribution (note the merge panels), while Bet3-KD perturbs profoundly GC architecture, but without strongly affecting *cis-trans* polarity.

179

4.2 Effect of sedlin and TRAPP depletion on PCII trafficking in chondrocytes

Control (mock) and sedlin-KD chondrocytes were analyzed for the trafficking of PCII using synchronization protocols. Similarly to PCI, the formation of PCII triple helices is temperature sensitive, and PCII stays trapped into the ER when cells are incubated at the non-permissive temperature (40°C block). The transport of both cargoes along the secretory pathway was synchronized by imposing this temperature block, resulting in reversible misfolding and retention in the ER, and then shifting the cells to 32°C to release the ER block. Neosynthesized PCII localised almost completely with the Golgi marker GRASP55 30 min after release of the trafficking block in mock-treated cells while the transport of PCII was severely impaired by sedlin depletion, with a marked inhibition of exit from the ER (**Figure 4.2**). PCII in sedlin-KD cells perfectly co-localized with the ER marker GRP78 (BiP, **Figure 4.2**).

Next, in order to determine whether the effects of sedlin depletion operated within the context of the TRAPP complex, I reduced the levels of the entire complex by depleting of the expression of the TRAPP subunit Bet3 in Rx chondrocytes, which induced destabilization and possibly degradation of the entire complex, as expected (**Figure 4.1**) and as reported above in other cell lines. (**Figures 3.1 and 3.9**)
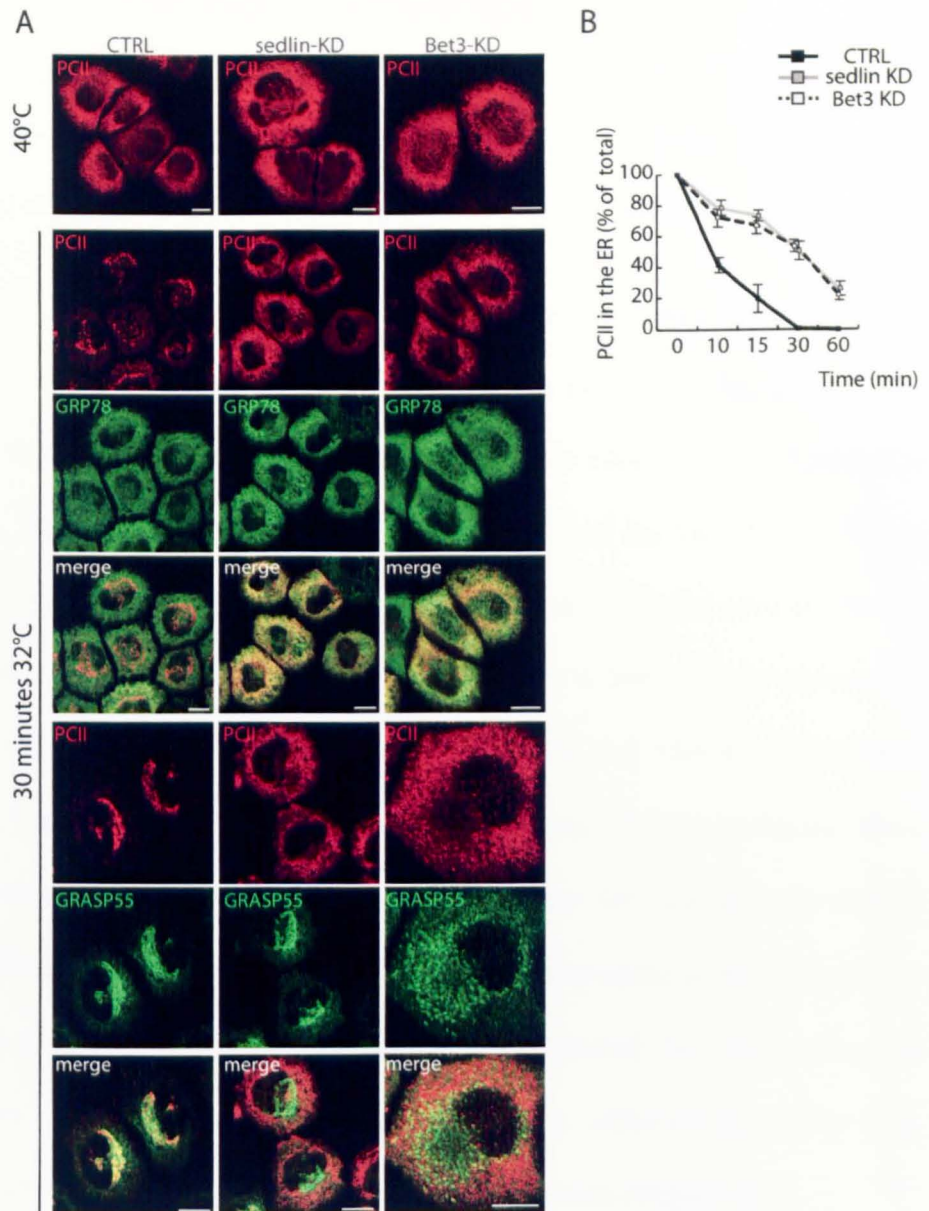
Figure 4.2 Sedlin is required for the selective exit of PCII in Rx chondrocytes. (A) PCII trafficking in chondrosarcoma cells (Rx chondrocytes). Mock-treated Rx chondrocytes or Rx chondrocytes treated with sedlin or Bet3 siRNAs were incubated for 3 hours at 40°C, shifted to 32°C for 30 min and then fixed and double stained with mAb against PCII (red) and an antibody against GRP78 (a marker for the ER compartment) or GRASP55 (a marker of the Golgi complex). Top panels show the PCII staining after the 40°C temperature block, a classical ER staining. After 30 minutes at the permissive temperature, PCII is concentrated in the perinuclear area in control cells and colocalises with GRASP55 but not with GRP78. PCII exhibits a clear ER pattern, as demonstrated by the almost complete co-localisation with GRP78, in sedlin-KD and Bet3-KD cells Scale bars 10 μM. (**B**) Quantification of the ER exit of PCII in sedlin, Bet3 siRNA-treated or mock-treated Rx chondrocytes. Cells were treated as described in (A) and fixed at the time points shown. The data are expressed as % of cells with PCII in the ER. Each experiment was repeated at least 4 times in duplicate (*n=200* cells each) and the data are represented as mean values (± SD).

Here too, the ER exit of PCII was strongly inhibited by TRAPP depletion (**Figure 4.2**). The depletion of TRAPP severely affected the structure of the Golgi complex, which appeared extensively vesiculated (**Figure 4.1**).

Then, I analysed the transport of VSV-G using the same synchronization protocols. By contrast, the transport of VSV-G to the GC (**Figure 4.3**) was indistinguishable in sedlin-depleted compared to control cells. In Bet3-KD cells, VSV-G reached the vesiculated structures of the GC (**Figure 4.3**). I measured also the VSV-G arrival to the PM, and found that after sedlin KD it was not altered compared to the control, while it was strongly inhibited in Bet3-KD cells (**Figure 4.3**). By analysing PCII and VSV-G in the same cells, I could observe that PCII was retained in the ER after sedlin and Bet3 depletion, while VSV-G appeared to reach the GC similarly to control conditions (**Figure 4.4**). Finally, I analyzed total protein secretion in pulse-chase experiments in chondrocytes (as also reported for HeLa cells, see **Figure 3.10**). Secretion was not significantly affected by sedlin KD, similarly to what I reported previously for HeLa cells (**Figure 4.5**).

To assess whether the selective impairment of ER exit of PCII in sedlin- and Bet3-KD cells was a specific and direct consequence of the depletion achieved during the three days of siRNA treatment, I adopted two alternative approaches. First, I verified the specificity of the transport delay by expressing siRNA-resistant forms of sedlin. A cDNA encoding the human sedlin (which encodes an identical protein but with a different mRNA, resistant to rat siRNA) was microinjected into the nuclei of control and sedlin-KD Rx chondrocytes. Four hours post-injection, the cells were subjected to the 40°C block and release protocol.
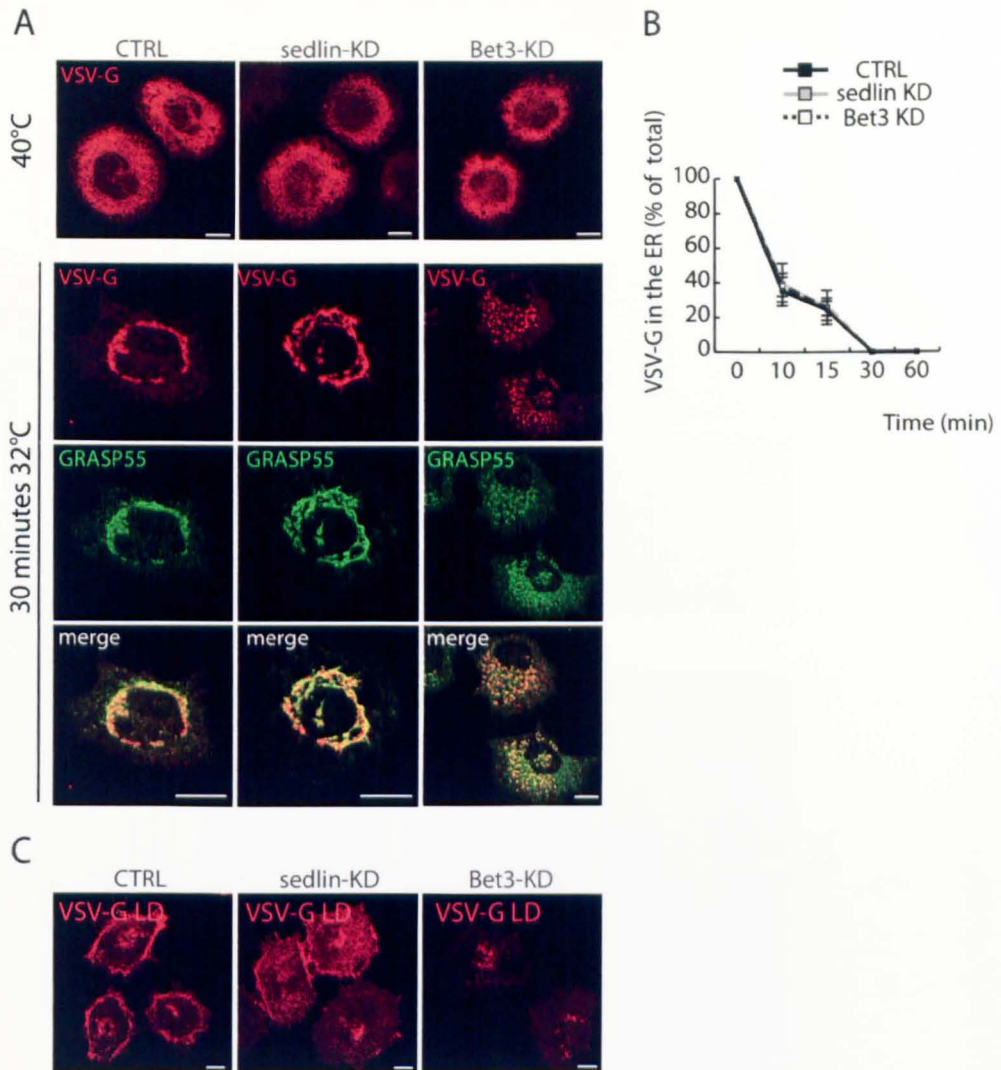
Figure 4.3 Sedlin is dispensible for the ER exit of VSV-G in Rx chondrocytes. (A) Mock-treated Rx chondrocytes or Rx chondrocytes treated with sedlin or Bet3 siRNAs were infected for 1 hour at 32°C with VSVts045 and then incubated at 40°C for 3 hours. Cells were shifted to the permissive temperature for 30 minutes. Here, VSV-G was localized using the P5D4VSV-g mAb (red). Top panels represent the starting point at 40°C, where VSV-G is in the ER under all conditions. After 30 minutues at 32°C, VSV-G reaches the GC in control, sedlin- and Bet3-KD cells (as demonstrated by the co-localisation with the Golgi marker GRASP55, green). Scale bars 10 μM. (B) Quantification of the ER exit of VSV-G in sedlin, Bet3 siRNA-treated or mock-treated Rx chondrocytes. Cells were treated as described in (A) and fixed at the time points shown. The data are expressed as % cells with VSV-G in the ER. Each experiment was repeated at least 4 times in duplicate and the data are represented as mean values (± SD). (C) VSV-G arrival to the PM. Cells were treated as described in (A) and then fixed but without detergent permeabilization. Control, sedlin- and Bet3-depleted cells were incubated with an antibody that recognizes the VSV-G luminal domain (LD). While in control and sedlin-KD cells VSV-G is clearly on the PM, in Bet3-KD cells its arrival is strongly impaired. Scale bars, 10 μM.

183
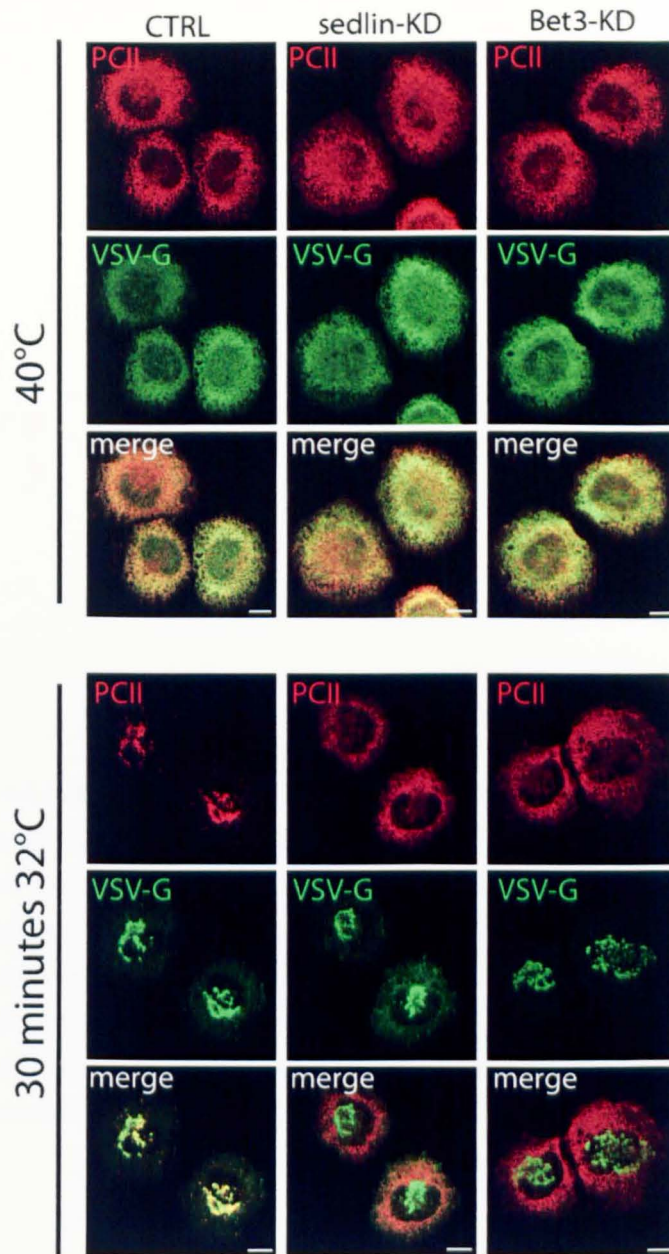
Figure 4.4 Sedlin and the TRAPP complex are required for the selective ER exit of PCII, but are dispensible for VSV-G in Rx chondrocytes. Mock-treated Rx chondrocytes or Rx chondrocytes treated with sedlin or Bet3 siRNAs were infected for 1 hour at 32°C with VSVts045 and then incubated at 40°C for 3 hours. Cells were shifted to the permissive temperature for 30 minutes. VSV-G was localized using the P5D4VSV-g pAb (green). Top panels represent the starting point at 40°C, where VSV-G and PCII (red) are in the ER under all three conditions. After 30 minutues at 32°C, VSV-G reaches the GC in control, sedlin- and Bet3-KD cells. In control cells, PCII exits the ER and concentrates in the perinuclear region. By contrast, PCII remains into the ER after sedlin and Bet3 depletion. Bars 10 μM.
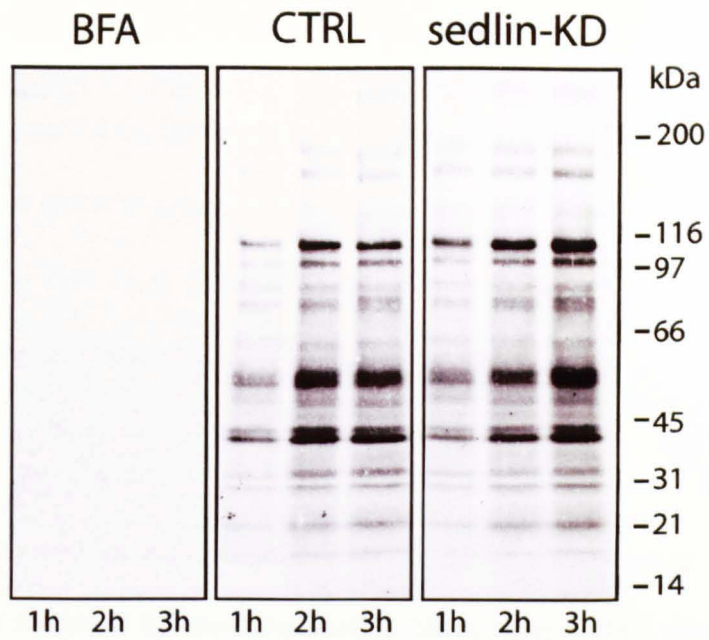
Figure 4.5 Sedlin KD does not affect total secretion in chondrocytes. Rx chondrocytes mock-treated (CTRL) or sedlin siRNA-treated (sedlin-KD) were pulsed with [^{35}S]-cystheine and methionine for 60 minutes, then washed and cultured in standard medium with unlabelled methionine. After 1, 2 and 3 hours the medium was analyzed by SDS-PAGE followed by autoradiography. As a negative control, mock cells were treated with 10μg/ml BFA (a blocker of protein secretion) for the last ten minutes of the pulse and during the chase. No significant difference is detectable between sedlin-KD and control cells, while BFA-treated cells fail to secrete any protein.

I observed that expression of human sedlin could rescue the secretory inhibition (**Figure 4.6**). Intriguingly, the co-expression of one of the disease related sedlin mutants (sedlinR90X) failed to rescue the PCII phenotype (**Figure 4.6**). This is a very important result, because it unequivocally correlates a sedlin mutation with the PCII phenotype.

Second, I devised an experimental protocol in which the acute block of TRAPP was achieved by microinjecting a blocking anti-Bet3 antibody. In De Matteis' laboratory, previous studies led to the finding that injection of the Bet3-Ab caused extensive fragmentation of the GC and impaired the ER exit of PCI in fibroblasts, while injection of pre-immune IgG did not (Scanu Ph.D. thesis, 2008 and see also Yu et al., 2006).

Neosynthesized PCII reached the Golgi complex 30 min after the temperature shift from 40°C to 32°C in pre-immune Ig-G-injected cells, but were retained in the ER of chondrocytes that had been injected with the anti-Bet3 antibody (**Figure 4.7**). Compared to the TRAPP depletion achieved through siRNAs, the acute block of TRAPP induced a pronounced and persistent inhibition of the ER exit PCII (**Figure 4.7** compared to **Figure 4.2**). The Golgi complex, however, was markedly fragmented in the Bet3-Ab injected cells, even more extensively then that induced by siRNA treatment (**Figure 4.7**). Consistent with the data reported above for the TRAPP depletion by Bet3 KD, VSV-G transport out of the ER was not impaired in the cells injected with the anti-Bet3 antibody (**Figure 4.7**).
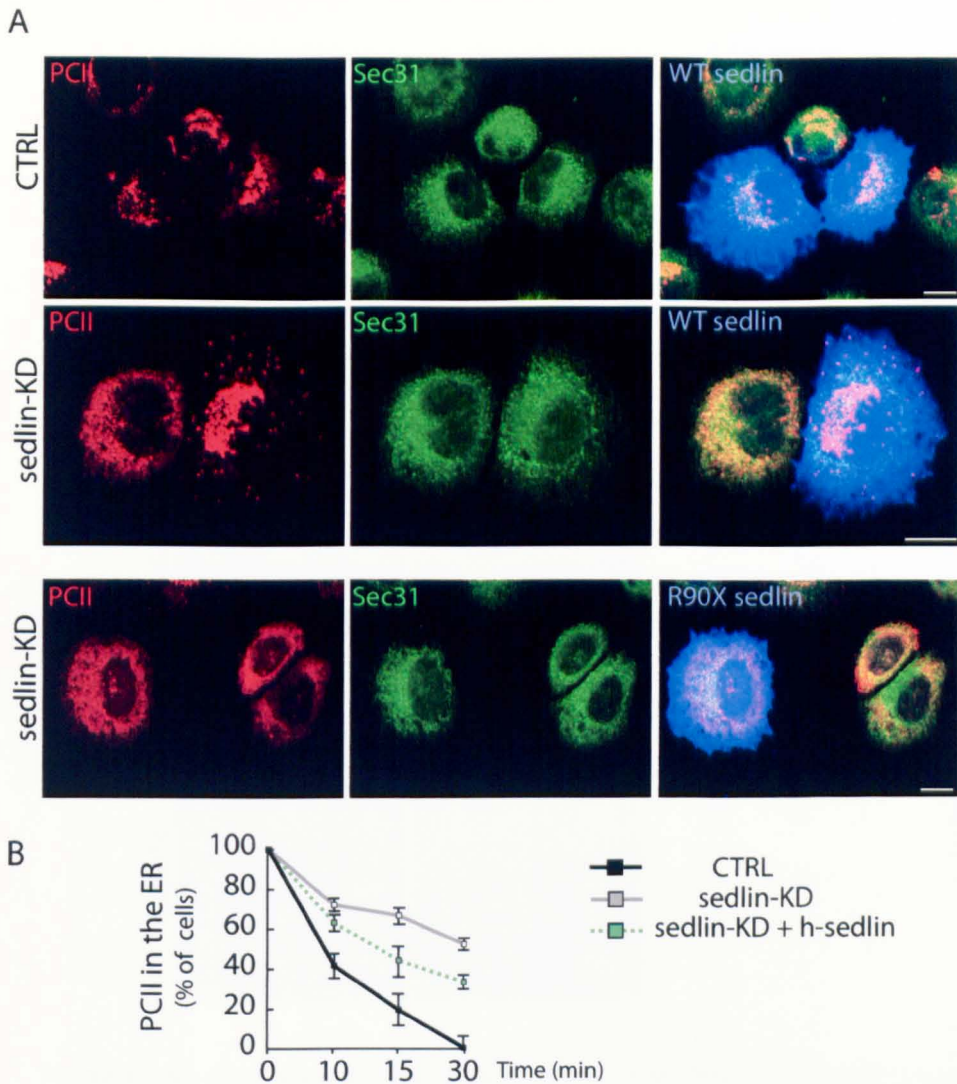
Figure 4.6 Re-expression of wild-type sedlin in sedlin-KD chondrocytes rescues the PCII exit from the ER while a disease-causing mutant does not. (A) Rx chondrocytes mock-treated (CTRL) or sedlin siRNA-treated chondrocytes (sedlin-KD) were microinjected with a plasmid encoding human wild-type sedlin, which is not sensitive to the RNAi treatment (two upper rows) or with a plasmid encoding a SEDT-causing mutation, R90X (bottom row). 4 hours post-injection, cells were incubated for 3 hours at 40°C and then shifted to the permissive temperature of 32°C for 30 minutes. Cells were then fixed and analysed by immunofluorescence. In control cells, the expression of WT-sedlin does not perturb PCII arrival to the Golgi, as observed in non-injected cells. In sedlin-KD chondrocytes, the expression of the sedlin protein restores the PCII exit from the ER. By contrast, the R90X-sedlin mutant fails to restore the ER exit of PCII. Scale bars, 10 μm. (B) Quantification of the ER exit of PCII in sedlin siRNA-treated or mock-treated Rx chondrocytes (CTRL) after the injection of sedlin RNA-resistant construct. Cells were treated as described in (A) and fixed at the time points shown. The data are expressed as % cells with PCII in the ER. Each experiment was repeated at least 3 times and the data are represented as mean values (± SD), n=100.
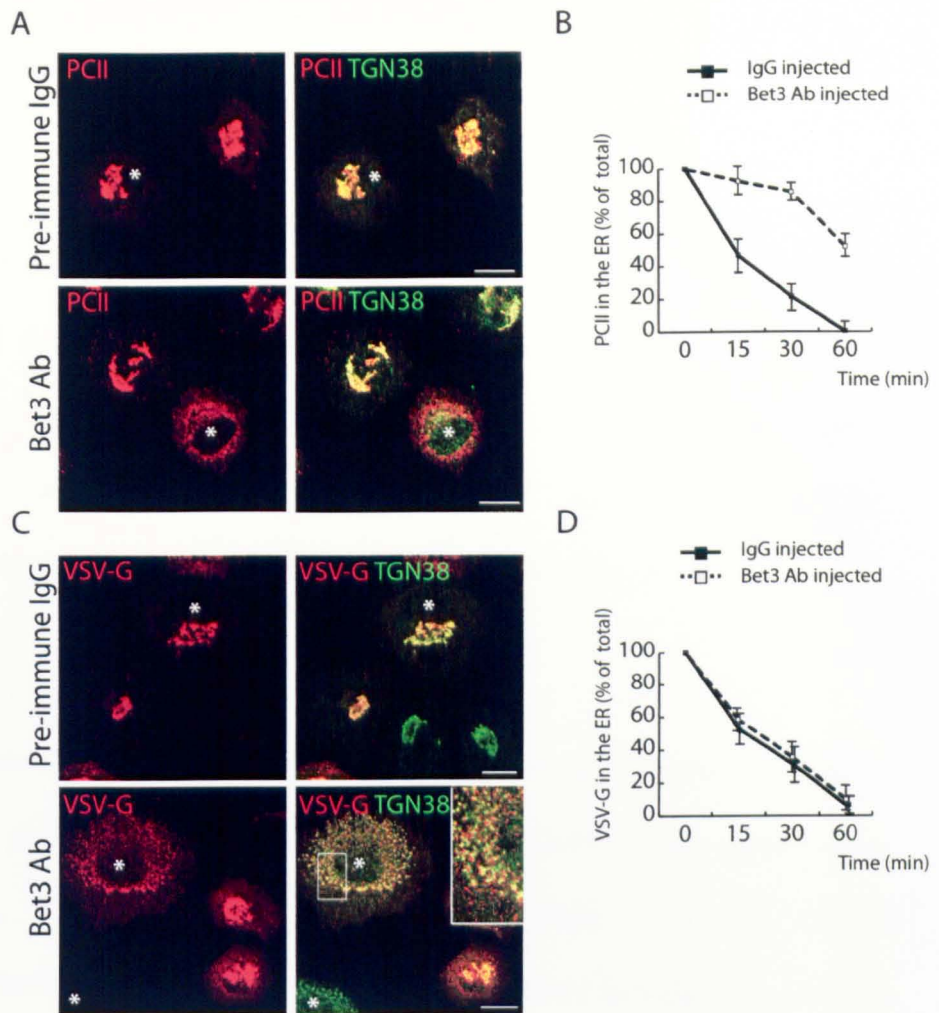
Figure 4.7 An acute block of TRAPP prevents PCII exit from the ER in Rx chondrocytes.
(**A**) Rx chondrocytes were microinjected with pre-immune IgG or an anti-Bet3 antibody (Bet3 Ab) during the second hour of the 40°C block. Immunofluorescence analysis was performed 30 min after shifting to the permissive temperature (32°C) using anti-PCII (red) and anti-TGN38 (green, a Golgi marker) antibodies. While in IgG-injected cells, PCII reaches the GC, in Bet3 Ab-injected cells, PCII exhibits an ER pattern. Asterisks indicate microinjected cells. Scale bars, 10 μm. (**B**) Quantitative analysis of PCII transport in IgG- and Bet3 Ab-injected Rx chondrocytes. Cells were treated as described in (A) and analyzed at the indicated time points. Mean values (± SD) from 4 independent experiments, n=100. (**C**) The acute block of TRAPP does not inhibit VSV-G exit from the ER in Rx chondrocytes. VSV-infected cells were microinjected with pre-immune IgG or an anti-Bet3 antibody (Bet3 Ab) during the 40°C block, similarly to the protocol used in (**A**). Immunofluorescence analysis was performed 30 min after shifting to the permissive temperature (32°C) using anti-VSV-G (red) and anti-TGN38 (green, a Golgi marker) antibodies. Asterisks indicate microinjected cells. Inset shows the colocalization of VSVS-G with the Golgi marker TGN38. Scale bars, 10 μm. (**D**) Quantitative analyses of VSV-G transport in VSV-infected Rx chondrocytes in IgG- and Bet3 Ab-injected cells. Cells were treated as described in C and analyzed at the indicated time points.

4.3 Sedlin role in aggrecan trafficking

Since I evaluated PCII trafficking in sedlin-KD chondrocytes, I wanted to extend the analysis to another major constituent of ECM secreted by chondrocytes, the aggrecan. Aggrecan is required to concentrate negative charges in the ECM, thereby providing the high degree of hydration necessary to maintain an expanded cartilage ECM volume.

This function reflects the covalent addition of several hundred chondroitin sulfate and keratan sulfate glycosaminoglycan chains to the aggrecan core protein. The 340 kDa core protein represents only 10% of the biosynthetically complete monomer and is further modified (N- and O-linked oligosaccharides). Aggrecan, link protein (a separate gene product) and hyaluronic acid are assembled in the extracellular space into large aggregates, which are further associated with the type II collagen-containing fibres. Biochemically, chondrocytes in culture synthesize the aggrecan core protein in the ER, process it to its mature form in the Golgi and secrete aggrecan into the medium.

Aggrecan is not a synchronysable cargo, so I set up a protocol to measure the ER "clearance" under sedlin depletion in chondrocytes. After siRNA treatment, chondrocytes (both mock and sedlin siRNA-treated) were incubated with hyaluronidase for 60 min to remove the ECM present on chondrocyte membranes, allowing the detection of the intracellular aggrecan. Then, cells were incubated with cycloheximide for an additional

30 minutes. In control cells, soon after hyaluronidase treatment, aggrecan localized at the ER and at the GC. By contrast, in sedlin-KD chondrocytes, aggrecan was mainly in the ER, with little or no evident Golgi localisation (**Figure 4.8**).

Moreover, after 30 minutes of CHX treatment in control cells, aggrecan was no longer localised at the GC but appeared at the PM. Conversely, in sedlin depleted chondrocytes aggrecan failed to reach the PM (**Figure 4.8**). Further and more detailed studies (such as pulse-chase and secretion experiments) will be required to dissect aggrecan intracellular transport in chondrocytes, but I can conclude that sedlin depletion perturbs aggrecan trafficking (**Figure 4.8**).

4.4 The inhibition of the ER exit of PCII by sedlin depletion does not involve Rab1

As Rab1 was found not to be involved in the TRAPP-mediated block of PCI in the ER (Chapter 3), I also controlled its possible involvement in the secretory phenotypes induced by sedlin and TRAPP depletion (inhibition of the ER exit of PCII) in chondrocytes.

Rab1A and B protein levels were depleted by using specific siRNAs in Rx chondrocytes. After three days of Rab1 siRNA treatment, Rab1 A and B were strongly reduced (up to 90%, **Figure 4.9**).
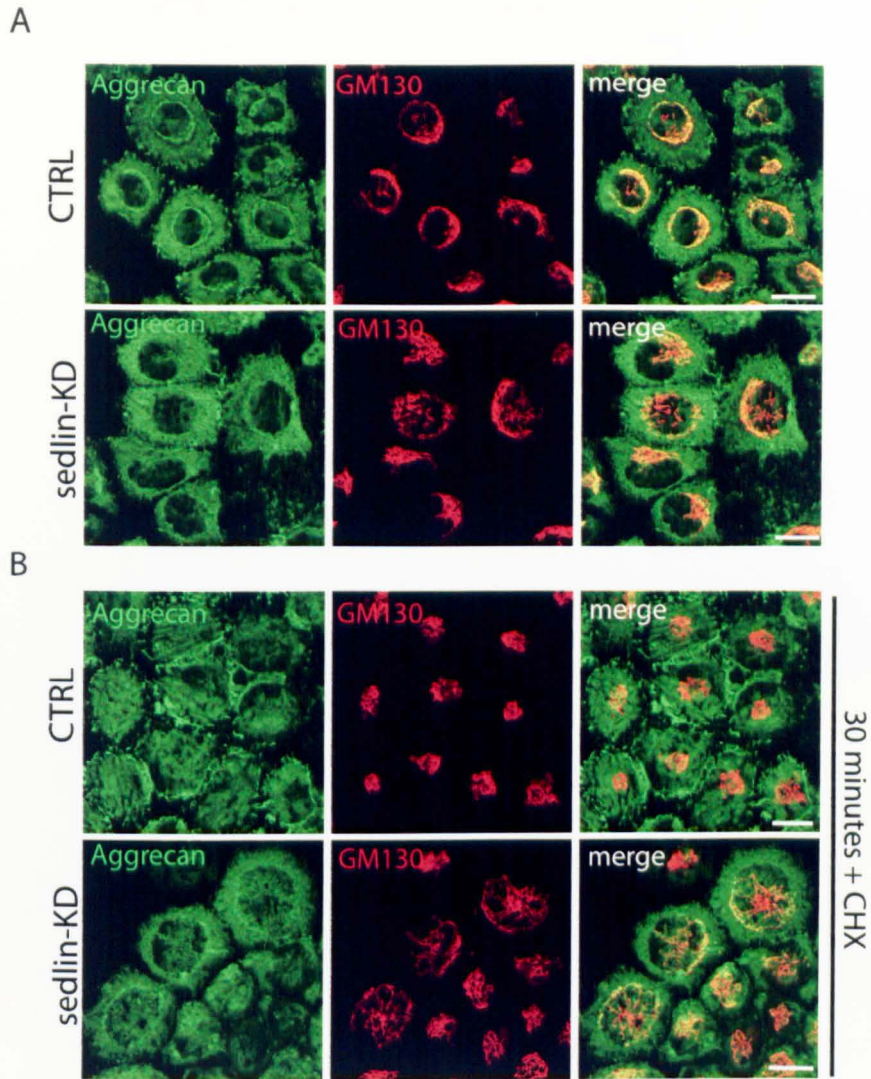
Figure 4.8 Aggrecan trafficking is affected in sedlin-KD chondrocytes. Rx chondrocytes were mock or sedlin siRNA treated for three days and then incubated for 1 hour at 37°C with hyaluronidase. After this treatment, control and KD cells were fixed (A) or incubated for an additional 30 minutes in presence of CHX (B) and then fixed and processed for immunofluorescence experiments. **(A)** After hyaluronidase treatment, aggrecan (green) shows an ER and Golgi pattern in control cells (as highlighted by the co-localisation with the Golgi marker GM130 in red). In sedlin-KD chondrocytes, aggrecan exhibits ER staining but not the Golgi staining. **(B)** 30 minutes after hyaluronidase removal, aggrecan is no longer present at the GC in control cells. By contrast, in sedlin-KD cells aggrecan begins to appear not only in the ER (as depicted at the steady state) but also in the GC. Scale bars, 10 μm.
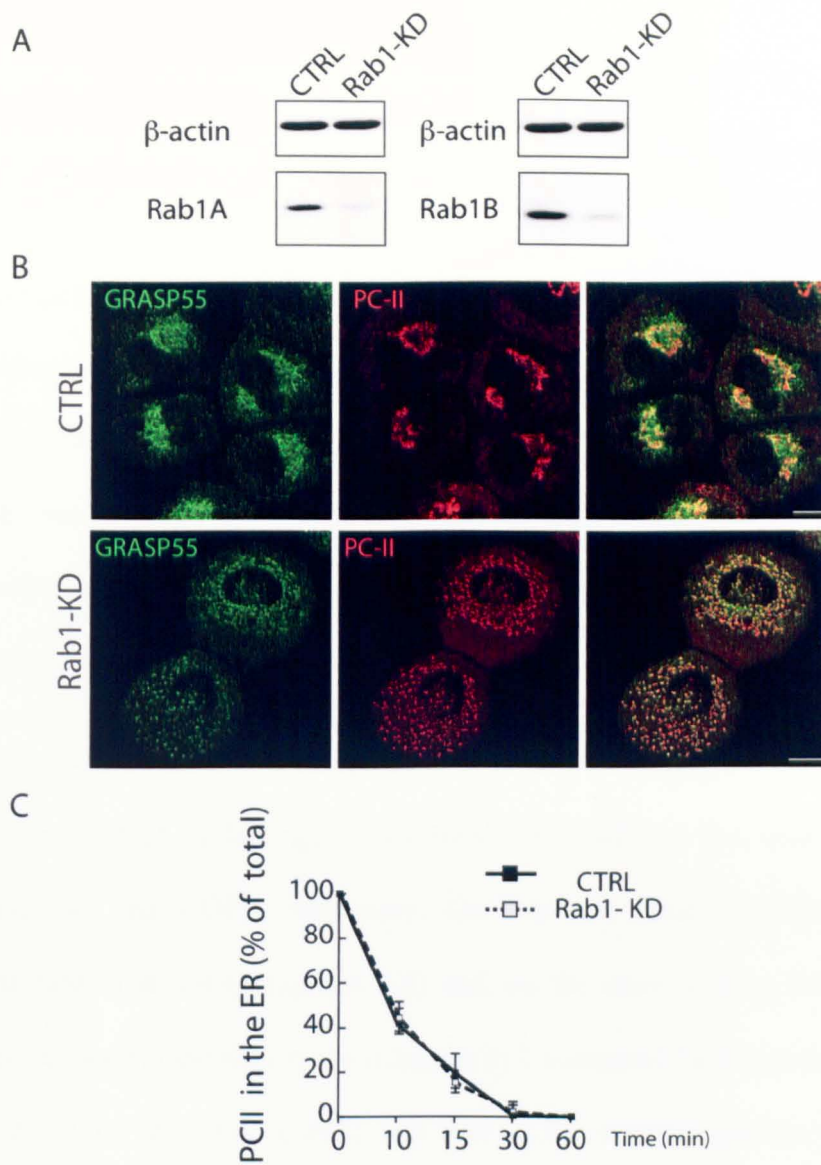
Figure 4.9 Rab1 KD does not affect the ER exit of PCII in Rx chondrocytes. Rx chondrocytes were mock-treated (CTRL) or treated with siRNAs against both Rab1A and Rab1B (Rab1AB) **(A)** Western blot analysis of siRNA treated cells: cell lystaes (60 µg/lane) were probed with an anti-Rab antibody. Both Rab1A and B are reduced. β-actin was used as a loading control. **(B)** After 72 hours of siRNA treatment, the cells were incubated for 3 hours at 40°C and then shifted to the permissive temperature (32°C) for 30 min. Cells were fixed and stained for PCII (red) and the Golgi marker GRASP55 (green). Note the extensive vesiculation of the Golgi complex after Rab1 KD, clearly visible by GRASP55 staining. Scale bars 10 µm. **(C)** Quantification of the ER localisation of PCII over time in mock-treated (CTRL) and Rab1AB silenced cells. PCII exit out the ER is similar between control and Rab1-KD cells. The values are the mean (±SD) from 3 independent experiments, n=200.

I performed a synchronisation protocol on control and Rab1-KD cells to evaluate PCII trafficking in these cells and found that PCII was not retained into the ER (**Figure 4.9**). In addition, the GC morphology appeared heavily compromised, as shown by the vesiculated GRASP55 staining (Figure 4.9). Therefore, Rab1 depletion obtained by the combined KD of Rab1a and Rab1b mimicked the effects of TRAPP depletion on the Golgi complex, which was extensively vesiculated but did not reproduce the selective inhibition of PCI and PCII ER exit observed upon sedlin (and TRAPP) depletion.

Having excluded a role for the GTPase Rab1 as part of the function exerted by sedlin in PCII trafficking, I considered the possibility that sedlin could act also on the COPII machinery. On the one hand I analyzed the localization of sedlin (paragraph 4.5) and, on the other, having found that sedlin can control the Sar1 cycle (Chapter 3) I compared the requirement for Sar1 cycle for the exit of PCII and that of the reporter protein VSV-G (paragraph 4.6)

4.5 Rx chondrocytes: sedlin localisation

I analysed sedlin distribution in wild type Rx chondrocytes to validate the localisation found in other cell lines. Also here sedlin localised at the ERES where it co-stained with the COPII component Sec31 (**Figure 4.10**).
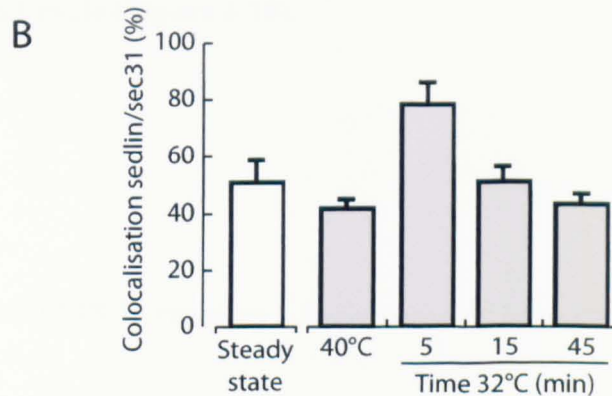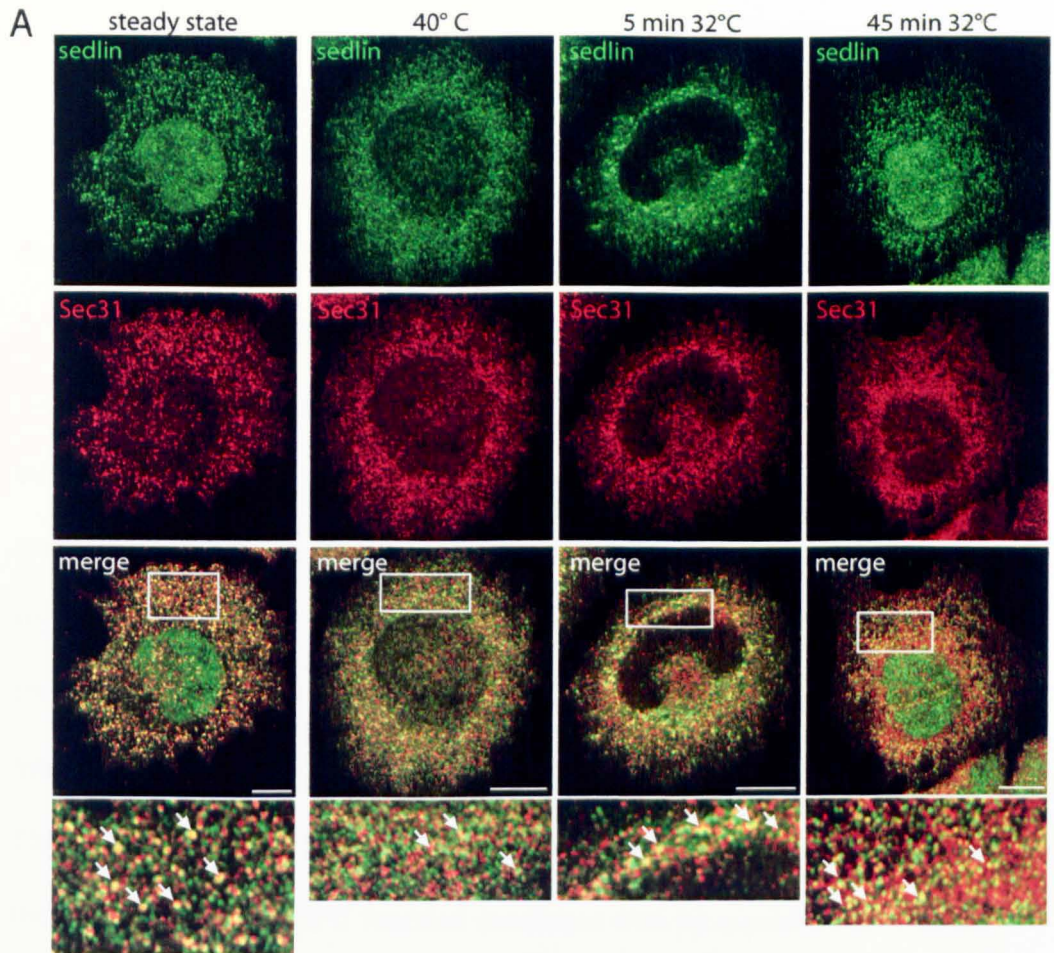
Figure 4.10 Sedlin is actively recruited to ERES during a traffic pulse in Rx chondrocytes. (**A**) Rx chondrocytes at steady state or during a 40°-32°C synchronisation protocol were paraformaldehyade-fixed, permeabilised with 0.1% Triton X-100 and processed for immunofluorescence analyses at the indicated times. Sedlin (green) co-localises with Sec31 (red) in all the analysed time points, with a clear increase at 5 minutes after the shift to the permissive temperature. White boxes indicate regions magnified in the lower panels. Arrows mark sedlin and Sec31 positive ERES. Scale bars, 10 μm. (**B**) Colocalisation analyses of sedlin and Sec31 were carried out under steady state conditions and during a trafficking wave (3 hours at 40°C and then 5, 15 and 45 minutes at 32°C). Three different single optical slices were taken for each cell (*n=20*), and the mean values (± SD) are shown.

Next, I studied the behaviour of sedlin in Rx chondrocytes during a synchronised wave of PCII transport induced by imposing the temperature block/release protocol. At 40 °C, no significant changes in sedlin distribution was detected compared to steady state conditions (**Figure 4.10**). After 5 minutes at 32 °C, sedlin appeared to be heavily recruited on roundish Sec31-positive structures. At later time-points (15 and 45 minutes), sedlin appeared less associated to Sec31 compared to 5 minutes, gradually restoring the steady state conditions (**Figure 4.10**). These data suggested that sedlin is involved in some early events of PCII carrier formation, because the increased co-localisation at ERES was a very transient event, likely coinciding with peak PCII-carrier formation at ERES. These data indicate the sedlin is actively recruited at the ERES, supporting the role of sedlin in COPII function consistent with its capability to bind and regulate the Sar1 cycle (**Figure 4.10**).

4.6 The ER exit of PCII requires a higher rate of Sar1 cycling than the exit of VSV-G

Altogether the previous findings both in chondrocytic and non-chondrocitic cell lines indicated that sedlin (and the TRAPP complex) are selectively required for the exit of PC (PCII and PCI) and can control the Sar1 cycle via the direct interaction of sedlin with Sar1.

I now wanted to assess whether the two activities are related, and thus whether the ER exit of PC have "special" requirement in term of Sar1 cycle compared to the exit of other cargoes (i.e. VSV-G).

As the slower Sar1/COPII cycle induced by sedlin/TRAPP depletion was still permissive for the export of many cargoes (including VSV-G) from the ER, but not for that of PCs, I tested the hypothesis that different cargoes require a different rate of Sar1 cycling to exit the ER. I evaluated the impact of progressively blocking the Sar1 GTP/GDP cycle on the ER exit of PCII and VSV-G by microinjecting increasing amounts of the GTP-locked mutant of Sar1 (Sar1H79G). At a low level of Sar1H79G (0.1 mg/ml) the exit of PCII and VSV-G from the ER was not affected, while at an intermediate level (0.5 mg/ml) the ER exit of PCI and PCII, but not of VSV-G, was selectively impaired (**Figure 4.11**). Higher levels of Sar1H78G (2.5 mg/ml) blocked the exit of all cargo, in agreement with previous reports (Pepperkok et al., 1998). I can conclude that ER exit of the large cargo molecules (such as PCII) requires a faster Sar1 cycle than that of VSV-G (**Figure 4.11**).

A possible explanation for the requirement of a higher rate of Sar1 cycling for the export of PCI (compared to the exit of VSV-G) might be found in the ability of Sar1-GTP to induce membrane bending/constriction (Long et al., 2010). A prolonged GTP-bound state of Sar1 at the ERES would induce local membrane narrowing that would remain permissive for the entry of small but not large cargoes into the nascent carriers.
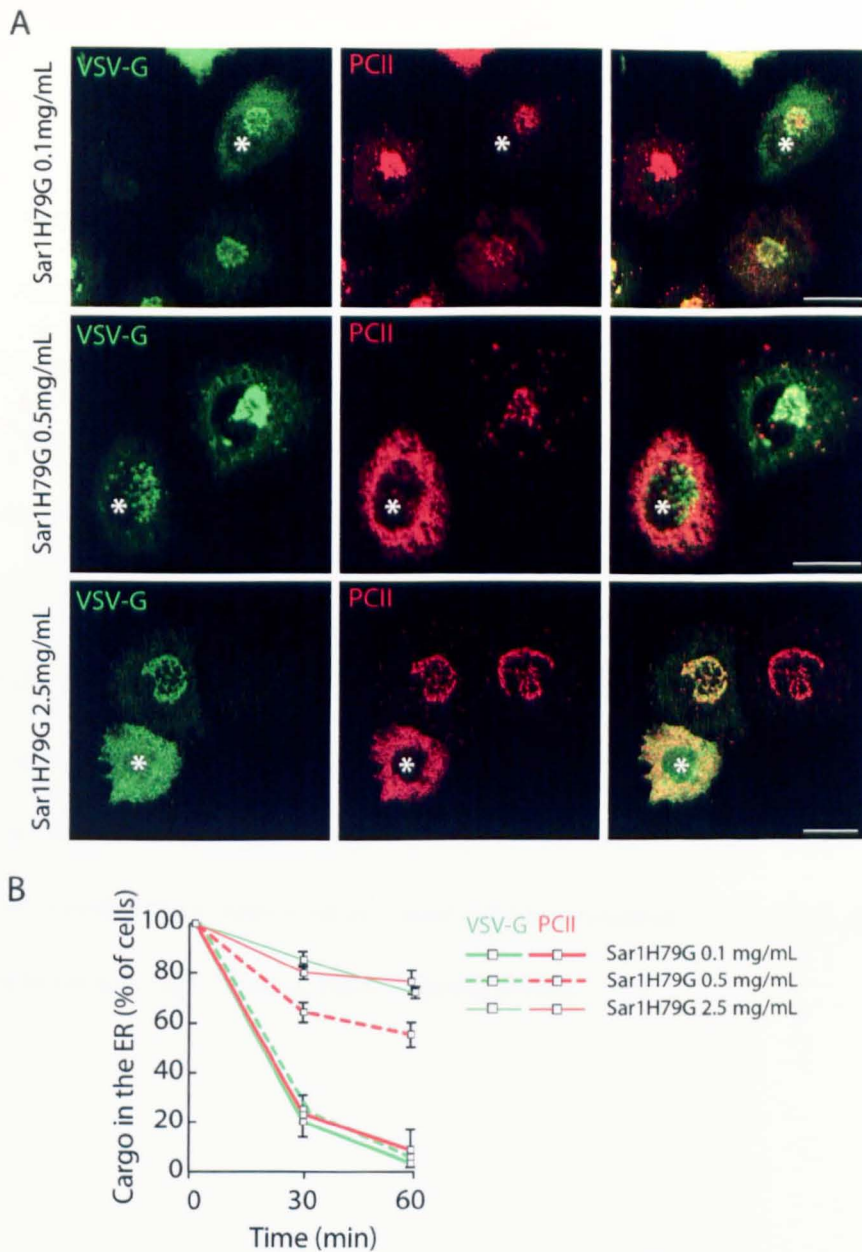
Figure 4.11 Efficient Sar1 cycling is required for the exit of PCII but not VSV-G from the ER. (A) Rx chondrocytes were VSVtsO45-infected for 1 hour at 32°C and then incubated at 40°C for three hours. During the last hour, cells were microinjected with His-Sar1H79G (asterisks) at the indicated dilutions (0.1, 0.5 and 2.5 mg/ml) and then shifted to the permissive temperature. 30 minutes after the shift to 32°C, the cells were fixed and processed for indirect immunofluorescence to analyse intracellular trafficking of VSV-G (green) and PCII (red). Scale bars, 10μm. A low concentration of Sar1H79G does not affect the ER exit of the two cargo molecules, while a high concentration completely blocks the ER exit of VSV-G and PCII. By contrast, at an intermediate concentration (0.5 mg/ml) Sar1H79G inhibits only PCII but not VSV-G exit from the ER. Scale bars, 10 μm **(B)** Quantification of the ER exit of VSV-G and PCII with increasing concentrations of His-Sar1H79G at the indicated time points. Data are reported as mean values (± SD) from three independent experiments.

A prolonged membrane association of Sar1-GTP leads to local increases in Sar1-GTP concentration which, by inducing closely-spaced membrane constrictions, might prevent the formation of carriers large enough to accommodate PC prefibrils. In order to test this hypothesis we performed IEM and tomographic analyses of ERES in TRAPP depleted cells. Indeed, the IEM analysis showed that, compared to control cells, TRAPP depleted cells had a twofold increase in Sar1 labeling density on the round and tubular profiles of the ERES (**Figure 4.12**).

Finally the tomographic analysis showed that the ERES in TRAPP-depleted cells, compared to those in mock treated cells (Scanu, Ph.D. Thesis, 2008), were characterized by a higher number of tubules with very narrow constrictions which appeared as round profiles connected with each other as "beads on a string" (Scanu, Ph.D. Thesis, 2008).
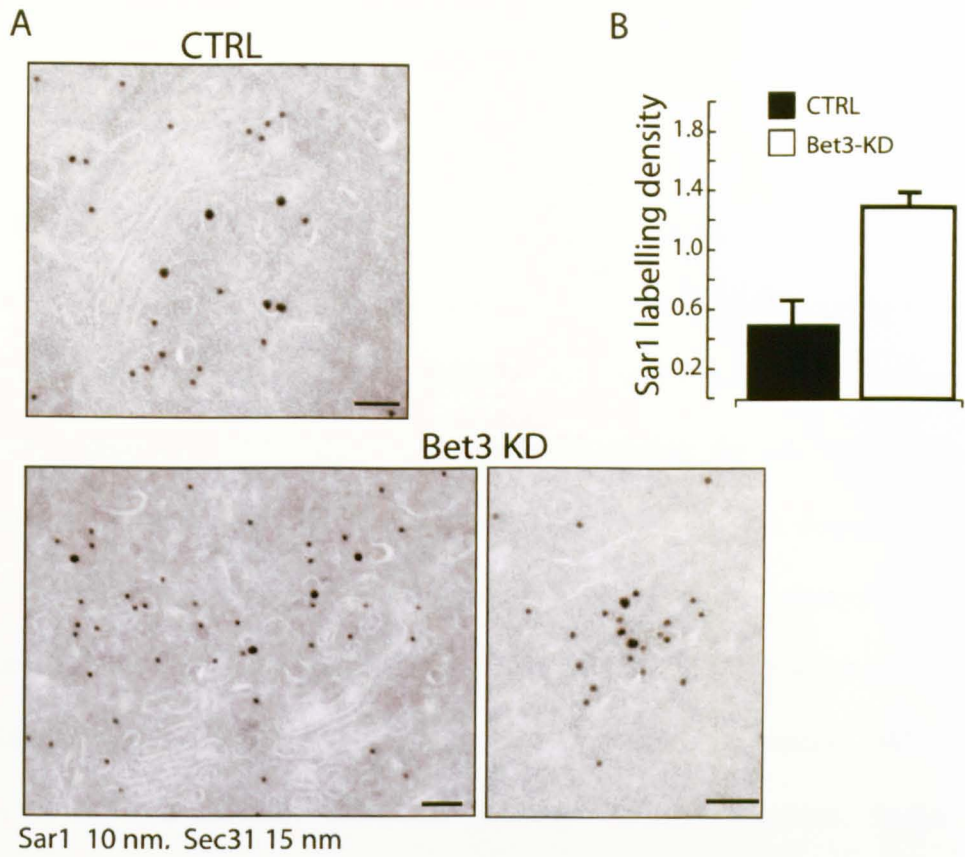
Figure 4.12 Sar1 is more associated to ERES membranes in TRAPP-depleted cells.
(**A**) Immunoelectron microscopic analyses of HeLa cells treated with non-targeting (CTRL) and Bet3 siRNAs (Bet3-KD) show that the KD of Bet3 causes an accumulation of Sar1 and Sec31 near the Golgi stack remnants. Scale bars, 200nm. (**B**) Quantitative analysis of Sar1 labelling (expressed as labelling density).

4.7 Analyses of disease-associated mutants of sedlin

At this stage of my studies it became crucial to assess the relevance of all these findings for the pathogenesis of SEDT. To this end, I first tested two disease-associated sedlin mutants (del387a and R90X) in the Sar1-binding assay. I produced GST-sedlin fusion proteins bearing the two mutations identified in SEDT patients. Next, I performed the GST pull down assay under the same conditions used to perform the other binding assays and I found that they exhibited a significantly lower affinity for Sar1 compared to wild-type (WT) sedlin (**Figure 4.13**). I tested also another mutation, D47Y, one of the four missense mutations identified in SEDT patients. Sedlin D47Y was still able to bind Sar1, but its affinity appeared higher compared to wild type sedlin (**Figure 4.13**).

Among the identified disease-causing mutations of sedlin, the majority result in early termination during translation, leading to degradation of partially translated peptides. Recent biochemical studies showed that three of the four missense mutations, S73L, F83S and V130D, caused misfolding of the mutant protein, activating protein degradation pathways when mutant sedlin proteins were over-expressed as GFP-tagged proteins in cells (Choi et al., 2009). These missense mutants also failed to bind known interacting proteins of sedlin, including MBP1, pituitary homeobox 1 (PITX1) and steroidogenic factor 1 (SF1; Jeyabalan et al., 2010).
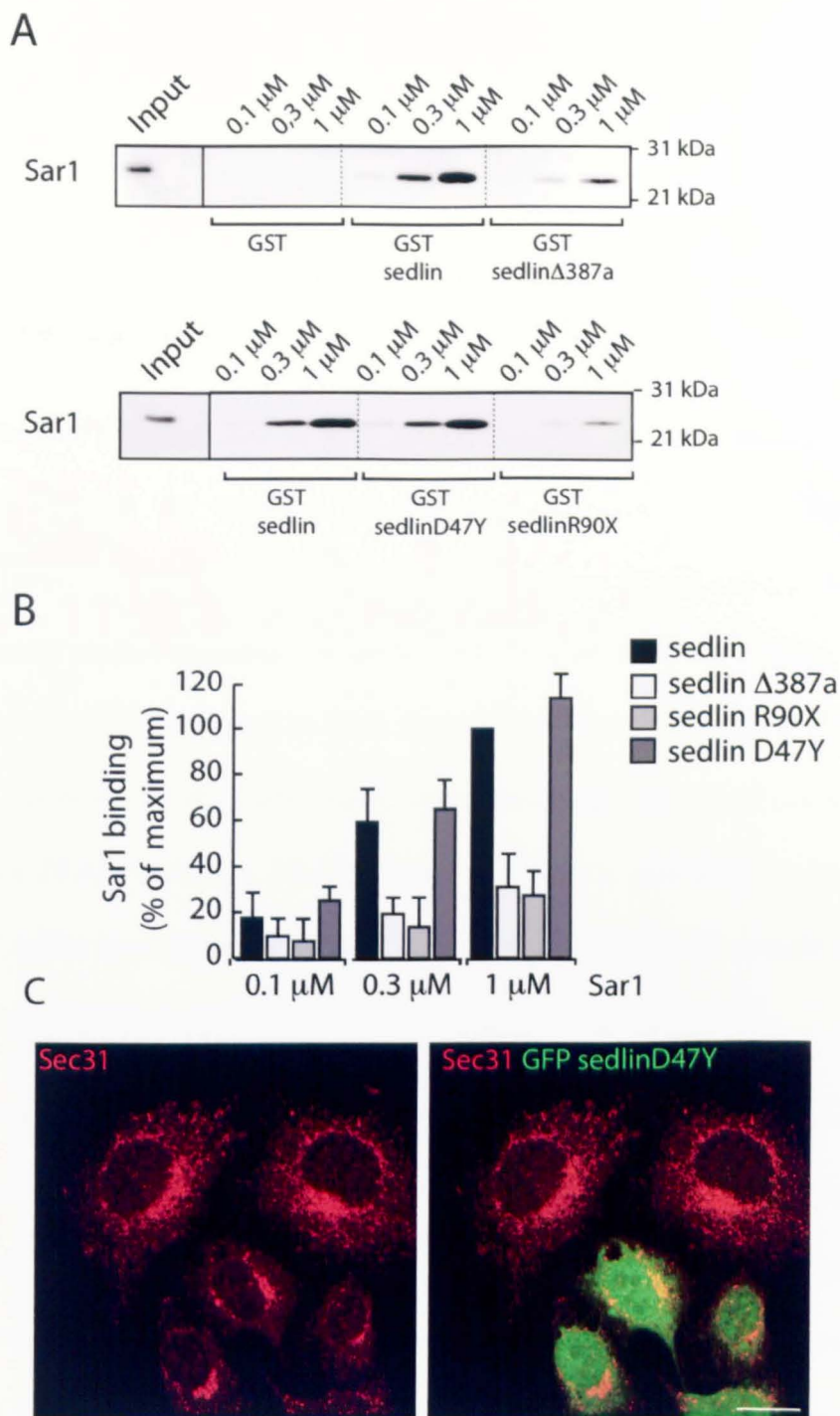
Figure 4.13 SEDT mutations result in an altered affinity for Sar1. (A) GST, GST-sedlin (WT) and the disease-associated sedlin mutants GST-sedlin del387a (upper panel) GST-sedlin D47Y and sedlin R90X (lower panel) were incubated with increasing concentrations of His-Sar1, as indicated. After overnight incubation, GSH-agarose beads were added to each sample, to perform the GST-pull down. Except for the D47Y mutant that exhibits slightly increased affinity for Sar1 (note the 0.1 μM point), all the mutants show a reduced affinity for Sar1. **(B)** Graph reports mean values (±SD) of three experiments performed in duplicate. Values are expressed as a percentage of the sedlin-Sar1 binding relative to 1 μM Sar1 (% of Maximum). **(C)** GFP sedlin D47Y perturbs the ERES distribution. HeLa cella were transfected for 16 hours with a plasmid encoding a GFP – tagged sedlinD47Y protein. Cells were fixed and stained with a Sec31 Ab. In sedlin D47Y expressing cells, Sec31 is strongly recruited to the perinuclear area as compared to non-transfected cells. Scale bar, 10 μm.

Since proteins encoded by sedlin mutants are more prone to degradation, one possibility is that the loss of interaction between sedlin mutants and its interactors in the cell might be due to the instability of proteins caused by protein degradation.

The D47Y mutant was of particular interest since the mutation *per se* does not perturb the stability of the protein. Moreover, the amino acid substitution does not cause a dramatic change in the protein properties. Recent studies revealed that sedlin-D47Y has an increased affinity for Bet3 and remains associated to Bet3 for a longer time compared to WT sedlin (Choi et al., 2009). Furthermore, this mutant has been found not to bind to two TRAPP subunits, TRAPPC8 and TRAPPC9, revealing the importance of sedlin as an adaptor protein for the assembly of TRAPP complexes (Zong et al., 2011).

On the basis of the finding that sedlin-D47Y has an altered affinity for Sar1, I decided to express a GFP-tagged version of this mutant in HeLa cells and I checked its impact on the COPII machinery by immunofluorescence. I found that the expression of GFP-sedlin-D47Y caused a recruitment of the COPII marker Sec31 to larger structures, similar to what was observed upon Sar1H79G over-expression. By contrast, GFP-sedlin at low levels of expression did not cause any significant changes in Sec31 distribution compared to control cells (**Figure 4.13**).

All the three tested sedlin mutants showed an altered affinity for Sar1 compared to WT sedlin. These findings suggest that this interaction is relevant for SEDT pathogenesis. This correlation was reinforced by the observation that while the WT sedlin was able to rescue the ER exit of PCII in sedlin-depleted chondrocytes, the disease-associated sedlin mutant (the R90X), unable to bind Sar1 *in vitro*, was not.

4.8 COPII dynamics and PCII trafficking in SEDT and control primary fibroblasts

As a final and most relevant test of our model, i.e. that sedlin is required for PCII exit and for a fast Sar1 cycle, I used fibroblasts isolated from a SEDT patient bearing one of the studied mutations: sedlin del387a. This mutation leads to a frameshift at the C-terminal that causes the loss of the last 6 amino acids (**Figure 4.14**).

I analysed the morphology of these primary fibroblasts first by immunofluorescence and secondly by ultrastructural analyses. I analysed the Golgi structure and the COPII Sec31 in SEDT fibroblasts and in primary fibroblasts isolated from a healthy subject. The GC of SEDT fibroblasts appeared indistinguishable from the GC of the control fibroblasts (**Figure 4.14**). A slight difference was evident regarding COPII staining: in SEDT fibroblasts Sec31 appeared more associated to membranes compared to control fibroblasts (**Figure 4.14**).

A

```
sedlin WT        MSGSFYFVIVGHHDNPVFEMEFLPAGKAESKDDHRHLNQFIAHAALDLVDENMWLSNNMY
sedlin del387a   MSGSFYFVIVGHHDNPVFEMEFLPAGKAESKDDHRHLNQFIAHAALDLVDENMWLSNNMY
                 ************************************************************

sedlin WT        LKTVDKFNEWFVSAFVTAGHMRFIMLHDIRQEDGIKNFFTDVYDLYIKFSMNPFYEPNSP
sedlin del387a   LKTVDKFNEWFVSAFVTAGHMRFIMLHDIRQEDGIKNFFTDVYDLYIKFSMNPFYEPNSP
                 ************************************************************

sedlin WT        IRSSAFDRKVQFLGKKHLLS
sedlin del387a   IRSSAFDRKFSFLGRNTF--
                 *********..***:: :
```

B

CTRL fibroblasts   SEDT fibroblasts

GM130   GM130

Sec31   Sec31

merge   merge

C

CTRL fibroblasts
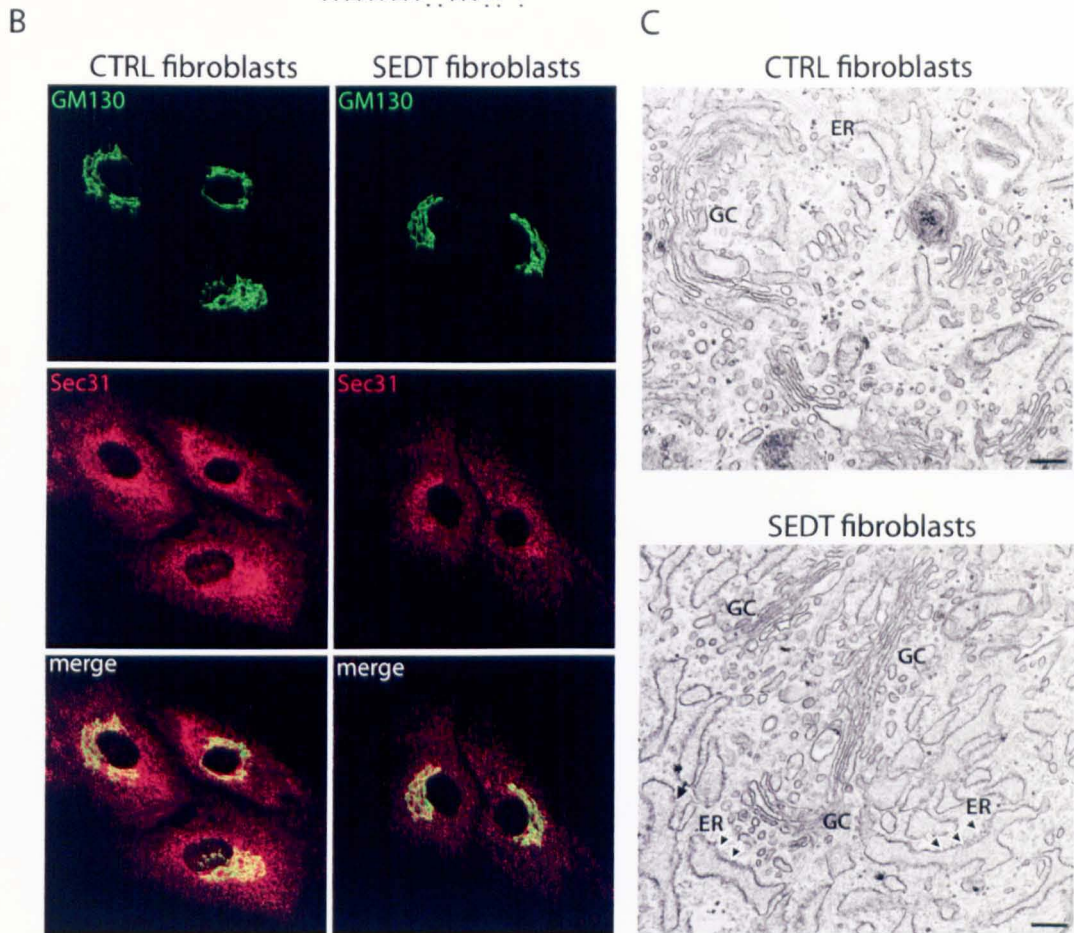
SEDT fibroblasts

Figure 4.14 SEDT fibroblasts show a normal Golgi morphology but a slightly altered ER exit site distribution. (**A**) Sequence alignment between wild-type sedlin and a mutant sedlin isolated from a SEDT patient. Deletion of a single nucleotide at position 387 causes a frameshift resulting in a truncation of the last C-terminal 9 amino acid. The alignment was generated using ClustalW. (**B**) Control (CTRL) and SEDT fibroblasts were seeded onto coverslips the day before the experiment. Cells were PFA fixed and processed for indirect immunofluorescence experiments. GM130 (green) was used to analyse the GC morphology, while Sec31 (red) to evaluate the ERES organisation. In both CTRL and SEDT fibroblasts the GC appears normal and is not vesiculated. On the other hand, ERES distribution appears slightly different between control and SEDT fibroblasts. While a large number of peripheral Sec31-positive spots are evident in control cells, Sec31 is more concentrated at the ERES in SEDT fibroblasts, with a slight reduction in the number of Sec31-positive spots. (**C**) SEDT fibroblasts exhibit dilated ER and a regular Golgi complex. Wild type (CTRL from a healthy subject) and SEDT fibroblasts were fixed and processed for electron microscopy analysis. GC, Golgi complex; ER, endoplasmic reticulum. Note that the GC in SEDT fibroblasts appears similar to CTRL fibroblasts. Arrowheads indicate dilated ER. Scale bars: 200 nm.

Notably, these SEDT fibroblasts exhibited a dilated ER at the EM level, a finding in accordance with what was observed in a SEDT bioptic sample reported previously (Tiller et al., 2001).

I then compared COPII dynamics in control and SEDT fibroblasts. The fibroblasts were injected with the Sec23-GFP plasmid and the FRAP half-life of single ERES was measured. Sec23-GFP exhibited remarkably slower dynamics in SEDT fibroblasts than in WT fibroblasts (**Figure 4.15**). Importantly, the expression of WT sedlin in the SEDT fibroblasts partially corrected the COPII cycle defect (**Figure 4.15**).

Finally, I assessed the trafficking of PC in control and SEDT fibroblasts. First, I analysed the ER-to-Golgi transport of endogenous PCI. I found that PCI exit from the ER was slower in SEDT fibroblasts compared to control fibroblasts (**Figure 4.16**). To follow the ER export of PCII, control and SEDT fibroblasts were transfected with a plasmid encoding a fluorescently-tagged PCII and subjected to a synchronized trafficking protocol.

During the 40° block, PCII was retained in the ER in both WT and SEDT cells.

After 30 minutes at the permissive temperature and in the presence of ascorbate and CHX, PCII was almost completely concentrated in the perinuclear region (positive for the Golgi marker TGN46) in WT fibroblasts
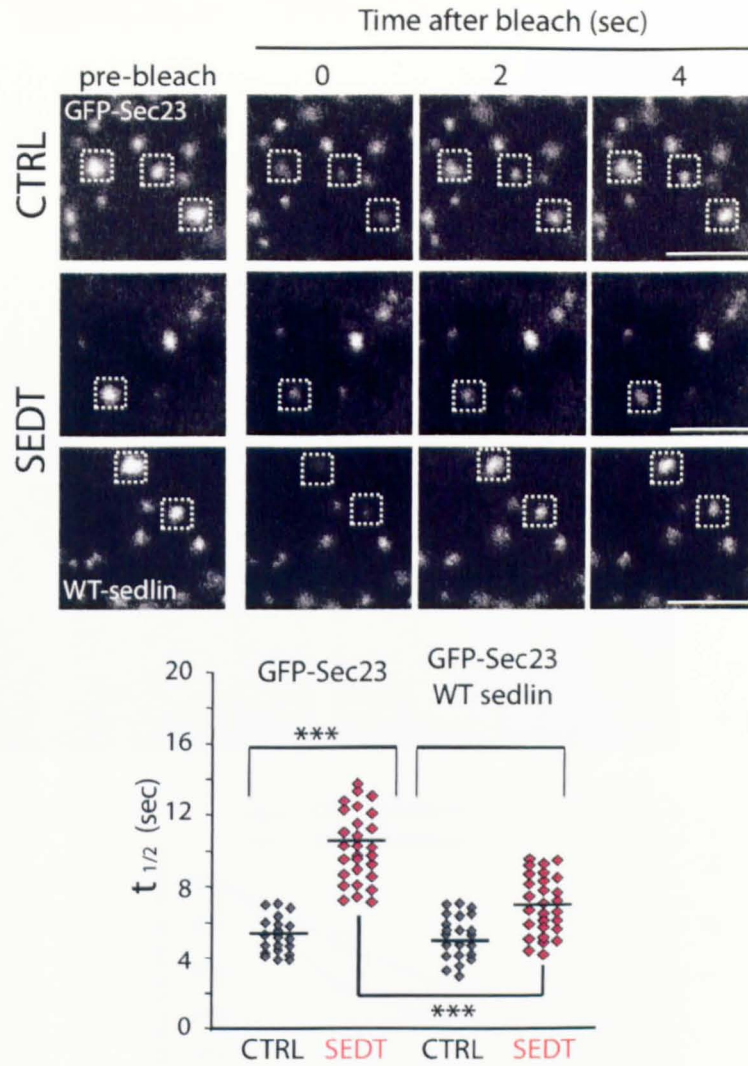
Figure 4.15 The COPII cycle is slower in SEDT fibroblasts. FRAP analysis of ERES (labelled with GFP-Sec23 and performed as described in Chapter 3) is shown in fibroblasts from a healthy subject (CTRL), in fibroblasts from a SEDT patient (SEDT) or in fibroblasts from a SEDT patient transfected with WT sedlin (SEDT+WT-sedlin). The four images show different time points of a time-lapse sequence. The white squares indicate the bleached ERES. "0" is the first image acquired after the bleaching. Scale bars, 2 μm. The graph reports the $t_{1/2}$ for the FRAP of single ERES in fibroblasts from a healthy donor (CTRL) or from a SEDT patient (SEDT) in the absence or in the presence of co-expressed WT sedlin (GFP-Sec23 + WT sedlin). GFP-Sec23 CTRL n=20, SEDT n=27; GFP-Sec23 + WT sedlin CTRL n=22 and SEDT n=29; n represents the number of analysed ERES. Asterisks indicate a P value < 0.0001. The experiment was repeated three indipendent times in duplicates, with similar results. At least 60 ERES were analysed for each experiments.

206
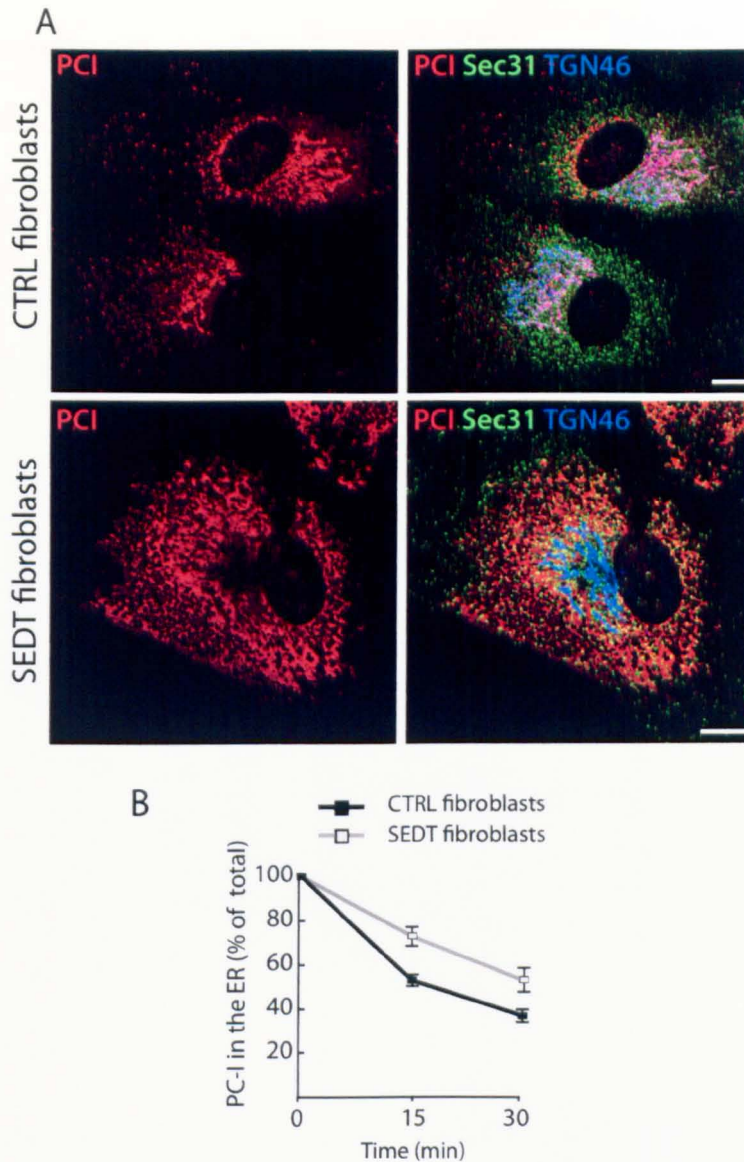
Figure 4.16 PCI exit from the ER is impaired in SEDT-isolated primary fibroblasts
(**A**) Primary fibroblasts isolated from a healthy subject (CTRL) or from a SEDT patient
(SEDT) were incubated for 3 hours at 40°C. After the temperature block, cells were
shifted to 32°C for 30 minutes in the presence of ascorbate and CHX. Cells were then
fixed and processed for immunofluorescence. In control fibroblasts, PCI (red) reaches the
GC (green), and it is not retained into the ER (PDI, blue). By contrast, PCI exit from the
ER is slower in SEDT fibroblasts, as shown by the co-localisation between PCI and PDI.
Scale bars, 10 μm. (**B**) The graph reports mean values (±SD) of three experiments
performed in duplicate (*n=100*). Values are expressed as a percentage of cells with PCI
into the ER.

but remained distributed in the ER throughout the cytoplasm in SEDT fibroblasts (**Figure 4.17**). Importantly, the expression of a full-length WT sedlin protein in SEDT fibroblasts could rescue the PCII export from the ER (**Figure 4.17**).

Collectively, the above results provide a molecular basis for the defective chondrogenesis resulting from sedlin mutations in SEDT patients.
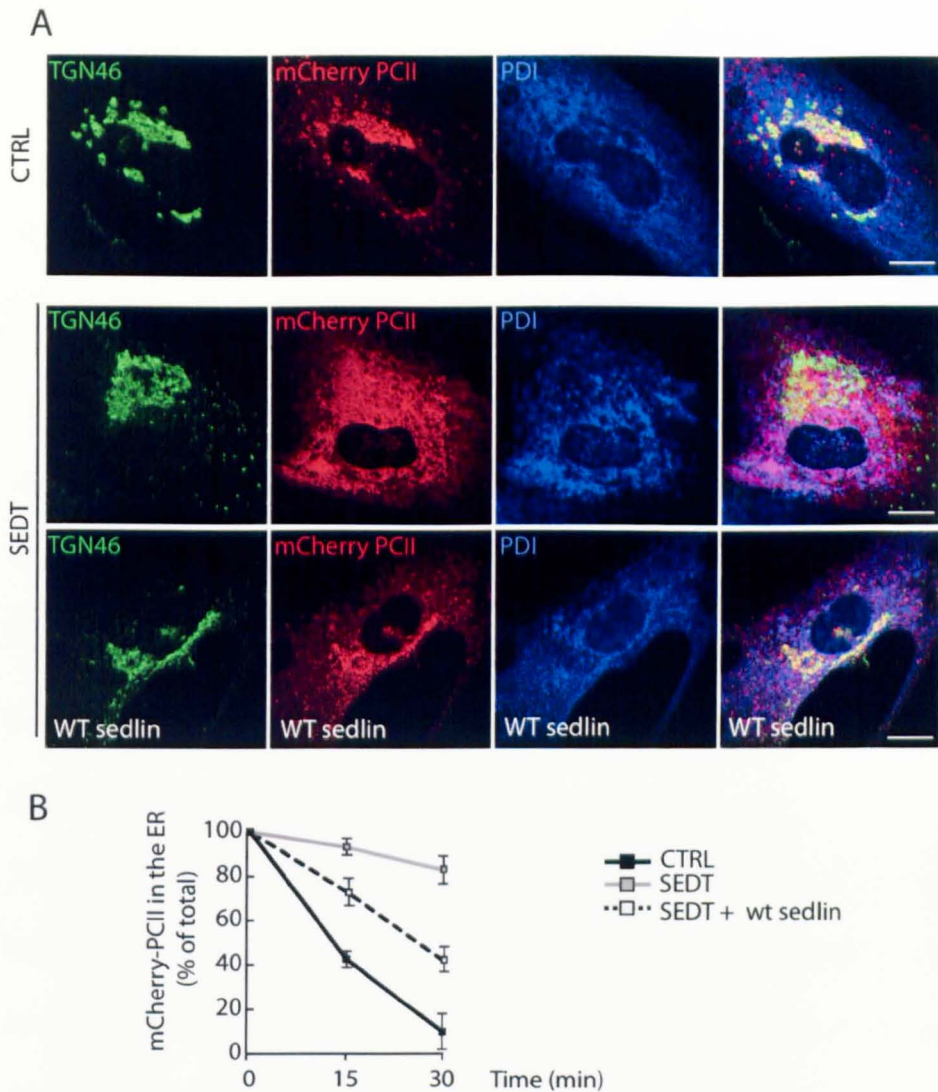
Figure 4.17 The exit of PCII from the ER is impaired in SEDT fibroblasts and corrected by WT sedlin. (A) A plasmid encoding fluorescently-tagged PCII (mCherry, red, top two rows) or the same construct together with a plasmid encoding full-length WT sedlin (bottom row) were microinjected into the nuclei of human fibroblasts isolated from from a healthy (CTRL) or a SEDT subject and incubated at 37°C for 3 hours. The cells were then incubated at 40°C for 3 hours, and subsequently shifted to the permissive temperature for 30 minutes. Cells were fixed and processed for indirect immunofluorescence using anti-TGN46 (a Golgi marker) or anti-PDI (and ER marker). In control fibroblasts, PCII reaches the GC after 30 minutes, while in SEDT fibroblasts it fails to leave the ER, as demonstrated by the co-localisation with PDI. The overexpression of a WT sedlin restores PCII transport. Scale bars, 10 μm. (B) Quantitative analyses of the transport of PCII out of the ER assessed as described in (A). Mean values (± SD) from 3 independent experiments are shown.

Discussion

The TRAPP complex is involved in several and important membrane trafficking steps along the secretory pathway.

Here, for the very first time, I provide different lines of evidence that correlates the function of the TRAPP complex and of its subunit sedlin in membrane trafficking and the onset of Spondyloepyphiseal dysplasia tarda (SEDT).

I analyzed the role of TRAPP in rat (Rx) chondrocytes, a cell line relevant for SEDT, where the main affected tissue is the cartilage (Tiller et al., 2001). As discussed in Chapter 3, sedlin/TRAPP are involved in controlling the ER exit of procollagen type I in fibroblasts by regulating Sar1. In this scenario, I wanted to verify whether also the trafficking of PCII, the major cargo in chondrocytes, was dependent on TRAPP (and sedlin).

PCII shares some similarities with PCI in terms of shape and size (a triple helix of 300 nm). Interestingly, mutations occurring in PCII are responsible for the onset of a similar pathology, Spondyloepyphiseal dysplasia congenita, highlighting the importance of PCII in endochondral bone formation processes.

I found that sedlin is selectively required for the ER exit of PCII but it is dispensable for VSV-G in chondrocytes. Similarly to sedlin, TRAPP depletion does not affect VSV-G trafficking out of the ER in chondrocytes, but strongly inhibits its arrival to the PM. Furthermore, as observed in HeLa

cells, total protein secretion is not compromised by sedlin depletion in Rx chondrocytes. On the other hand, the loss/impairment of the entire TRAPP complex affects the trafficking of all the analyzed cargoes at the level of the Golgi complex that appears fragmented under these conditions.

The molecular mechanism underlying the specific requirement for sedlin in ER-exit of PCII does not involve Rab1. As observed also for PCI, selective impairment of Rab1 does not affect the ER exit of PCII in Rx chondrocytes. Thus, sedlin and TRAPP exert their function on ER exit of selected cargoes independently of the TRAPP exchange factor activity on Rab1.

I found instead that the role of the TRAPP complex in controlling the ER exit of PCII involves the COPII machinery. Bet3 is known to bind Sec23, and I have shown here that sedlin contacts the Sar1 GTPase, controlling its cycle.

Furthermore, sedlin is actively recruited to the ERES during a PCII trafficking wave, pointing out a very early step of transport in which sedlin is involved.

Sar1 dictates the timing of COPII carrier formation, and its cycling is fundamental for the proper exit of large molecules such as PCII. To determine whether prolonging the active (GTP-bound) state of Sar1 differentially affects the ER exit of PCII or VSV-G in chondrocytes, the Sar1H79G mutant was expressed in cells during a synchronised wave of transport. I found that PCII is more sensitive to Sar1H79G mutant than VSV-G. In the light of this evidence, I can conclude that a highly efficient COPII cycle is necessary for the ER exit of PCII.

Thus, these results lead to the conclusion that sedlin regulates PCII exit from the ER by regulating Sar1 GDP-GTP cycle. But what is the relevance of these findings for SEDT pathogenesis? To address this important issue I studied a cell line derived from one SEDT patient where I could confirm the importance of sedlin in the control of Sar1 cycle. Indeed, studies aimed at evaluating COPII dynamics reveal that Sec23 was more persistently associated with ER membranes in SEDT fibroblasts compared to fibroblasts isolated from a control healthy subject. This important finding definitively correlates the alteration of the COPII and Sar1 cycle to the disease.

Furthermore, the co-expression of a WT sedlin in the SEDT fibroblasts almost completely rescued the phenotype, revealing the importance of sedlin for COPII cycling.

Finally, the alteration of the COPII cycle in SEDT fibroblasts causes a delay in ER exiting of PCI and PCII (fluorescently tagged version), again almost completely rescued by the re-introduction of a functional sedlin molecule.

Chapter 5

Results

Establishing a SEDT animal model

Having an animal model to test the results from *in vitro* and cellular model systems represents an important step towards the development of therapeutic strategies but presently no animal model of SEDT is available.

Establishing this animal model is the natural evolution of my studies on sedlin and as a model vertebrate organism we have selected medaka fish (*Oryzias latipes*). This medaka sedlin-KD model will be developed in collaboration with Sandro Banfi and Ivan Conte who have established the medaka system at TIGEM. The medaka-based approach offers the indisputable advantage, compared to other animal models, of obtaining a KD animal in an extremely efficient and "fast" way with the use of anti-sense morpholino oligonucleotides. Importantly, medaka is a well-established model system to study chondrogenesis.

Medaka, Oryzias latipes (order Beloniformes), is a small egg-laying freshwater teleost fish that is primarily indigenous to Japan, Korea, Taiwan, and China. The adult is approximately 2-4 cm long, and the female lays every day a cluster of eggs (10–30 eggs). The embryos develop externally, and both the embryo and chorion are transparent. The embryos hatch seven days after fertilization at 28°C and grow to sexual maturity within 2 to 2.5 months. These biological features are mostly shared by zebrafish (*Danio rerio*).

During the last two decades, zebrafish research has been increased enormously, while medaka has more recently generated much interest. There are, however, several advantages of using medaka over the more commonly used zebrafish. First of all, the medaka genome is smaller (800 Mb). It corresponds in size to one-third of the human genome and less than half that of the zebrafish.

Second, there are highly polymorphic inbred medaka strains available, which can be used for mutagenesis screening and genetic mapping.

Finally, unlike zebrafish, which are tropical, embryos of the temperate medaka can develop at a wider range of temperatures, 6°C to 40°C, which facilitates the isolation of temperature-sensitive mutants and the staging of developing embryos by temperature. Moreover, medaka is more resistant than zebrafish and less susceptible to disease. In contrast with zebrafish, medaka has clearly defined sex chromosomes, and sex determination is intensively studied.

For decades, medaka was regarded as an important test system for ecotoxicology and carcinogenesis studies. Notably, medaka has many attributes that make it a perfect model laboratory organism, among them the clarity of its eggs, hardiness, and lack of aggression.

Furthermore, a fish model has been recently adopted to study bone and cartilage development and defects. In particular, fish animal models were used for studying defects occurring in members of early secretory pathway machinery such as COPII (Sarmah et al., 2010; Ohisa et al., 2010; Schwarz et al., 2009; Townley et al., 2008; Boyadjiev et al., 2006; Lang et al., 2006).

Since the medaka model is available at TIGEM, and since a SEDT animal model has not been created yet, I decided to start generating a medaka animal model for the SEDT disease.

First of all, I performed in silico analyses to search for a sedlin gene in the medaka genome. This analysis showed that there is a gene closely related to the human sedlin (**Figure 5.1**)

Sedlin is highly conserved in the medaka genome and importantly it is present as a single gene (**Figure 5.1**). This is very noteworthy information, since sedlin possesses a very complex genomic organisation in mammals, with the presence of several additional pseudogenes. The nucleotide sequence of medaka sedlin (ENSORLT0000022285.1) was obtained from the medaka genome sequence database at NCBI.

Next, I decided to verify whether the medaka sedlin gene is also transcribed. The sequence obtained from NCBI was used to design specific primers to detect sedlin mRNA.

```
Mus        MSGSFYFVIVGHHDNPVFEMEFLPPGKAESKDDHRHLNQFIAHAALDLVDENMWLSNNMY
Homo       MSGSFYFVIVGHHDNPVFEMEFLPAGKAESKDDHRHLNQFIAHAALDLVDENMWLSNNMY
Rattus     MSGSFYFVIVGHHDNPVFEMEFLPAGKTESKDEHRHLNQFIAHAALDLVDENMWLSNNMY
Medaka     MSGSFYFVMVGHHDNPVFELEFLPPGKAESKDDHRHLNQFIAHAALDLVDENMWLSNNMY
Xenopus    MSGSFYFVIVGHHDNPVFEMEFLPQGKTESKDDHRHLNQFIAHAALDLVDENMWLSNNMY
           ********:**********:****  **:****:**************************

Mus        LKTVDKFNEWFVSAFVTAGHMRFIMLHDVRQEDGIKNFFTDVYDLYIKFAMNPFYEPNSP
Homo       LKTVDKFNEWFVSAFVTAGHMRFIMLHDIRQEDGIKNFFTDVYDLYIKFSMNPFYEPNSP
Rattus     LKTVDKFNEWFVSAFVTAGHMRLIMLHDVRQEDGIKNFFTDVYDLYIKFAMNPFYEPNSP
Medaka     LKTVDKFNEWFVSAFVTAGHMRFIMLHDVRQEDGIKNFFNDVYDLYVKFAMNPFYEVNAP
Xenopus    LKTVDKFNEWFVSAFVTAGHMRFIMLHDVRQEDGIKNFFNEAYDLYIKFAMNPFYEINSP
           **********************:*****:**********  :: ****:**:****** *:*

Mus        IRSSAFDRKVQFLGKKHLLS
Homo       IRSSAFDRKVQFLGKKHLLS
Rattus     IRSTAFERKVQFLGKKHLLS
Medaka     IRSTAFERKVQFLGKKHLLS
Xenopus    LRSTAFDRKIQFLGKKHLLS
           :**:**:**:**********
```

Figure 5.1 Sedlin is highly conserved in Orytias latipes genome (medaka). Sequence alignment of sedlin proteins from different species shows that the protein is evolutionarily highly conserved. This alignment was generated using ClustalW program.

Using these probes I verified that the sedlin gene is expressed and is present as a single variant corresponding to the entire spliced coding sequence (**Figure 5.2**). Sedlin mRNA is also translated in medaka, as detected by Western Blot using an antibody raised against the human sedlin (**Figure 5.3**).

Then, to monitor sedlin localisation in medaka, embryos were morphologically staged according to Iwamatsu (Iwamatsu et al., 2004, stage 32) and fixed in 4% paraformaldehyde overnight. Sections were stained by indirect immunofluorescence using several antibodies.

As observed in mammals, sedlin is ubiquitously expressed in medaka (**Figure 5.4**). I also stained the sections with an anti-type PCII antibody and I observed staining of the extracellular space in different tissues, including the spine (**Figure 5.4**). These are very positive premises for the development of the sedlin KD medaka model and for the analysis of a possible phenotype on PCII trafficking. I have already designed specific anti-sedlin morpholinos from GeneTools. Further studies will be necessary also to verify whether medaka can recapitulate the symptoms of the SEDT disease, but undoubtedly these are very encouraging preliminary data that allow to work with medaka to generate a SEDT animal model.

Moreover, in De Matteis' laboratory we will also consider the possibility, if necessary, of generating a transgenic fish by injection of circular plasmids into medaka with mutant forms of sedlin described in patients, as mCherry or GFP fusion proteins to follow their fate during fish development.
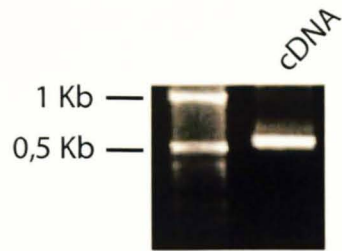
Figure 5.2 Sedlin gene is transcribed in Orytias latipes (medaka). Total mRNA from medaka was isolated, reverse-transcribed and amplified by RT-PCR using primers specific for the sedlin transcript. A single product was detected, supporting the hypothesis that sedlin is expressed as a single not-processed mRNA.
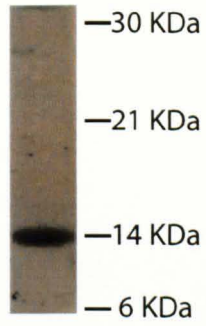
Figure 5.3 Sedlin gene is translated in Orytias latipes (medaka). Western analysis of a medaka protein extract (all developmental stages) with an anti-sedlin antibody. A single band corresponding of 14 kDa was detected.
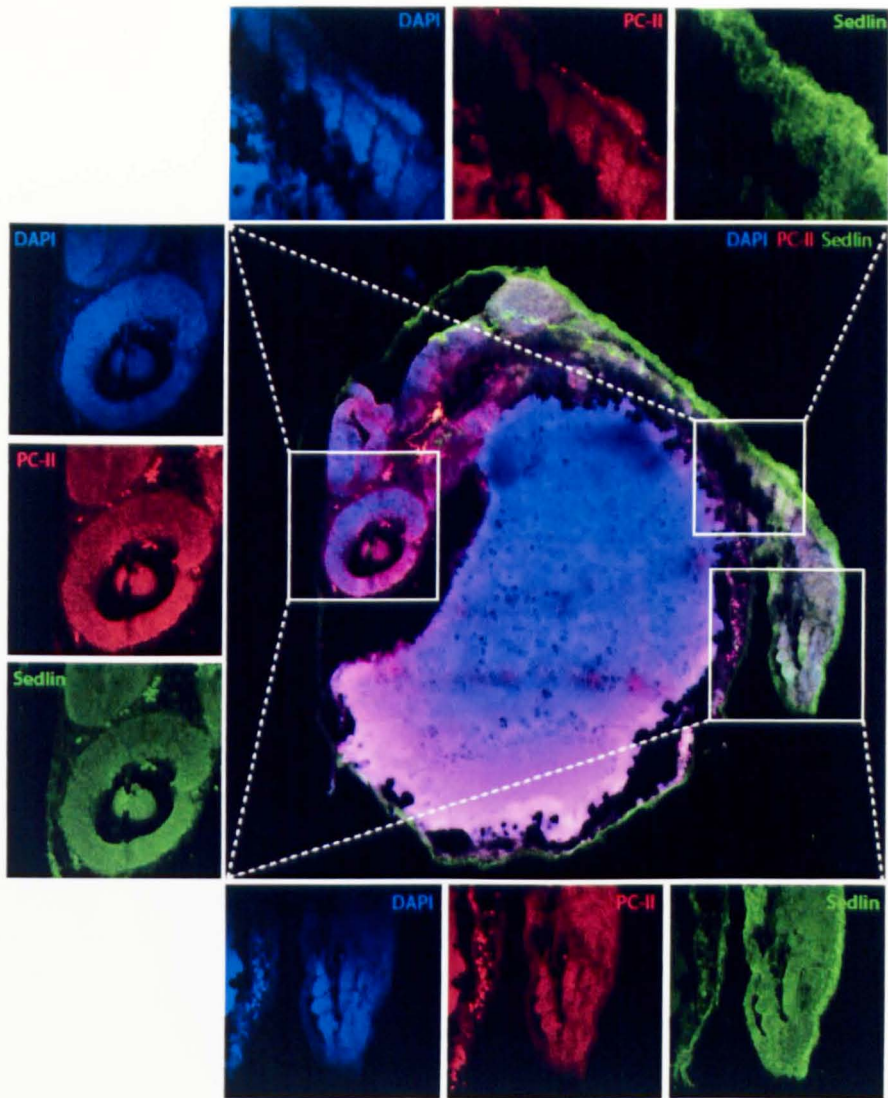
Figure 5.4 Sedlin localisation in embryonyc sections of Orytias latipes (medaka). Immunofluorescence of frozen medaka embryos. Sedlin is ubiquitously expressed. At this developmental stage (stage 32), PCII is easily detectable in the extracellular space.

Chapter 6

Final discussion

A huge variety of cargo proteins, in terms of size and composition, is exported from the ER in a COPII dependent manner. A central question is whether they leave the ER using different types of carriers. The COPII complex is remarkably versatile and able to form assemblies with a variety of shapes and sizes (Stagg et al., 2008), but what regulates this differential assembly?

A specific combination of Sec23 or Sec24 isoforms might favour a given COPII geometry, but there is space for yet undiscovered accessory proteins to regulate this event, the example of TANGO1 for PCVII being one (Saito et al., 2009; Wilson et al., 2011). Indeed a growing body of evidence indicates that different carriers form at the ER with differential molecular requirements. Studies in yeast have shown that different carriers can form in a COPII-dependent manner at the ER with differential molecular requirements. Two different types of carriers have been described: one containing GPI-anchored protein and another containing non GPI- anchored protein. Uso1p, Sec34/35 and Ypt1p are required for the formation of GPI-

containing carriers, but are dispensable for the other carriers. Again, these findings support the hypothesis that different cargoes might use different machinery for exiting the ER.

Manifold approaches have been undertaken to address this question in mammals but a definitive answer is still missing, with reports suggesting that PCI uses either distinct carriers or the same carriers used by "generic" cargo proteins.

In fact, the strongest line of evidence that supports the existence of different molecular machinery that control ER exit of different cargoes comes from the identification of tissue-specific genetic diseases caused by mutations in components of the presumed general secretory transport machinery that, however, affect selected tissues, possibly because these tissues express special cargoes.

For instance, mutations of COPII components cause tissue-specific pathology. Sar1B if mutated leads to the onset of Chylomicron Retention Disease, characterized by the failure of enterocytes to secrete large lipoprotein particles, which in turn accumulate inside the ER. Cranio-lenticulo sutural dysplasia is a rare genetic disease associated to mutations in the Sec23a gene. Why should widely expressed and highly conserved genes when mutated generate a tissue specific phenotype? A possible answer is that tissue-specific cargoes might be exquisitely sensitive to a defect in given components of the secretory machinery.

Indeed, the study of monogenic diseases of membrane trafficking can be revealing in addressing the question as to whether special cargoes, in terms

of size or composition, do have special trafficking requirements in terms of molecular machinery, and I have provided here an example of how the study of the cellular pathogenesis of SEDT has revealed an unsuspected role for the TRAPP complex in the early secretory pathway. .

So far, multiple trafficking steps in the exocytic, endocytic and autophagy pathways have been shown to be controlled by the TRAPP complex via the direct involvement of individual components of the complex. Here I report that TRAPP, through sedlin, intervenes in the earliest trafficking step along the exocytic pathway, i.e. the exit of (selected) cargoes from the ER, and I show that sedlin controls this step by modulating the residence time and concentration of Sar1-GTP at the ERES.

I have provided several independent lines of evidence demonstrating that TRAPP, through sedlin, accelerates the membrane-cytosol cycle of Sar1. Compared to control cells, sedlin/TRAPP-depleted cells have 1) a higher fraction of Sar1 associated with membranes, 2) a higher labelling density of Sar1 at the ERES membranes, 3) lower values of cytosolic Sar1 GAP activity, and 4) higher values for the membrane Koff of COPII components. Furthermore, this sedlin-mediated acceleration of Sar1 cycling is required for the export of PC, but not of many other cargoes, from the ER.

These findings, together with the observation that the ER export of PC, but not of the reporter cargo VSV-G, is inhibited by low concentrations of the GTP-locked Sar1 mutant Sar1H79G and the report that Sec13-31 (which enhances the Sar1 GAP activity of Sec23) is required for the ER export of PC but not of VSV-G (Townley et al., 2008), converge on the conclusion

that the full-efficiency of the Sar1 activation/inactivation cycle is required for PC but dispensable for VSV-G export from the ER (Stephens and Pepperkok, 2004).

The activation of Sar1 at the ERES by Sec12 (leading to Sar1-GTP) is required to initiate the recruitment of the Sec23-24 prebudding complex. However, Sec23-24 can temporarily remain associated with membranes once Sar1 is released from membranes (upon GTP hydrolysis promoted by Sec23 itself) thanks to the interaction of Sec24 with cargo through specific export signals (Barlowe, 2003; Miller et al., 2003; Forster et al., 2006). Thus, while the recruitment of "new" COPII invariably occurs with a 1:1 ratio between COPII and Sar1-GTP (which is continuously supplied by Sec12), the subsequent moulding of the COPII coat and the sculpting of the nascent bud proceeds under higher COPII:Sar1-GTP ratios. Indeed, Sar1-GTP is efficiently and actively released from membranes through the GAP activity of Sec23/24, which is enhanced by Sec13/31 (Bi et al., 2007), by cargo (Sato and Nakano, 2004, 2005; Forster et al., 2006) and by TRAPP, as described in this Thesis. Given the flexibility of the COPII coat (Stagg et al., 2008), its assembly in the presence of substoichiometric amounts of Sar1-GTP may allow the budding of carriers suitable for differently sized cargoes (**Figure 6.1**, upper panel). By contrast, higher local concentrations of Sar1-GTP during the budding process (as upon sedlin/TRAPP depletion) induce constrictions along the nascent carriers, as Sar1-GTP, due to the insertion of its N-terminal alpha helix in the phospholipid bilayer, (Lee et al., 2005; Long et al., 2010) can bend membranes.
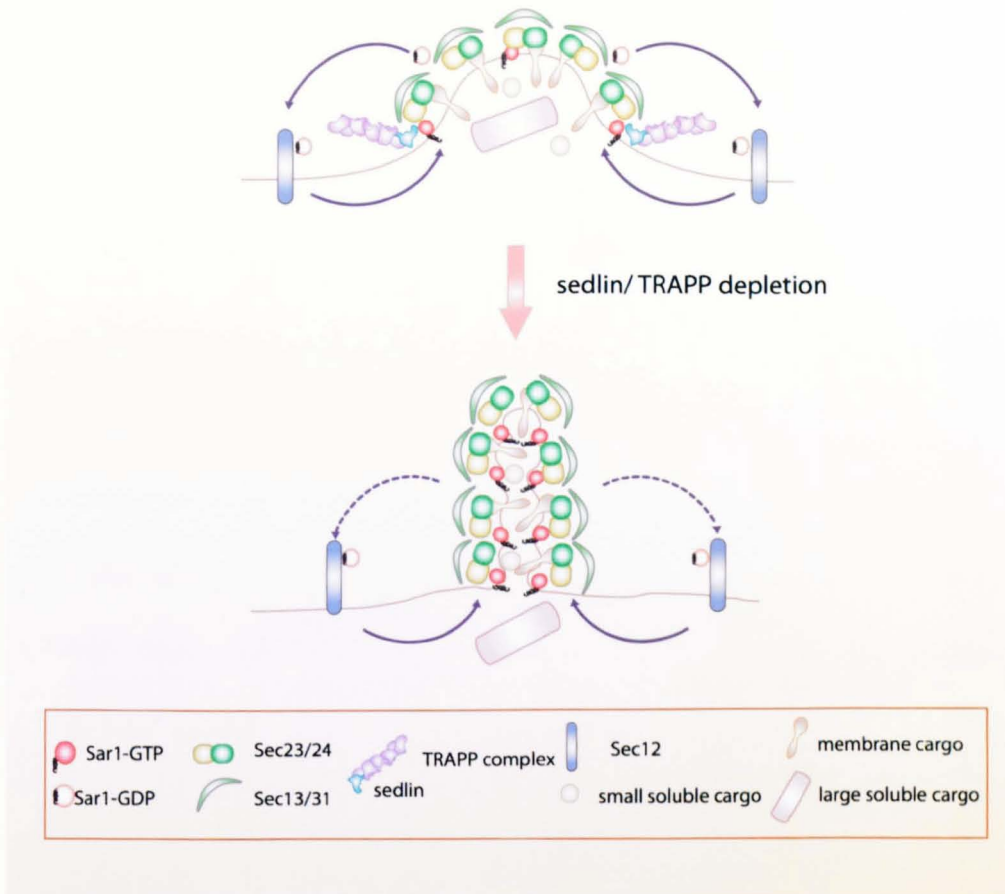
Figure 6.1 Model of the role of sedlin/TRAPP in the budding of transport carriers from the ER. Upper panel: under control conditions the activation of Sar1 by Sec12 at the ERES initiates the recruitment of the COPII complex. The inactivation of Sar1-GTP is triggered by Sec23 and positively controlled by cargo and sedlin/TRAPP. The release of Sar1-GDP from membranes is faster than the release of COPII, which can remain temporarily bound to membranes through membrane cargo-Sec24 interaction. The carriers formed under these conditions are competent for both small and large cargoes. Bottom: upon sedlin/TRAPP depletion or sedlin mutations the inactivation of Sar1-GTP is slowed down and its concentration in the nascent carrier increases. Higher local concentrations of Sar1-GTP induce membrane constrictions along the nascent carriers that are unsuited to host large cargoes, but are still able to accommodate small cargoes. See Final Discussion for details.

These "constricted" carriers may be unsuited to host large cargoes, but are still competent for smaller cargo (Figure 6.1, bottom panel). In this scenario, the dynamics of Sar1-GTP inactivation dictates the size and shape of the ER-derived carriers.

In line with this, TRAPP depletion (which slows down the inactivation of Sar1-GTP) leads to the proliferation of membrane structures (tubules with constriction sites), which are inaccessible to the 300 nm PC triple helices but permissive for smaller cargoes (such as VSV-G, which is indeed found inside these membrane profiles, data not shown Mironov, personal communication).

Interestingly, a higher concentration of Sar1 and the presence of constricted tubular profiles at the ERES have been also observed in cells expressing mutant Sec23a, which is responsible for cranio-lenticulo-sutural dysplasia (Fromme et al., 2007). This is another condition characterized by impaired PC secretion (Boyadjiev et al., 2011) in which a defective coupling between Sec23 and Sec31 slows down the rate of the Sar1 GTP/GDP cycle (Fromme et al., 2007). All of the above conditions, i.e. sedlin depletion (this Thesis), Sec23a mutation (Fromme et al., 2007; Boyadjiev S. et al 2011) and Sec13 depletion (Townley et al., 2008), selectively affect PC export from the ER through a convergent mechanism involving a more stable association of Sar1-GTP with the ERES membranes.

Sedlin binds Sar1, and this finding adds a further layer to the interactions between TRAPP and COPII, as Bet3 can bind Sec23 (Cai et al., 2007). The Bet3-Sec23 interaction is reported to mediate the tethering of COPII vesicles, preceding their homotypic fusion in mammals and their heterotypic fusion with the Golgi complex in yeast (Cai et al., 2007; Sacher et al., 2001). More recently, it has been shown that Bet3 competes with Sar1-GTP for its binding to Sec23 (Lord et al., 2011), thus indicating that the Bet3-Sec23-mediated interaction between TRAPP and COPII complexes can occur only after Sec23 is disengaged from Sar1 binding, i.e. only after Sar1 has been released from membranes and only after vesicles have detached from the donor ER membranes (Lord et al., 2011).

What I have reported here refers to an earlier interaction event between TRAPP and COPII complexes that involves sedlin and Sar1. This interaction occurs at a transport step (i.e. budding) that precedes the release of COPII-coated vesicles and is required to accelerate the release of Sar1 from membranes, thus allowing the next layer of interaction between COPII and TRAPP involving Sec23 and Bet3. TRAPP would then remain associated with budded transport carriers to play a role in subsequent events, such as Rab1 activation and the homotypic and heterotypic tethering of these carriers with the Golgi complex (Yu et al., 2006; Lord et al., 2011).

The TRAPP complex thus appears to be endowed with the ability to couple the cycles of two GTPases acting in series in ER-to-Golgi transport as it promotes the inactivation of Sar1 and the activation of Rab1, in line with the

proposal that the sequential activation of small GTPases acts as a switch controlling subsequent steps of intracellular trafficking (Segev, 2011; Poteryaev et al., 2010).

TRAPP mediates the first GTPase switch in the early secretory pathway: it deactivates Sar1 (acting as a co-GAP) and ensures Rab1 activation (functioning as a GEF), providing a sequential control in different trafficking steps. Furthermore, this dual activity of TRAPP is exerted through distinct subunits, with sedlin mediating the inactivation of Sar1 but being dispensable for the activation of Rab1.

Finally, my findings provide important mechanistic insights into the pathophysiology of SEDT, as indicated by the observation that SEDT-causing sedlin mutations shows defects in Sar1 binding and that cells from SEDT patients have abnormal COPII dynamics and impaired PCII transport. While these results on the selective requirement of sedlin for the trafficking of PCII provide a possible explanation for the chondrocyte-restricted involvement in SEDT, additional factors may contribute to this selective sensitivity of chondrocytes to sedlin mutations. These include the possibility that the chondrocytes of SEDT male patients express lower levels of sedlin pseudogene products (Gécz et al., 2000; Scrivens et al., 2009) or the ability of sedlin to exert "extra-TRAPP" and/or extra-trafficking functions, such as the regulation of transcription (Jeyabalan et al., 2010).

The involvement of these factors in the pathogenesis of SEDT remains a topic for future investigation. Moreover, a demanding task at this stage is the generation of a SEDT animal model (i.e. using Medaka animal model

228

system) to validate the identified molecular mechanism responsible for the onset of the disease and also to define therapeutic targets.

List of abbreviations

ARF   ADP-ribosylation factor

ATP   adenosine 5'-triphosphate

BFA   brefeldin A

BSA   bovine serum albumin

cDNA complementary DNA

CGN   Cis-Golgi network

COG   Conserved oligomeric complex

COPI/COPII coat protein I/II or coatomer

CPY   carboxypeptidase Y

CS   calf serum

Cvt   cytoplasm to vacuole targeting

DAB   3 5'-diaminobenzidine

DEAE diethylaminoethyl

DMEM   Dulbecco's modified minimal essential medium

DNA   deoxyribonucleasic acid

DTT   dithiothreitol

ECM   extracellular matrix

EDTA ethylenediamine tetraacetic acid

EGC endoplasmic reticulum-to-Golgi carriers

EGTA thyleneglycol-bis-(2-aminoethyllether)-N,N,N',N'-tetracetic acid

EM electron microscopy

ER endoplasmic reticulum

ERES endoplasmic reticulum exit sites

ERGIC ER-Golgi intermediate compartment

FCS fetal calf serum

FRAP fluorescence recovery after photobleaching

GalT galactosyl transferase

GEF Guanine Exchange Factor

GM Golgi matrix

GFP green fluorescence protein

GPC Golgi-to-plasma membrane carriers

GST glutathione S-transferase

GTP guanosine 5'-triphosphate

GTPase guanosine triphosphatese

HEPES N-2-hydroxyethylpiperazine-N-2-ethanesulfonic acid

Hfs Human fibroblast

HRP horseradish peroxidase

IC Intermediate compartment

IEM Immuno electron microscopy

IF immunofluorescence

IgG Immunoglobuline G

KD Knockdown

kDa kilo Dalton

LB Luria Broth

LSCM laser scan confocal microscopy

MannII mannosidase II

MOPS 4-morpholinepropanesulfonic acid

MW molecular weight

NSF N-ethylmaleimide-sensitive fusion

NZ nocodazole

ORF open reading frame

PAGE polyacrylamide gel electrophoresis

PAS pre-autophagosomal structure

PBS phosphate buffered saline

PCI procollagen type I

PCII procollagen type II

PCR polymerase chain reaction

PM plasma membrane

rpm revolution per minute

SDS Sodium dodecyl sulfate

SEDL spondyloepiphyseal dysplasia late

SNARE N-ethylmaleimide-sensitive fusion attachment protein receptor

TBS 150 mM NaCl, 50 mM Tris-HCl pH 7.5

tER transitional exit sites

TGN trans-Golgi network

TRIS tris(hydroxymethyl)aminomethane

TRAPP Transport Protein Particles

TTBS 0.05% Tween 20, 150 mM NaCl, 50 mM Tris-HCl pH 7.5

VSV vesicular stomatitis virus

VSV-G vesicular stomatitis virus G protein

VTC vesicular-tubular cluster

Bibliography

Allan, B.B., Moyer, B.D., and Balch, W.E. (2000). Rab1 recruitment of p115 into a cis-SNARE complex: programming budding COPII vesicles for fusion. Science *289*, 444-448.

Alvarez, C., Fujita, H., Hubbard, A., and Sztul, E. (1999). ER to Golgi transport: Requirement for p115 at a pre-Golgi VTC stage. J Cell Biol *147*, 1205-1222.

Alvarez, C., Garcia-Mata, R., Brandon, E., and Sztul, E. (2003). COPI recruitment is modulated by a Rab1b-dependent mechanism. Mol Biol Cell *14*, 2116-2127.

Anderson, C.M., Townley, R.R., Freemanm, and Johansen, P. (1961). Unusual causes of steatorrhoea in infancy and childhood. Med J Aust *48(2)*, 617-622.

Antonny, B., Madden, D., Hamamoto, S., Orci, L., and Schekman, R. (2001). Dynamics of the COPII coat with GTP and stable analogues. Nat Cell Biol *3*, 531-537.

Aridor, M., Bannykh, S.I., Rowe, T., and Balch, W.E. (1995). Sequential coupling between COPII and COPI vesicle coats in endoplasmic reticulum to Golgi transport. J Cell Biol *131*, 875-893.

Aridor, M., Bannykh, S.I., Rowe, T., and Balch, W.E. (1999). Cargo can modulate COPII vesicle formation from the endoplasmic reticulum. J Biol Chem *274*, 4389-4399.

Aridor, M., Fish, K.N., Bannykh, S., Weissman, J., Roberts, T.H., Lippincott-Schwartz, J., and Balch, W.E. (2001). The Sar1 GTPase coordinates biosynthetic cargo selection with endoplasmic reticulum export site assembly. J Cell Biol *152*, 213-229.

Aridor, M., Weissman, J., Bannykh, S., Nuoffer, C., and Balch, W.E. (1998). Cargo selection by the COPII budding machinery during export from the ER. J Cell Biol *141*, 61-70.

Balch, W.E., and Keller, D.S. (1986). ATP-coupled transport of vesicular stomatitis virus G protein. Functional boundaries of secretory compartments. J Biol Chem *261*, 14690-14696.

Banfield, D.K., Lewis, M.J., and Pelham, H.R. (1995). A SNARE-like protein required for traffic through the Golgi complex. Nature *375*, 806-809.

Bannykh, S.I., Rowe, T., and Balch, W.E. (1996). The organization of endoplasmic reticulum export complexes. J Cell Biol *135*, 19-35.

Barlowe, C. (2003). Molecular recognition of cargo by the COPII complex: a most accommodating coat. Cell *114*, 395-397.

Barlowe, C., d'Enfert, C., and Schekman, R. (1993). Purification and characterization of SAR1p, a small GTP-binding protein required for transport vesicle formation from the endoplasmic reticulum. J Biol Chem *268*, 873-879.

Barlowe, C., Orci, L., Yeung, T., Hosobuchi, M., Hamamoto, S., Salama, N., Rexach, M.F., Ravazzola, M., Amherdt, M., and Schekman, R. (1994). COPII: a membrane coat formed by Sec proteins that drive vesicle budding from the endoplasmic reticulum. Cell *77*, 895-907.

Barrowman, J., Bhandari, D., Reinisch, K., and Ferro-Novick, S. TRAPP complexes in membrane traffic: convergence through a common Rab. Nat Rev Mol Cell Biol *11*, 759-763.

Barrowman, J., Sacher, M., and Ferro-Novick, S. (2000). TRAPP stably associates with the Golgi and is required for vesicle docking. EMBO J *19*, 862-869.

Berger, A.H., Knudson, A.G., and Pandolfi, P.P. A continuum model for tumour suppression. Nature *476*, 163-169.

Bhattacharyya, D., and Glick, B.S. (2007). Two mammalian Sec16 homologues have nonredundant functions in endoplasmic reticulum (ER) export and transitional ER organization. Mol Biol Cell *18*, 839-849.

Bi, X., Corpina, R.A., and Goldberg, J. (2002). Structure of the Sec23/24-Sar1 pre-budding complex of the COPII vesicle coat. Nature *419*, 271-277.

Bi, X., Mancias, J.D., and Goldberg, J. (2007). Insights into COPII coat nucleation from the structure of Sec23.Sar1 complexed with the active fragment of Sec31. Dev Cell *13*, 635-645.

Bielli, A., Haney, C.J., Gabreski, G., Watkins, S.C., Bannykh, S.I., and Aridor, M. (2005). Regulation of Sar1 NH2 terminus by GTP binding and hydrolysis promotes membrane deformation to control COPII vesicle fission. J Cell Biol *171*, 919-924.

Bleasel, J.F., Bisagni-Faure, A., Holderbaum, D., Vacher-Lavenu, M.C., Haqqi, T.M., Moskowitz, R.W., and Menkes, C.J. (1995). Type II procollagen gene (COL2A1) mutation in exon 11 associated with spondyloepiphyseal dysplasia, tall stature and precocious osteoarthritis. J Rheumatol *22*, 255-261.

Bonfanti, L., Mironov, A.A., Jr., Martinez-Menarguez, J.A., Martella, O., Fusella, A., Baldassarre, M., Buccione, R., Geuze, H.J., Mironov, A.A., and Luini, A. (1998). Procollagen traverses the Golgi stack without leaving the lumen of cisternae: evidence for cisternal maturation. Cell *95*, 993-1003.

Bonifacino, J.S., and Glick, B.S. (2004). The mechanisms of vesicle budding and fusion. Cell *116*, 153-166.

Bos, J.L., Rehmann, H., and Wittinghofer, A. (2007). GEFs and GAPs: critical elements in the control of small G proteins. Cell *129*, 865-877.

Boyadjiev, S., Kim, S.D., Hata, A., Haldeman-Englert, C., Zackai, E., Naydenov, C., Hamamoto, S., Schekman, R., and Kim, J. Cranio-lenticulo-sutural dysplasia associated with defects in collagen secretion. Clin Genet *80*, 169-176.

Boyadjiev, S.A., Fromme, J.C., Ben, J., Chong, S.S., Nauta, C., Hur, D.J., Zhang, G., Hamamoto, S., Schekman, R., Ravazzola, M., *et al.* (2006). Cranio-lenticulo-sutural dysplasia is caused by a SEC23A mutation leading to abnormal endoplasmic-reticulum-to-Golgi trafficking. Nat Genet *38*, 1192-1197.

Boyadjiev, S.A., Justice, C.M., Eyaid, W., McKusick, V.A., Lachman, R.S., Chowdry, A.B., Jabak, M., Zwaan, J., Wilson, A.F., and Jabs, E.W. (2003). A novel dysmorphic syndrome with open calvarial sutures and sutural cataracts maps to chromosome 14q13-q21. Hum Genet *113*, 1-9.

Brigance, W.T., Barlowe, C., and Graham, T.R. (2000). Organization of the yeast Golgi complex into at least four functionally distinct compartments. Mol Biol Cell *11*, 171-182.

Brodsky, B., and Persikov, A.V. (2005). Molecular structure of the collagen triple helix. Adv Protein Chem *70*, 301-339.

Brown, W.J., Plutner, H., Drecktrah, D., Judson, B.L., and Balch, W.E. (2008). The lysophospholipid acyltransferase antagonist CI-976 inhibits a late step in COPII vesicle budding. Traffic *9*, 786-797.

Burton, J., and De Camilli, P. (1994). A novel mammalian guanine nucleotide exchange factor (GEF) specific for rab proteins. Adv Second Messenger Phosphoprotein Res *29*, 109-119.

Cai, H., Yu, S., Menon, S., Cai, Y., Lazarova, D., Fu, C., Reinisch, K., Hay, J.C., and Ferro-Novick, S. (2007). TRAPPI tethers COPII vesicles by binding the coat subunit Sec23. Nature *445*, 941-944.

Cai, H., Zhang, Y., Pypaert, M., Walker, L., and Ferro-Novick, S. (2005). Mutants in trs120 disrupt traffic from the early endosome to the late Golgi. J Cell Biol *171*, 823-833.

Cai, Y., Chin, H.F., Lazarova, D., Menon, S., Fu, C., Cai, H., Sclafani, A., Rodgers, D.W., De La Cruz, E.M., Ferro-Novick, S., *et al.* (2008). The structural basis for activation of the Rab Ypt1p by the TRAPP membrane-tethering complexes. Cell *133*, 1202-1213.

Cao, X., Ballew, N., and Barlowe, C. (1998). Initial docking of ER-derived vesicles requires Uso1p and Ypt1p but is independent of SNARE proteins. EMBO J *17*, 2156-2165.

Cao, X., and Barlowe, C. (2000). Asymmetric requirements for a Rab GTPase and SNARE proteins in fusion of COPII vesicles with acceptor membranes. J Cell Biol *149*, 55-66.

Castillon, G.A., Watanabe, R., Taylor, M., Schwabe, T.M., and Riezman, H. (2009). Concentration of GPI-anchored proteins upon ER exit in yeast. Traffic *10*, 186-200.

Choi, C., Davey, M., Schluter, C., Pandher, P., Fang, Y., Foster, L.J., and Conibear, E. Organization and assembly of the TRAPPII complex. Traffic *12*, 715-725.

Clermont, Y., Rambourg, A., and Hermo, L. (1995). Trans-Golgi network (TGN) of different cell types: three-dimensional structural characteristics and variability. Anat Rec *242*, 289-301.

Cole, N.B., Sciaky, N., Marotta, A., Song, J., and Lippincott-Schwartz, J. (1996). Golgi dispersal during microtubule disruption: regeneration of Golgi stacks at peripheral endoplasmic reticulum exit sites. Mol Biol Cell *7*, 631-650.

Connerly, P.L., Esaki, M., Montegna, E.A., Strongin, D.E., Levi, S., Soderholm, J., and Glick, B.S. (2005). Sec16 is a determinant of transitional ER organization. Curr Biol *15*, 1439-1447.

Cox, R., Chen, S.H., Yoo, E., and Segev, N. (2007). Conservation of the TRAPPII-specific subunits of a Ypt/Rab exchanger complex. BMC Evol Biol *7*, 12.

d'Enfert, C., Wuestehube, L.J., Lila, T., and Schekman, R. (1991). Sec12p-dependent membrane binding of the small GTP-binding protein Sar1p promotes formation of transport vesicles from the ER. J Cell Biol *114*, 663-670.

Dalton, A.J., and Felix, M.D. (1954). Cytologic and cytochemical characteristics of the Golgi substance of epithelial cells of the epididymis in situ, in homogenates and after isolation. Am J Anat *94*, 171-207.

De Matteis, M.A., Santini, G., Kahn, R.A., Di Tullio, G., and Luini, A. (1993). Receptor and protein kinase C-mediated regulation of ARF binding to the Golgi complex. Nature *364*, 818-821.

Delepine, M., Nicolino, M., Barrett, T., Golamaully, M., Lathrop, G.M., and Julier, C. (2000). EIF2AK3, encoding translation initiation factor 2-alpha kinase 3, is mutated in patients with Wolcott-Rallison syndrome. Nat Genet *25*, 406-409.

Delprato, A., and Lambright, D.G. (2007). Structural basis for Rab GTPase activation by VPS9 domain exchange factors. Nat Struct Mol Biol *14*, 406-412.

Doudna, J.A., and Batey, R.T. (2004). Structural insights into the signal recognition particle. Annu Rev Biochem *73*, 539-557.

Duarte, D.T., Hul, S., and Sacher, M. A yeast two hybrid screen identifies SPATA4 as a TRAPP interactor. FEBS Lett *585*, 2676-2681.

Dumas, J.J., Zhu, Z., Connolly, J.L., and Lambright, D.G. (1999). Structural basis of activation and GTP hydrolysis in Rab proteins. Structure *7*, 413-423.

Ehl, S., Uhl, M., Berner, R., Bonafe, L., Superti-Furga, A., and Kirchhoff, A. (2004). Clinical, radiographic, and genetic diagnosis of progressive pseudorheumatoid dysplasia in a patient with severe polyarthropathy. Rheumatol Int *24*, 53-56.

Espenshade, P., Gimeno, R.E., Holzmacher, E., Teung, P., and Kaiser, C.A. (1995). Yeast SEC16 gene encodes a multidomain vesicle coat protein that interacts with Sec23p. J Cell Biol *131*, 311-324.

Ethell, I.M., Hagihara, K., Miura, Y., Irie, F., and Yamaguchi, Y. (2000). Synbindin, A novel syndecan-2-binding protein in neuronal dendritic spines. J Cell Biol *151*, 53-68.

Ethell, I.M., and Yamaguchi, Y. (1999). Cell surface heparan sulfate proteoglycan syndecan-2 induces the maturation of dendritic spines in rat hippocampal neurons. J Cell Biol *144*, 575-586.

Eyre, D.R. (1991). The collagens of articular cartilage. Semin Arthritis Rheum *21*, 2-11.

Faiyaz ul Haque, M., King, L.M., Krakow, D., Cantor, R.M., Rusiniak, M.E., Swank, R.T., Superti-Furga, A., Haque, S., Abbas, H., Ahmad, W., *et*

al. (1998). Mutations in orthologous genes in human spondyloepimetaphyseal dysplasia and the brachymorphic mouse. Nat Genet *20*, 157-162.

Fan, L., Yu, W., and Zhu, X. (2003). Interaction of Sedlin with chloride intracellular channel proteins. FEBS Lett *540*, 77-80.

Farhan, H., Weiss, M., Tani, K., Kaufman, R.J., and Hauri, H.P. (2008). Adaptation of endoplasmic reticulum exit sites to acute and chronic increases in cargo load. EMBO J *27*, 2043-2054.

Farquhar, M.G., and Palade, G.E. (1981). The Golgi apparatus (complex)- (1954-1981)-from artifact to center stage. J Cell Biol *91*, 77s-103s.

Fath, S., Mancias, J.D., Bi, X., and Goldberg, J. (2007). Structure and organization of coat proteins in the COPII cage. Cell *129*, 1325-1336.

Filippini, F., Rossi, V., Galli, T., Budillon, A., D'Urso, M., and D'Esposito, M. (2001). Longins: a new evolutionary conserved VAMP family sharing a novel SNARE domain. Trends Biochem Sci *26*, 407-409.

Forster, R., Weiss, M., Zimmermann, T., Reynaud, E.G., Verissimo, F., Stephens, D.J., and Pepperkok, R. (2006). Secretory cargo regulates the turnover of COPII subunits at single ER exit sites. Curr Biol *16*, 173-179.

Franzusoff, A., and Schekman, R. (1989). Functional compartments of the yeast Golgi apparatus are defined by the sec7 mutation. EMBO J *8*, 2695-2702.

Fromme, J.C., Orci, L., and Schekman, R. (2008). Coordination of COPII vesicle trafficking by Sec23. Trends Cell Biol *18*, 330-336.

Fromme, J.C., Ravazzola, M., Hamamoto, S., Al-Balwi, M., Eyaid, W., Boyadjiev, S.A., Cosson, P., Schekman, R., and Orci, L. (2007). The genetic basis of a craniofacial disease provides insight into COPII coat assembly. Dev Cell *13*, 623-634.

Fromme, J.C., and Schekman, R. (2005). COPII-coated vesicles: flexible enough for large cargo? Curr Opin Cell Biol *17*, 345-352.

Futai, E., Hamamoto, S., Orci, L., and Schekman, R. (2004). GTP/GDP exchange by Sec12p enables COPII vesicle bud formation on synthetic liposomes. EMBO J *23*, 4146-4155.

Gavin, A.C., Bosche, M., Krause, R., Grandi, P., Marzioch, M., Bauer, A., Schultz, J., Rick, J.M., Michon, A.M., Cruciat, C.M., *et al.* (2002). Functional organization of the yeast proteome by systematic analysis of protein complexes. Nature *415*, 141-147.

Gecz, J., Hillman, M.A., Gedeon, A.K., Cox, T.C., Baker, E., and Mulley, J.C. (2000). Gene structure and expression study of the SEDL gene for spondyloepiphyseal dysplasia tarda. Genomics *69*, 242-251.

Gecz, J., Shaw, M.A., Bellon, J.R., and de Barros Lopes, M. (2003). Human wild-type SEDL protein functionally complements yeast Trs20p but some naturally occurring SEDL mutants do not. Gene *320*, 137-144.

Gedeon, A.K., Colley, A., Jamieson, R., Thompson, E.M., Rogers, J., Sillence, D., Tiller, G.E., Mulley, J.C., and Gecz, J. (1999). Identification of the gene (SEDL) causing X-linked spondyloepiphyseal dysplasia tarda. Nat Genet *22*, 400-404.

Gedeon, A.K., Tiller, G.E., Le Merrer, M., Heuertz, S., Tranebjaerg, L., Chitayat, D., Robertson, S., Glass, I.A., Savarirayan, R., Cole, W.G., *et al.* (2001). The molecular basis of X-linked spondyloepiphyseal dysplasia tarda. Am J Hum Genet *68*, 1386-1397.

Georges, A., Bonneau, J., Bonnefont-Rousselot, D., Champigneulle, J., Rabes, J.P., Abifadel, M., Aparicio, T., Guenedet, J.C., Bruckert, E., Boileau, C., *et al.* Molecular analysis and intestinal expression of SAR1

genes and proteins in Anderson's disease (Chylomicron retention disease). Orphanet J Rare Dis *6*, 1.

Ghosh, A.K., Steele, R., and Ray, R.B. (2003). Modulation of human luteinizing hormone beta gene transcription by MIP-2A. J Biol Chem *278*, 24033-24038.

Gimeno, R.E., Espenshade, P., and Kaiser, C.A. (1996). COPII coat subunit interactions: Sec24p and Sec23p bind to adjacent regions of Sec16p. Mol Biol Cell *7*, 1815-1823.

Groesch, M.E., Ruohola, H., Bacon, R., Rossi, G., and Ferro-Novick, S. (1990). Isolation of a functional vesicular intermediate that mediates ER to Golgi transport in yeast. J Cell Biol *111*, 45-53.

Grosshans, B.L., Ortiz, D., and Novick, P. (2006). Rabs and their effectors: achieving specificity in membrane traffic. Proc Natl Acad Sci U S A *103*, 11821-11827.

Guo, Y., and Linstedt, A.D. (2006). COPII-Golgi protein interactions regulate COPII coat assembly and Golgi size. J Cell Biol *174*, 53-63.

Gurkan, C., Lapp, H., Alory, C., Su, A.I., Hogenesch, J.B., and Balch, W.E. (2005). Large-scale profiling of Rab GTPase trafficking networks: the membrome. Mol Biol Cell *16*, 3847-3864.

Gwynn, B., Smith, R.S., Rowe, L.B., Taylor, B.A., and Peters, L.L. (2006). A mouse TRAPP-related protein is involved in pigmentation. Genomics *88*, 196-203.

Hammond, A.T., and Glick, B.S. (2000). Dynamics of transitional endoplasmic reticulum sites in vertebrate cells. Mol Biol Cell *11*, 3013-3030.

Heimpel, H., and Wendt, F. (1968). Congenital dyserythropoietic anemia with karyorrhexis and multinuclearity of erythroblasts. Helv Med Acta *34*, 103-115.

Hicke, L., Yoshihisa, T., and Schekman, R. (1992). Sec23p and a novel 105-kDa protein function as a multimeric complex to promote vesicle budding and protein transport from the endoplasmic reticulum. Mol Biol Cell *3*, 667-676.

Hong, W. (2005). SNAREs and traffic. Biochim Biophys Acta *1744*, 493-517.

Huang, M., Weissman, J.T., Beraud-Dufour, S., Luan, P., Wang, C., Chen, W., Aridor, M., Wilson, I.A., and Balch, W.E. (2001). Crystal structure of Sar1-GDP at 1.7 A resolution and the role of the NH2 terminus in ER export. J Cell Biol *155*, 937-948.

Hughes, H., Budnik, A., Schmidt, K., Palmer, K.J., Mantell, J., Noakes, C., Johnson, A., Carter, D.A., Verkade, P., Watson, P., *et al.* (2009). Organisation of human ER-exit sites: requirements for the localisation of Sec16 to transitional ER. J Cell Sci *122*, 2924-2934.

Hurvitz, J.R., Suwairi, W.M., Van Hul, W., El-Shanti, H., Superti-Furga, A., Roudier, J., Holderbaum, D., Pauli, R.M., Herd, J.K., Van Hul, E.V., *et al.* (1999). Mutations in the CCN gene family member WISP3 cause progressive pseudorheumatoid dysplasia. Nat Genet *23*, 94-98.

Huxley-Jones, J., Robertson, D.L., and Boot-Handford, R.P. (2007). On the origins of the extracellular matrix in vertebrates. Matrix Biol *26*, 2-11.

Iceton, J.A., and Horne, G. (1986). Spondylo-epiphyseal dysplasia tarda. The X-linked variety in three brothers. J Bone Joint Surg Br *68*, 616-619.

Iinuma, T., Shiga, A., Nakamoto, K., O'Brien, M.B., Aridor, M., Arimitsu, N., Tagaya, M., and Tani, K. (2007). Mammalian Sec16/p250 plays a role in

membrane traffic from the endoplasmic reticulum. J Biol Chem *282*, 17632-17639.

Iolascon, A., D'Agostaro, G., Perrotta, S., Izzo, P., Tavano, R., and Miraglia del Giudice, B. (1996). Congenital dyserythropoietic anemia type II: molecular basis and clinical aspects. Haematologica *81*, 543-559.

Iolascon, A., Servedio, V., Carbone, R., Totaro, A., Carella, M., Perrotta, S., Wickramasinghe, S.N., Delaunay, J., Heimpel, H., and Gasparini, P. (2000). Geographic distribution of CDA-II: did a founder effect operate in Southern Italy? Haematologica *85*, 470-474.
I
sherwood, S.G., Williams, C.M., and Gould, B.J. (1997). Apolipoprotein B-48 as a marker for chylomicrons and their remnants: studies in the postprandial state. Proc Nutr Soc *56*, 497-505.

Itzen, A., Rak, A., and Goody, R.S. (2007). Sec2 is a highly efficient exchange factor for the Rab protein Sec4. J Mol Biol *365*, 1359-1367.
Ivan, V., de Voer, G., Xanthakis, D., Spoorendonk, K.M., Kondylis, V., and Rabouille, C. (2008). Drosophila Sec16 mediates the biogenesis of tER sites upstream of Sar1 through an arginine-rich motif. Mol Biol Cell *19*, 4352-4365.

Jahn, R., and Scheller, R.H. (2006). SNAREs--engines for membrane fusion. Nat Rev Mol Cell Biol *7*, 631-643.

Jang, S.B., Kim, Y.G., Cho, Y.S., Suh, P.G., Kim, K.H., and Oh, B.H. (2002). Crystal structure of SEDL and its implications for a genetic disease spondyloepiphyseal dysplasia tarda. J Biol Chem *277*, 49863-49869.

Jeyabalan, J., Nesbit, M.A., Galvanovskis, J., Callaghan, R., Rorsman, P., and Thakker, R.V. SEDLIN forms homodimers: characterisation of SEDLIN mutations and their interactions with transcription factors MBP1, PITX1 and SF1. PLoS One *5*, e10646.

Jiang, Y., Scarpa, A., Zhang, L., Stone, S., Feliciano, E., and Ferro-Novick, S. (1998). A high copy suppressor screen reveals genetic interactions between BET3 and a new gene. Evidence for a novel complex in ER-to-Golgi transport. Genetics *149*, 833-841.

Jones, B., Jones, E.L., Bonney, S.A., Patel, H.N., Mensenkamp, A.R., Eichenbaum-Voline, S., Rudling, M., Myrdal, U., Annesi, G., Naik, S., *et al.* (2003). Mutations in a Sar1 GTPase of COPII vesicles are associated with lipid absorption disorders. Nat Genet *34*, 29-31.

Jones, S., Newman, C., Liu, F., and Segev, N. (2000). The TRAPP complex is a nucleotide exchanger for Ypt1 and Ypt31/32. Mol Biol Cell *11*, 4403-4411.

Julius, D., Brake, A., Blair, L., Kunisawa, R., and Thorner, J. (1984). Isolation of the putative structural gene for the lysine-arginine-cleaving endopeptidase required for processing of yeast prepro-alpha-factor. Cell *37*, 1075-1089.

Kadler, K.E., Holmes, D.F., Trotter, J.A., and Chapman, J.A. (1996). Collagen fibril formation. Biochem J *316 (Pt 1)*, 1-11.

Karsenty, G., and Wagner, E.F. (2002). Reaching a genetic and molecular understanding of skeletal development. Dev Cell *2*, 389-406.
Keenan, R.J., Freymann, D.M., Stroud, R.M., and Walter, P. (2001). The signal recognition particle. Annu Rev Biochem *70*, 755-775.

Kepes, F., Rambourg, A., and Satiat-Jeunemaitre, B. (2005). Morphodynamics of the secretory pathway. Int Rev Cytol *242*, 55-120.

Kim, Y.G., Raunser, S., Munger, C., Wagner, J., Song, Y.L., Cygler, M., Walz, T., Oh, B.H., and Sacher, M. (2006). The architecture of the

multisubunit TRAPP I complex suggests a model for vesicle tethering. Cell *127*, 817-830.

Kindel, T., Lee, D.M., and Tso, P. The mechanism of the formation and secretion of chylomicrons. Atheroscler Suppl *11*, 11-16.

King, K.B., and Kimura, J.H. (2003). The establishment and characterization of an immortal cell line with a stable chondrocytic phenotype. J Cell Biochem *89*, 992-1004.

Klausner, R.D., Donaldson, J.G., and Lippincott-Schwartz, J. (1992). Brefeldin A: insights into the control of membrane traffic and organelle structure. J Cell Biol *116*, 1071-1080.

Kreis, T.E. (1986). Microinjected antibodies against the cytoplasmic domain of vesicular stomatitis virus glycoprotein block its transport to the cell surface. EMBO J *5*, 931-941.

Kuehn, M.J., Herrmann, J.M., and Schekman, R. (1998). COPII-cargo interactions direct protein sorting into ER-derived transport vesicles. Nature *391*, 187-190.

Ladinsky, M.S., Mastronarde, D.N., McIntosh, J.R., Howell, K.E., and Staehelin, L.A. (1999). Golgi structure in three dimensions: functional insights from the normal rat kidney cell. J Cell Biol *144*, 1135-1149.

Lang, M.R., Lapierre, L.A., Frotscher, M., Goldenring, J.R., and Knapik, E.W. (2006). Secretory COPII coat component Sec23a is essential for craniofacial chondrocyte maturation. Nat Genet *38*, 1198-1203.

Lederkremer, G.Z., Cheng, Y., Petre, B.M., Vogan, E., Springer, S., Schekman, R., Walz, T., and Kirchhausen, T. (2001). Structure of the Sec23p/24p and Sec13p/31p complexes of COPII. Proc Natl Acad Sci U S A *98*, 10704-10709.

Lee, M.C., Orci, L., Hamamoto, S., Futai, E., Ravazzola, M., and Schekman, R. (2005). Sar1p N-terminal helix initiates membrane curvature and completes the fission of a COPII vesicle. Cell *122*, 605-617.

Lippincott-Schwartz, J. (1998). Cytoskeletal proteins and Golgi dynamics. Curr Opin Cell Biol *10*, 52-59.

Liu, X., Wang, Y., Zhu, H., Zhang, Q., Xing, X., Wu, B., Song, L., and Fan, L. Interaction of Sedlin with PAM14. J Cell Biochem *109*, 1129-1133.

Loh, E., Peter, F., Subramaniam, V.N., and Hong, W. (2005). Mammalian Bet3 functions as a cytosolic factor participating in transport from the ER to the Golgi apparatus. J Cell Sci *118*, 1209-1222.

Long, K.R., Yamamoto, Y., Baker, A.L., Watkins, S.C., Coyne, C.B., Conway, J.F., and Aridor, M. Sar1 assembly regulates membrane constriction and ER export. J Cell Biol *190*, 115-128.

Lord, C., Bhandari, D., Menon, S., Ghassemian, M., Nycz, D., Hay, J., Ghosh, P., and Ferro-Novick, S. Sequential interactions with Sec23 control the direction of vesicle traffic. Nature *473*, 181-186.

Luirink, J., and Sinning, I. (2004). SRP-mediated protein targeting: structure and function revisited. Biochim Biophys Acta *1694*, 17-35.
Lupashin, V., and Sztul, E. (2005). Golgi tethering factors. Biochim Biophys Acta *1744*, 325-339.

Lynch-Day, M.A., Bhandari, D., Menon, S., Huang, J., Cai, H., Bartholomew, C.R., Brumell, J.H., Ferro-Novick, S., and Klionsky, D.J. Trs85 directs a Ypt1 GEF, TRAPPIII, to the phagophore to promote autophagy. Proc Natl Acad Sci U S A *107*, 7811-7816.

Mansbach, C.M., and Siddiqi, S.A. The biogenesis of chylomicrons. Annu Rev Physiol *72*, 315-333.

Marra, P., Maffucci, T., Daniele, T., Tullio, G.D., Ikehara, Y., Chan, E.K., Luini, A., Beznoussenko, G., Mironov, A., and De Matteis, M.A. (2001). The GM130 and GRASP65 Golgi proteins cycle through and define a subdomain of the intermediate compartment. Nat Cell Biol *3*, 1101-1113.

Marra, P., Salvatore, L., Mironov, A., Jr., Di Campli, A., Di Tullio, G., Trucco, A., Beznoussenko, G., Mironov, A., and De Matteis, M.A. (2007). The biogenesis of the Golgi ribbon: the roles of membrane input from the ER and of GM130. Mol Biol Cell *18*, 1595-1608.

Matsuoka, K., Orci, L., Amherdt, M., Bednarek, S.Y., Hamamoto, S., Schekman, R., and Yeung, T. (1998). COPII-coated vesicle formation reconstituted with purified coat proteins and chemically defined liposomes. Cell *93*, 263-275.

Mayne, R. (1989). Cartilage collagens. What is their function, and are they involved in articular disease? Arthritis Rheum *32*, 241-246.

McCray, B.A., Skordalakes, E., and Taylor, J.P. Disease mutations in Rab7 result in unregulated nucleotide exchange and inappropriate activation. Hum Mol Genet *19*, 1033-1047.

Meiling-Wesse, K., Epple, U.D., Krick, R., Barth, H., Appelles, A., Voss, C., Eskelinen, E.L., and Thumm, M. (2005). Trs85 (Gsg1), a component of the TRAPP complexes, is required for the organization of the preautophagosomal structure during selective autophagy via the Cvt pathway. J Biol Chem *280*, 33669-33678.

Menon, S., Cai, H., Lu, H., Dong, G., Cai, Y., Reinisch, K., and Ferro-Novick, S. (2006). mBET3 is required for the organization of the TRAPP complexes. Biochem Biophys Res Commun *350*, 669-677.

Miller, E.A., and Barlowe, C. Regulation of coat assembly--sorting things out at the ER. Curr Opin Cell Biol *22*, 447-453.

Miller, E.A., Beilharz, T.H., Malkus, P.N., Lee, M.C., Hamamoto, S., Orci, L., and Schekman, R. (2003). Multiple cargo binding sites on the COPII subunit Sec24p ensure capture of diverse membrane proteins into transport vesicles. Cell *114*, 497-509.

Miller, E.A., Liu, Y., Barlowe, C., and Schekman, R. (2005). ER-Golgi transport defects are associated with mutations in the Sed5p-binding domain of the COPII coat subunit, Sec24p. Mol Biol Cell *16*, 3719-3726.

Miller, J.D., Tajima, S., Lauffer, L., and Walter, P. (1995). The beta subunit of the signal recognition particle receptor is a transmembrane GTPase that anchors the alpha subunit, a peripheral membrane GTPase, to the endoplasmic reticulum membrane. J Cell Biol *128*, 273-282.

Mironov, A.A., Beznoussenko, G.V., Nicoziani, P., Martella, O., Trucco, A., Kweon, H.S., Di Giandomenico, D., Polishchuk, R.S., Fusella, A., Lupetti, P., *et al.* (2001). Small cargo proteins and large aggregates can traverse the Golgi by a common mechanism without leaving the lumen of cisternae. J Cell Biol *155*, 1225-1238.

Mironov, A.A., Mironov, A.A., Jr., Beznoussenko, G.V., Trucco, A., Lupetti, P., Smith, J.D., Geerts, W.J., Koster, A.J., *Burger, K.N.,* Martone, M.E., *et al.* (2003). ER-to-Golgi carriers arise through direct en bloc protrusion and multistage maturation of specialized ER exit domains. Dev Cell *5*, 583-594.

Mochida, G.H., Mahajnah, M., Hill, A.D., Basel-Vanagaite, L., Gleason, D., Hill, R.S., Bodell, A., Crosier, M., Straussberg, R., and Walsh, C.A. (2009). A truncating mutation of TRAPPC9 is associated with autosomal-recessive intellectual disability and postnatal microcephaly. Am J Hum Genet *85*, 897-902.

Montpetit, B., and Conibear, E. (2009). Identification of the novel TRAPP associated protein Tca17. Traffic *10*, 713-723.

Moreno, F., Ochoa, A.G., Gascon, S., and Villanueva, J.R. (1975). Molecular forms of yeast invertase. Eur J Biochem *50*, 571-579.

Morozova, N., Liang, Y., Tokarev, A.A., Chen, S.H., Cox, R., Andrejic, J., Lipatova, Z., Sciorra, V.A., Emr, S.D., and Segev, N. (2006). TRAPPII subunits are required for the specificity switch of a Ypt-Rab GEF. Nat Cell Biol *8*, 1263-1269.

Morsomme, P., Prescianotto-Baschong, C., and Riezman, H. (2003). The ER v-SNAREs are required for GPI-anchored protein sorting from other secretory proteins upon exit from the ER. J Cell Biol *162*, 403-412.

Morsomme, P., and Riezman, H. (2002). The Rab GTPase Ypt1p and tethering factors couple protein sorting at the ER to vesicle targeting to the Golgi apparatus. Dev Cell *2*, 307-317.

Mossessova, E., Bickford, L.C., and Goldberg, J. (2003). SNARE selectivity of the COPII coat. Cell *114*, 483-495.

Mumm, S., Zhang, X., Gottesman, G.S., McAlister, W.H., and Whyte, M.P. (2001). Preonset studies of spondyloepiphyseal dysplasia tarda caused by a novel 2-base pair deletion in SEDL encoding sedlin. J Bone Miner Res *16*, 2245-2250.

Nakano, A., Brada, D., and Schekman, R. (1988). A membrane glycoprotein, Sec12p, required for protein transport from the endoplasmic reticulum to the Golgi apparatus in yeast. J Cell Biol *107*, 851-863.

Nakano, A., and Muramatsu, M. (1989). A novel GTP-binding protein, Sar1p, is involved in transport from the endoplasmic reticulum to the Golgi apparatus. J Cell Biol *109*, 2677-2691.

251

Nishimura, N., Bannykh, S., Slabough, S., Matteson, J., Altschuler, Y., Hahn, K., and Balch, W.E. (1999). A di-acidic (DXE) code directs concentration of cargo during export from the endoplasmic reticulum. J Biol Chem *274*, 15937-15946.

Nuoffer, C., Wu, S.K., Dascher, C., and Balch, W.E. (1997). Mss4 does not function as an exchange factor for Rab in endoplasmic reticulum to Golgi transport. Mol Biol Cell *8*, 1305-1316.

Pagano, A., Letourneur, F., Garcia-Estefania, D., Carpentier, J.L., Orci, L., and Paccaud, J.P. (1999). Sec24 proteins and sorting at the endoplasmic reticulum. J Biol Chem *274*, 7833-7840.

Pasqualato, S., Senic-Matuglia, F., Renault, L., Goud, B., Salamero, J., and Cherfils, J. (2004). The structural GDP/GTP cycle of Rab11 reveals a novel interface involved in the dynamics of recycling endosomes. J Biol Chem *279*, 11480-11488.

Pepperkok, R., Lowe, M., Burke, B., and Kreis, T.E. (1998). Three distinct steps in transport of vesicular stomatitis virus glycoprotein from the ER to the cell surface in vivo with differential sensitivities to GTP gamma S. J Cell Sci *111 (Pt 13)*, 1877-1888.

Pereira-Leal, J.B., and Seabra, M.C. (2001). Evolution of the Rab family of small GTP-binding proteins. J Mol Biol *313*, 889-901.

Peretti, N., Sassolas, A., Roy, C.C., Deslandres, C., Charcosset, M., Castagnetti, J., Pugnet-Chardon, L., Moulin, P., Labarge, S., Bouthillier, L., *et al.* Guidelines for the diagnosis and management of chylomicron retention disease based on a review of the literature and the experience of two centers. Orphanet J Rare Dis *5*, 24.

Pfeffer, S., and Aivazian, D. (2004). Targeting Rab GTPases to distinct membrane compartments. Nat Rev Mol Cell Biol *5*, 886-896.

Philippe, O., Rio, M., Carioux, A., Plaza, J.M., Guigue, P., Molinari, F., Boddaert, N., Bole-Feysot, C., Nitschke, P., Smahi, A., *et al.* (2009). Combination of linkage mapping and microarray-expression analysis identifies NF-kappaB signaling defect as a cause of autosomal-recessive mental retardation. Am J Hum Genet *85*, 903-908.

Pind, S.N., Nuoffer, C., McCaffery, J.M., Plutner, H., Davidson, H.W., Farquhar, M.G., and Balch, W.E. (1994). Rab1 and Ca2+ are required for the fusion of carrier vesicles mediating endoplasmic reticulum to Golgi transport. J Cell Biol *125*, 239-252.

Pinnel, S.R., Murad, S., and Darr, D. (1987). Induction of collagen synthesis by ascorbic acid. A possible mechanism. Arch Dermatol *123*, 1684-1686.

Poliseno, L., Salmena, L., Zhang, J., Carver, B., Haveman, W.J., and Pandolfi, P.P. A coding-independent function of gene and pseudogene mRNAs regulates tumour biology. Nature *465*, 1033-1038.

Poteryaev, D., Datta, S., Ackema, K., Zerial, M., and Spang, A. Identification of the switch in early-to-late endosome transition. Cell *141*, 497-508.

Presley, J.F., Cole, N.B., Schroer, T.A., Hirschberg, K., Zaal, K.J., and Lippincott-Schwartz, J. (1997). ER-to-Golgi transport visualized in living cells. Nature *389*, 81-85.

Queisser, W., Spiertz, E., Jost, E., and Heimpel, H. (1971). Proliferation disturbances of erythroblasts in congenital dyserythropoietic anemia type I and II. Acta Haematol *45*, 65-76.

Ralston, E., Ploug, T., Kalhovde, J., and Lomo, T. (2001). Golgi complex, endoplasmic reticulum exit sites, and microtubules in skeletal muscle fibers are organized by patterned activity. J Neurosci *21*, 875-883.

Rambourg, A., and Clermont, Y. (1990). Three-dimensional electron microscopy: structure of the Golgi apparatus. Eur J Cell Biol *51*, 189-200.

Ramshaw, J.A., Peng, Y.Y., Glattauer, V., and Werkmeister, J.A. (2009). Collagens as biomaterials. J Mater Sci Mater Med *20 Suppl 1*, S3-8.

Rao, Y., Bian, C., Yuan, C., Li, Y., Chen, L., Ye, X., Huang, Z., and Huang, M. (2006). An open conformation of switch I revealed by Sar1-GDP crystal structure at low Mg2+. Biochem Biophys Res Commun *348*, 908-915.

Reggiori, F., Wang, C.W., Nair, U., Shintani, T., Abeliovich, H., and Klionsky, D.J. (2004). Early stages of the secretory pathway, but not endosomes, are required for Cvt vesicle and autophagosome assembly in Saccharomyces cerevisiae. Mol Biol Cell *15*, 2189-2204.

Roberts, B., Clucas, C., and Johnstone, I.L. (2003). Loss of SEC-23 in Caenorhabditis elegans causes defects in oogenesis, morphogenesis, and extracellular matrix secretion. Mol Biol Cell *14*, 4414-4426.

Rossi, G., Kolstad, K., Stone, S., Palluault, F., and Ferro-Novick, S. (1995). BET3 encodes a novel hydrophilic protein that acts in conjunction with yeast SNAREs. Mol Biol Cell *6*, 1769-1780.

Rossi, V., Banfield, D.K., Vacca, M., Dietrich, L.E., Ungermann, C., D'Esposito, M., Galli, T., and Filippini, F. (2004). Longins and their longin domains: regulated SNAREs and multifunctional SNARE regulators. Trends Biochem Sci *29*, 682-688.

Ruohola, H., Kabcenell, A.K., and Ferro-Novick, S. (1988). Reconstitution of protein transport from the endoplasmic reticulum to the Golgi complex in

yeast: the acceptor Golgi compartment is defective in the sec23 mutant. J Cell Biol *107*, 1465-1476.

Russell, C., and Stagg, S.M. New insights into the structural mechanisms of the COPII coat. Traffic *11*, 303-310.

Sacher, M. (2003). Membrane traffic fuses with cartilage development. FEBS Lett *550*, 1-4.

Sacher, M., Barrowman, J., Wang, W., Horecka, J., Zhang, Y., Pypaert, M., and Ferro-Novick, S. (2001). TRAPP I implicated in the specificity of tethering in ER-to-Golgi transport. Mol Cell *7*, 433-442.

Sacher, M., Jiang, Y., Barrowman, J., Scarpa, A., Burston, J., Zhang, L., Schieltz, D., Yates, J.R., 3rd, Abeliovich, H., and Ferro-Novick, S. (1998). TRAPP, a highly conserved novel complex on the cis-Golgi that mediates vesicle docking and fusion. EMBO J *17*, 2494-2503.

Sacher, M., Kim, Y.G., Lavie, A., Oh, B.H., and Segev, N. (2008). The TRAPP complex: insights into its architecture and function. Traffic *9*, 2032-2042.

Saito, K., Chen, M., Bard, F., Chen, S., Zhou, H., Woodley, D., Polischuk, R., Schekman, R., and Malhotra, V. (2009). TANGO1 facilitates cargo loading at endoplasmic reticulum exit sites. Cell *136*, 891-902.

Salama, N.R., Yeung, T., and Schekman, R.W. (1993). The Sec13p complex and reconstitution of vesicle budding from the ER with purified cytosolic proteins. EMBO J *12*, 4073-4082.

Saraste, J., Lahtinen, U., and Goud, B. (1995). Localization of the small GTP-binding protein rab1p to early compartments of the secretory pathway. J Cell Sci *108 (Pt 4)*, 1541-1552.

Sato, K., and Nakano, A. (2004). Reconstitution of coat protein complex II (COPII) vesicle formation from cargo-reconstituted proteoliposomes reveals the potential role of GTP hydrolysis by Sar1p in protein sorting. J Biol Chem *279*, 1330-1335.

Sato, K., and Nakano, A. (2005). Dissection of COPII subunit-cargo assembly and disassembly kinetics during Sar1p-GTP hydrolysis. Nat Struct Mol Biol *12*, 167-174.

Sato, M., Sato, K., and Nakano, A. (1996). Endoplasmic reticulum localization of Sec12p is achieved by two mechanisms: Rer1p-dependent retrieval that requires the transmembrane domain and Rer1p-independent retention that involves the cytoplasmic domain. J Cell Biol *134*, 279-293.

Scheel, J., Pepperkok, R., Lowe, M., Griffiths, G., and Kreis, T.E. (1997). Dissociation of coatomer from membranes is required for brefeldin A-induced transfer of Golgi enzymes to the endoplasmic reticulum. J Cell Biol *137*, 319-333.

Schlenker, O., Hendricks, A., Sinning, I., and Wild, K. (2006). The structure of the mammalian signal recognition particle (SRP) receptor as prototype for the interaction of small GTPases with Longin domains. J Biol Chem *281*, 8898-8906.

Schwartz, T., and Blobel, G. (2003). Structural basis for the function of the beta subunit of the eukaryotic signal recognition particle receptor. Cell *112*, 793-803.

Schwarz, K., Iolascon, A., Verissimo, F., Trede, N.S., Horsley, W., Chen, W., Paw, B.H., Hopfner, K.P., Holzmann, K., Russo, R., *et al.* (2009). Mutations affecting the secretory COPII coat component SEC23B cause congenital dyserythropoietic anemia type II. Nat Genet *41*, 936-940.

Sciaky, N., Presley, J., Smith, C., Zaal, K.J., Cole, N., Moreira, J.E., Terasaki, M., Siggia, E., and Lippincott-Schwartz, J. (1997). Golgi tubule

traffic and the effects of brefeldin A visualized in living cells. J Cell Biol *139*, 1137-1155.

Scrivens, P.J., Noueihed, B., Shahrzad, N., Hul, S., Brunet, S., and Sacher, M. C4orf41 and TTC-15 are mammalian TRAPP components with a role at an early stage in ER-to-Golgi trafficking. Mol Biol Cell *22*, 2083-2093.

Scrivens, P.J., Shahrzad, N., Moores, A., Morin, A., Brunet, S., and Sacher, M. (2009). TRAPPC2L is a novel, highly conserved TRAPP-interacting protein. Traffic *10*, 724-736.

Seabra, M.C., Mules, E.H., and Hume, A.N. (2002). Rab GTPases, intracellular traffic and disease. Trends Mol Med *8*, 23-30.

Seabra, M.C., and Wasmeier, C. (2004). Controlling the location and activation of Rab GTPases. Curr Opin Cell Biol *16*, 451-457.

Segev, N. Coordination of intracellular transport steps by GTPases. Semin Cell Dev Biol *22*, 33-38.

Shaw, M.A., Brunetti-Pierri, N., Kadasi, L., Kovacova, V., Van Maldergem, L., De Brasi, D., Salerno, M., and Gecz, J. (2003). Identification of three novel SEDL mutations, including mutation in the rare, non-canonical splice site of exon 4. Clin Genet *64*, 235-242.

Shoulders, M.D., and Raines, R.T. (2009). Collagen structure and stability. Annu Rev Biochem *78*, 929-958.

Siddiqi, S., Saleem, U., Abumrad, N.A., Davidson, N.O., Storch, J., Siddiqi, S.A., and Mansbach, C.M., 2nd A novel multiprotein complex is required to generate the prechylomicron transport vesicle from intestinal ER. J Lipid Res *51*, 1918-1928.

Siddiqi, S.A., Gorelick, F.S., Mahan, J.T., and Mansbach, C.M., 2nd (2003). COPII proteins are required for Golgi fusion but not for endoplasmic

reticulum budding of the pre-chylomicron transport vesicle. J Cell Sci *116*, 415-427.

Snapp, E.L., Altan, N., and Lippincott-Schwartz, J. (2003). Measuring protein mobility by photobleaching GFP chimeras in living cells. Curr Protoc Cell Biol *Chapter 21*, Unit 21 21.

Spranger, J., Winterpacht, A., and Zabel, B. (1994). The type II collagenopathies: a spectrum of chondrodysplasias. Eur J Pediatr *153*, 56-65.

Stagg, S.M., LaPointe, P., Razvi, A., Gurkan, C., Potter, C.S., Carragher, B., and Balch, W.E. (2008). Structural basis for cargo regulation of COPII coat assembly. Cell *134*, 474-484.

Starkuviene, V., and Pepperkok, R. (2007). Differential requirements for ts-O45-G and procollagen biosynthetic transport. Traffic *8*, 1035-1051.

Stephens, D.J., Lin-Marq, N., Pagano, A., Pepperkok, R., and Paccaud, J.P. (2000). COPI-coated ER-to-Golgi transport complexes segregate from COPII in close proximity to ER exit sites. J Cell Sci *113 (Pt 12)*, 2177-2185.

Stephens, D.J., and Pepperkok, R. (2002). Imaging of procollagen transport reveals COPI-dependent cargo sorting during ER-to-Golgi transport in mammalian cells. J Cell Sci *115*, 1149-1160.

Stephens, D.J., and Pepperkok, R. (2004). Differential effects of a GTP-restricted mutant of Sar1p on segregation of cargo during export from the endoplasmic reticulum. J Cell Sci *117*, 3635-3644.

Stevens, T., Esmon, B., and Schekman, R. (1982). Early stages in the yeast secretory pathway are required for transport of carboxypeptidase Y to the vacuole. Cell *30*, 439-448.

Su, A.I., Wiltshire, T., Batalov, S., Lapp, H., Ching, K.A., Block, D., Zhang, J., Soden, R., Hayakawa, M., Kreiman, G., *et al.* (2004). A gene atlas of the mouse and human protein-encoding transcriptomes. Proc Natl Acad Sci U S A *101*, 6062-6067.

Supek, F., Madden, D.T., Hamamoto, S., Orci, L., and Schekman, R. (2002). Sec16p potentiates the action of COPII proteins to bud transport vesicles. J Cell Biol *158*, 1029-1038.

Tajima, S., Lauffer, L., Rath, V.L., and Walter, P. (1986). The signal recognition particle *receptor is a complex* that contains two distinct polypeptide chains. J Cell Biol *103*, 1167-1178.

Tiller, G.E., Hannig, V.L., Dozier, D., Carrel, L., Trevarthen, K.C., Wilcox, W.R., Mundlos, S., Haines, J.L., Gedeon, A.K., and Gecz, J. (2001). A recurrent RNA-splicing mutation in the SEDL gene causes X-linked spondyloepiphyseal dysplasia tarda. Am J Hum Genet *68*, 1398-1407.

Tiller, G.E., Polumbo, P.A., Weis, M.A., Bogaert, R., Lachman, R.S., Cohn, D.H., Rimoin, D.L., and Eyre, D.R. (1995). Dominant mutations in the type II collagen gene, COL2A1, produce spondyloepimetaphyseal dysplasia, Strudwick type. Nat Genet *11*, 87-89.

Tisdale, E.J. (1999). A Rab2 mutant with impaired GTPase activity stimulates vesicle formation from pre-Golgi intermediates. Mol Biol Cell *10*, 1837-1849.
Tisdale, E.J., and Balch, W.E. (1996). Rab2 is essential for the maturation of pre-Golgi intermediates. J Biol Chem *271*, 29372-29379.

Tisdale, E.J., Bourne, J.R., Khosravi-Far, R., Der, C.J., and Balch, W.E. (1992). GTP-binding mutants of rab1 and rab2 are potent inhibitors of vesicular transport from the endoplasmic reticulum to the Golgi complex. J Cell Biol *119*, 749-761.

Tisdale, E.J., and Jackson, M.R. (1998). Rab2 protein enhances coatomer recruitment to pre-Golgi intermediates. J Biol Chem *273*, 17269-17277.

Townley, A.K., Feng, Y., Schmidt, K., Carter, D.A., Porter, R., Verkade, P., and Stephens, D.J. (2008). Efficient coupling of Sec23-Sec24 to Sec13-Sec31 drives COPII-dependent collagen secretion and is essential for normal craniofacial development. J Cell Sci *121*, 3025-3034.

Turner, J.R., and Tartakoff, A.M. (1989). The response of the Golgi complex to microtubule alterations: the roles of metabolic energy and membrane traffic in Golgi complex organization. J Cell Biol *109*, 2081-2088.

Ullrich, O., Stenmark, H., Alexandrov, K., Huber, L.A., Kaibuchi, K., Sasaki, T., Takai, Y., and Zerial, M. (1993). Rab GDP dissociation inhibitor as a general regulator for the membrane association of rab proteins. J Biol Chem *268*, 18143-18150.

Ungermann, C., and Langosch, D. (2005). Functions of SNAREs in intracellular membrane fusion and lipid bilayer mixing. J Cell Sci *118*, 3819-3828.

Vetter, I.R., and Wittinghofer, A. (2001). The guanine nucleotide-binding switch in three dimensions. Science *294*, 1299-1304.

Votsmeier, C., and Gallwitz, D. (2001). An acidic sequence of a putative yeast Golgi membrane protein binds COPII and facilitates ER export. EMBO J *20*, 6742-6750.

Walter, P., and Blobel, G. (1980). Purification of a membrane-associated protein complex required for protein translocation across the endoplasmic reticulum. Proc Natl Acad Sci U S A *77*, 7112-7116.

Walter, P., and Blobel, G. (1982). Signal recognition particle contains a 7S RNA essential for protein translocation across the endoplasmic reticulum. Nature *299*, 691-698.

Wang, W., and Ferro-Novick, S. (2002). A Ypt32p exchange factor is a putative effector of Ypt1p. Mol Biol Cell *13*, 3336-3343.

Wang, W., Sacher, M., and Ferro-Novick, S. (2000). TRAPP stimulates guanine nucleotide exchange on Ypt1p. J Cell Biol *151*, 289-296.

Watson, P., Forster, R., Palmer, K.J., Pepperkok, R., and Stephens, D.J. (2005). Coupling of ER exit to microtubules through direct interaction of COPII with dynactin. Nat Cell Biol *7*, 48-55.

Watson, P., Townley, A.K., Koka, P., Palmer, K.J., and Stephens, D.J. (2006). Sec16 defines endoplasmic reticulum exit sites and is required for secretory cargo export in mammalian cells. Traffic *7*, 1678-1687.

Weissman, J.T., Plutner, H., and Balch, W.E. (2001). The mammalian guanine nucleotide exchange factor mSec12 is essential for activation of the Sar1 GTPase directing endoplasmic reticulum export. Traffic *2*, 465-475.

Westlake, C.J., Baye, L.M., Nachury, M.V., Wright, K.J., Ervin, K.E., Phu, L., Chalouni, C., Beck, J.S., Kirkpatrick, D.S., Slusarski, D.C., *et al.* Primary cilia membrane assembly is initiated by Rab11 and transport protein particle II (TRAPPII) complex-dependent trafficking of Rabin8 to the centrosome. Proc Natl Acad Sci U S A *108*, 2759-2764.

Whyte, M.P., Gottesman, G.S., Eddy, M.C., and McAlister, W.H. (1999). X-linked recessive spondyloepiphyseal dysplasia tarda. Clinical and radiographic evolution in a 6-generation kindred and review of the literature. Medicine (Baltimore) *78*, 9-25.

261

Wild, K., Sinning, I., and Cusack, S. (2001). Crystal structure of an early protein-RNA assembly complex of the signal recognition particle. Science *294*, 598-601.

Wilson, B.S., Nuoffer, C., Meinkoth, J.L., McCaffery, M., Feramisco, J.R., Balch, W.E., and Farquhar, M.G. (1994). A Rab1 mutant affecting guanine nucleotide exchange promotes disassembly of the Golgi apparatus. J Cell Biol *125*, 557-571.

Wilson, D.G., Phamluong, K., Li, L., Sun, M., Cao, T.C., Liu, P.S., Modrusan, Z., Sandoval, W.N., Rangell, L., Carano, R.A., *et al.* Global defects in collagen secretion in a Mia3/TANGO1 knockout mouse. J Cell Biol *193*, 935-951.

Wittmann, J.G., and Rudolph, M.G. (2004). Purification, crystallization and preliminary X-ray analysis of the GTP-binding protein Rab9 implicated in endosome-to-TGN vesicle trafficking. Acta Crystallogr D Biol Crystallogr *60*, 580-582.

Yamasaki, A., Menon, S., Yu, S., Barrowman, J., Meerloo, T., Oorschot, V., Klumperman, J., Satoh, A., and Ferro-Novick, S. (2009). mTrs130 is a component of a mammalian TRAPPII complex, a Rab1 GEF that binds to COPI-coated vesicles. Mol Biol Cell *20*, 4205-4215.

Yoshihisa, T., Barlowe, C., and Schekman, R. (1993). Requirement for a GTPase-activating protein in vesicle budding from the endoplasmic reticulum. Science *259*, 1466-1468.

Yu, S., Satoh, A., Pypaert, M., Mullen, K., Hay, J.C., and Ferro-Novick, S. (2006). mBet3p is required for homotypic COPII vesicle tethering in mammalian cells. J Cell Biol *174*, 359-368.

Zankl, A., Zabel, B., Hilbert, K., Wildhardt, G., Cuenot, S., Xavier, B., Ha-Vinh, R., Bonafe, L., Spranger, J., and Superti-Furga, A. (2004).

Spondyloperipheral dysplasia is caused by truncating mutations in the C-propeptide of COL2A1. Am J Med Genet A *129A*, 144-148.

Zong, M., Wu, X.G., Chan, C.W., Choi, M.Y., Chan, H.C., Tanner, J.A., and Yu, S. The Adaptor Function of TRAPPC2 in Mammalian TRAPPs Explains TRAPPC2-Associated SEDT and TRAPPC9-Associated Congenital Intellectual Disability. PLoS One *6*, e23350.

Acknowledgements